PREPARATION AND PROPERTIES OF CERAMIC AND SURFACE MODIFIED CERAMIC MEMBRANES

Thesis Submitted to the University of Glasgow

for the Degree of Ph.D.

by

HÉLIO DE LUCENA LIRA

FACULTY OF SCIENCE

CHEMISTRY DEPARTMENT

December 1996

Summary

In this research anodic alumina membranes are prepared and improved. Experimental method for preparation of novel small pore size asymmetric anodic alumina membranes is described. The method consists in to reduce the anodisation voltage and maintain constant in this low voltage for a long period of time. After the aluminium substrate and caps are removed by using a large voltage pulse for a very short time and the membrane is separated instantly. The barrier layer formed on the anodic alumina film is removed and all pores are open. Normally anodic alumina membrane are released from the aluminium substrate by chemical attack, either by dissolution of the aluminium foil or by dissolution of the barrier film of alumina. All these method involve dissolution of the pore wall and membrane with small pore size can not be produced

Scanning electron microscopy (SEM), atomic force microscopy (AFM) and gas permeation methods were used for the characterisation of pore size of anodic alumina membranes. Gas permeation measurements were performed using flat membranes with different pore sizes. It is shown that the permeation mechanism for anodic alumina membranes is Knudsen diffusion. This mechanism of gas permeation have been used to determine pore diameters. A good agreement between the anodisation voltage, direct observation by SEM and AFM and Knudsen predictions was observed. The anodic alumina samples studied in this research were 65, 50, 40, 11 and 5 nm diameters approximately. For the smallest pore size direct observation by SEM and AFM were difficult.

N-dodecyl-phosphate (nDP) and octadecyl-phosphate (ODP) were used to modify anodic alumina membrane. The analysis made by FTIR showed that nDP and ODP formed a stable monolayer on surface of anodic alumina membrane. Also the gas

permeation studies showed that the modification effectively reduced the pore size of the membrane and the permeability of the tested gases decrease by 4 times, approximately, for nDP treatment and 60 times, approximately, for ODP treatment. The modification with ODP shows a high separation factor for CO_2 and C_3H_8 when compared with helium and this results is interesting for use of separation of these gases. Also the pore diameter of the anodic alumina was estimated by gas permeation combined with surface modification. In this study the results obtained for pore diameter using nDP and ODP modifications are smaller than the results predicted by pure gas permeation.

A new way to prepare hydrophobic γ-alumina membranes is also reported. Polydimethylsiloxane oil was grafted onto a porous alumina membrane by heating, to 180 °C, producing a covalently grafted monolayer of silicone oil, chemically and thermally stable, unaffected by organic solvents but susceptible to alkali attack (as is the silicone oil itself). The membrane is totally impermeable to pure water, and organic solvents may be extracted from water mixtures by pervaporation. Very high permeation fluxes were obtained, suggesting possible use of these silicone/ceramic membranes in extraction of volatile organic compounds (VOCs). This simple modification can be applied to macroporous membranes increasing hydrophobiticy without pore blocking.

Also stable trichloro-octadecyl silane (ODS) derivatives of a 5nm -alumina ceramic membrane were prepared. Gas permeabilites of the untreated membrane did not show Knudsen diffusion at 20 °C. Gas permeabilities of the ODS membrane were three orders of magnitude lower. He, Ne, Ar, CO_2 , C_3H_8 have near constant permeabilities 360×10^{-11} mole s^{-1} m^{-2} Pa^{-1} except methane which has the highest permeability of the

group, 481×10^{-11} mole s^{-1} m^{-2} Pa^{-1}. The mechanism of diffusion is solution/diffusion. Remarkably, permeabilities of ODS-alumina membrane were reduced by 5x after exposure to a pressure difference of 1atm (active layer side) against vacuum for only ten minutes. The effect was metastable but could be reversed on standing for several hours, reversal of pressure difference or after washing with (hydrocarbon solvent) toluene. The mechanism was presumed to be due to movement of the octadecyl-hydrocarbon chains of the silane monolayer causing a partially blocked pore structure; perhaps a unique example of self-fouling.

Acknowledgements

Declaration

The work described in Chapters 7 and 8 was published in the Journal of Membrane Science. These publications were made jointly with Dr. Russell Paterson and Dr. Christian Leger.

Table of Contents

Chapter 7 Surface Modification of γ-Alumina Membrane Using Polydimethylsiloxane (PDMS)

Chapter 1

General Introduction

1.1 Introduction

The preparation of inorganic membranes has received great attention in the past few years. A number of excellent reviews have been published recently [1-4]. Ceramic oxide membranes, anodic alumina membranes, glass membranes and others membranes have been of most interest [1] because of their potential application in gas separation and high temperature membrane reactors [2] as well as in liquid separation processes. Ceramic membranes are today successfully applied to a wide variety of separation, concentration and purification problems in many industries [3].

The most generally applicable method of preparation is by a sol-gel process and in a smaller scale by anodic oxidation. By refinements of these methods membranes may be prepared with very thin active layers, excellent permeabilities and almost any desired porosities down to ultrafiltration levels and some experimental membranes even show pore sizes below 2 nm which is acceptable for nanofiltration. However ceramic membrane materials are limited in practice to four insoluble oxides , silica, alumina, titania and zirconia: there is very little choice of membrane material. The limited range of ceramic materials compared with the almost limitless range of organic polymers make the unmodified ceramic membranes less attractive. For this reason, there has been renewed interest in surface modification of inorganic membranes as a means to improve and expand their use in separation and other processes. A selection of these can be found in the Proceedings of the International Conferences on Inorganic Membranes [5-13]. Most treatments either involved the production of composites or membrane coating using polyelectrolytes. Clearly the properties of the membrane are

determined by its surface and if this is modified a new membrane is produced with properties which depend primarily upon the new surface created and have little or no relation to the original. In general, the mechanical properties are dictated primarily by the ceramic support, while the permeability is influenced principally by the chemistry and configuration of the covalently-bonded compound.

The research presented in this thesis begins with the preparation of anodic alumina membranes, described in Chapter 2. A new technique to remove the aluminium substrate and barrier from anodic film is applied. This is followed by discussions on the preparation of asymmetric structures that can lead to a new small pore size membrane.

In Chapter 3, the general microstructure of the anodic alumina membrane is discussed. Scanning electron microscopy (SEM) and atomic force microscopy (AFM) are used to study the general features of the anodic alumina membrane, mainly thickness, pore density and porosity.

Although the microstructure of anodic alumina membranes has been studied by high resolution scanning electron microscope and also by the newer atomic force microscope, the pore diameters measured by this techniques are limited to large pores (>40 nm, particularly in this study). However, due to a very high regularity of the features of the anodic alumina membranes a geometrical model, discussed in Chapter 4, was applied from the SEM and AFM data to extrapolate the small pore diameter of the asymmetric membranes prepared when the formation voltage is reduced at the end of the anodisation.

Although individual estimates of the pore diameter for the small pore size anodic alumina membranes were predicted from geometric considerations an additional independent method to confirm these results was necessary. In Chapter 5, a gas permeation method was designed for the characterisation of pore size of homogeneous and asymmetric anodic alumina membranes. In this technique the measurement of the gas permeability coefficient as a function of the mean pressure across a membrane was used to determine a mean pore diameter of the membranes.

The last three chapters (Chapters 6, 7 and 8) are devoted to a preparation of surface modified ceramic membranes and their gas permeation properties. Chapter 6 describes the chemical treatment of anodic alumina membranes by organo phosphate compounds and their characterisation by the gas permeation method. The measurements are performed using flat anodic alumina membranes after chemical surface modification by n-Dodecylphosphate and Octadecylphosphate. The permeation mechanism for untreated and treated membranes is applied to estimate the pore diameter of the anodic alumina. A new method to prepare hydrophobic membranes is reported in Chapter 7. Polydimethlsiloxane oil is grafted onto a porous γ-alumina membrane. The covalently grafted monolayer of silicone oil produces a stable (chemically and thermally) silicone/ceramic membrane. The composite membrane produced is totally impermeable to pure water. Finally, Chapter 8 describes the modification of γ-alumina membranes by silane compounds. Surprisingly, when the membrane is treated by trichloro-octadecylsilane the gas permeabilities are reduced drastically and show a metastable behaviour and can be reversed on reversal of pressure difference or after

washing with hydrocarbon solvent. This mechanism is presumed to be due to movement of the octadecyl carbon chains of the silane monolayer causing a self-fouling.

1.2 Background To Ceramic Membranes

Ceramic membranes were first developed in the 1940's for nuclear applications, and essentially for the separation of uranium isotopes by the process of gaseous diffusion applied to UF_6 [14, 15]. These materials were porous alumina and zirconia. The preference for these oxide materials may be due to several factors, one of which is the apparent corrosive nature of uranium hexafluoride, for example, toward metals [15]. Non-nuclear applications of these membranes started at the beginning of the 1980's in France and in USA. Today more than twenty companies have introduced inorganic membranes on the market and the number is increasing rapidly. European, American and Japanese companies are now competing [16], in the emergent market.

Ceramic membranes has been commercialised first in the microfiltration applications. The major evolution in the characteristics of the ceramic membranes during the last few years is the decrease in the pore size of the products. Commercial ceramic membranes for ultrafiltration began to emerge and ceramic nanofiltration membranes have just became available [17].

Several methods can be used to prepare ceramic membranes, but slip casting of fine particle dispersions, from sol-gel process, is the most widely used technique for preparing ceramic membranes.

Another completely different type of ceramic membrane also has its origin in nuclear industry [18] and is obtained by the anodic oxidation of an aluminium sheet. Today this method is used to produce commercial anodic alumina membrane.

1.2.1 Anodic Alumina Membranes

Throughout the present thesis, a difference between anodic alumina films and anodic alumina membranes is made. Anodic alumina films are taken to be those oxide layers produced by anodically oxidising aluminium in suitable electrolytes and comprise a porous "relatively pure alumina" film with a impermeable barrier layer (or caps) at the end of the pores (see Figs. 2.3a and 2.3b, in Chapter 2). Anodic alumina membranes are taken to be those anodic alumina films with the barrier layer (or caps) removed by electrochemical treatment or acid dissolution (see Fig. 2.3c, in Chapter 2).

Anodic Alumina Films

The process of anodic oxidation of aluminium and the resulting structures which have been realised were described in 1953 [19]. A review by Diggle et al [20] has covered this field from 1930 up to 1969. The thorough review by Thompson and Wood [21] contains valuable information about structure, composition and mechanism of growth of anodic films on aluminium surfaces. Many of these aspects were studied in the period of 1970-1983.

O'Sullivan and Wood [21] made an extended study on the morphology and mechanism of formation of porous anodic films on aluminium. Structural studies were also carried

out by Takahashi et al [22], Thompson *et al* [23], Furneaux, Thompson and Wood [24] and Pavlovic and Ignatiev [25]. Some conclusion listed from the above studies are:

1. Pore initiation in anodic films produced at constant current density occurs by the merging of locally thickening oxide regions, with appear related to the substrate substructure, and the subsequent concentration of current into the residual thin regions.

2. The pores grow in such a way that their diameter remains proportional to the applied voltage as the steady state is approached.

3. The barrier-layer thickness, cell diameter and pore diameter are directly proportional to the formation voltage.

4. Increase and/or decrease of the voltage during anodisation leads to a redistribution of pore and cell populations, requiring pore merging or termination and pore initiation, respectively.

5. Use of relatively weak electrolytes produces porous films with thicker barrier layers, larger cell and larger pores next to the barrier layer than strong electrolytes under constant current density conditions.

6. Pore widening, film distortion and film collapsed upon drying, produced by chemical dissolution during prolonged contact with the electrolyte are more severe with strong electrolytes.

Anodic alumina films have most commonly been formed in sulphuric, phosphoric, chromic and oxalic acid electrolytes [26]. Commercially pure aluminium has been

potentiostatically anodised in phosphoric acid for a range of voltages and anodising times. The microstructure, of these anodic layers, consists of hexagonal columnar cells, with a centrally situated pore that runs down the column of each cell. The regularity of this structure allows the pore diameter and percentage porosity to be controlled and measured within each film. The fabrication of inorganic membranes, through anodisation of aluminium, requires control of voltage, electrolyte temperature and composition, and anodisation time. The pore size decreases directly with anodic voltage.

According to Thompsom and Wood [27] and Furneaux *et al* [28] the pores grow in diameter and change in number until the steady-state morphology is established. The steady-state barrier-layer thickness, cell diameter and pore diameter are all observed to be directly proportional to the formation voltage. It becomes evident that the barrier-layer thickness, decided largely by an equilibrium established between oxide formation in the barrier-layer and field-assisted dissolution (probably thermally enhanced) at the pore bases, determines the cell and pore sizes by a simple geometrical mechanism. Shimizu et al [29] suggest a model to explain the growth of anodic alumina films at the metal/film interface based on migration of O^{2-} and Al^{3+} ions, inward and outward, across the thickening barrier oxide. Current is subsequently concentrated into the thin film regions between protuberance of locally thicker films which become the preferred regions for pore development.

Anodic Alumina Membranes

The process for producing an anodic alumina membrane was first described by Mårtensson *et al* [18] and patented by Smith [30, 31]. Anodic alumina membranes have been produced since 1986 on a commercial scale by Anotec Separations [32]. Basically two type of membranes in laboratory-scale modules are available; (1) a homogeneous membrane with pores of 200 nm and a porosity of 65% or higher; and (2) an asymmetric membrane with pores of 20 nm in the top layer and porosity about 50%.

In the process patented by Smith [30] for producing an anodic alumina membrane a sheet of aluminium is mounted in a cell in such a way that the sheet can be exposed to different solutions on both sides of the sheet. The preparation procedure can be summarised as follow: Aluminium foil (thickness 12 μm) was anodised by placing a solution of 15% solution of H_2SO_4 on one side of the foil for a period of 37 minutes. After rinsing, the sample was etched with H_2SO_4 on unanodised side and in pure distilled water on the anodised side. After rinsing again, the sample was washed for 20 min at 50-60 °C and allowed to cool slowly.

Rai and Ruckenstein [33] describe a process to produce a porous anodic alumina film by using two sheets of aluminium pressed together to produce pores extending across the entire thickness of one sheet. In this method oxalic acid at room temperature was used with anodisation voltages between 10 and 40 V. The pore size obtained was about 18 nm and it was shown that the cell size increase linearly with increasing anodising voltage.

Itaya *et al* [34] report a method to prepare anodic alumina membranes by using a cell for anodising where only one face of the aluminium sheet was anodised. This used sulphuric and oxalic acids as electrolytes. The aluminium substrate was etched by HCl and the barrier layer (or caps) were removed by H_2SO_4 concentrated. In this study the pore size of the membranes was measured by SEM and the diameters were found to be > 20 nm.

Furneaux *et al* [35- 37] described a method to prepare an anodic film with an asymmetric structure by a programmed voltage reduction during the anodisation. To detach the film from the aluminium metal the anodised material was briefly immersed in orthophosphoric acid and the anodic membrane was lifted from the aluminium. The pore diameters are in the range 28-51nm by this method.

Recently, Paterson *et al* [38] and Mardilovich *et al* [39-42] have developed polycrystalline anodic alumina membranes by controlled calcination of amorphous anodic alumina membranes. In these studies the polycrystalline anodic alumina membranes, formed by calcination at temperature >800°C, have an exceptionally high resistance to acid and base.

Itoh *et al* [43] also describe the preparation of a tubular anodic alumina membrane using an aluminium tube of 45 mm length, 0.5 mm thick and 6mm in its outer diameter. The tubular anodic alumina membrane obtained was 35-40μm thick and has pore diameters between 20-50nm.

1.2.2 Sol-Gel Membranes

Basically, a sol-gel ceramic membrane can be described as an asymmetric porous ceramic formed by a macroporous support with successive thin layers deposited on it. The support provides mechanical resistance, intermediate layers offer satisfactory support properties for the upper layer, and the top layer is the active one. The intermediate layer should prevent the penetration of the precursor of the top layer material into the pores of the support during the synthesis and the collapse of the thin finished top layer into the large pores of the support. Depending on the application different techniques are applied to prepare porous ceramic membranes. For microfiltration in which pores of less than one micrometer are needed suspensions of submicron powders have to be processed using spin coating, slip-casting or tape-casting techniques depending on the support shape (flat or tubular). For ultrafiltration and nanofiltration colloidal particles are needed and cannot be handled as dry powders, in this case colloidal suspensions are used. These particles and colloidal suspensions are obtained mainly by the technique known as the sol-gel process.

At least two main routes can be described in sol-gel process: the colloidal suspension route and the polymeric gel route [44]. The general steps involved in these two routes for making ceramic membranes are shown schematically in Fig. 1.1. In both cases, a precursor is hydrolysed while a condensation or polymerisation reaction occurs simultaneously. The precursor is either an inorganic salt or a metal organic compound.

In the colloidal route, a faster hydrolysis rate is obtained by using an excess of water. A precipitate of gelatinous hydroxide or hydrated oxide particles is formed which is peptised in a subsequent step to a stable colloidal suspension. The primary colloidal particles so obtained are usually in the range of 5 to 15 nm. Acid or base are added to break up the precipitate into small particles. Various reactions based on electrostatic interactions at the surface of the particles then take place. The result is a stable colloidal solution. Organic binders are then added to the solution and a physical gel is formed, this gel is then heat treated to form the ceramic membrane.

In the polymeric gel route which hydrolyses rate is kept low by adding successively small amounts of water and by choosing a precursor with hydrolyses only relatively slowly. The final stage of this process is a strongly interlinked gel network with a structure different from that obtained from the colloidal route. The gel layer is dried and head treated to form a rigid oxide network held together by chemical bonds.

1.3 References

[1] H. P. Hsieh, Inorganic Membranes for Separation and Reaction, Elsevier Science Publishing Co., New York, 1996.

[2] J. Zaman and A. Chakma, Inorganic membrane reactors: review, J. Membr. Sci., 92 (1994) 1.

[3] E. Drioli and L. Giorno, Catalytic membrane reactors, Chemistry & Industry, 22 (1996) 19-22.

[4] R. R. Bhave, Inorganic Membranes: Synthesis, Characteristics and Applications, Reinhold, New York, 1991.

[5] C. Guizard, A. Labort, L. Cot, A new generation of membranes based on inorganic-organic polymers, Proc. Ist. Int. Conf. Inorganic Membranes, July 3-6, 1990, Montpellier, p. 55.

[6] S. N. Gaeta, H. Zang and E. Drioli, Preparation of polyphosphazene membranes for gas & liquid separations, Proc. 1st. Int. Conf. Inorganic Membranes, July 3-6, 1990, Montpellier, p. 65.

[7] T. Tanigami, Y. Kobayashi, S. Nakano, K. Yamaura and S. Matsuzawa, Thin film of poly(bis(β-phenoxythoxy)phosphazene) as a microporous membrane, Proc. 1st. Int. Conf. Inorganic Membranes, July 3-6, 1990, Montpellier, p. 75.

[8] M. S. Suwandi, and M. S. Lefebvre, Flexible organic-inorganic composite membranes, Proc. 1st. Int. Conf. Inorganic Membranes, July 3-6, 1990, Montpellier, p. 81.

[9] C. Eyraud, J. Lenoir, J. Charpin, P. Bergez, and J. M. Matinet, Elaboration & caracterisation de nouvelles membranes d'UF fonctionnalisees organo-minerales, Proc. 1st. Int. Conf. Inorganic Membranes, July 3-6, 1990, Montpellier, p. 87.

[10]W. Doyen, A. Bassier, P. Traest, E. Post and R. Leysen, Tubular organo-mineral membranes: and interesting alternative for ultrafiltration, Proc. 2nd. Int. Conf. Inorganic Membranes, July 1-4, 1991, Montpellier, p. 201.

[11]B. Chaufer, M. Rollin, A. Grangeon and J. Dulieu, Tetracycline removal or concentration with an inorganic ultrafiltration membrane modified by a quaternized polyvinylimidazole coating, Proc. 2nd. Int. Conf. Inorganic Membranes, July 1-4, 1991, Montpellier, p. 249.

[12]J. Randon, H. L. Lira and R. Paterson, Improved separations using surface modification of ceramic membranes, Proc. 3rd. Int. Conf. Inorganic Membranes, July 10-14, 1994, Worcester, p. 429.

[13]T. T. Tsotsis and Y. Zhu, The preparation of composite polymeric/inorganic membranes and their use in continuous pervaporation membrane reactors, Book of Abstracts of the 4th. Int. Conf. Inorganic Membranes, July 14-18, 1996, Gatlinburg, Section 4-A.

[14]J. Gillot, The developing use of inorganic membranes: A historical perspective, in R. Bhave (Ed.), Inorganic Membranes, Van Nostrand, New York, 1991, Chap. 1.

[15]H. P. Hsieh, Inorganic Membranes for Separation and Reaction, Elsevier, Netherlands, 1996, Chap. 2.

[16]R. Soria, Overview on industrial membranes, Catalysis Today, 25 (1995) 285-290.

[17]J. Sarrazin, A. Larbot, C. Kiefer and M. Persin, Preparation of ceramic nanofiltration membranes: Functionality in the filtration of ionic solutions and in the separation of organic mixtures, Proc. XIth Annual Summer School, 12-16 September, Glasgow, 1994.

[18]M. Mårtensson, K. E. Holmberg, C. Lofman and E. I. Eriksson, Some type of membranes for isotope separation by gaseous diffusion, Proc. 2nd. U. N. Int. Conf. Peaceful Uses At. Energy, 4 (1958) 395-404.

[19]F. Keller, M. S. Hunter and D. L. Robinson, Structural features of oxide coatings on aluminium, J. Electrochem. Soc., 100 (1953) 411-419.

[20]J. W. Diggle, T. C. Downie and C. W. Goulding, Anodic oxide films on aluminum, Chemical Reviews, 69, 3 (1969) 365-405.

[21]G. E. Thompson and G. C. Wood, Anodic films on aluminium, Treatise on Materials Science and Technology, Edited by Scully, J. C., Academic Press, vol. 23, (1983) 205-327.

[22]H.Takahashi, H. Nagayama, H. Akahori and A. Kitahara, Electron-microscopy of porous anodic films on aluminum by ultrathin section technique. Part 1. The structural change of the film during the current recovery, J. Electro. Microscopy, 22 (2) (1973) 149-57.

[23]G. E. Thompson, R. C. Furneaux, G. C. Wood, H. A. Richardson and J. S. Goode, Nucleation and growth of porous anodic films on aluminum, Nature, 272 (1978) 433-35.

[24]R. C. Furneaux, G. E. Thompson and B. C. Wood, The application of ultramicrotomy to the electronoptical examination of surface films on aluminum, Corrosion Science, 18 (1978) 853-81.

[25]T. Parlovic and A. Ignatiev, Optical and microstructural properties of anodically oxidized aluminum, Thin Solid Films, 138 (1986) 97-109.

[26]P. A. Kestin, R. R. Biederman, Y. H. Ma, The effects of anodizing parameters on alumina membrane synthesis, Key Eng. Mater., 61 (1991) 387-390.

[27]G. E. Thompson and G. C. Wood, Porous anodic film formation on aluminium, Nature, 290 (1981) 230.

[28]R. C. Furneaux, W. R. Rigby, and A. P. Davidson, Porous films and method of forming them, EP 0,178,831 Al (1986); US Pat. 4,687,551 (1987).

[29]K. Shimizu, K. Kobayashi, G. E. Thompson and G. C. Wood, Development of porous anodic films on aluminium, Phil. Mag. A, 66, 4(1992) 643-652.

[30]A. W. Smith, Process for producing an anodic aluminum oxide membrane. U.S. Patent 3,850,762 (1974)

[31]A. W. Smith, Porous anodic aluminum oxide membrane, J. Electrochem. Soc., 120(8)(1973) 1068-69.

[32]Anotec Separations. Anopore-A new inorganic membrane unique in the world of microfiltration. Brochure.

[33]K. N. Rai and E. Ruckenstein, Alumina substrates with cylindrical parallel pores, J. Catalysis, 40 (1975) 117-123.

[34]K. Itaya, S. Sugawara, K. Arai and S. Saito, Properties of porous anodic aluminum oxide films as membranes, J. Chem. Eng. Japan, 17 (1984) 514-520.

[35]R. C. Furneaux and M. C. Thornton, Porous "ceramic" membranes produced from anodizing aluminium, Adv. Ceram. Chem. Process Eng., 43 (1988) 93-101.

[36]R. C. Furneaux, W. R. Rigby, and A. P. Davidson, The formation of controlled porosity membranes from anodically oxidized aluminum, Nature, 337 (1989) 147.

[37]R. C. Furneaux, R. W. Philpott and D. M. Jenkins, Controlled pore-size membranes produced by anodizing aluminium, Proceedings of the First International Conference on Inorganic Membranes, Montpellier, 1989, 47-53.

[38]R. Paterson, P. P. Mardilovich, A. N. Govyadinov, N. I. Mazurenko, Permeable anodic alumina film, UK Patent WO 9534371, Dec, 1995.

[39]P. P. Mardilovich, A. N. Govyadinov, N. I. Mukhurov, A. M. Rzhevskii, and R. Paterson, New and modified anodic alumina membranes. Part. I. Thermotreatment of anodic alumina membranes, J. Membr. Sci., 98 (1995) 131.

[40]P. P. Mardilovich, A. N. Govyadinov, N. I. Mazurenko, and R. Paterson, New and modified anodic alumina membranes. Part. II. Comparison of solubility of amorphous (normal) and polycrystalline anodic alumina membranes, J. Membr. Sci., 98 (1995) 143.

[41]P. P. Mardilovich, A. N. Govyadinov, V. Kozharinov, and R. Paterson, Polycrystalline anodic alumina - New ceramic membranes and matrices, Ceramics: Charting the Future, P. Vincenzini Editor, Techna Srl, (1995), 2763.

[42]P. P. Mardilovich, A. N. Govyadinov, J. Randon, S. McFadzean and R. Paterson, New high temperature chemically resistant anodic alumina membranes: preparation, modification, properties, Proc. 3th Intern. Conf. on Inorg. Membr., Worchester, Massachusetts, USA, 1994, 457.

[43]N. Itoh, K. Kato, T. Tsuji and M. Hongo, Preparation of a tubular anodic aluminum oxide membrane, J. Membr. Sci., 117 (1996) 189-196.

[44]A. J. Burggraaf and K. Keizer, Synthesis of inorganic membranes, in R. Bhave (Ed.), Inorganic Membranes, Van Nostrand, New York, 1991, Chap. 2.

[45]R. Paterson, J. Randon and H. L. Lira, Functionalisation of ceramic membrane surfaces for improved separations, Proc. of the XIth Annual Summer School, on functional membranes, Glasgow, 12-16 September, 1994.

[46]J. Randon, P. Blanc and R. Paterson, Modification of ceramic membrane surfaces using phosphoric acid and alkyl phosphonic acids and its effects on ultrafiltration of BSA protein, J. Membr. Sci., 98 (1995) 119-129.
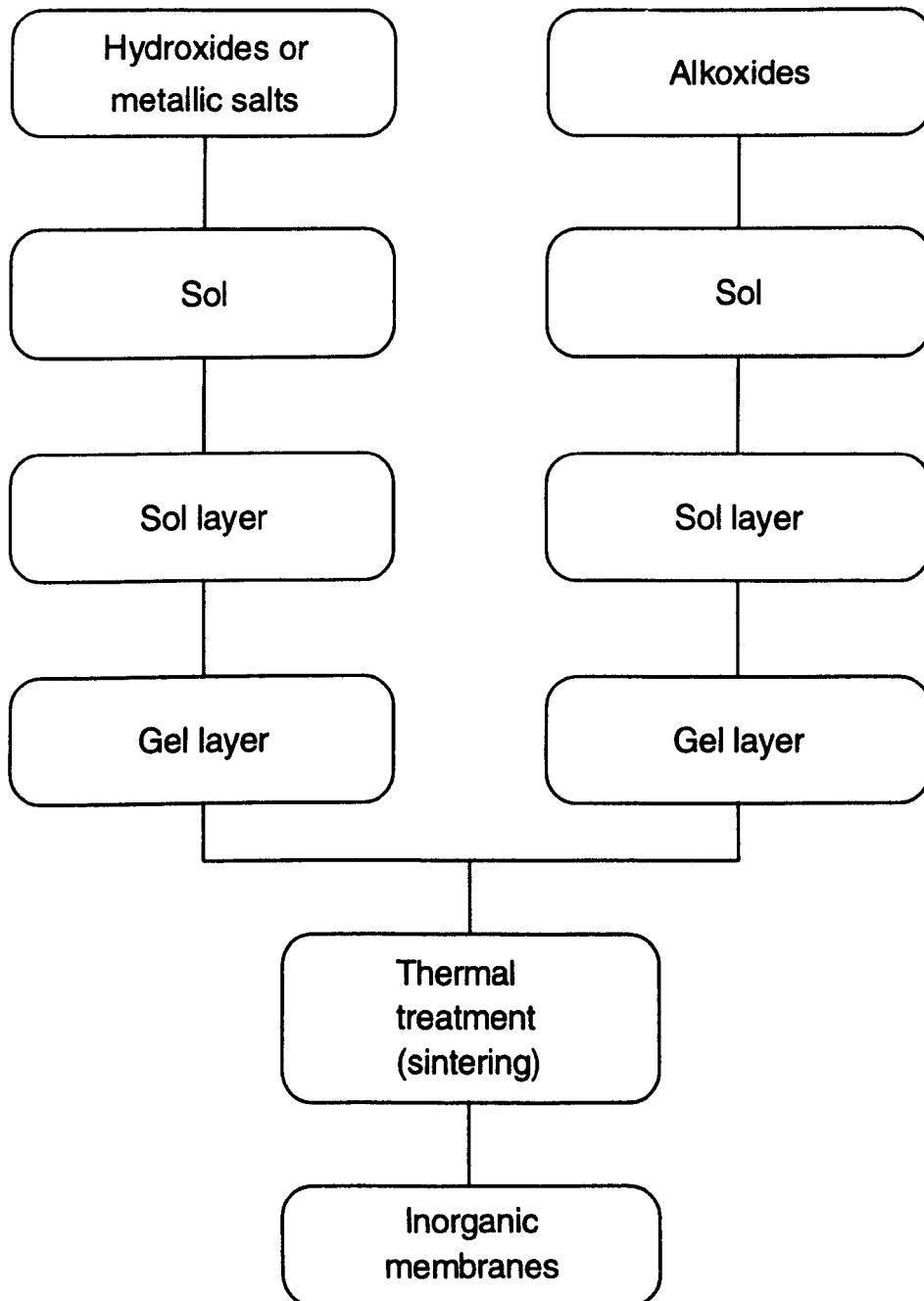
Fig. 1.1- Different route for the preparation of oxide ceramic membranes

Chapter 2

Preparation of Anodic Alumina Membrane

2.1 Introduction

Synthetic membranes are used in a number of diverse applications, such filtration, bioreactors, tissue culture, analytical devices including sensors, and as supports for active materials. Narrow pore size distribution, high pore density and thinness are often important attributes. It has long been observed that when aluminium oxidizes on its surface [1], the resulting structure of the oxide is rather unique in having cylindrical pores normal to the film surface. The anodising voltage controls the pore size and pore density, whereas the thickness is determined by the amount of charge transferred. The ability to design porous films of pre-determined morphology makes the anodic alumina films potentially well-suited for use as porous membranes. Researchers have turned this unique phenomenon into synthesis of controlled membrane morphology [2-9]. A major problem with this technique, however, is that the porous anodic alumina film layer adheres strongly to the aluminium anode metal with the pore base closed by an oxide barrier layer which is difficult to remove. In order to create 'through' pores it is necessary to detach the film from the aluminium and remove the barrier layer [6]. Normally anodic alumina films are release from the aluminium substrate by chemical attack, either by dissolution of the aluminium foil or by dissolution of the barrier film of alumina [2, 3, 5, 6, 8, 9]. Both methods, and particularly the second, can lead to enlargement of pores due to partial dissolution of pore walls.

Furneaux *et al* [5, 6, 9] describe a method to separate anodic alumina film and perforate the barrier layer by progressively reducing the anodising voltage to a very low value to reduce the barrier layer thickness and subsequently by chemical attack of

the aluminium to detach the anodic alumina film. The membrane produced by this method has an asymmetric morphology with larger pores interconnected with smaller pores at the interface originally adjacent to the aluminium. Membranes produced by these methods are limited to pore size (>15 nm) due to chemical dissolution.

Paterson *et al* [10] and Mardilovich *et al* [11, 12] developed a method in which a very large voltage pulse is applied for a very short time to the aluminium anode at the end of the anodisation which removes the barrier layer and separates the membrane instantly. By this method the barrier film of anodic alumina is completely removed and all pores are open. The greater advantage of this new method is that it is electrical and so fully quantifiable and does not involve dissolving chemicals which need to be applied carefully and washed off quickly to prevent damage or even total dissolution of the membrane.

The research presented in this chapter is an extension of the technology for the preparation of anodic alumina membranes, using the new technique to disclose the film formed from the aluminium substrate and used to prepare membranes with small pore size (<13 nm) impossible by early technologies. The pore diameter of all these anodic alumina membranes is effectively determined by the formation voltage of the anodisation process.

2.2 Experimental

2.2.1 Anodisation System

An automated anodisation system was developed in the course of this research. This system enabled the production of anodic alumina films to be fully controlled. It was designed to apply precise anodic voltages for precise times and to record and monitor current/voltage curves as a function of time during the anodisation. With this system it is possible to obtain a extremely reproducible membrane. Fig. 2.1 shows schematically the connection between the computer and the power supply on one hand and the anodisation cell and the circulator bath on the other. The system was controlled by a Buchler programmable power supply (1000 VDC and 400 mA) from CP Instruments Ltd. and the Grant LTD-20 refrigerated circulator bath was obtained from Orme Scientific Ltd.

The anodisation cell (Fig. 2.2) consist of a metallic container coated by a chemically resistant insulating varnish to isolate the electrolyte solution and prevent electrical leak. The volume of electrolyte solution in the cell was 2 litres, approximately. A thermostated bath with refrigerated distilled water circulated through the walls was used to control the temperature during the anodisation (usually maintained at 10 °C). A circulation pump in "Teflon" was designed and constructed to stir the electrolyte solution. The temperature difference between the distilled water in the refrigerated circulator bath and the electrolyte solution was 0.1 °C. Two electrode holders built in "Teflon" were used to support a platinum mesh cathode (10 x 10 cm^2 of area) and an aluminium anode. Typically an electrode was (5 x 5 cm^2 of total area and 8.04 cm^2 of

exposed area). The distance between the platinum mesh cathode and the aluminium

sample was 2.5 cm.

2.2.2 Preparation of Anodic Alumina Film

Anodic alumina membranes were prepared by anodisation of aluminium foil, purity 99.999% and 70 μm thick supplied by Johnson Matthey, Materials Technology, UK. The aluminium foil was first degreased in a Soxhlet apparatus using boiling 1,1,1-tri-chloro-ethane for 30 min., then cleaned ultrasonically three times with fresh isopropanol and finally washed in distilled water. To prepare membranes with precisely defined shapes some part of the aluminium was protected with a photoresist (OFPR-800 positive resist, viscosity 20.0 ±15 cps, acquired from Dynachem Corporation, UK). To assist the adhesion of the photoresist on the aluminium surface a very thin layer of anodic alumina was created using an applied voltage of 40 V for 2 min. The electrolyte was oxalic acid 3% w/w and the process performed at room temperature (20 °C). The coated electrode layer was then washed with distilled water and dried at 140 °C for 30 minutes. Some drops of photoresist was put in the center of the aluminium surface, which was then centrifuged at 1500 rpm for 10 seconds and dried at 70 °C for 20 minutes. A uniform coating of photoresist was obtained by this method. In this process it was necessary to protect the coated surface from light. Using a mask with desired shape of the membrane and the opaque remainder was exposed in UV for 5 minutes, then developed in a solution of tetramethyl ammonium hydroxide (TBAH 1.2%, from Dynachem Corporation, UK) for 2 minutes. It was then washed in distilled water and baked at 80, 100, 120 and 140 °C for 20 minutes in each temperature. After, backside of the aluminium was protected by varnish. At this stage only the area selected for membrane production is exposed. To re-establish electrical

contact and initiate the production of a uniform anodic film layer, the initial thin layer of oxide, created only to stick the photoresist, was removed by dissolution using a solution (20 g CrO_3, 35 ml H_3PO_4 88% w/w, make up to 1.0 litre with distilled water) at 90 °C for 2 minutes. Finally, the aluminium was washed in distilled water and mounted on its Teflon holder to be anodised. The anodisation process was performed by using oxalic solution 3% w/w, at 10 °C under constant voltage conditions (the larger the voltage the larger in pore diameter). Oxalic acid was chosen as electrolyte because it permits anodisation at low voltages with enough current flow and also according to [13] the pore and cell diameters are smaller for the films formed in oxalic acid than for those observed for films formed in phosphoric acid, for instance. Basically, two different programmes were used in this study to produce different structures of the anodic alumina film; 1) at constant anodising voltage, to obtain a regular anodic alumina film; 2) at constant anodising voltage, followed by progressively reducing the anodising voltage to attain final constant but low final anodising voltage. This latter produced asymmetric anodic alumina film with two uniform pore layers one large the other small with a very thin branched pore structure intermediate. Conditions of preparations are summarised on Table 2.1. Afterwards, remaining aluminium was removed by electrochemistry treatment (see next Section).

2.2.3 Electrochemistry Treatment to Release the Anodic Film from the Aluminium

Normally the film produced by the anodisation on the aluminium sample is removed either by the dissolution of the remain metal, barrier layer [5] or by reversing the polarity of the electrodes at the final stage of anodisation [14]. In this research the aluminium substrate was removed from the alumina layer by an electrochemical treatment. For this propose it was constructed a special power supply capable to produce a voltage pulse up to 150 V and current up to 15 A. In this technique the anodic film produced with aluminium substrate was deep in a mixture of perchloric acid ($HClO_4$, 70 ml; 72% w/w) and acetic anhydride (($CH_3CO)_2O$, 130 ml 98%, d=1.08 g/ml) and voltage of 15 V greater then the final voltage of anodisation was applied during 1-3 seconds, approximately, stirring was not necessary. In this case anodic alumina film was separated from the aluminium panel immediately, and the barrier layer was removed from the film according to the sequence in Fig. 2.3 (a, b, c). The film was washed in distilled water and allowed to dry at room temperature. Fig. 2.4 show a flow-chart of the preparation process for anodic alumina films.

2.3 Porous Anodic Film Formation on Aluminium

The anodic alumina membrane preparation described in this research successfully obtained small and regular pores diameter (<13 nm). Films were formed at various constant voltages in the range 5 to 72 V, using oxalate ($H_2C_2O_4$ 3% w/w) as an electrolyte and controlled temperature (10 °C).

The code used to identify the method of preparation of various samples discussed throughout this thesis was as follows:

72/1 - represents anodic alumina film prepared at constant voltage, 72 V for 1 hour.

60/3 - refer to sample prepared at constant voltage, 60 V for 3 hours.

40/5 - refer to sample prepared at constant voltage, 40 V for 5 hours.

72/1/10/16 - refer to sample prepared at constant voltage, 72 V for 1 hour, followed by a progressively reduction from 72 to 10 V in decrements of 2 V/min and then maintained in 10 V for 16 hours. Other description follow the same code, for example, 72/1/5/20 and 72/1/5/40 - refer to samples prepared at constant voltage, 72 V for 1 hour, followed by a progressively reduction from 72 to 5 V in decrements of 2 V/min and then maintained in 5 V for 20 and 40 hours, respectively.

Figs. 2.5 to 2.9 show the voltage and current density versus time recorded direct from the anodisation system during the preparation of the samples 72/1, 60/3, 40/5, 72/1/10/16 and 72/1/5/20, respectively. The exposed area on the aluminium sheet, during the anodisation was normally formed by four circular sections with 1.6 cm in diameter (total area 8.04 cm^2). For sample 72/1 in the Fig. 2.5, as the voltage was limited to constant 72 V, current density rises to 45 mA/cm^2 and declines rapidly to a

low value, 13 mA/cm^2 , due to formation of the anodic film in the beginning. Subsequently the current density increase to 24 mA/cm^2, due to formation of porous on anodic film. After this initial stage the current density declines to a relatively constant steady-stage for the duration of the run. According to O'Sullivan and Wood [15] at this steady-stage pore and cell structure are created with rather constant dimensions. The cell diameter[1] and pore diameter[1] are all directly proportional to the formation voltage. For samples 60/3 and 40/5 formed at 60 and 40 V, Figs. 2.6 and 2.7, respectively, the same effect appear on the begin of anodisation, where the current density rises a maximum value close to 45 mA/cm^2, for both samples, followed by a decline to a steady-state of relatively constant current density, approximately 7 and 2.5 mA/cm^2, respectively, where the development of the porous anodic film was observed. For samples 72/1/10/16 and 72/1/5/20, Figs. 2.8 and 2.9, respectively, first a support layer was created at constant anodisation voltage, 72V, for 1 hour, with the same behaviour as discussed before. Subsequently, the anodisation voltage was progressively reduced from 72 V to 10 and 5 V, respectively, in decrements of 2V/min. During these voltage reduction process, after each decrement, the current density fell to a minimum value and rose after towards the steady state associated with the new barrier-layer thickness. The process took about 30-35 minutes when the final voltage was achieved. At the final voltage, the current densities maintain constant at values of 0.87 and 0.37 mA/cm^2, and the rates of formation film were found to be

---

[1] Cell diameter and pore diameter are defined in Fig. 4.1, Chapter 4, and refer to the size of the cell, D, and internal diameter of the pore, d, created in the anodic film.

0.56 µm per 10V/h and 0.37 µm per 5V/h, for the samples 72/110/16 and 72/1/5/20, respectively.

2.4 Separation of Anodic Alumina Film from Aluminium Substrate

In the new technique developed by Paterson *et al* [10] to remove the aluminium substrate and the barrier layer to produce anodic alumina membrane a voltage greater then the final anodisation voltage was applied, using a mixture of perchloric acid ($HClO_4$) and acetic anhydride $((CH_3CO)_2O)$. In this case a high current density was reached (greater than 1000 mA/cm^2 for the sample 72/1 when a pulse of 85 V was applied). Evidence shown in the micrographs, in Chapter 3, suggest that the high current density produced by the applied voltage pulse during the separation of the aluminium substrate cause a local heating between the barrier layer and aluminium substrate. A combination of dissolving process by the effect of electrolyte and local heating induce to a cracking and removing of the caps. The schematic representation of the mechanism of separation is shown in the Fig. 3.3. Some parts of the caps stay on the surface of the aluminium substrate after separation of the anodic film formed, this can be seen in Plate III, Chapter 3. It was also realised that the barrier layer and the aluminium substrate was removed more easily from the anodised film, by the electrochemical method, for anodisation in small voltage when compared with high voltage. This effect can be explained by the fact that the barrier layer become very thin at small anodising voltage. In this situation, when the anodising voltage decreases, the current decreases exponentially, as shown in the Section before, and then the rate of film growth decrease from the film/aluminium interface and there is a continue

chemical dissolution from inside the pore. So a new barrier layer thickness was formed. It is important in this stage to decrease the voltage slowly to recover the current to stabilise this new barrier layer. Furneaux *et al* [16] and Takahashi *et al* [17] observed that for a large voltage decrement a non-uniform pores propagation is created and subtle local variation in barrier layers at the base of different pores allow preferential dissolution due to concentration of current at certain sites. The same effect was observed in this study. However it was observed (see SEM characterisation in Chapter 3) that even with the irregularities created during the voltage decrement all caps were removed and this effect not affect the pore opening on the film. Also the reduction of anodisation voltage produced an asymmetric structure with large pores interconnected with smaller pores which increased in pore density and maintains the porosity constant (this was shown in details in Chapter 4, Section 4.5). Moreover after the lower final anodisation voltage was reached it was kept for a long time in this voltage and a new continuous layer with small pores was created.

2.5 References

[1] Hoar, T. P. and N. F. Mott, Mechanism for the formation of porous anodic oxide films on aluminium, J. Phys. Chem. Solids, 9 (1959) 97-99.

[2] Smith, A. W., Process for producing an anodic aluminum oxide membrane. U.S. Patent 3,850,762 (1974)

[3] Smith, A. W., Porous anodic aluminum oxide membrane, J. Electrochem. Soc., 120(8)(1973) 1068-69.

[4] G. E. Thompson, R. C. Furneaux, G. C. Wood, H. A. Richardson and J. S. Goode, Nucleation and growth of porous anodic films on aluminum, Nature, 272 (1978) 433-35.

[5] R. C. Furneaux, W. R. Rigby, and A. P. Davidson, Porous films and method of forming them, EP 0,178,831 Al (1986); US Pat. 4,687,551 (1987).

[6] R. C. Furneaux, W. R. Rigby, and A. P. Davidson, The formation of controlled porosity membranes from anodically oxidized aluminum, Nature, 337 (1989) 147.

[7] G. E. Thompson and G. C. Wood, Porous anodic film formation on aluminium, Nature, 290 (1981) 230.

[8] Anotec Separations. Anopore-A new inorganic membrane unique in the world of microfiltration. Brochure, Whatman International Ltd., Maidstone, UK.

[9] R. C. Furneaux, R. W. Philpott and D. M. Jenkins, Controlled pore-size membranes produced by anodizing aluminium, Proceedings of the First International Conference on Inorganic Membranes, Montpellier, 1989, 47-53.

[10] R. Paterson, P. P. Mardilovich, A. N. Govyadinov, N. I. Mazurenko, Permeable anodic alumina film, UK Patent WO 9534371, Dec, 1995.

[11] P. P. Mardilovich, A. N. Govyadinov, N. I. Mukhurov, A. M. Rzhevskii, and R. Paterson, New and modified anodic alumina membranes. Part. I. Thermotreatment of anodic alumina membranes, J. Membr. Sci., 98 (1995) 131.

[12] P. P. Mardilovich, A. N. Govyadinov, N. I. Mazurenko, and R. Paterson, New and modified anodic alumina membranes. Part. II. Comparison of solubility of amorphous (normal) and polycrystalline anodic alumina membranes, J. Membr. Sci., 98 (1995) 143.

[13] P. A. Kestin, R. R. Biederman, Y. H. Ma, The effects of anodizing parameters on alumina membrane synthesis, Key Eng. Mater., 61 (1991) 387-390.

[14] K. K. Wada, K. N. Baba, S. Ono, T. Yoshino, Porous aluminum oxide film and method of forming of the same, US Pat. 5,061,544 (1991).

[15] J. P. O'Sullivan and G. C.Wood, The morphology and mechanism of formation of porous anodic films on aluminum. Proc. R. Soc. London, Ser. A , 317 (1970) 511-43.

[16] R. C. Furneaux, G. E. Thompson and B. C. Wood, The application of ultramicrotomy to the electronoptical examination of surface films on aluminum, Corros. Sci., 18 (1978) 853-81.

[17] H.Takahashi, H. Nagayama, H. Akahori and A. Kitahara, Electron-microscopy of porous anodic films on aluminum by ultrathin section technique. Part 1. The

structural change of the film during the current recovery, J. Electron Micros., 22

(2) (1973) 149-57.

Table 2.1 - Conditions of preparation of homogeneous anodic alumina membranes

Sample Ref.	Oxalic (%)	t (h)	T (°C)	U_{1st} (Volts)
72/1	3	1	10	72
60/3	3	3	10	60
40/5	3	5	10	40

U_{1st} - Initial voltage of anodisation
T - Temperature of electrolyte solution
t - Time of anodisation

Table 2.2 - Conditions of preparation of asymmetric anodic alumina membranes

Sample Ref.	Oxalic (%)	T (°C)	U_{1st} (Volts)	t_{1st} (h)	U_{2nd} (Volts)	t_{2nd} (h)
72/1/10/16	3	10	72	1	10	16
72/1/5/20	3	10	72	1	5	20
72/1/5/40	3	10	72	1	5	40

U_{1st} - Initial voltage of anodisation
U_{2nd} - Final voltage of anodisation
T - Temperature of electrolyte solution
t_{1st} - Time of anodisation for initial voltage
t_{2nd} - Time of anodisation for final voltage
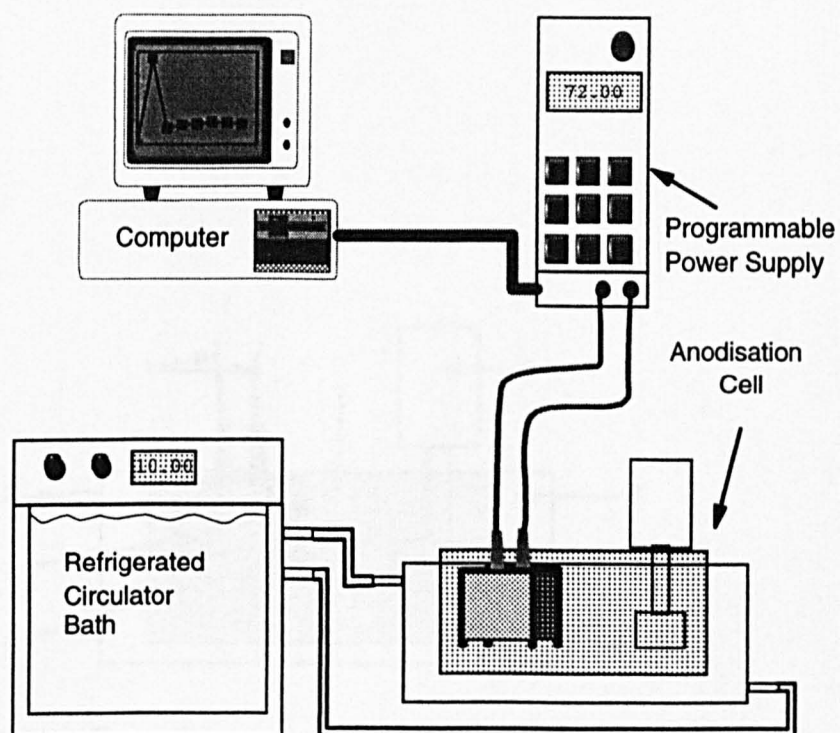
Fig. 2.1- Schematic representation of the anodisation system

1 Electrode Connections
2 Thermostat Water Outlet (10 $^\circ$C)
3 Platinium Mesh Cathode
4 Aluminium Anode

5 Stirring Motor
6 Electrolysis Bath
7 Circulating Pump in Teflon
8 Thermostat Water Inlet (10°C)
9 Electrolyte Solution
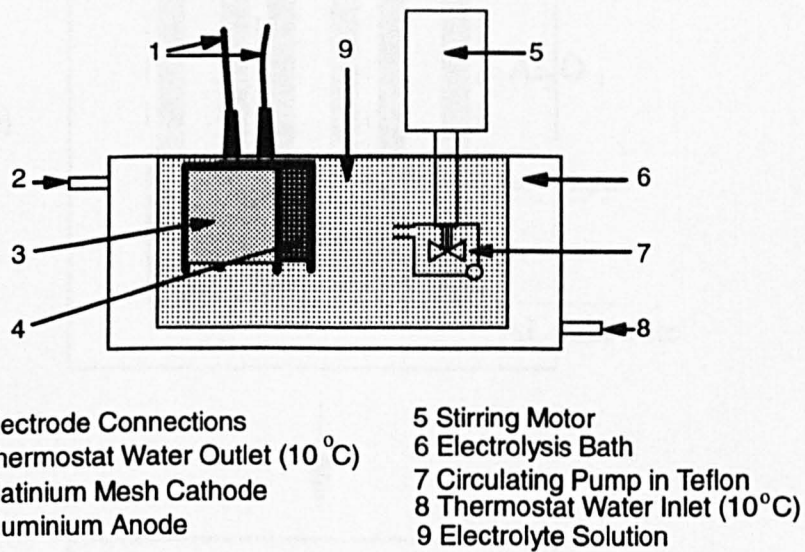
Fig 2.2 - Schematic Representation of the Anodisation Cell

(a) Anodic film with aluminium substrate and barrier layer

(b) pore Al$_2$O$_3$ barrier layer Al substrate

(c) Anodic alumina membrane after removing aluminium and the barrier layer
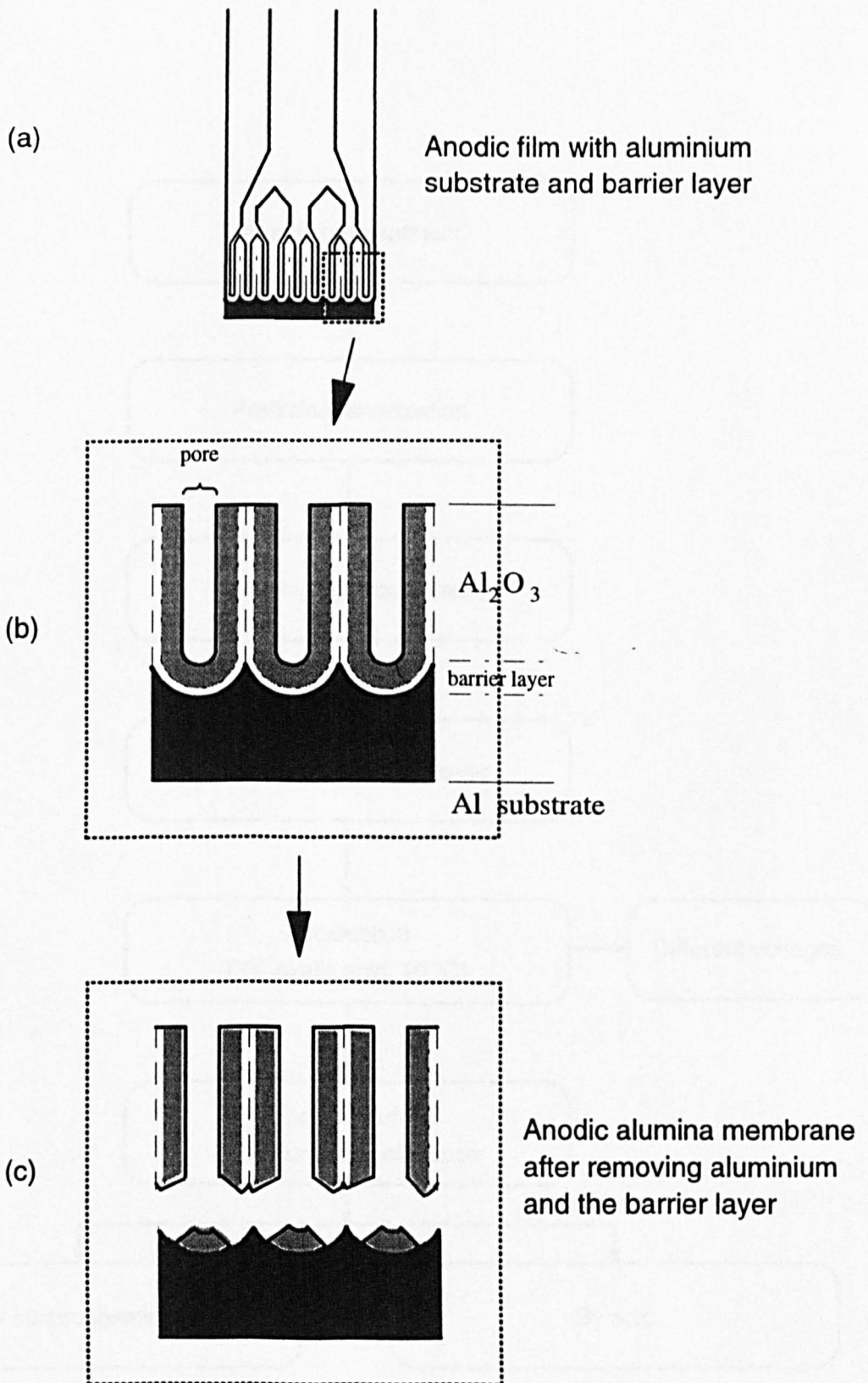
Fig.2.3 - Representation of anodic alumina film with (a) assymetric pore structure created with reduction of anodisation voltage . A cross-section view (b) shows anodic film with a impermeable barrier layer and aluminium substrate on the botton. In (c) the barrier layer and the aluminium was removed and a porous anodic alumina membrane is produced.

2.18
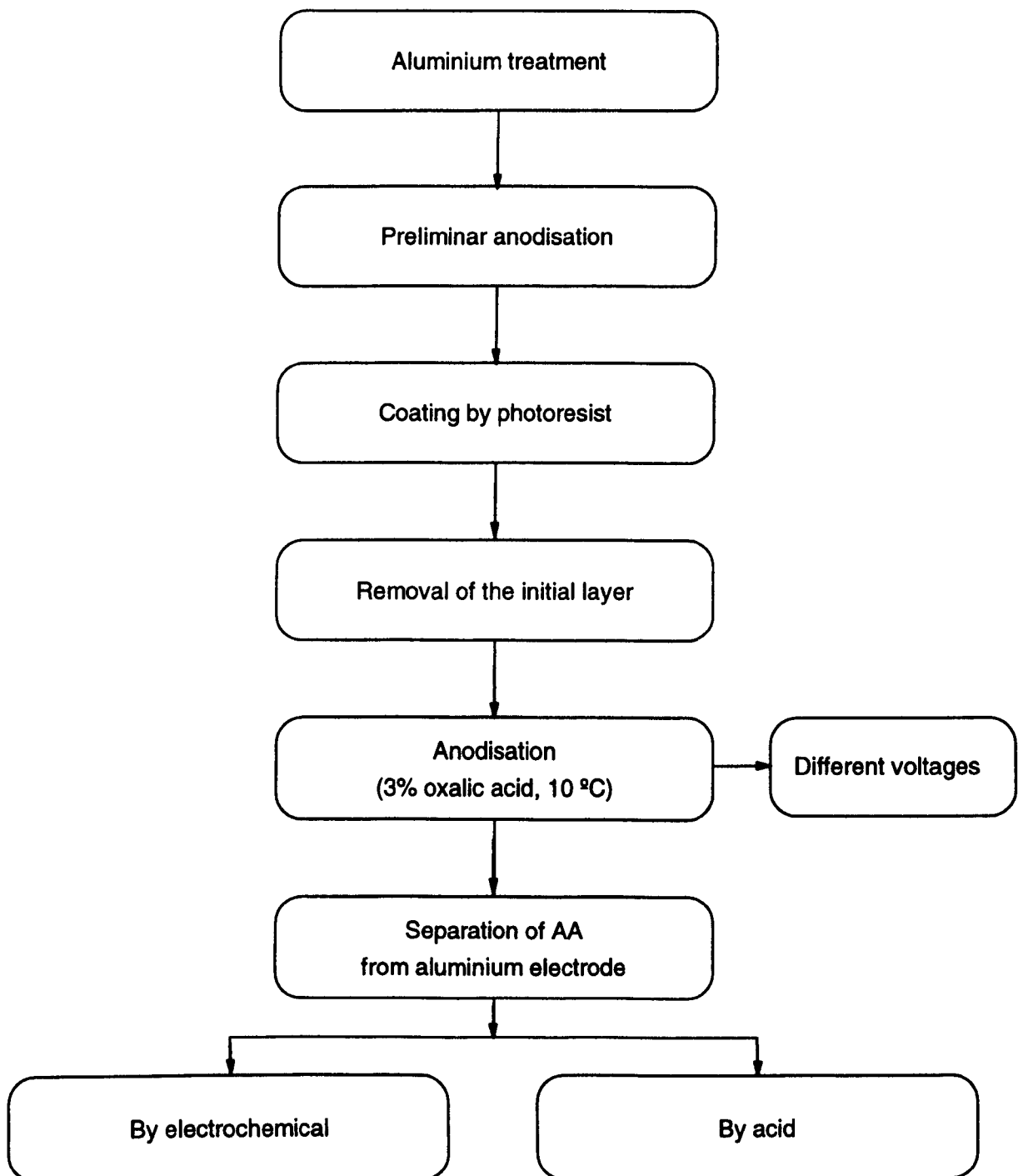
Fig. 2.4 - Flow-chart of preparation of anodic alumina films

Fig. 2.5 - Current density-time and voltage-time behaviour observed for sample 72/1 with constant anodisation voltage (72 V for 1 hour, exposed area 8.04 cm2).

Fig. 2.6 - Current density-time and voltage-time behaviour observed for sample 60/3 with constant anodisation voltage (60 V for 3 hour, exposed area 8.04 cm2).

Fig. 2.7 - Current density-time and voltage-time behaviour observed for sample 40/5 with constant anodisation voltage (40 V for 5 hour, exposed area 8.04 cm2).

Fig. 2.8 - Current density-time and voltage-time behaviour observed for sample
72/1/10/16 with constant anodisation voltage (72 V for 1 hour and reduced
to 10 V for 16 hours,exposed area 8.04 cm2).
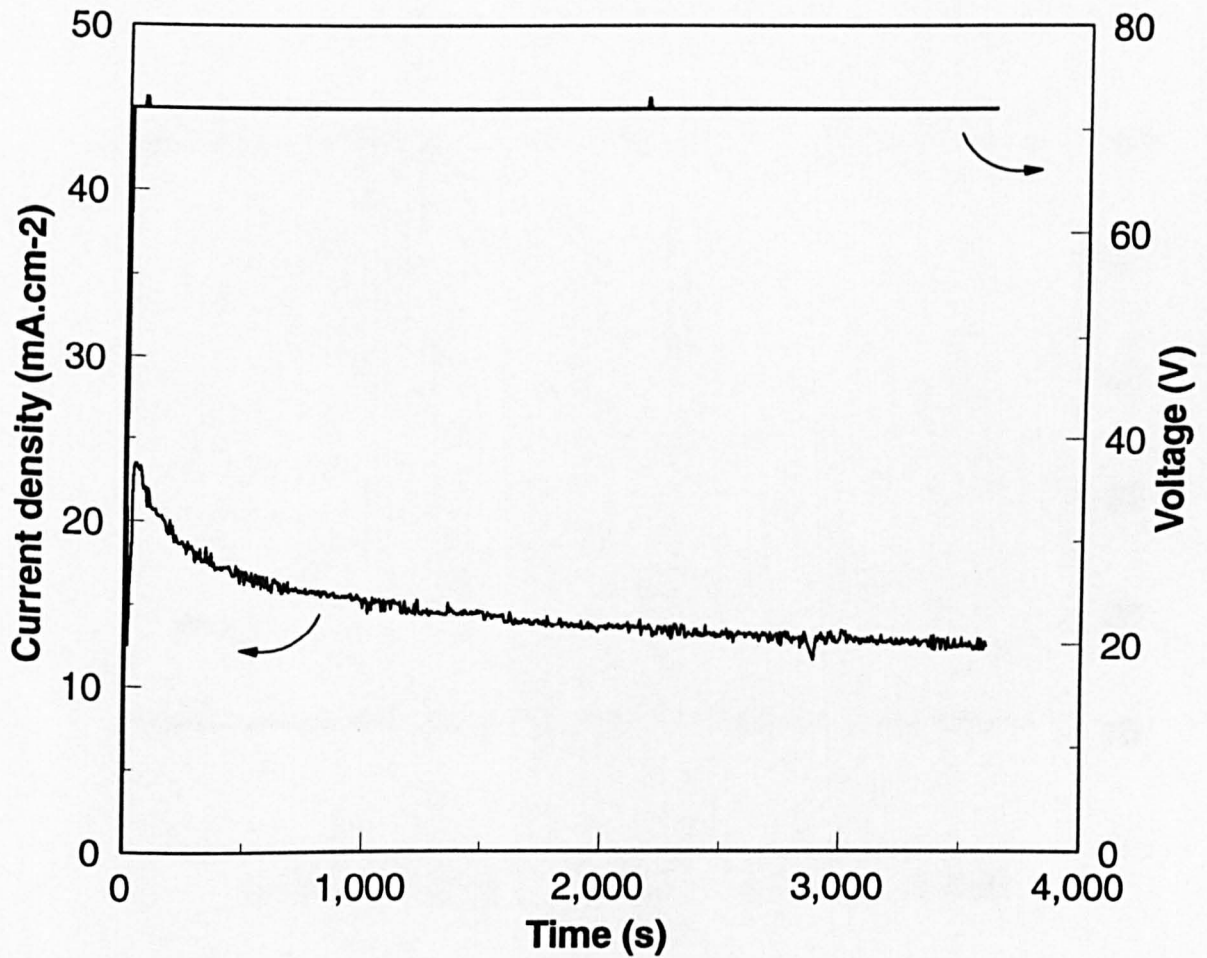
Fig. 2.9- Current density-time and voltage-time behaviour observed for sample
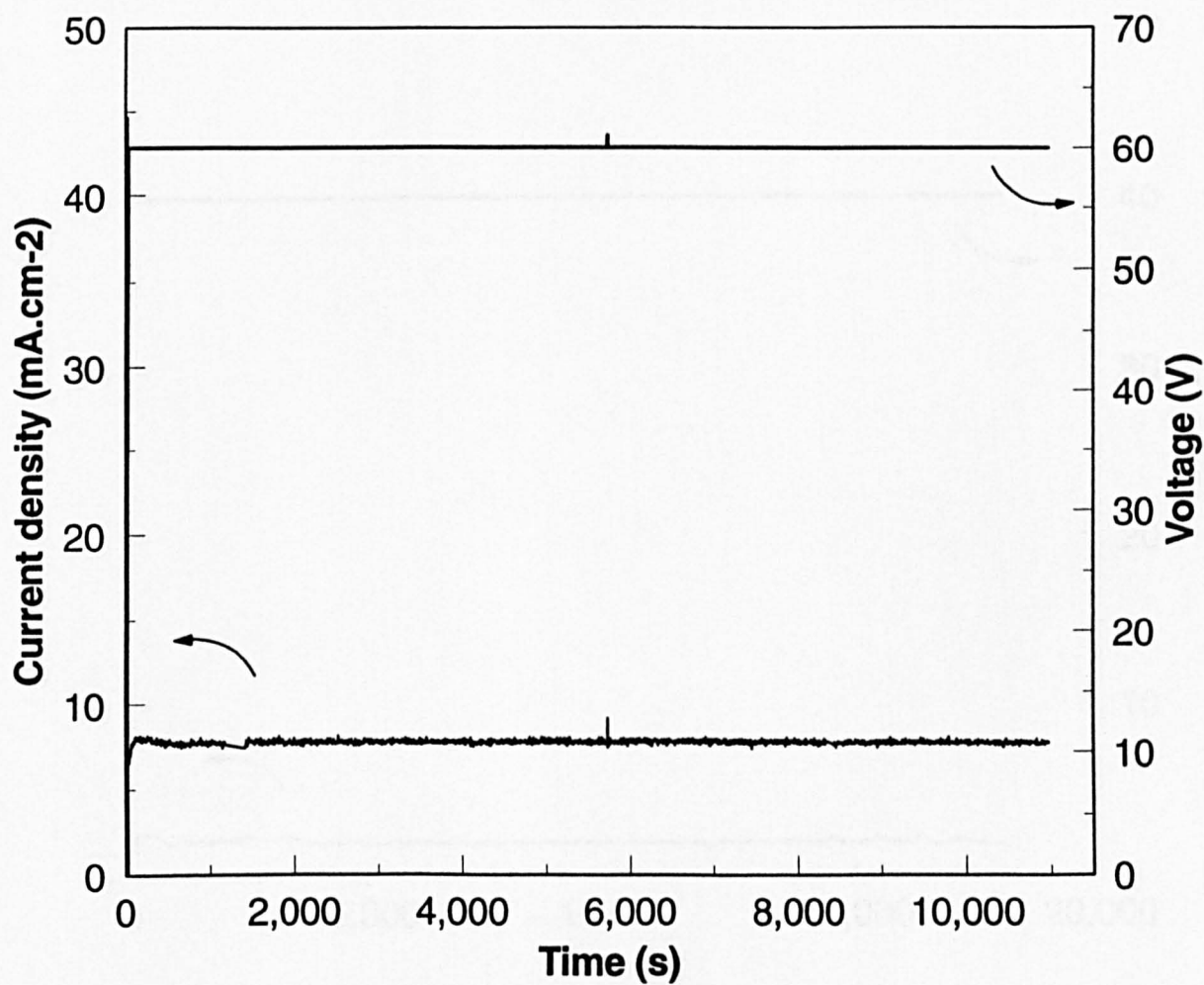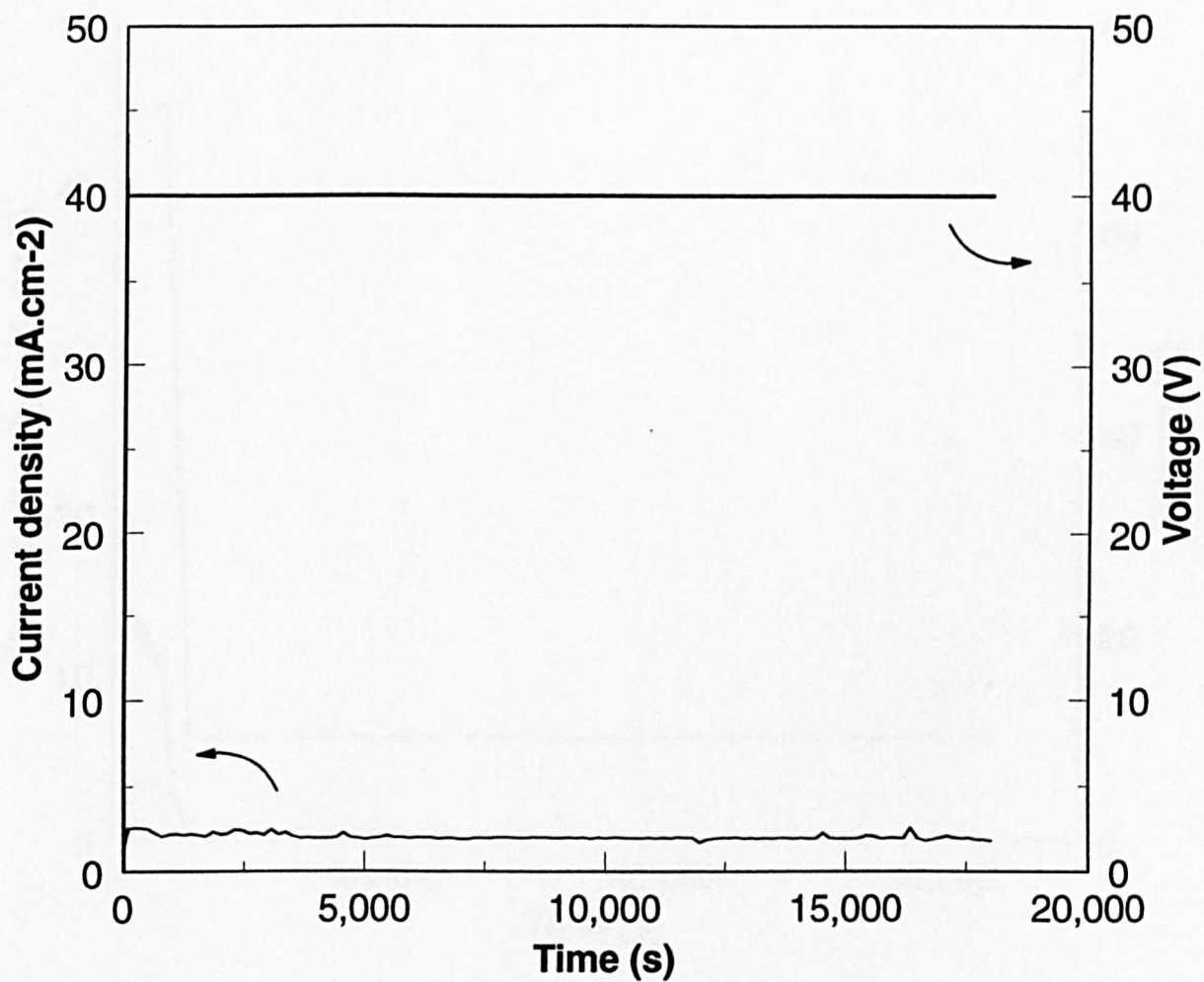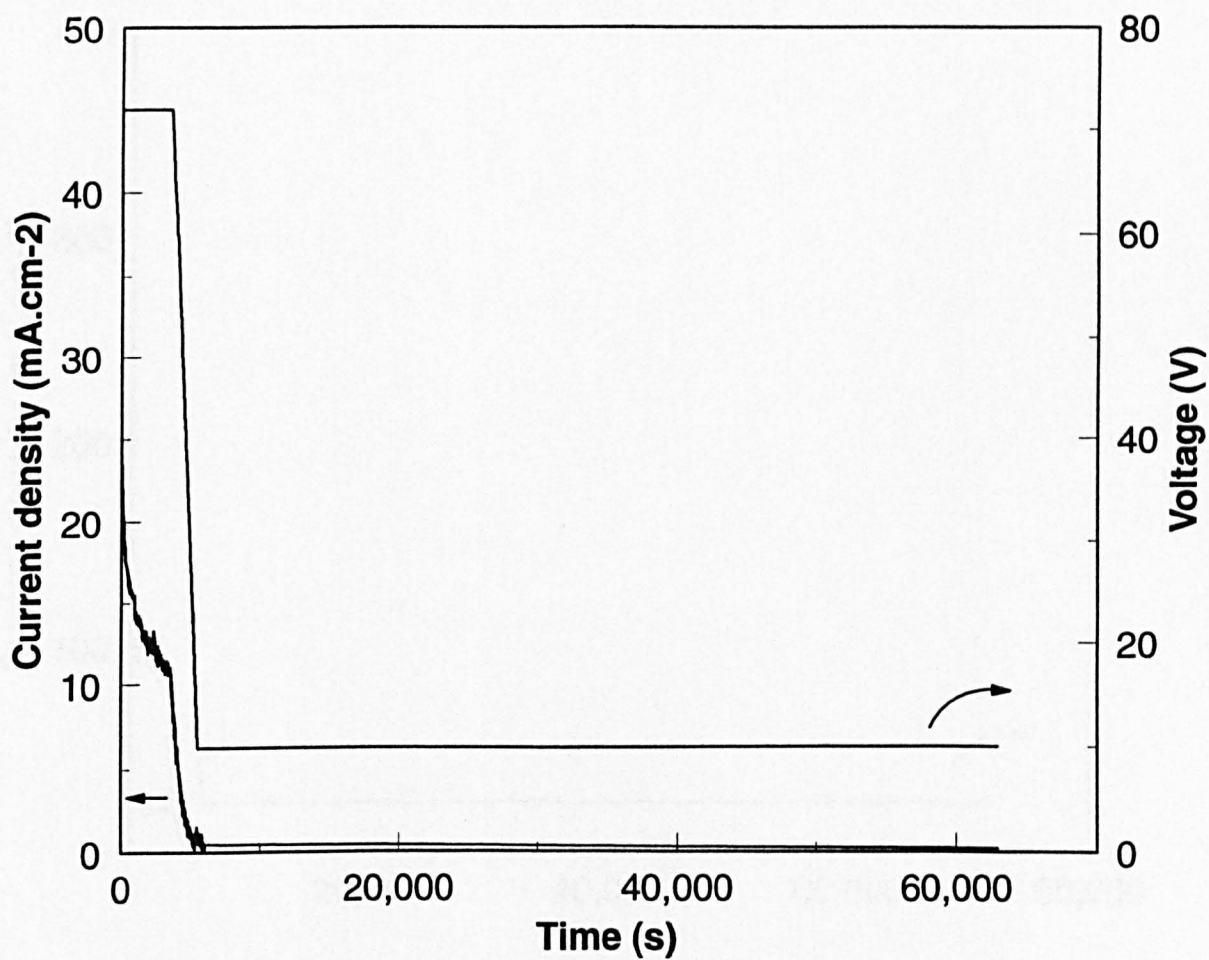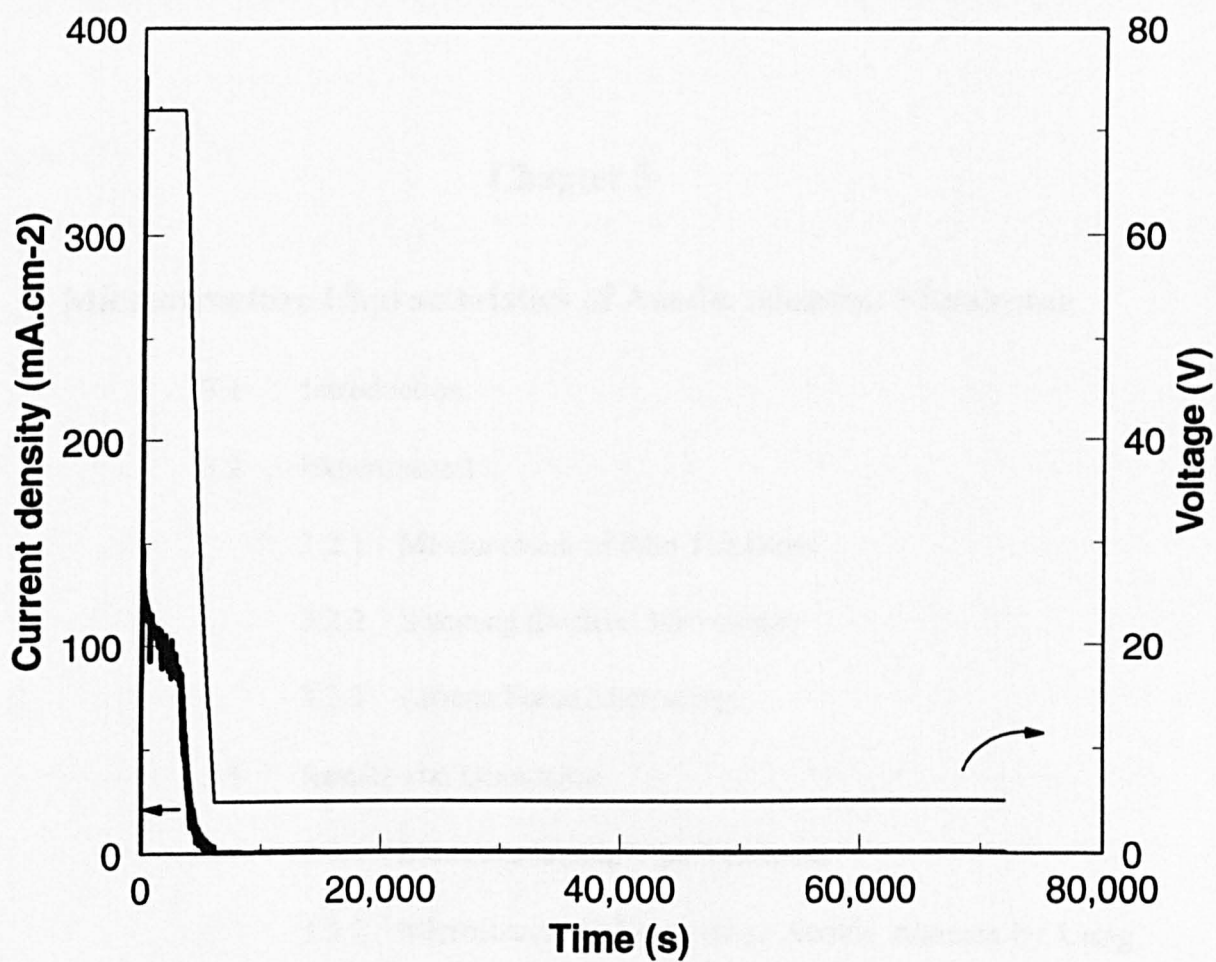72/1/5/20 with constant anodisation voltage (72 V for 1 hour and reduced
to 5 V for 20 hours,exposed area 8.04 cm2).

Chapter 3

Microstructure Characteristics of Anodic Alumina Membrane

3.1 Introduction

The preparation methods and the conditions reported in Chapter 2 describe the general mechanism of formation of the anodic alumina membranes. The structural features will be examined in this chapter using scanning electron microscopy and atomic force microscopy.

The most widely used method of characterising the morphology of membranes, particularly ceramic membranes, is scanning electron microscopy. A scanning electron microscope (SEM) is based on the principle that an image is formed when the electrons it emits interact with the atoms of the specimen. SEMs can provide higher-resolution images than reflected light microscopes. Because of this advantage, as a result of recent advanced technology, SEMs have become the workhorse of many surface and microstructural characterisation tools in various material applications, including membrane separation [1, 2]. Its disadvantage (which proved important in this study) is that the sample examined by this method require to have electrically conducting surfaces. This involves deposit by either carbon or gold on the surface as a pre-treatment.

Atomic force microscopy is an emerging surface characterisation tool in a wide variety of materials science fields. The method is relatively easy to use and allows the surface study of non-conducting materials down to the nanometer scale, as a result no sample preparation is required for oxide materials. Although it is a relatively novel technique, its application to synthetic membranes is growing rapidly [3-6]. The basic principle involved is to utilise a integrated tip in the end of a spring cantilever with constant

spring weaker than the equivalent atomic forces between sample and tip. This way the sharp tip of the cantilever, which is microfabricated from silicon, silicon oxide or silicon nitride using photolithography, mechanically scans over a sample surface to image its topography. Typical lateral dimension of the cantilever are on the order of 100 μm and the thickness on the order of 1 μm. Cantilever deflections on the order of 0.01 nm can be measured in modern atomic force microscopes.

So, in this chapter the anodic alumina membranes, prepared in Chapter 2, will be examined by scanning electron microscopy (SEM) and atomic force microscopy (AFM) and the results of pore diameter obtained from direct observation in these two methods will be compared.

3.2 Experimental

3.2.1 Measurement of Film Thickness

The measurement of the film thickness was carried out using a Comparator Stand Mitutoyo model IDC-112B-5. Thickness was determined to an accuracy of ±0.001mm. At least ten readings were taken from each film to be tested, and from them the average was determined.

3.2.2 Scanning Electron Microscopy

The pore structure of the membrane was observed with scanning electron microscope (SEM) Leica Cambridge, model Stereoscan 360, with energy dispersive (x-ray) spectroscopy (EDS), and ultrahigh resolution scanning electron microscope Hitachi, model S-900. The anodic alumina films were first coated with thin layer of carbon or gold by sputtering. It also made analysis of the aluminium substrate after the film removed.

3.2.3 Atomic Force Microscopy

The surface pore structure of anodic alumina was investigate by atomic force microscopy (AFM) model ARIS-3300 Personal AFM, from Burleigh Instruments Inc. This equipment is connected to a computer (IBM 486DX). To acquire images it was used a "True Image SPM™" software written as a Windows™ -based product. Silicon cantilever with a high aspect ratio tip of typical radius of curvature 10 nm were used. The tip was held about 5 to 10 nm above the sample surface during the scan.

3.3 Results and discussion

3.3.1 Measurements of Film Thickness

The thickness of the anodic alumina membranes were presented on Tables 3.1 and 3.2. For homogeneous membranes the values range from 23 μm (sample 72/1) to 37 μm (sample 60/3). These membranes were thick enough to provide mechanical strength and support a gas pressure up to 1.5×10^5 Pa (used in experimental tests, in Chapter 5) without damage the membrane. Asymmetric membranes was prepared for small pore diameter and the basic idea is to minimise the overall resistance of the permeation (of gas or liquid) through the membrane structure. As the permeation is inversely proportional to the layer thickness (see Equation 5.2, Chapter 5) it was desirable to have an active layer as thin as possible. So, a support layer with 23 μm in thickness was used for asymmetric membranes. The thickness of the active layer of the sample 72/1/10/16 was obtained by the difference between the total thickness of the membrane and the thickness of the sample 72/1 (as prepared in the same conditions). This thickness was equal to 9 μm and it was in good agreement with the value obtained by SEM on Plate XIII. Also for the samples 72/1/5/20 and 72/1/5/40 the values of thickness of the active layer were obtained from the difference between the sample 72/1 and the total thickness of the membranes. In these cases a good agreement was achieved between the two samples, since the time of preparation of the sample 72/1/5/40 was two times the sample 72/1/5/20 and a double of thickness of the active layer was expected for the sample 72/1/5/40 in relation to the sample 72/1/5/20.

3.3.2 Microstructural Features of Anodic Alumina by Using SEM and AFM

The microstructural features of anodic alumina films prepared in this study, as observed from scanning electron microscopy and atomic force microscopy are discussed independently, for each sample separately. The sample 72/1 is discussed in more details since the other samples follow almost the same features in a different scale.

Sample 72/1

Plates I, II, III and IV show scanning electron micrographs of the anodic alumina film for the sample 72/1. The top surface (Plate I) shows caps formed during the anodisation using acid to remove aluminium substrate. As can be seen in this plate there are no open pores in this film and all caps have a semi-spherical shape evenly distributed on the surface. This sample was prepared by dissolving the remaining aluminium by acid. The caps remain and all pores are closed, no gas permeation was observed in this case. Plate II shows the cross-sectional view for the anodic film after remove the caps by electrochemistry. The micrograph shows high regularity in the structure with straight and parallel pores and all caps removed. It interest to note on the top of the pores some marks or small channels along the exposed pore wall on the top, showing some evidence of local dissolution by this method. Micrographs of the aluminium substrate after electrochemical separation of the anodic film (Plate III) show small particles distributed on the surface. Chemical analysis by energy dispersive spectroscopy (EDS) in the Fig. 3.1 show these have the same composition as the anodic film (the main chemical elements are oxygen (at 0.5keV) and aluminium (at

1.5keV)). This shows in the electrochemical method part of the caps stay on the aluminium surface. Plate IV shows the top surface with all pores open. The pore density is equal to 4.0×10^{13} pores/cm^2. The pore diameter is not so clear since a shadow effect appear on the top of the pore due to gold (or carbon) deposited unevenly in the open pore. However, with this picture it was possible to estimate the distance between the center of the pores, 180 ± 14nm. This distance can be used to estimate pore diameters and will be discussed in Chapter 4.

Plates V and VI show AFM micrographs of the sample 72/1 with and without caps on surface, respectively. All images are given in top view representation using the same area, that is, 1×1 μm^2. The colour bar at the left side of each image shows the vertical profile of the samples, with the light regions being the highest points, and the dark regions the depressions. Plate V shows the high by regular distribution of the caps on the surface with well defined hexagonal array. The cell size measured in this image is 190 ± 27nm , the same range was observed by SEM (Plate IV), and the pore density found is 3×10^{13}pores/m^2. On the other hand the Plate VI show open pores (caps removed, Fig. 2.3(c)), for the same sample, distributed non-uniformly over the surface and the individual pores are not as regular as the caps shown in the Plate V, although pore density obtained in both Plates were in good agreement. The surface roughness is probably responsible for the greater difficulty in imaging the sample without caps and also the pores are funnel-shaped, as discussed in SEM analysis above. So, the diameter may not be determined directly by surface AFM due to convolution between the tip shape and the pore.

Sample 60/3

Plate VII presents scanning electron micrograph for the sample prepared at 60 Volts (sample 60/3). It can be observed from these images that almost the pores are well distributed on the surface and all pores are open and directly comparable to Plate IV apart from scale. To predict some value for pore diameter from this image is relatively hard due to the effect caused by the shadow effect (due to the metal film deposit) just on the top of the pore as discussed for the sample 72/1. This effect can lead to an error on pore size estimations. The distance between center of pores is better defined approximately 150±15 nm.

Plates VIII and IX show AFM images for the sample 60/3 with and without caps, respectively. Plate VIII shows caps with size in the range of 147±24 nm, slightly smaller than from SEM measurement. Also the pore density determined in this plate is $6.2x10^{13}$pores/m^2, slightly different from the value found in SEM analysis. In addition it is clear that the sharpness of the images is poorer and the surface much rougher than larger pore samples 72/1, Plate V. A depression in the middle of the plate indicate some defect on the original surface aluminium before start the anodisation. Plate IX shows the top surface for the same sample without caps. Again the resolution is poor and pores are not well defined and it is not possible to estimate pore diameters. However the estimate value for pore density in this plate is ~6x10^{13} pores/m^2, the same as found in the Plate VII. Also similar roughness is found in this picture and confirm some defects in the original aluminium surface. This can be caused by the interaction

between tip and film structure, once AFM images have to be interpreted as a convolution between tip shape and caps shape.

Sample 40/5

Plate X shows the scanning electron micrograph of the top surface of the sample 40/5 prepared at 40 Volts. Also it can be observed from these images that almost the pores are well distributed on the surface and all pores are open. From this picture the distance between center of pores is 120 ± 9 nm.

Plate XI shows the AFM image of the top surface with open pores for sample 40/5. Once again roughness is found in this micrograph and to estimate some pore diameter is difficult. However pore density estimated from this micrograph is $\sim 8 \times 10^{13}$ pores/m^2, compared with a better defined value of 7.1×10^{13} pores/m^2 from SEM.

Sample 72/1/10/16

Plates XII, XIII and XIV show scanning electron micrographs of the anodic alumina film for the sample 72/1/10/16. The top surface, corresponding to the small pore active layer, (Plate XII) also showed that all pores were open. It interesting to note in this micrograph that despite of the image apparently showing pores (dark area dimensions) with ~ 30 nm of diameter, the value predicted by other method of estimation (anodisation voltage Chapter 4 and gas permeation, Chapter 5) is close to 11nm. This is explained by the same shadow effect discussed before. There is some evidence, see discussion of sample 72/1/5/20 below, of small pore in the middle of this dark area. The pore density can be estimated from this image if each hole corresponds to a small pore. This value was equal to 7×10^{14} pores/m^2. The cross-section views

(Plates XIII and XIV) show the area in the interface layer when the pore (~65nm) was branched into small pores when the anodisation voltage was reduced. The Plate XIV is a magnification of the Plate XIII and shows details of the interface layer. Thickness of support formed at 72 V for 1 hour estimated in the Plate XIII was 23μm, this value is in good agreement with measurement made by using a micrometer (for sample 72/1) in Table 3.1, and the thickness for active layer formed at 10 V for 16h was 9μm.

Sample 72/1/5/20

Plate XV shows the scanning electron micrograph of the top surface for sample 72/1/5/20. From this micrograph it observed that all caps were removed and the opening on the surface show size approximately 15nm in diameter. However a magnification of this view (Plate XVI) indicates a small pore in the middle of this opening. Distance between center of pores, measured from this picture, was 24.9 nm approximately. This value is used to estimate pore diameter (see Section 4.3.3),. Pore density, from Plate XV, was 1.5×10^{15} pores/m^2.

3.4 Conclusions

The SEM images show well defined pore structures for large pore samples >30 nm. The technique is however limited to such large pores due to the effect of gold or carbon deposits (sample preparation) in masking small features. Although AFM does

not require such deposits its results are much poorer and depth of focus limited. The AFM images were in good agreement with SEM, that is, both techniques showed the same features. However for samples 72/1/10/16 and 72/1/5/20 it was not possible to scanning by AFM due to a small contrast on the surface in these two sample and also due to the limitation of the available tip with 10nm diameter of curvature. For membranes with pores <20nm it is clear that pores sizes can not be estimated with any degree of confidence for direct microscopic observation.

One of the major objectives in characterising membranes is to estimate pore sizes. For pore sizes < 20nm it is clear that nether SEM or AFM are suitable for quantitative estimations. Other methods were required. These are discussed in detail in Chapter 4 and Chapter 5.

3.6 References

[1] R. R. Bhave (Editor), Inorganic Membranes Synthesis, Characteristics and Applications, Van Nostrand Reinhold, New York, 1991, pgs. 67-72.

[2] H. P. Hsieh, Inorganic Membranes for Separation and Reaction, Elsevier, Netherlands, 1996, pgs. 93-96.

[3] A. K. Fritzsche, A. R. Arevalo, A. F. Connolly, M. D. Moore, V. B. Eling, K. Kjoller and C. M. Wu, The structure and morphology of the skin of polyethersulfone ultrafiltration membranes. A comparative atomic force microscope and a scanning electron microscope study, J. Appl. Polym. Sci., 45 (1992) 1945-1956.

[4] P. Dietz, P. K. Hansma, O. Inacker, H. D. Lehmann and K. H. Herrmann, Surface and pore structures of micro- and ultrafiltration membranes imaged with atomic force microscope, J. Membr. Sci., 65 (1992) 101-111.

[5] A. K. Fritzsche, A. R. Arevalo, M. D. Moore and C. O'Hara, The surface structure and morphology of polyacrylonitrile membranes by atomic force microscopy, J. Membr. Sci., 81 (1993) 109-120.

[6] W. R. Bowen, N. Hilal, R. W. Lovitt and P. M. Williams, Atomic force microscope studies of membranes: surface pore structures of Cyclopore and Anopore membranes, J. Membr. Sci., 110 (1996) 233-238.

Table 3.1 - Thickness of homogeneous anodic alumina membranes

Sample Reference	δ_{tot} (μm)
72/1	23
60/3	37
40/5	25

δ_{tot} - Total thickness of the membrane

Table 3.2 -Thickness of asymmetric anodic alumina membranes, support and active layers.

Sample Reference	δ_{tot} (μm)	a (μm)	b (μm)
72/1/10/16	32	23	9
72/1/5/20	29	23	6
72/1/5/40	35	23	12

δ_{tot} - Total thickness of the membrane
a - Thickness of the support layer
b - Thickness of the active layer
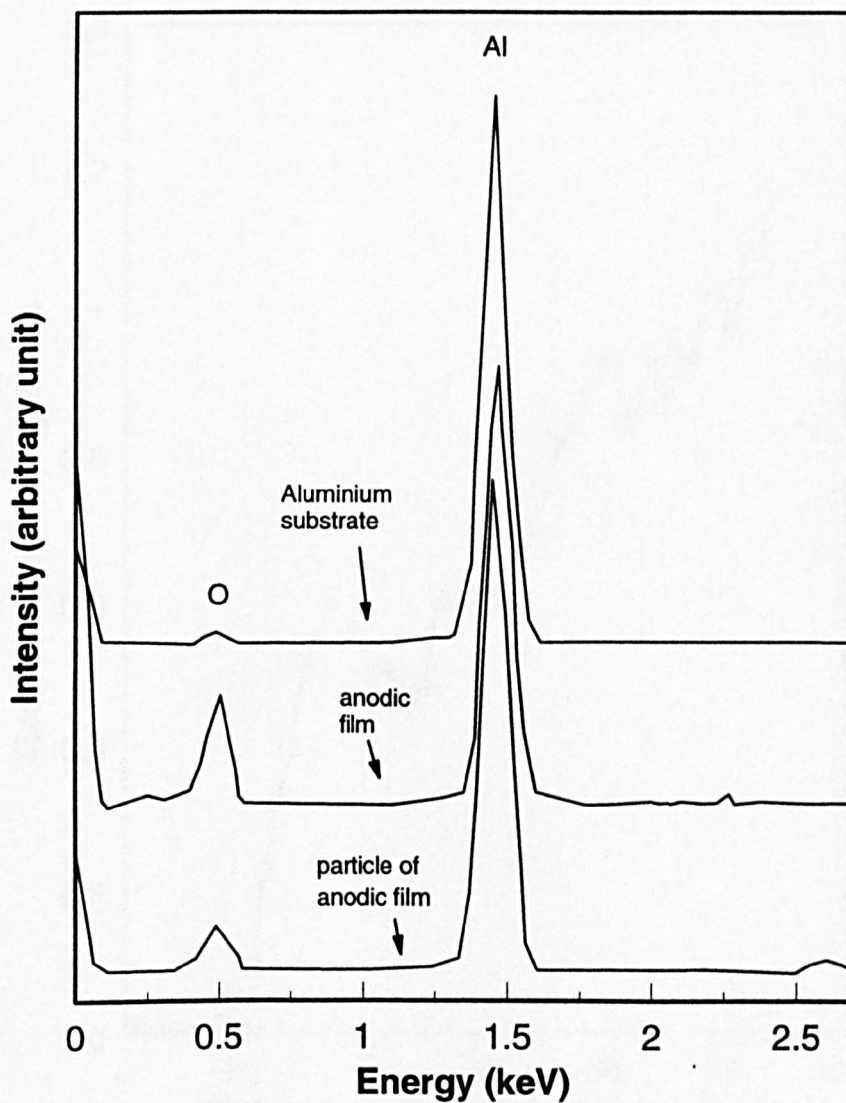
Fig. 3.1 Energy dispersive spectra of anodic film, aluminium substrate and particle of alumina film on the surface of aluminium substrate.
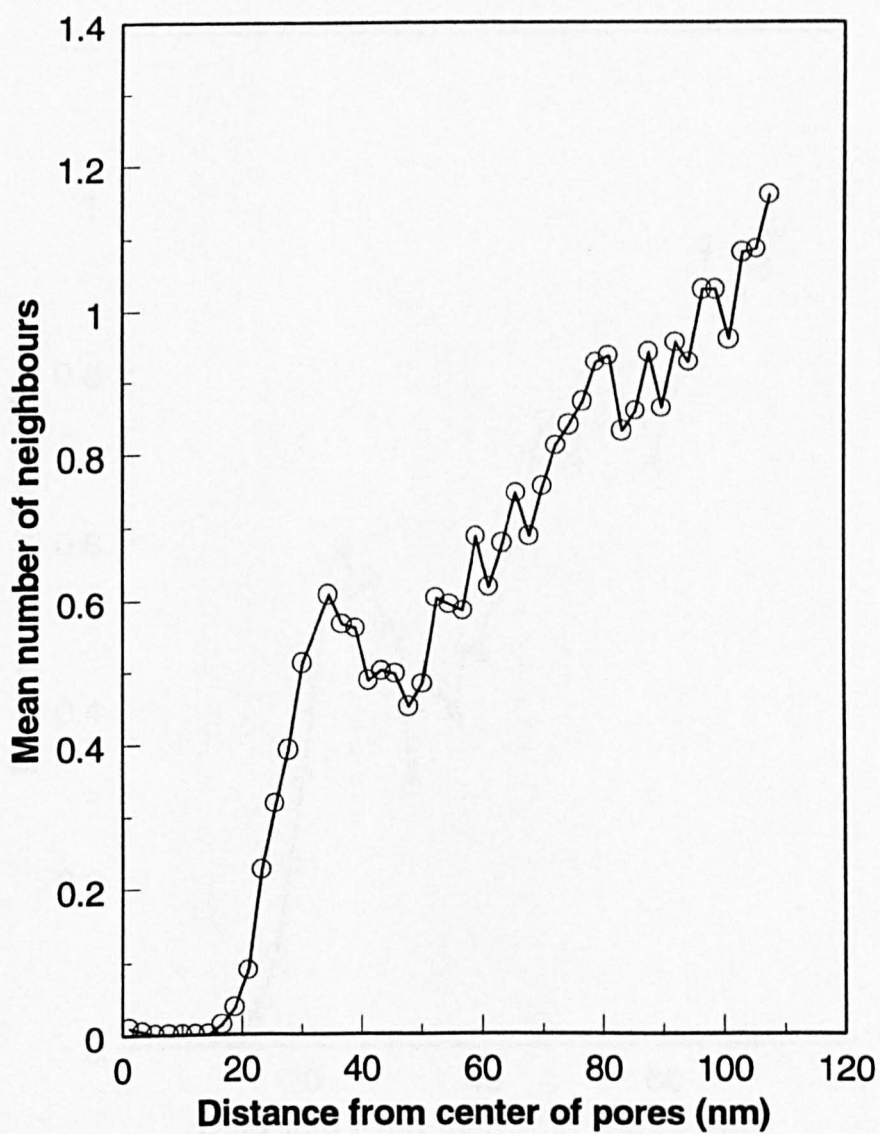
Fig. 3.2 Radial function of distribution of geometrical centers of
pores for sample 72/1/10/16.
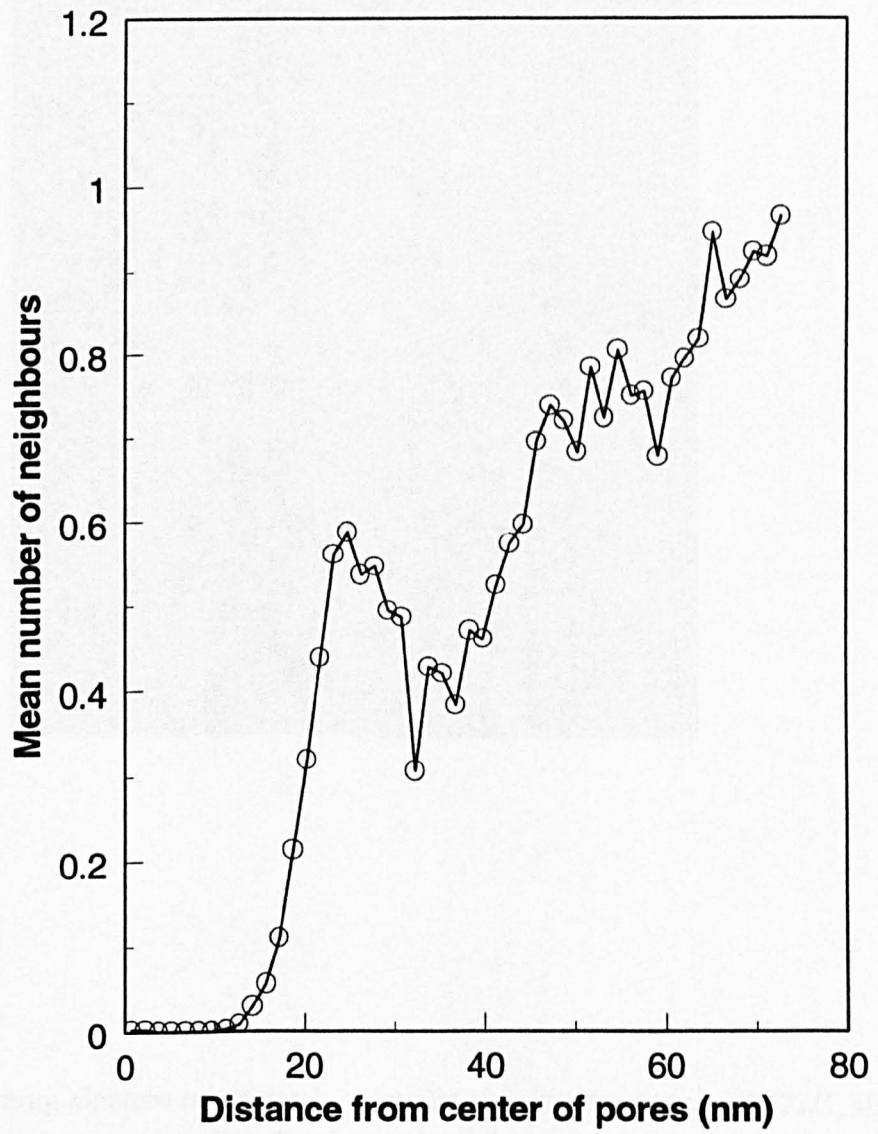
Fig. 3.3 Radial function of distribution of geometrical centers of
pores for sample 72/1/5/20.

Plate I. Scanning electron micrograph of anodic alumina film for sample 72/1, showing caps on top surface after dissolving aluminium substrate by acid. (Magnification: 50,000x)

Plate II. Scanning electron micrograph of anodic alumina film for sample 72/1, showing cross-section view with open pores on top surface after removing caps and aluminium substrate by electrochemical treatment. (Magnification: 50,000x)

Plate III. Scanning electron micrograph of aluminium substrate showing some part of caps from alumina film after removing by electrochemical technique. (Magnification: 30,000x)

Plate IV. Scanning electron micrograph of anodic alumina film for sample 72/1, showing top surface view with open pores after remove caps and aluminium substrate by the electrochemical method. (Magnification: 50,000x)
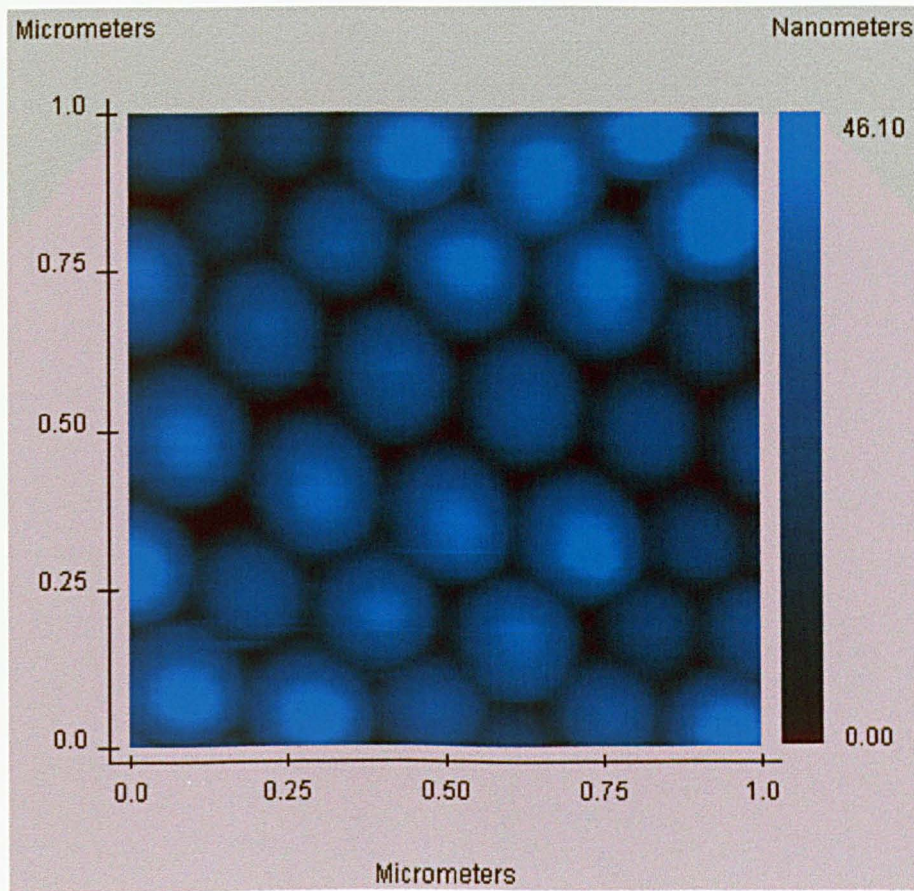
Plate V. Atomic force micrograph of anodic alumina film for sample 72/1, showing caps on top surface view after dissolving aluminium substrate by acid.
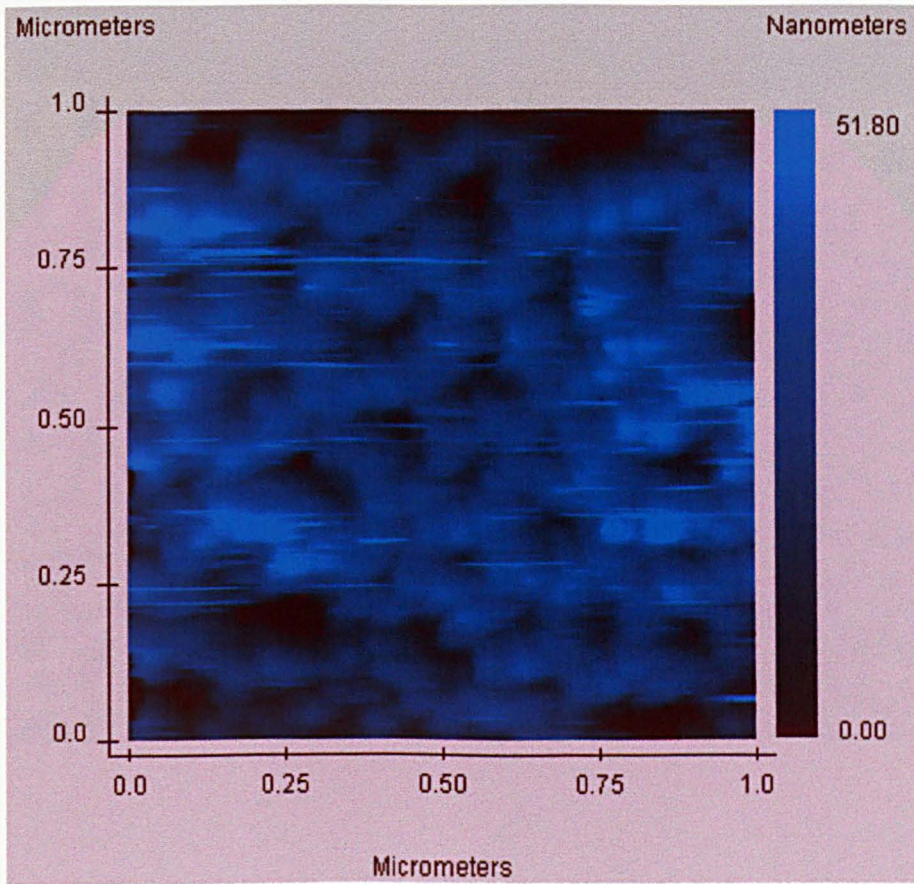
Plate VI. Atomic force micrograph of anodic alumina film for sample 72/1, showing pores on top surface view after removing caps and aluminium substrate by the electrochemical method.
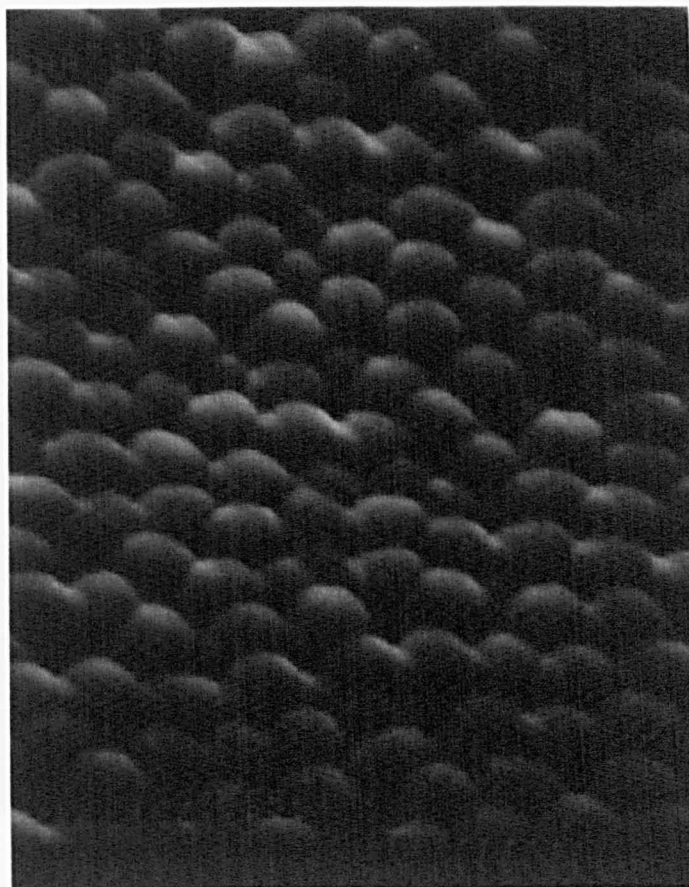
Plate VII. Scanning electron micrograph of anodic alumina film for sample 60/3, showing top surface view with open pores on top surface after removing caps and aluminium substrate by electrochemical treatment. (Magnification: 60,000x)
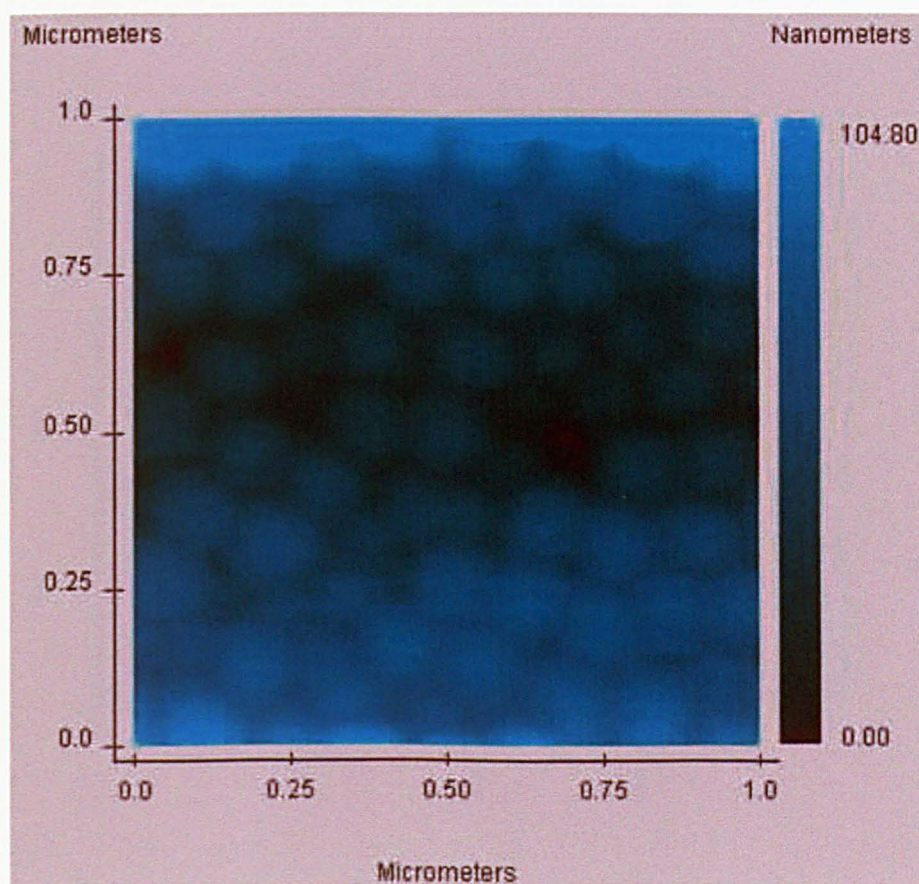
Plate VIII. Atomic force micrograph of anodic alumina film for sample 60/3, showing caps on top surface view after dissolving the aluminium substrate by acid.
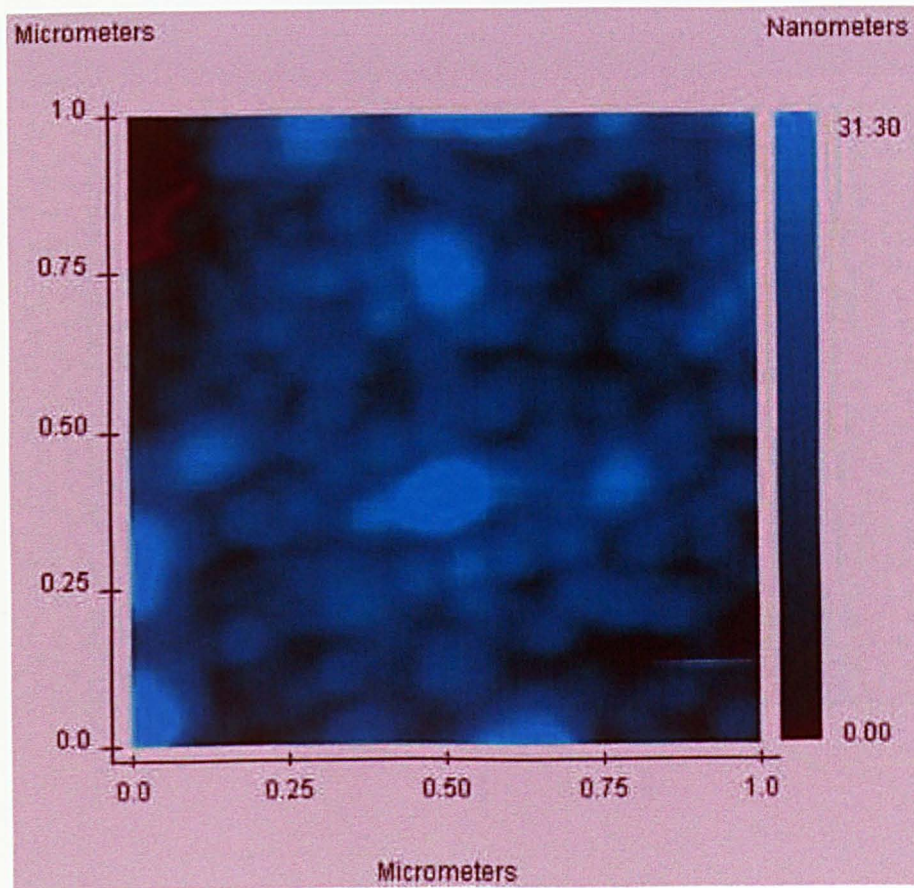
Plate IX. Atomic force micrograph of anodic alumina film for sample 60/3, showing pores on top surface view after removing caps and the aluminium substrate by the electrochemical method.
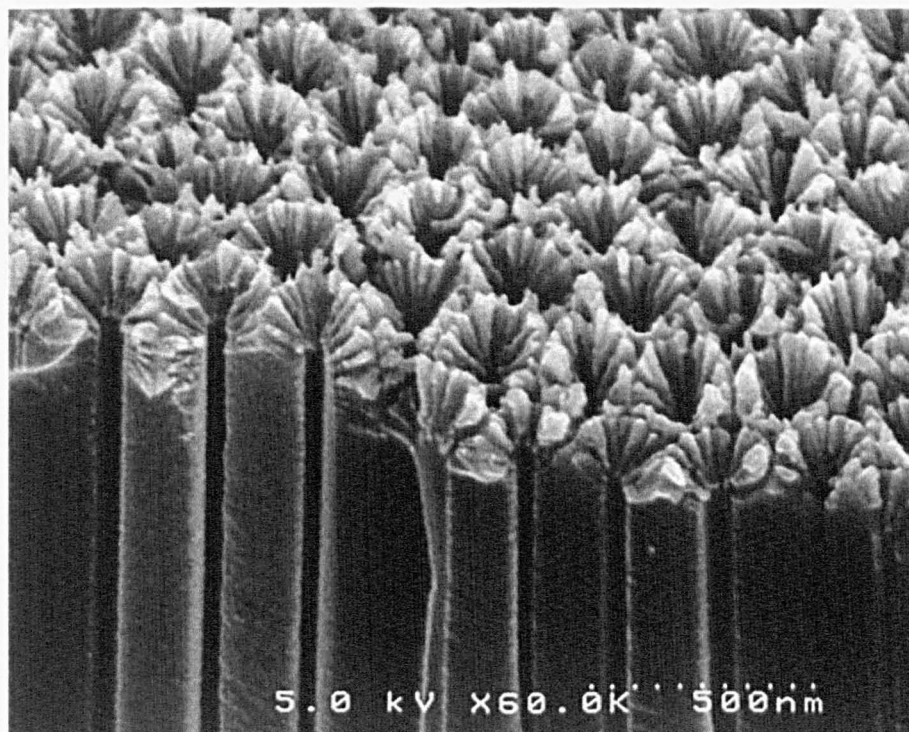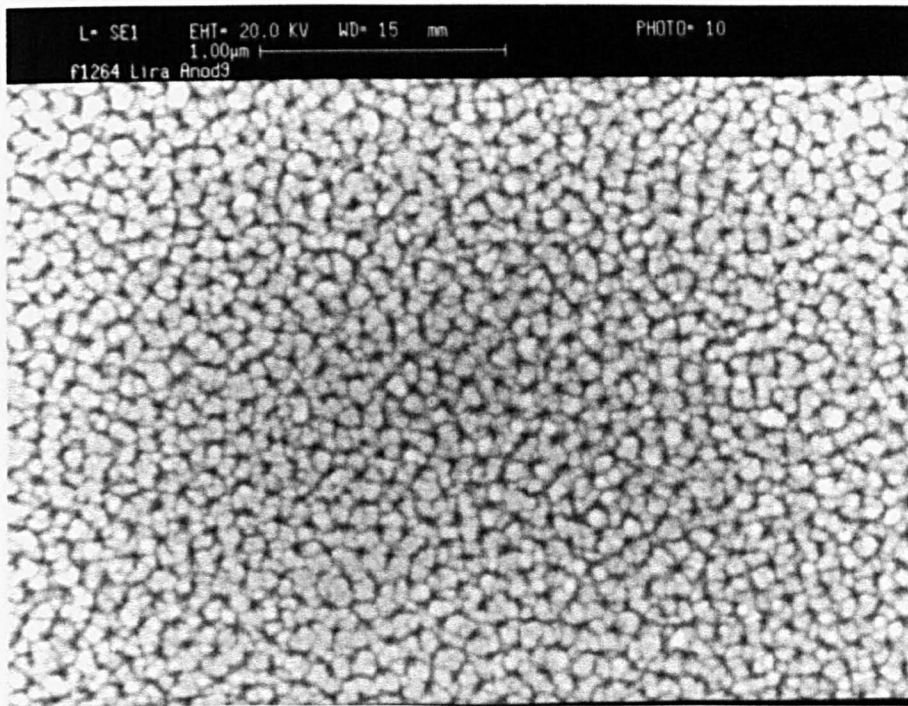
Plate X. Scanning electron micrograph of anodic alumina film for sample 40/5, showing top surface view with open pores on top surface after removing caps and aluminium substrate by electrochemical treatment. (Magnification: 31,500x)
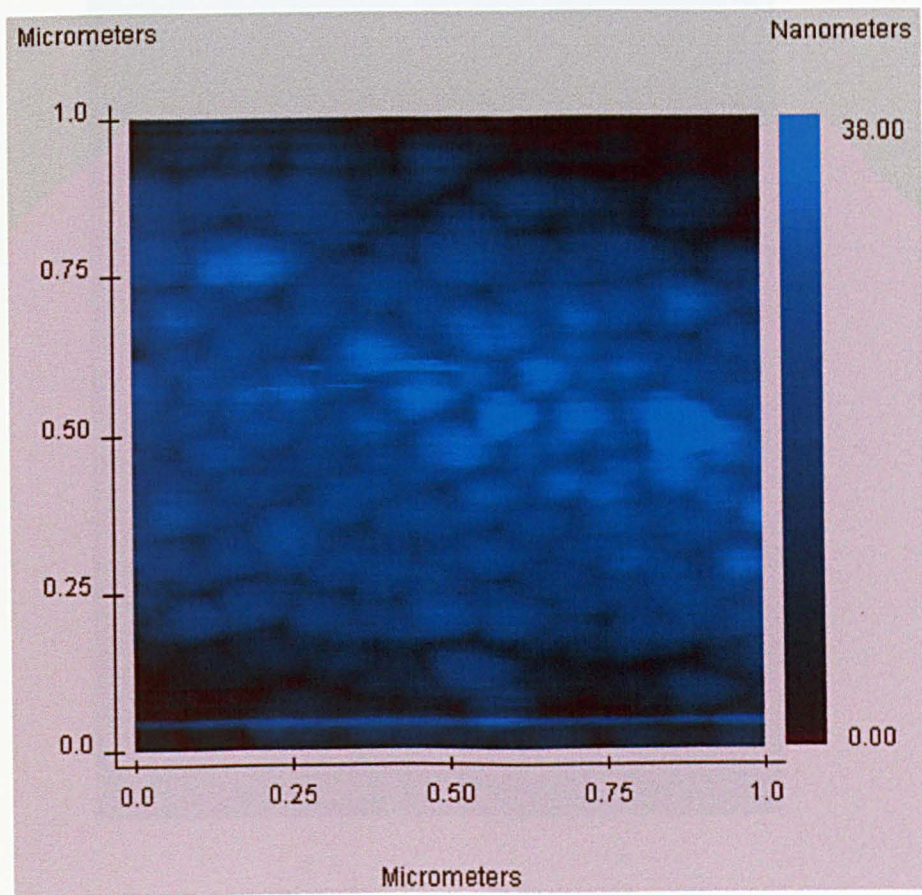
Plate XI. Atomic force micrograph of anodic alumina film for sample 40/5, showing pores on top surface view after removing caps and the aluminium substrate by the electrochemical method.
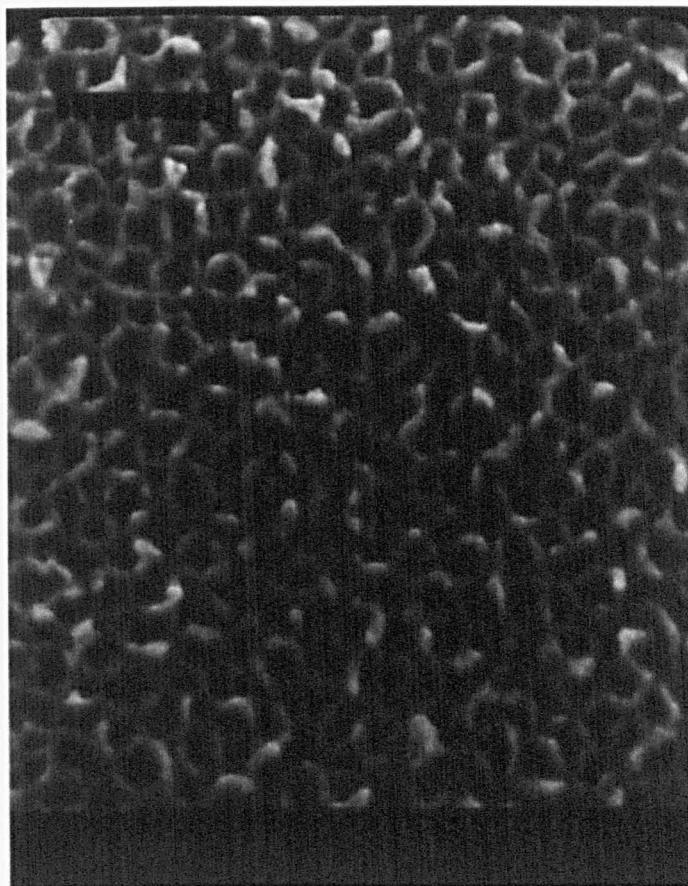
Plate XII. Scanning electron micrograph of anodic alumina film for sample 72/1/10/16, showing top surface view with open pores on top surface after removing caps and aluminium substrate by electrochemical treatment. (Magnification: 112,500x)
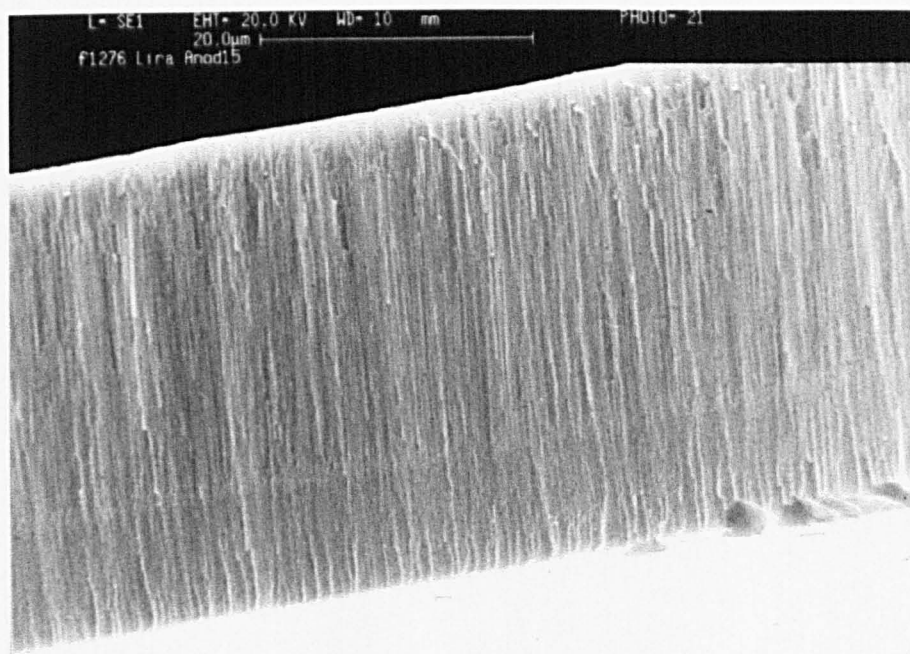
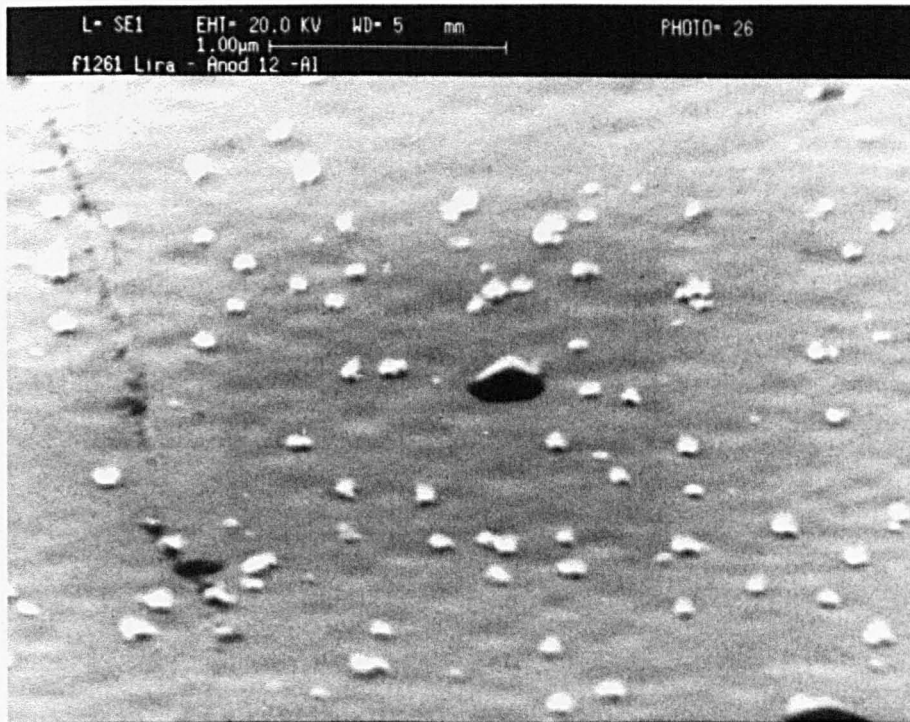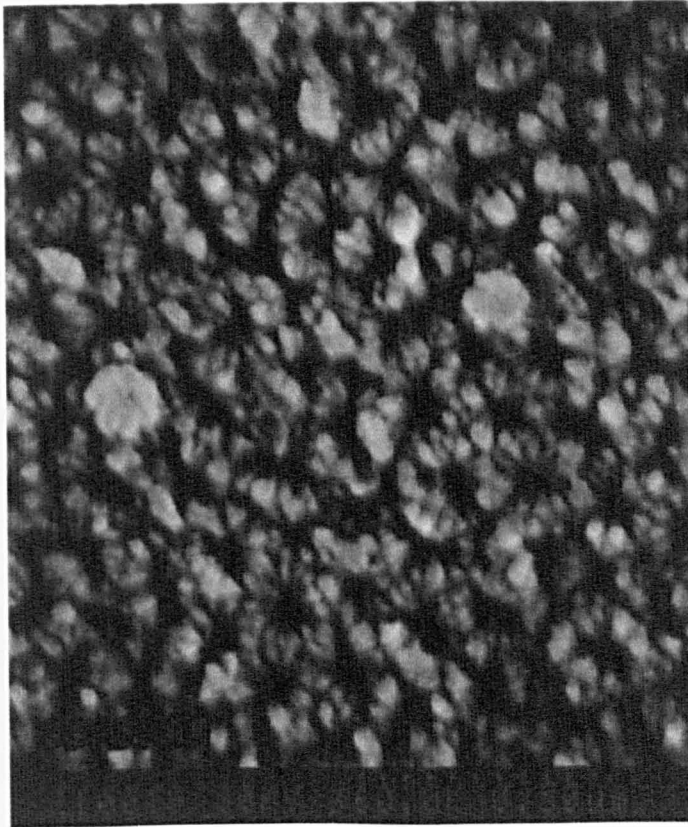Plate XIII. Scanning electron micrograph of anodic alumina film for sample 72/1/10/16, showing cross-section view with two layer (23 µm created at 72V for 1 h and 9 µm at 10 V for 16 hs). (Magnification: 1,450x)

L- SE1   EHT- 20.0 KV   WD- 10   mm   PHOTO- 20
         2.00µm
f1276 Lira Anod15
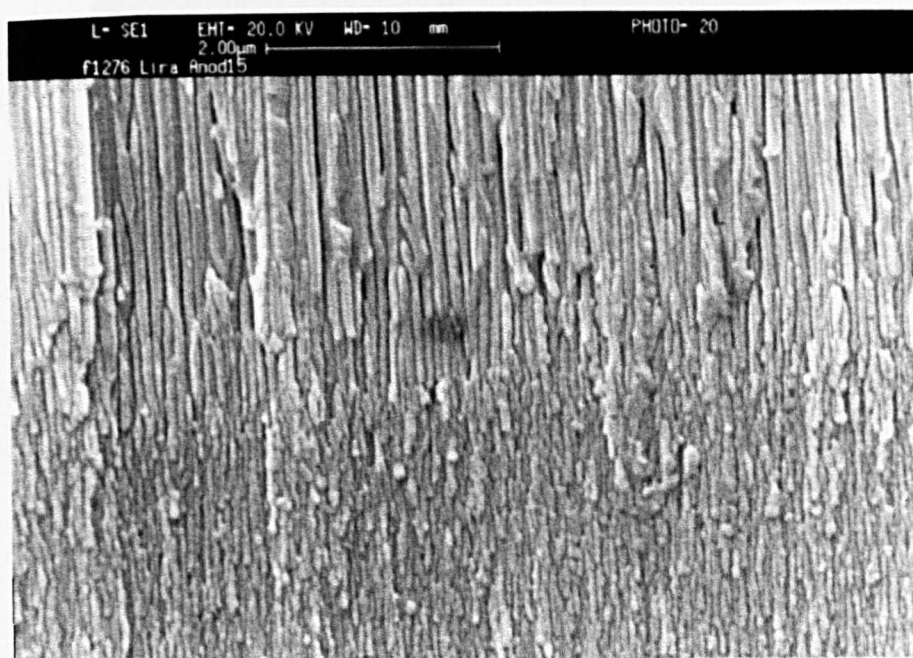
Plate XIV. Scanning electron micrograph of anodic alumina film for sample 72/1/10/16, showing cross-section view with detail of interface layer when big pores are branched into small pores during reduction of anodisation voltage. (Magnification: 12,250x)
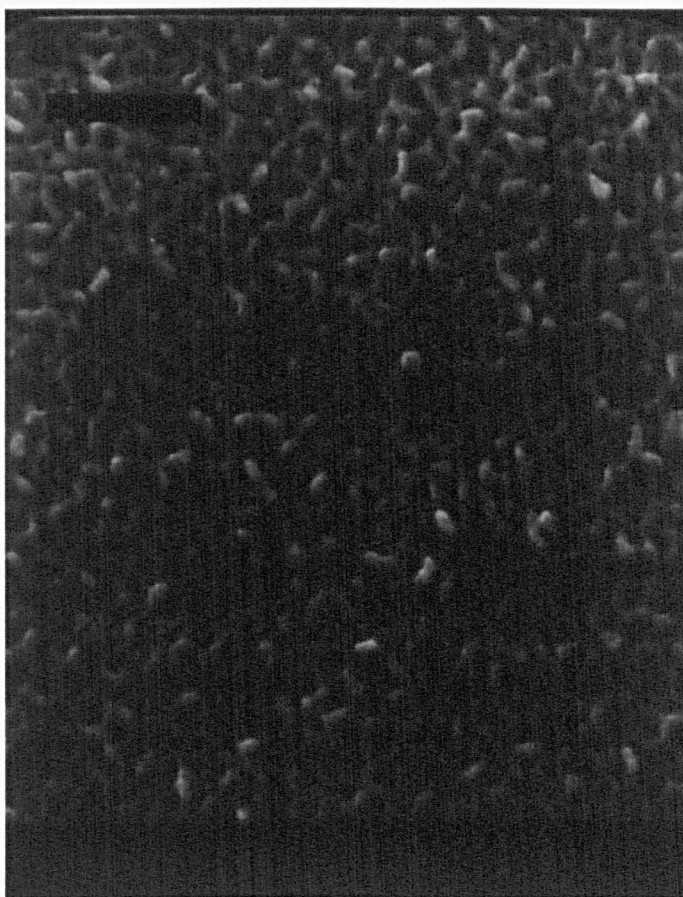
Plate XV. Scanning electron micrograph of anodic alumina film for sample 72/1/5/20, showing top surface view with open pores on top surface after removing caps and aluminium substrate by electrochemical treatment. (Magnification: 112,500x)
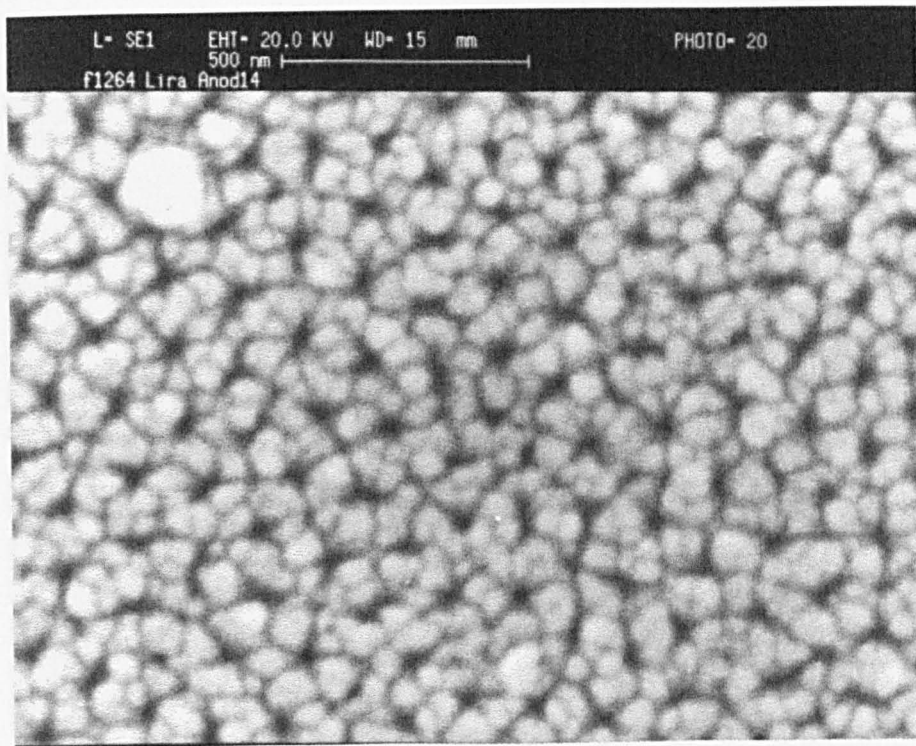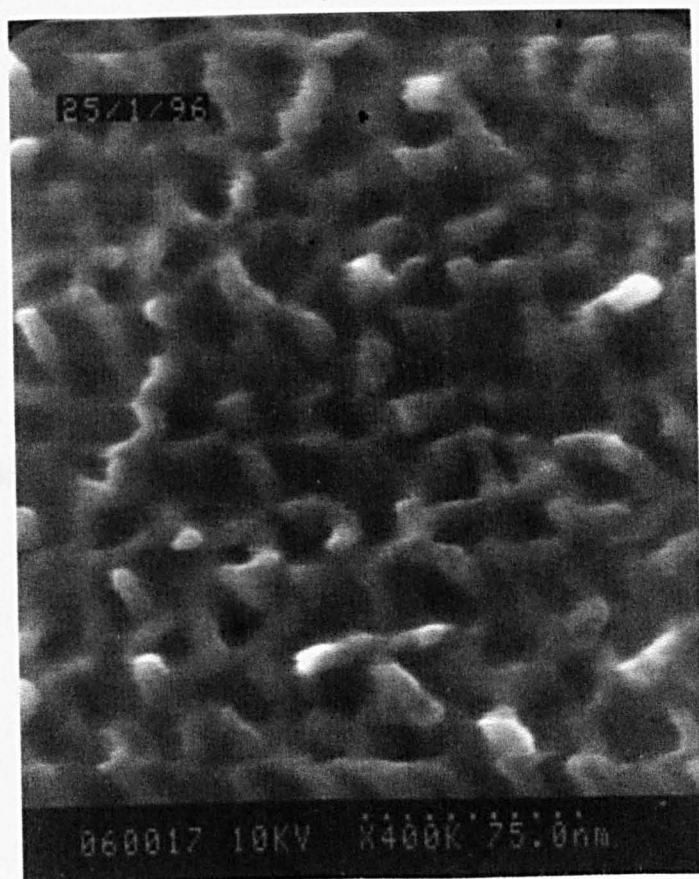
Plate XVI. Scanning electron micrograph of anodic alumina film for sample 72/1/5/20, showing magnfication of top surface view (Plate X) with small pores in the middle of the big holes on top surface after removing caps and aluminium substrate by electrochemical treatment. (Magnification: 300,000x)

Chapter 4

Geometric Considerations of Anodic Alumina Membranes

4.1 Introduction

The images presented in Chapter 3 describes the structural features of anodic alumina membranes. When aluminium is anodised in certain acid electrolytes, a porous oxide develops which exhibits a remarkably uniform array of cells, each containing a cylindrical pore. Microscopy studies, in Chapter 3, showed an asymmetric membrane with small pore was prepared. To measure the pore diameter with SEM and AFM was not possible. However the structural features obtained for large pore size anodic alumina membranes can be generalised and used be extrapolate the pore diameter of the asymmetric small pore size anodic alumina membranes.

Essentially every pore in these asymmetric membranes had divided into smaller pores and the membrane has an asymmetric structure: large pores extending through the bulk of its thickness interconnected with an array of smaller pores.

In this chapter a geometric model was used to describe how the pore size and pore density are related to the formation voltage, during growth at constant voltage of anodisation. The predict value for morphological parameters from geometrical model were compared with SEM and AFM data obtained in Chapter 3.

4.2 Hexagonal Cell Model

From the analysis of the scanning electron micrographs and atomic force images of the samples prepared in this study and discussed in Chapter 3 the microstructure features of anodic alumina films can be idealised (Plates I, II, V). It consists of hexagonal columnar cells, with a centrally situated pore that runs down the column of each cell, Fig. 4.1(a, b). This geometry was clearly (as showing in Plate V, Chapter 3) obtained by using ultra-pure aluminium pre-treated to decrease the concentration of defects on the aluminium surface. The regularity of this structure allows the pore diameter and percent porosity to be controlled and estimated within each film (this technique is one of several used in this study to assess the smallest pore diameter under condition that scanning electron microscopy and atomic force microscopy technique fail). The fabrication of inorganic membranes, through anodisation of aluminium, requires control of voltage, electrolyte temperature and composition, and anodisation time. It was observed in this study and is a well known fact [1-20] that the hexagonal cell diameter, D, and the pore diameter, d, decrease with the anodisation voltage. Also there is ample evidence [8, 10, 11, 13, 17, 20] that the ratio of the hexagonal cell diameter, D, and the pore diameter, d, defined in Fig. 4.1(b), is constant and independent of electrolysis voltage for the same electrolyte and the same condition of temperature, solution concentration, aluminium purity.

In order to investigate the validity of the D/d assumption, the size of the cell, D, and the diameter of the pores, d, were estimated from the SEM and AFM images. The measurements was done for homogeneous membrane samples, 72/1, 60/3 and 40/5,

and a compilation of the values are given in Table 4.1. The ratio between the cell

diameter (D) and anodisation voltage is almost constant and approximately equal to

2.8 nm/V. Also the relation between D/d is practically constant (3.0±0.2). This result

is in a excellent agreement with the results obtained from the literature [8, 10, 11, 13,

17, 20].

In the next section (4.3) these observations are used to estimate pore diameter of small

pore size anodic alumina samples prepared in this study.

4.3 Estimations of Pore Diameter From D/d Ratios

At least two different ways was used to estimate the pore diameter by D/d relation.

First, the values of D and d were estimate from direct microscopic observation of the

membranes prepared with anodisation voltage >30 V (samples 72/1, 60/3, and 40/5)

and the value of the relation D/d was used to extrapolate the pore diameter for the

smaller pore sizes of the asymmetric membranes. Second, the D values of samples

72/1/10/16 and 72/1/5/20 were estimate from measurement of the distance between

pore centres in micrographs[1] using a statistical analysis and after the pore diameter

was estimated by using the relation D/d.

---

[1]The images presented in Chapter 3 describes the structural features of anodic alumina membranes. These structural features can be generalised and used be extrapolate the pore diameter of these asymmetric anodic alumina membranes.

4.3.1 Extrapolation of Pore Diameter for Samples 72/1/10/16 and 72/1/5/20 Based on D/d From Direct Microscopy Observation

Based on cell diameter values per anodisation voltage (D=2.8 nm/V) and D/d relation (D/d=3.0) obtained by direct microscopy observation, on Chapter 3, the pore diameters for membranes prepared at 10 V (sample 72/1/10/16) and 5 V (sample 72/1/5/20) can be extrapolated from the equation:

$$d = \frac{D}{3} = \frac{2.8 \times U}{3} \tag{4.1}$$

where U (Volts) is the formation anodisation voltage. So in this case the pore diameter of the active layer for the samples 72/1/10/16 and 72/1/5/20 extrapolated from the equation (4.1) are 9.3 and 4.6 nm, respectively.

4.3.2 Estimation of Pore Diameter for Samples 72/1/10/16 and 72/1/5/20 Based on Measurement of Mean Distance Between Adjacent Pores (D) and Statistical Analysis

Average distance between adjacent pores for samples 72/1/10/16 and 72/1/5/20 was calculated by using a software called Digitize-Pro™ version 2.2. In this program a scanned SEM image was used to obtain the co-ordinates X, Y of the centre of each pore and saved to a file. The mean distance of first neighbours was calculated by using a radial function distribution as a function of the distance from each centre of pore [17]. For the sample 72/1/10/16 a total of 434 points, Fig. 4.2, was used and the

calculated first neighbours distance was 34nm. For the sample 72/1/5/20 a total of 751 points, Fig. 4.3, was used and the corresponding distance was 25nm. So, if the distance between adjacent pores is equal to D and the relation D/d=3.0, the samples 72/1/10/16 and 72/1/5/20 give values of 11.3 and 8.3nm, respectively. These pore diameters values are bigger than the values predict by D/d relation using direct microscopy observation.

Although individual estimates of pore diameter of the samples 72/1/10/16 and 72/1/5/20 were predict from the relation D/d, based on the observation that this ratio is constant, an additional independent method to confirm these results was necessary and this will be discussed in Chapter 5.

4.4 Porosity of Anodic Alumina Membranes

The porosity, ε, of a membrane is the fractional pore volume and for a uniform layer with uniform parallel pore normal to its surface, this is identical to the fractional area of pores per unit surface, that is;

$$\varepsilon = \frac{total\ pore\ volume}{volume\ of\ membrane} = \frac{total\ area\ of\ pores \times thickness}{total\ area\ of\ membrane \times thickness} \tag{4.2}$$

Based on the idealised hexagonal cell model for anodic alumina membranes, the porosity can be calculated by the area of the pore divided by the area of hexagonal cell, see Fig. 4.1 (b);

$$\varepsilon = \frac{area \; of \, pore}{area \; of \; hexagonal \; cell} \qquad\qquad (4.3)$$

Also in Fig. 4.1(b), the area of the hexagonal cell is $\frac{\sqrt{3}}{2}D^2$, and the area of the pore is $\pi d^2/4$. Consequently, the porosity becomes;

$$\varepsilon = \frac{\pi}{2\sqrt{3}}\left(\frac{d}{D}\right)^2 \qquad\qquad (4.4)$$

When D/d is constant it is clear from equation (4.4) that porosity, ε, is constant and independent of pore diameter (for these membrane when D/d=3.0, the porosity ε=0.1). This means that even for asymmetric anodic alumina membrane, when the voltage is reduced at the end of anodisation, the fractional pore area remain constant. Based on this consideration theoretical calculations for pore diameter, porosity and pore density were made. A compilation of these values and observed ones are given in Table 4.2. The observed values are in good agreement with the theoretical one. For asymmetric membranes (72/1/10/16 and 72/1/5/20) it was not possible to estimate the pore diameter and the porosity from microscopy studies, however the value of pore density can be estimated since each hole in the micrograph correspond to a pore, independently of the size of the pore. So, the observed pore density, from SEM micrograph, for these two sample are close to the calculated one.

4.6 References

[1] T. P. Hoar and N. F. Mott, Mechanism for the formation of porous anodic oxide films on aluminium, J. Phys. Chem. Solids, 9 (1959) 97-99.

[2] J. P. O'Sullivan, 1968, The formation and sealing of porous anodic oxide films on aluminium, PhD Thesis, University of Manchester.

[3] J. P. O'Sullivan and G. C.Wood, The morphology and mechanism of formation of porous anodic films on aluminum. Proc. R. Soc. London, Ser. A, 317 (1970) 511-43.

[4] A. W. Smith, Porous anodic aluminum oxide membrane, J. Electrochem. Soc., 120(8)(1973) 1068-69.

[5] H.Takahashi, H. Nagayama, H. Akahori and A. Kitahara, Electron-microscopy of porous anodic films on aluminum by ultrathin Section technique. Part 1. The structural change of the film during the current recovery, J. Electron Microsc., 22 (2) (1973) 149-57.

[6] A. W. Smith, Process for producing an anodic aluminum oxide membrane. U.S. Patent 3,850,762 (1974)

[7] R. C. Furneaux, 1977, Sealing anodised aluminium, PhD Thesis, University of Manchester.

[8] G. E. Thompson, R. C. Furneaux, G. C. Wood, H. A. Richardson and J. S. Goode, Nucleation and growth of porous anodic films on aluminum, Nature, 272 (1978) 433-35.

[9] Y. Xu, 1983. The growth mechanisms of anodic films on aluminium, PhD Thesis, University of Manchester.

[10] G. E. Thompson and G. C. Wood, Porous anodic film formation on aluminium, Nature, 290 (1981) 230.

[11] T. Parlovic and A. Ignatiev, Optical and microstructural properties of anodically oxidized aluminum, Thin Solid Films, 138 (1986) 97-109.

[12] R. C. Furneaux, W. R. Rigby, and A. P. Davidson, Porous films and method of forming them, EP 0,178,831 Al (1986); US Pat. 4,687,551 (1987).

[13] R. C. Furneaux, W. R. Rigby, and A. P. Davidson, The formation of controlled porosity membranes from anodically oxidized aluminum, Nature, 337 (1989) 147.

[14] R. C. Furneaux, R. W. Philpott and D. M. Jenkins, Controlled pore-size membranes produced by anodizing aluminium, Proc. of the 1st Inter. Conf. on Inorganic Membranes, Montpellier, 1989, 47-53.

[15] P. A. Kestin, R. R. Biederman, Y. H. Ma, The effects of anodizing parameters on alumina membrane synthesis, Key Eng. Mater., 61 (1991) 387-390.

[16] K. Shimizu, K. Kobayashi, G. E. Thompson and G. C. Wood, Development of porous anodic films on aluminium, Philos. Mag. A, 66, 4 (1992) 643-652.

[17] J. Randon, P. P. Mardilovich, A. N. Govyadinov, and R. Paterson, Computer simulation of inorganic membrane morphology. Part 3. Anodic alumina films and membranes, J. Colloid Interface Sci., 169 (1995) 335.

[18] P. P. Mardilovich, A. N. Govyadinov, N. I. Mukhurov, A. M. Rzhevskii, and R. Paterson, New and modified anodic alumina membranes. Part. I. Thermotreatment of anodic alumina membranes, J. Membr. Sci., 98 (1995) 131.

[19] R. Paterson, P. P. Mardilovich, A. N. Govyadinov, N. I. Mazurenko, UK Patent WO 9534371, Permeable anodic alumina film, Dec, 1995.

[20] J. Randon, P. P. Mardilovich, A. N. Govyadinov, and R. Paterson, Modelling the pore structure of anodic alumina membranes, Proc. 3th Intern. Conf. on Inorg. Membr., Worchester, Massachusetts, USA, 1994, 613.

Table 4.1 - Values of cell diameter, D, and pore diameter, d, of homogeneous anodic alumina membranes from direct microscopy observation.

Sample	Anodisation Voltage (V)	Cell diameter, D (nm)(*)	Cell diam./Voltage (nm/V)	Pore diameter, d (nm)(**)	Cell diameter/ Pore diameter D/d
72/1	72	180±14	2.5	64±14	2.8
60/3	60	160±14	2.7	50±6	3.2
40/5	40	120±9	3.0	40±8	3.0
Average value	-	-	2.8	-	3.0

(*)Value estimated from SEM and AFM images.
(**)Value estimated from SEM images.

Table 4.2 - Comparison of calculated and observed values for pore diameter, pore

density and porosity of anodic alumina membranes

	Calculated			Observed		
Sample	Pore diameter (nm)(*)	Pore density (pores/m^2)	Porosity	Pore diameter (nm)(**)	Pore density (pores/m^2)	Porosity
72/1	67.0	2.8×10^{13}	0.10	64 ± 14	4.0×10^{13}	0.13 ± 0.06
60/3	55.8	4.1×10^{13}	0.10	50 ± 6	5.6×10^{13}	0.11 ± 0.02
40/5	37.2	9.2×10^{13}	0.10	40 ± 8	7.1×10^{13}	0.09 ± 0.03
72/1/10/16 (***)	9.3 11.3(+)	1.5×10^{15} 9.7×10^{14}	0.10	-	7×10^{14}	-
72/1/5/20 (***)	4.6 8.3(+)	6.0×10^{15} 1.8×10^{15}	0.10	-	1.5×10^{15}	-

(*)   Value calculated based on D=2.8 nm/V, D/d = 3.0.

(**) Value estimated from SEM.

(***)The value of the pore diameter refer to the active layer (small pore) surface of the asymmetric membrane.

(+)   Value calculated based on the distance between pore center from statistical analysis of SEM micrographs, Section 4.3.2.
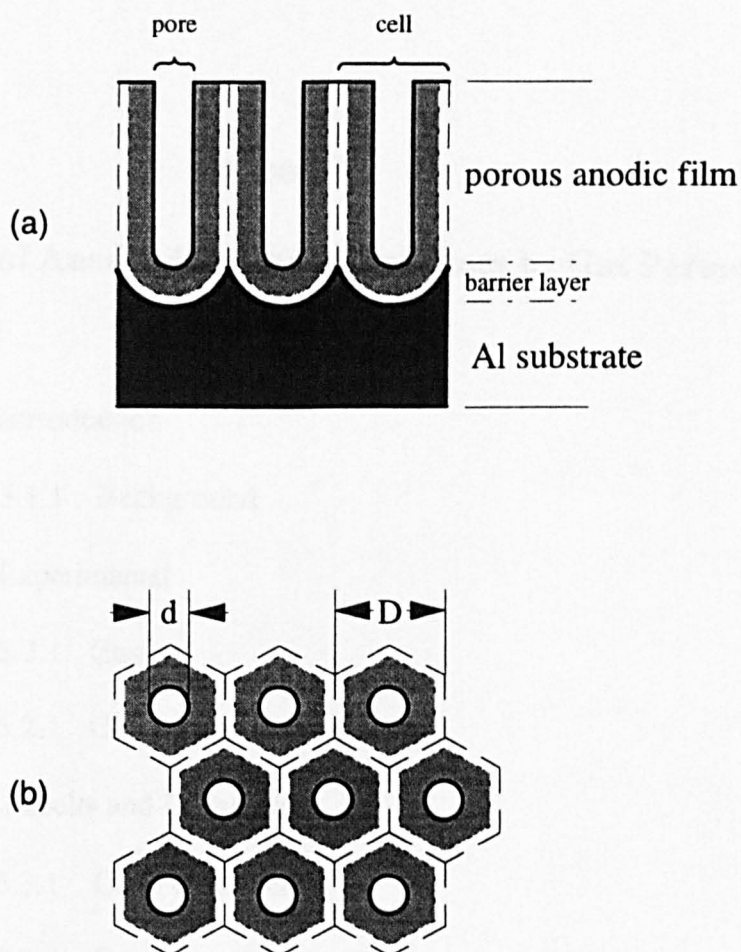
Fig. 4.1- Representation of anodic alumina structure with a cross-section view (a) shows anodic film with a impermeable barrier layer and aluminium substrate on the botton and uniform pores (b) placed in a center of a hexagon cell organised in a hexagonal network

Chapter 5

Characterisation of Anodic Alumina Membranes by Gas Permeation

5.1 Introduction

The pore size of a membrane plays the most important role in the function of porous membranes and their applications. Despite several methods to estimate mean pore size of porous membranes been available [1-3], these methods generally involve some ambiguity and/or are require sample modification, for example, in a high-resolution scanning electron microscopy used to measure pore size of anodic alumina membranes, discussed in Chapter 3, the alumina sample must be electrically conductive and precoated with some conductive material. This can lead to a reduction in the pore size of the membrane. Others methods, such as coulter porometry, is limited by the pore radii of approximately 25nm [4]; the penetration of mercury under pressure to estimate porosity may alter the pore sizes of original membranes [1].

The measurement of the gas permeability coefficient as a function of the mean pressure across a membrane can be used to determine a mean pore diameter of the membrane. This method has been applied by several authors to characterise microporous and asymmetric ultrafiltration membranes [5-8]. Some reported results show good correlation between experimental data and theoretical simulations, although the difficulty to control the porous structure of the membranes, in terms of pore shape, layer thickness and even to obtain a membrane free of defects and reproducible.

The anodic alumina membrane has special features (see Chapter 4) which make it an ideal system to be studied by gas permeations. The membrane has a uniform planar

structure with regular pores in an hexagonal array. All pores are parallel to each other, without intersection. Also membrane can be prepared with high reproducibility.

Chapter 2 described the preparation of anodic alumina membranes with small pore size and in Chapters 3 and 4 the characterisation of these membranes by SEM, AFM and geometrical considerations methods. Even with the use of powerful techniques such as high resolution scanning microscopy and atomic force microscopy, the characterisation of small pore size anodic alumina membrane has been achieved only partially, mainly because of the conductive coating, in the case of SEM, and the shape of the pore on the active layer that causes a shadow and covers the pores. The objective of this chapter is to characterise these membranes by gas a permeation method. For this study flat anodic alumina membranes with different pore sizes will be tested. The mechanism of gas permeation will be investigated and applied to determine the pore diameter of the samples studied. Finally, the results obtained will be compared with direct observation by SEM and the predictions with anodisation voltage discussed in Chapter 4.

5.1.1 Background

There is a large literature on transport of gases and vapours through porous membranes [9-17]. In multi-layered porous membranes several transport mechanisms can occur. However for membranes with a pore size between 1 nm and 100 nm, at least, three mechanisms can apply separately or in combination. These are, surface, Knudsen and Poiseuille diffusion [16]. Surface diffusion appears when the molecules of the gas interact with or are adsorbed physically/chemically on the material of the pore wall of the membrane. Knudsen diffusion occurs when the size of the pore is smaller than the mean free path of the gas molecules [18]. In this case the gas molecules collide much more frequently with the pore wall than with one another and low molecular weight gases therefore are able to diffuse more rapidly than heavier ones. For Poiseuille diffusion gas molecules collide exclusively with each other, in fact, they seem to ignore the existence of the membrane or pore wall. These mechanisms are illustrated in Fig. 5.1. The gas flux density through a membrane per unit area per unit time is defined by

$$J = P \Delta p \tag{5.1}$$

Where J is the gas flux density (mole.s^{-1}.m^{-2}), P is the permeability (mole.s^{-1}.m^{-2}.Pa^{-1}) and p is the pressure (Pa). If all the transport mechanism described previously are applied for a single gas, the transport equation becomes:

$$P = P_p + P_k + P_s = \frac{\varepsilon \mu_p r^2 p}{8 \eta R T \delta} + \frac{2 \varepsilon \mu_k v r}{3 R T \delta} + \frac{2 \varepsilon \mu_s D_s}{r A N \delta} \frac{dx_s}{dp} \tag{5.2}$$

5.3

Where **P** is the total permeability (in $mole.s^{-1}.m^{-2}.Pa^{-1}$), P_p, P_k and P_s are the permeabilities by Poiseuille diffusion, Knudsen diffusion and surface diffusion, respectively. In equation (5.2), ε is the porosity, which is $n\pi r^2$, where n is the number of pores per m^2, r is the mean pore radius of the membrane (m), η is the viscosity of the gas (Pa.s), μ_p, μ_k and μ_s are shape factors, which are all equal to unity for uniform straight pores normal to the planar surface of the membrane, δ is the thickness of the membrane (m), R is the gas constant (8.314 $J.mol^{-1}.K^{-1}$), T is the absolute temperature (K), **A** is the surface area occupied by one molecule (m^2), D_s the surface diffusion coefficient ($m^2.s^{-1}$), N Avogrado's number, x_s the surface coverage as compared with a monolayer, p is the pressure (Pa) and v is the average velocity ($m.s^{-1}$) which is:

$$v = \left(\frac{8RT}{\pi M}\right)^{\frac{1}{2}}$$
(5.3)

Where M is the molecular mass of the gas ($kg.mol^{-1}$).

For pore sizes smaller than 100 nm and at low pressures, Poiseuille diffusion and surface diffusion can be negligible [17] and the transport is determined solely by Knudsen flow and so from equation (5.1),

$$P = P_k = \frac{2\varepsilon\mu_k v r}{3RT\delta}$$
(5.4)

Substituting the average velocity of gases and porosity in to equation (5.4), we obtain

5.4

$$P = P_k = \frac{8n\mu_k r^3}{3\delta}\left(\frac{2\pi}{RTM}\right)^{\frac{1}{2}} \tag{5.4a}$$

Since the value of $\frac{8\mu_k}{3}\left(\frac{2\pi}{RT}\right)^{\frac{1}{2}}$ is constant (c), it is possible to write equation (5.4a) as,

$$P = \frac{cr^3}{\delta\sqrt{M}} \tag{5.5}$$

Especially for membranes with small pores a multilayer structure is preferred to provide maximum strength and minimum thickness of the active layer. For a multilayer membrane, with m layers of uniform thickness, if each layer obeys Knudsen law independently the total permeability **P** of the multilayer membrane is also related to those of the individual layers as equation (5.5) and show a $\sqrt{M}$ relationship.

$$\frac{1}{P} = \frac{1}{P_1} + \frac{1}{P_2} + \ldots + \frac{1}{P_m} = \frac{1}{\frac{cr_1^3}{\delta_1\sqrt{M}}} + \frac{1}{\frac{cr_2^3}{\delta_2\sqrt{M}}} + \ldots + \frac{1}{\frac{cr_m^3}{\delta_m\sqrt{M}}} = \frac{\sqrt{M}}{c}\left(\frac{\delta_1}{r_1^3} + \frac{\delta_2}{r_2^3} + \ldots + \frac{\delta_m}{r_m^3}\right) \tag{5.6}$$

where **P** is the permeability of the multilayer membrane, P_m is the permeability of each layer, c is constant and dependent of the shape of the pores, M is the molecular mass of the gas, δ_m is the thickness of each layer of the membrane and r_m is the mean pore radius of each layer of the membrane.

In the experimental measurements the test membrane is placed in an experimental cell. Due to a pressure difference, $\Delta p = p' - p'' > 0$, across the membrane gas permeates from the high to the low pressure side. Under experimental conditions the high pressure p' is

kept constant and as the experiment proceeds the low pressure p" increases. The low pressure side has constant volume V" and the rate of permeation of gas dn/dt can be evaluated from the rate of pressure increased dp"/dt. Since

$$p"V"=nRT \tag{5.7}$$

the rate of permeation of gas becomes equal to,

$$\frac{dn}{dt} = \frac{V"}{RT}\frac{dp"}{dt} \tag{5.8}$$

Defined as a gradient per unit area of membrane, A

$$J = \frac{1}{A}\frac{dn}{dt} = \frac{V"}{ART}\frac{dp"}{dt} \tag{5.9}$$

Since $\frac{d\Delta p}{dt} = \frac{dp'}{dt} - \frac{dp"}{dt}$ and $\frac{dp'}{dt} = 0$ as p' constant,

$$\frac{d\Delta p}{dt} = -\frac{dp"}{dt} \tag{5.10}$$

Substituting for $\dfrac{dp"}{dt}$ in the equation (5.9) becomes

$$J = -\frac{V"}{ART}\frac{d\Delta p}{dt} \tag{5.11}$$

In the steady state dΔp/dt is constant and equation (5.11) can be approximated by:

$$J = -\frac{V"}{ART}\frac{d\Delta p}{dt} \approx -\frac{V"}{ART}\frac{\Delta p}{\Delta t} \tag{5.12}$$

By using Equation (5.12) the flux density can be estimated experimentally from recorded values of the pressure in the high and low pressure sides and time, when the gas permeates through the membrane. Additionally from the slope of the graph of flux density versus transmembrane pressure, the permeability can be calculated.

Alternatively, if the permeability is defined by equation (5.1) where $\Delta p = p'-p"$, then

$$P = -\frac{V"}{ART}\left(\frac{d\Delta p}{dt}\frac{1}{\Delta p}\right) \tag{5.13}$$

Since the value of $\frac{V"}{ART}$ is constant and is related with the characteristic of the cell system. We can call $\beta = \frac{V"}{ART}$, then substituting in the equation (5.13) becomes

$$-\beta\left(\frac{d\Delta p}{\Delta p}\right) = P dt \tag{5.14}$$

Integrating equation (5.14) between the limits $t=0 \to \Delta p^0$ and $t = t \to \Delta p^t$, where Δp is the transmembrane pressure difference, becomes

$$\ln \Delta p' = -\frac{P}{\beta}t + \ln \Delta p^0 \tag{5.15}$$

If $\ln \Delta p$ is plotted versus t/β , the permeability P can be directly calculated by the inclination of the this graph.

5.2 Experimental

5.2.1 Gases

Nitrogen and carbon dioxide were purchase from BOC Limited, UK. Neon, propane, argon, nitrogen, hydrogen, helium were supplied by Messer Griesheim, Germany. All gases were at least 99.99 % of purity. The physical properties of these gases are summarised in Table 5.1.

5.2.2 Gas Permeation System

An automated gas system was constructed in the course of this research. This system enabled the determination gas permeability through a flat membrane. It was designed to apply a gas pressure in one side of the membrane cell (high pressure side) and collect the gas passing through the membrane in a well known collecting volume (V") in the other (low pressure side) side.

The gas permeation studies were carried out using the apparatus shown in Fig. 5.2. The equipment consisted of a pressurised gas cylinder, pressure regulator, membrane cell (detail of the membrane cell is shown in Fig. 5.3), pressure transducers and computer link for data logging. Membrane samples 10 mm in diameter and different thickness were supported in the cell and sealed by a rubber O-ring with 2 mm inner diameter (the exposed membrane area A (m^2) was $\pi.d^2/4$). The gas was fed into the high pressure side of the cell after it had been completely filled with the pure used gas. The permeability of pure gases was measured by monitoring pressure in both the high

and low pressure sides of the permeation cell as function of time. The low pressure side is constituted by a constant volume cylinder and the pressure tends to increase in this side when the gas permeate through the membrane. For each gas three test runs were made. The experiments were performed in a thermostated room at 293 K. The gas flow (J) in the steady state was obtained from equation (5.12) and calculated using equation:

$$J = \frac{1}{A}\frac{dn}{dt} \approx \frac{V''}{ART}\frac{\Delta p}{\Delta t}$$

where V'' (m^3) is the volume in the low pressure side of the cell, A (m^2) is the permeation area, R is the gas constant ($J.mol^{-1}.K^{-1}$), T is the temperature (K), Δp is the difference between the pressure in the high pressure side and low pressure side (Pa), Δt is the time difference (s) and n is the amount of moles of the gas permeated through the membrane. The permeability was calculated by two different ways: 1) by the gas flux per pressure drop through the membrane; and 2) by logarithm scale of the pressure difference versus time. In both case the permeability will be expressed in $mol.s^{-1}.m^{-2}.Pa^{-1}$.

5.3 Results and discussion

5.3.1 Gas permeability

Figures 5.4 to 5.9 show the transmembrane pressure dependence of the flux of various gases at a constant temperature (293K) for samples 72/1, 60/3, 40/5, 72/1/10/16, 72/1/5/20 and 72/1/5/40, respectively. The observed fluxes for these membranes were perfectly linear with the upstream transmembrane pressure, indicating that the permeabilities were constant at the experimental temperature. These results are better presented in the Figs. 5.10 to 5.15, where the pressure difference between the high pressure side and low pressure side, in log scale, is plotted against the time divided by the cell constant ($\frac{V''}{ART}$). It is interesting to note in second case the excellent linearity even for small pressure difference since in the first set of graphs (Figs. 5.4 to 5.9) there are superposition of the points for small pressure difference and the behaviour is not clear in this situation. In both situations, the permeability can be calculated directly by the slope of the curves. Table 5.2 shows a compilation of the permeabilities of the gases studied. The sample 60/3 shows a permeability slightly smaller than the sample 40/5. This occurs due to the difference in thickness between these samples, all at once a reduction in the pore diameter is expected with small voltage of anodisation. To better compare these results, the permeabilities of theses membranes are multiplied by the thickness of each membrane and the results for homogeneous membrane are compiled in Table 5.3. The results for the sample 72/1 are approximately 1.3 and 1.6 times bigger than the values obtained for the samples

60/3 and 40/5, respectively. This shows that pore size reduction occurs during the preparation of the samples when the voltage is reduced.

For asymmetric membranes, samples 72/1/10/16, 72/1/15/20 and 72/1/5/40, the permeabilities of the active layer are calculated from the multilayer permeability relationship, equation (5.6),

$$\frac{1}{P_{72/1/10/16}} = \frac{1}{P_{72/1}} + \frac{1}{P_{10/16}}$$ (5.13)

$$\frac{1}{P_{72/1/5/20}} = \frac{1}{P_{72/1}} + \frac{1}{P_{5/20}}$$ (5.14)

$$\frac{1}{P_{72/1/5/40}} = \frac{1}{P_{72/1}} + \frac{1}{P_{5/40}}$$ (5.15)

where $P_{72/1}$ $P_{72/1/10/16}$, $P_{72/1/5/20}$ and $P_{72/1/5/40}$ are experimental permeabilities for the samples 72/1, 72/10/16, 72/1/5/20 and 72/1/5/40, respectively, and $P_{10/16}$, $P_{5/20}$ and $P_{5/40}$ are the permeabilities for the active layer of the samples 72/1/10/16, 72/1/5/20 and 72/1/5/40, respectively. A compilation of these calculations are shown in Table 5.4. It can be observed that the permeability of the active layer of the sample 72/1/10/16 has increased by more than 30% in relation to the total permeability of the sample 72/1/10/16. In other words, the active layer of the sample 72/1/10/16 is responsible for approximately 70% of the resistance of the permeation of the gas. For samples 72/1/5/20 and 72/1/5/40 the contribution of the active layers to the resistance to the permeation of the gas are approximately 88 and 96%, respectively. It can also be

observed that the values of the permeabilities for active layer of the sample 72/1/10/16 are approximately 3.5 and 10.9 times larger than the samples 72/1/5/20 and 72/1/5/40, respectively. However, to better compare these results the permeabilities of the active layer of these samples were also multiplied by the thickness of the active layer for each sample and the results are on shown in Table 5.5. It was observed from these results that the values obtained for sample 71/1/10/16 are approximately 5.2 and 8.2 times larger than the values obtained for samples 72/1/5/20 and 72/1/5/40, respectively. These magnitudes are reasonable since it expected double of pore size for the sample 72/1/10/16 in relation to the samples 72/1/5/20 and 72/1/5/40, according to the formation voltage discussed in the Chapter 4. Also the permeability of the active layer multiplied by the thickness for sample 72/1/5/20 is 1.6 times, approximately, the value for the sample 72/1/5/40 and this value is bigger than it was expected, since the pore size of these sample could be similar according to the formation voltage, as discussed in Chapter 4. Furthermore from the Figures 5.4 to 5.15 and on the tables 5.2 and 5.4 it can be observed that in all samples the permeability show a tendency to increase when the molecular weight of the gases tend to decrease. This suggest that the mechanism of permeation can be due to Knudsen diffusion in a open pore, as indicate by the Equations 5.4 and 5.6, where the permeability show a inverse square root of molecular mass of the gas correspondence.

To clarify the contribution of Knudsen flow in each sample the inverse of the square root of the molecular weight of the gases dependence of the permeability was plotted in the Figures 5.16 to 5.21. Also the permeabilities of the gases for the active layer of

the samples 72/1/10/16, 72/1/5/20 and 72/1/5/40 are plotted against the inverse square root of molecular mass of the gases, according to equations 5.6, in Figs. 5.22 to 5.24. All gases show a good linearity for different samples. The gas least likely to be more stable is helium and on this base an ideal Knudsen line was plotted in these graphs. These results strongly demonstrate that the permeation of gases through these membranes follow Knudsen diffusion under the conditions of this study. This suggests that the pore diameter of the samples are obviously less than the mean free path of the gases (Table 5.1) in the pressure range from 1 to 2 atm and 293K. At these low pressures, the contribution of Poiseuille flow to the overall permeation is generally very small for the gases examined. All these results indicate that gas permeation is just due only to Knudsen diffusion when the pore diameter decreases to values from less than 70 nm.

5.3.2 Pore size characterisation

It was demonstrated in the previous Section (5.3.1) that Knudsen flow is the main mechanism of gas permeation for the samples studied and that Pouseuille contribution to overall the gas flow rate is negligible. So, in this case the pore diameter for the samples can be evaluated by applying Equation (5.4) and using the following values: velocity of gas (v) on Table 5.1, shape factor $\mu=1$, and thickness (δ) of the samples on tables 3.1 and 3.2 (Chapter 3), permeability (P) on Table 5.2 for the samples 72/1, 60/3 and 40/5 and on Table 5.3 for samples 72/1/10/16, 72/1/5/20 and 72/1/5/40. The calculation has been done in two different ways: 1) using the density of pores (n)

determined from SEM images, on Table 4.3, and the modified Knudsen Equation (5.4a); and 2) using constant porosity (ε=0.1, this value was estimated using Equation (4.1), in Chapter 4) and equation 5.4. Tables 5.6 and 5.7 show a compilation of the pore diameter and statistical calculations of the population for each sample. It can be immediately seen that the pore diameter is reduced with decreasing voltage of anodisation, from samples 72/1 to 72/1/5/40. The average values of the pore diameter estimated using constant porosity for samples 72/1, 60/3 are larger than the values estimated using pore density. On the other hand, the average pore diameter estimated by constant porosity for samples 40/5, 72/1/10/16, 72/1/5/20 and 72/1/5/40 are smaller than the values estimated by using pore density, mainly for small pore size, where the values are smaller by a factor of two. Furthermore, the pore diameter estimated by using constant porosity show greater standard deviation when compared to the values estimated by using pore density and also confirm that the most stable gas is helium, with values of pore diameter very close to the average values. If the values of pore diameter estimated by the Knudsen equations are compared with the values estimated by SEM and formation voltage (D/d), on Table 5.6 and Fig. 5.21, we observed a good agreement between SEM and the values calculated by gas permeation and also by formation voltage. For the samples 72/1/10/16, 72/1/5/20 and 72/1/5/40, which the pore diameter could not be estimated by SEM, the results obtained by gas permeation are very close to the formation voltage, except for sample 72/1/5/20 and 72/1/5/40 using gas permeation and constant porosity. In this case the values of pore diameter are half the values estimated by formation voltage and by gas permeation using pore

5.14

density. These different results obtained by gas permeation and voltage formation suggest different explanations. Firstly, the method used based on pore density has a cubic relation between pore radii and permeability of the gases, see equation 5.4a, and a small variation in permeability can cause a large variation on the pore diameter estimation. Secondly, the method based on voltage formation is very simply and is based on D=2.8V, although it was observed in Chapter 2 that for small voltages (<4V) the electrode is polarised and current is zero. Another hypothesis that can be formulated from the pore diameter calculations using gas permeation is that when the voltage formation is reduced from 72 to 5 V it is not only the pore size of the membrane that is reduced but also the number of pores per area, at least for the samples analysed is this study.

5.4 Conclusions

Gas permeation measurements were performed using flat anodic alumina membranes with different pore sizes and high structure regularity prepared in Chapter 2. It has been demonstrated that the main mechanism of gas permeation on anodic alumina membranes was controlled by Knudsen diffusion. The pore size diameters of the samples are readily measurable by two different methods described here. When the results of gas permeation are compared with predictions from the formation voltage it was found that small differences between pore diameters mainly for 72/1, 60/3 and 40/5 samples arise. Also good agreement between the direct observation by SEM and Knudsen predictions were observed for sample 72/1, 60/3 and 40/5. The study of gas permeation suggests that when the formation voltage is reduced from 72 to 5 V the pore size of the membrane is also reduced, the number of pores per area is similarly reduced.

5.5 References

[1] J. Rocek and P. Uchytil, Evaluation of selected methods for characterization of ceramic membranes, J. Membr. Sci., 89 (1994) 119.

[2] P. Dietz, P. K. Hansma, O. Inacker, H. D. Lehmann, and K. H. Hermann, Surface pore structures of micro- and ultrafiltration membranes imaged with the atomic force microscope, J. Membr. Sci., 65 (1992) 101.

[3] P. Neufeld, N. K. Nagpaul, R. Ashdown and M. Akbar, Crystallization of anodic Al_2O_3, Electrochim. Acta, 17 (1972) 1543-1546.

[4] Y. Yuxun and W. Diyong, Pore size of composite inorganic membrane, Proceedings of the third International Conference on Inorganic Membranes, Worcester, July, 1994, pp. 525.

[5] P. Uchytil, Gas Permeation in ceramic membranes. Part I. Theory and testing of ceramic membranes, J. Membr. Sci., 97 (1994) 139.

[6] P. Uchytil and Zdenek Broz, Gas permeation in ceramic membranes. Part II. Modelling of gas permeation through ceramic membrane with one supported layer, J. Membr. Sci., 97 (1994) 145.

[7] F. W. Altena, H. A. M. Knoef, H. Heskamp, D Bargeman, and C. A. Smolders, Some comments on the applicability of gas permeation methods to characterize porous membranes based on improved experimental accuracy and data handling, J. Membr. Sci., 12 (1983) 313.

[8] P. Uchytil, Z. Wagner, J. Rocek, Z. Broz, Possibility of pore size determination in separation layer of ceramic membrane using permeation method, J. Membr. Sci., 103 (1995) 151.

[9] P. Uchytil, X. Q. Nguyen, and Z. Broz, Characterization of membrane skin defects by gas permeation method, J. Membr. Sci. 73 (1992) 47.

[10]K. Keizer, R. J. R. Uhlhorn, R. J. Van Vuren, and A. J. Burggraaf, Gas separation mechanisms in microporous modified γ-Al$_2$O$_3$ membranes, J. Membr. Sci., 39 (1988) 285.

[11]R. J. R. Uhlhorn, K. Keizer, and A. J. Burggraaf, Gas transport and separation with ceramic membranes. Part I. Multilayer diffusion and capillary condensation, J. Membr. Sci., 66 (1992) 259

[12]P. Levitz, Knudsen diffusion and excitation transfer in random porous media, J. Phys. Chem., 97 (1993) 3818.

[13]R. L. Rowell, S. A. Carrano, A. J. Bethune, and A. P. Malinauskas, Gas and vapour permeability: surface flow through porous media, J. Colloid Interface Sci., 37 (1971) 242.

[14]R. W. Schofield, A. G. Fane, and C. J. D. Fell, Gas and vapour transport through microporous membranes. I. Knudsen-Poiseuille transition, J. Membr. Sci., 53 (1990) 159.

[15]R. Datta, S. Dechapanichkul, J. S. Kim, L. Y. Fang, and . Uehara, A generalized model for the transport of gases in porous, non-porous, and leaky membranes. I. Application to single gases, J. Membr. Sci., 75 (1992) 245.

[16]M. Bhandarkar, A. B. Shelekhin, A. G. Dixon, and Y. H. Ma, Adsorption, permeation, and diffusion of gases in microporous membranes. I. Adsorption of gases on microporous glass membranes, J. Membr. Sci., 75 (1992) 221.

[17]R. J. R. Uhlhorn, K. Keizer, and A. J. Burggraaf, Gas and surface diffusion in modified γ-alumina systems, J. Membr. Sci., 46 (1989) 225.

[18]K. Keizer, R. J. R. Uhlhorn, V. T. Zaspalis, and A. J. Burggraaf, Transport and related (gas and vapour) separation in ceramic membranes, Key Eng. Mater., 61 & 62 (1991) 143.

[19]M. Knudsen, Kinetic theory of gases. Some modern aspects, 3rd Ed., Methuen & Co. Ltd., 1950.

[20]J. Randon, P. P. Mardilovich, A. N. Govyadinov, and R. Paterson, Computer simulation of inorganic membrane morphology. Part 3. Anodic alumina films and membranes, J. Colloid Interface Sci., 169 (1995) 335.

[21]P. P. Mardilovich, A. N. Govyadinov, J. Randon, S. McFadzean and R. Paterson, New high temperature chemically resistant anodic alumina membranes: preparation, modification, properties, Proc. 3th Intern. Conf. on Inorg. Membr., Worchester, Massahusetts, USA, 1994, 457.

[22]J. Randon, P. P. Mardilovich, A. N. Govyadinov, and R. Paterson, Modelling the pore structure of anodic alumina membranes, Proc. 3th Intern. Conf. on Inorg. Membr.., Worchester, Massachusetts, USA, 1994, 613.

[23]R.C. Furneaux and M. C. Thornton, Porous "Ceramic" membranes from anodizing aluminium, Adv. Ceram. Chem. Process Eng., 43 (1988) 93.

[24]Handbook of Chemistry and Physics, CRC Press Inc., USA, 75th Ed., 1994.

[25]P. W. Atkins, Physical Chemistry, 3th Ed, Oxford University Press, Oxford, pg. 652, 1987.

[26]D. W. Breck, Zeolite Molecular Sieve, John Wiley and Sons, New York, 1974.

Table 5.1 - Physical Properties of Measured Gases

Gas	H_2	He	Ne	N_2	O_2	Ar	CO_2	C_3H_8
Mw (g/mol)	2.00	4.00	20.17	28.04	32.00	39.94	44.00	44.10
λ(nm)([a])	111.00	174.00	124.00	59.00	63.00	63.00	55.0([b])	-
σ(Å)([c])	2.89	2.60	2.75	3.64	3.46	3.40	3.30	4.30
v(m/s)([d])	1760.70	1245.00	556.80	470.60	440.20	393.70	375.40	375.40

([a]) Mean free path (λ) of gases at pressure of 1 atm and 273 K [24]

([b]) Mean free path (λ) of the gas CO_2 at 1 atm and 298 K [25].

([c]) Minimum kinetic (sieving) diameters (σ) from the zeolite literature [26].

([d]) Velocity of gases (v) calculated using the Equation $(8RT/\pi M)^{1/2}$ at 293 K.

Table 5.2 - Experimental gas permeabilities for anodic alumina membranes, including support plus active layer (multilayer)

	Permeability $(mole.s^{-1}.m^{-2}.Pa^{-1}) \times 10^7$					
	Membrane					
Gas	72/1	60/3	40/5	72/1/10/16	72/1/5/20	72/1/5/40
H_2	592.30	314.30	394.10	207.00	70.50	23.75
He	463.50	223.20	287.90	154.90	54.60	17.47
Ne	215.60	108.50	133.70	54.80	25.30	9.54
N_2	200.80	86.30	110.00	64.80	23.50	7.23
O_2	176.10	79.30	94.60	66.60	22.60	7.49
Ar	158.10	74.20	84.80	51.70	21.40	6.86
CO_2	138.70	72.50	76.90	45.00	16.40	6.45
C_3H_8	159.40	72.70	82.20	49.50	19.80	8.99

Table 5.3 - Experimental gas permeabilities multiplied by the thickness for homogeneous anodic alumina membranes

	Permeability x thickness $(mole.s^{-1}.m^{-1}.Pa^{-1}) \times 10^{10}$		
	Membrane		
Gas	72/1	60/3	40/5
H_2	13.62	11.63	9.85
He	10.66	8.26	7.20
Ne	4.96	4.01	3.34
N_2	4.62	3.19	2.75
O_2	4.05	2.93	2.37
Ar	3.64	2.75	2.12
CO_2	3.19	2.68	1.92
C_3H_8	3.67	2.69	2.06

Table 5.4 - Experimental permeability for the active layer of the multilayer membranes

	Permeability $(mole.s^{-1}.m^{-2}.Pa^{-1}) \times 10^7$		
	Membrane		
Gas	72/1/**10/16** (*)	72/1/**5/20** (*)	72/1/**5/40** (*)
H_2	318.21	80.02	24.74
He	232.65	61.89	18.15
Ne	73.48	28.66	9.98
N_2	95.68	26.61	7.50
O_2	107.11	25.93	7.82
Ar	76.82	24.75	7.17
CO_2	66.61	18.60	6.76
C_3H_8	71.80	22.61	9.53

(*) Value calculated based on Equations (5.13), (5.14) and (5.15) and experimental value of the support 72/1, on Table 5.2.

Table 5.5 - Experimental permeability multiplied by the thickness of the active layer of the multilayer anodic alumina membranes

	Permeability x thickness $(mole.s^{-1}.m^{-1}.Pa^{-1})x10^{10}$		
	Membrane		
Gas	72/1/**10/16**	72/1/**5/20**	72/1/**5/40**
H_2	2.86	0.48	0.30
He	2.09	0.37	0.22
Ne	0.66	0.17	0.12
N_2	0.86	0.16	0.09
O_2	0.96	0.16	0.09
Ar	0.69	0.15	0.09
CO_2	0.60	0.11	0.08
C_3H_8	0.65	0.14	0.11

Table 5.6 - Pore diameter of active layer of anodic alumina membrane estimated by using Knudsen law and pore density estimated by SEM.

Pore diameter (nm)(*)					
Membrane					
Gas	72/1	60/3	40/5	72/1/**10/16** (**)	72/1/**5/20** (**)	72/1/**5/40** (**)
H_2	56.45	47.87	41.85	12.93	5.53	4.71
He	58.39	47.94	42.31	13.07	5.70	4.77
Ne	59.16	49.29	42.84	11.64	5.76	5.11
N_2	61.11	48.30	42.46	13.45	5.95	4.91
O_2	59.81	48.02	41.29	14.28	6.03	5.09
Ar	59.88	48.74	41.32	13.26	6.16	5.14
CO_2	58.24	49.14	40.63	12.85	5.69	5.12
C_3H_8	61.01	49.19	41.55	13.18	6.07	5.74
Average	59.26	48.56	41.78	13.08	5.86	5.07
Stan. Dev.	1.45	0.56	0.68	0.68	0.21	0.30

(*) Based on Knudsen law (Equation 5.4a) and using pore density from SEM.
(**) The pore diameter refer to active layer in these asymmetric membranes.

Table 5.7 - Pore diameter of active layer of anodic alumina membrane estimated by using Knudsen law and constant porosity.

	Pore diameter (nm)(*)					
	Membrane					
Gas	72/1	60/3	40/5	72/1/**10/16** (**)	72/1/**5/20** (**)	72/1/**5/40** (**)
H_2	56.50	48.24	40.87	11.88	2.00	1.23
He	62.53	48.45	42.23	12.28	2.18	1.28
Ne	65.03	52.67	43.85	8.68	2.26	1.57
N_2	71.67	49.57	42.69	13.37	2.48	1.40
O_2	67.19	48.69	39.25	16.00	2.58	1.56
Ar	67.44	50.94	39.33	12.83	2.76	1.60
CO_2	62.06	52.20	37.41	11.67	2.17	1.58
C_3H_8	71.32	52.34	39.99	12.57	2.64	2.23
Average	65.47	50.39	40.70	12.41	2.38	1.55
Stan. Dev.	4.75	1.75	1.99	1.90	0.25	0.29

(*) Based on Knudsen law (Equation 5.4) and using constant porosity (ε=0.1).
(**) The pore diameter refer to active layer in these asymmetric membranes.

Table 5.8 - Comparison of pore size estimated by anodisation voltage, gas permeation and SEM.

Pore diameter (nm)				
Membrane sample	based on Permeability [2]	based on Permeability [3]	based on D/d [4]	based on SEM
72/1	59.3±1.4	65.5±4.7	67.00	64±14
60/3	48.7±0.6	50.4±1.7	55.80	50±6
40/5	41.8±0.7	40.7±2.0	37.20	40±8
72/1/**10/16**[1]	13.08±0.68	12.41±1.90	9.30	-
72/1/**5/20**[1]	5.86±0.21	2.38±0.25	4.60	-
72/1/**5/40**[1]	5.07±0.30	1.55±0.29	4.60	-

[1] Pore size is relate to the active layer of the membrane.
[2] Based on Knudsen law (Equation 5.4a) and using pore density from SEM.
[3] Based on Knudsen law (Equation 5.4) and using constant porosity (ε=0.1).
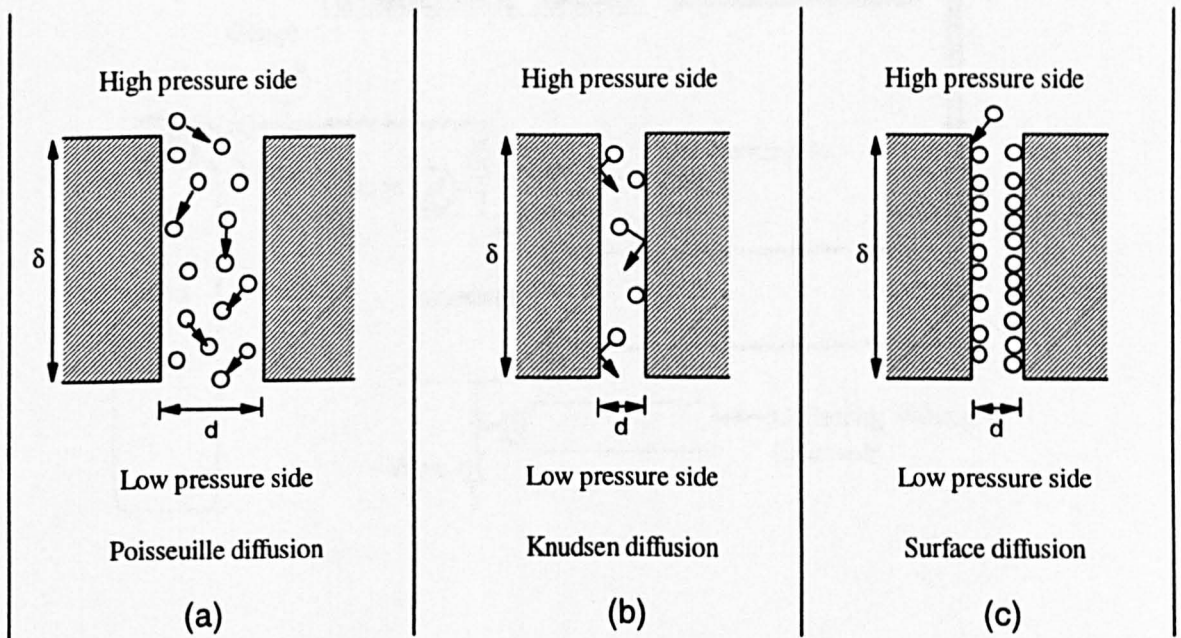[4] Value calculated based on D=2.8 nm/V, D/d = 3.0.

Fig. 5.1 - Schematic drawings showing membrane gas transport:
(a) Poisseuille, (b) Knudsen and (c) surface diffusion.

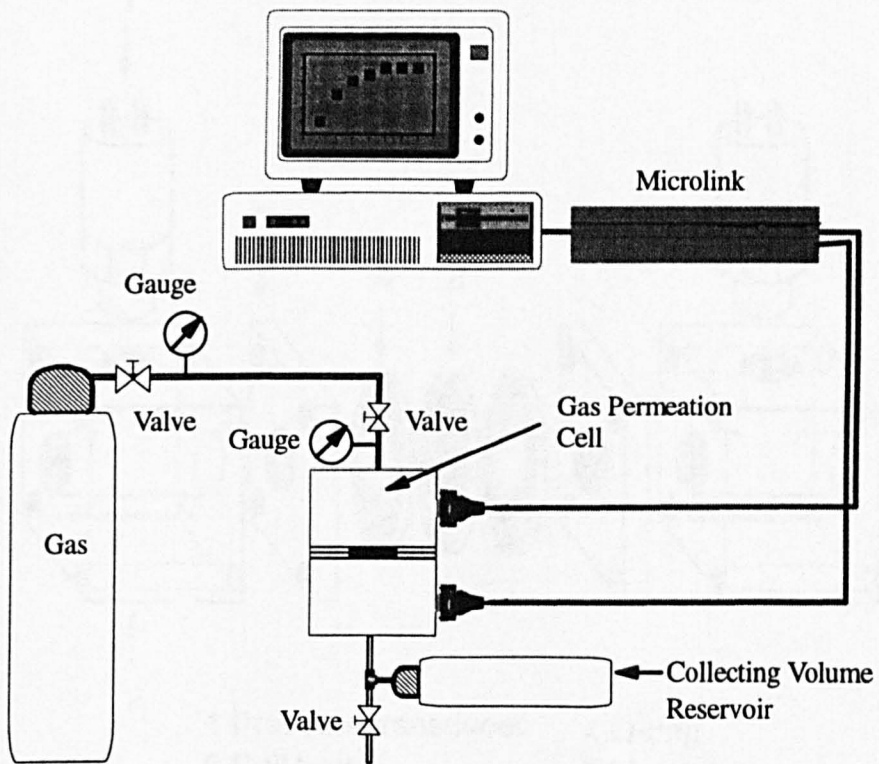Fig. 5.2 - Schematic diagram of gas permeation system

1

3

4 5

2

1 Pressure transducer 4 O-ring
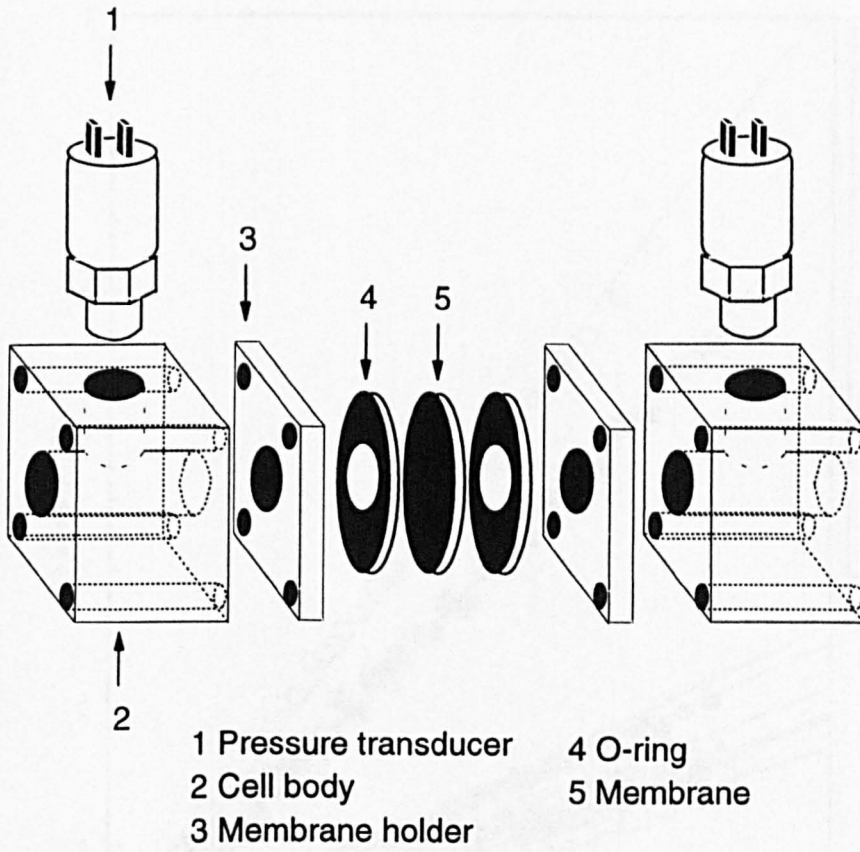2 Cell body 5 Membrane
3 Membrane holder

Fig. 5.3- Schematic diagram for gas permeation cell

Fig. 5.4 - Gas flux versus transmembrane pressure with different gases for the sample 72/1

Fig. 5.5 - Gas flux versus transmembrane pressure with different
gases for the sample 60/3
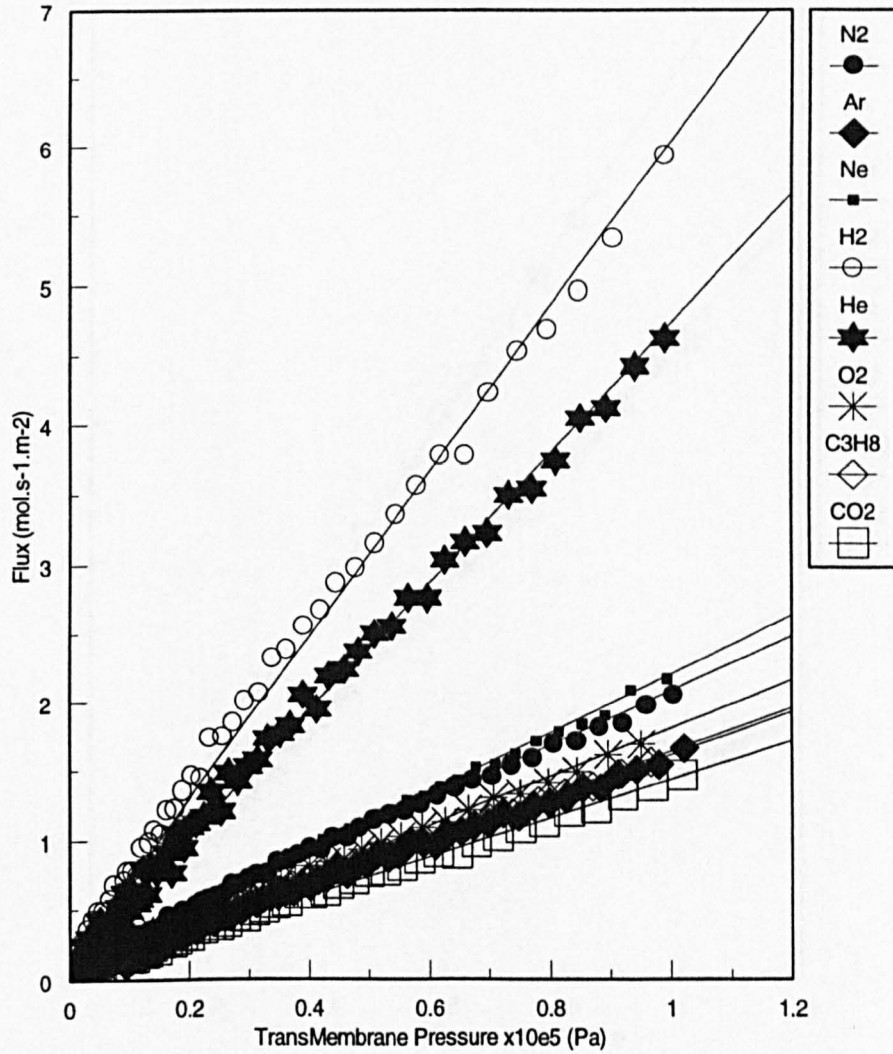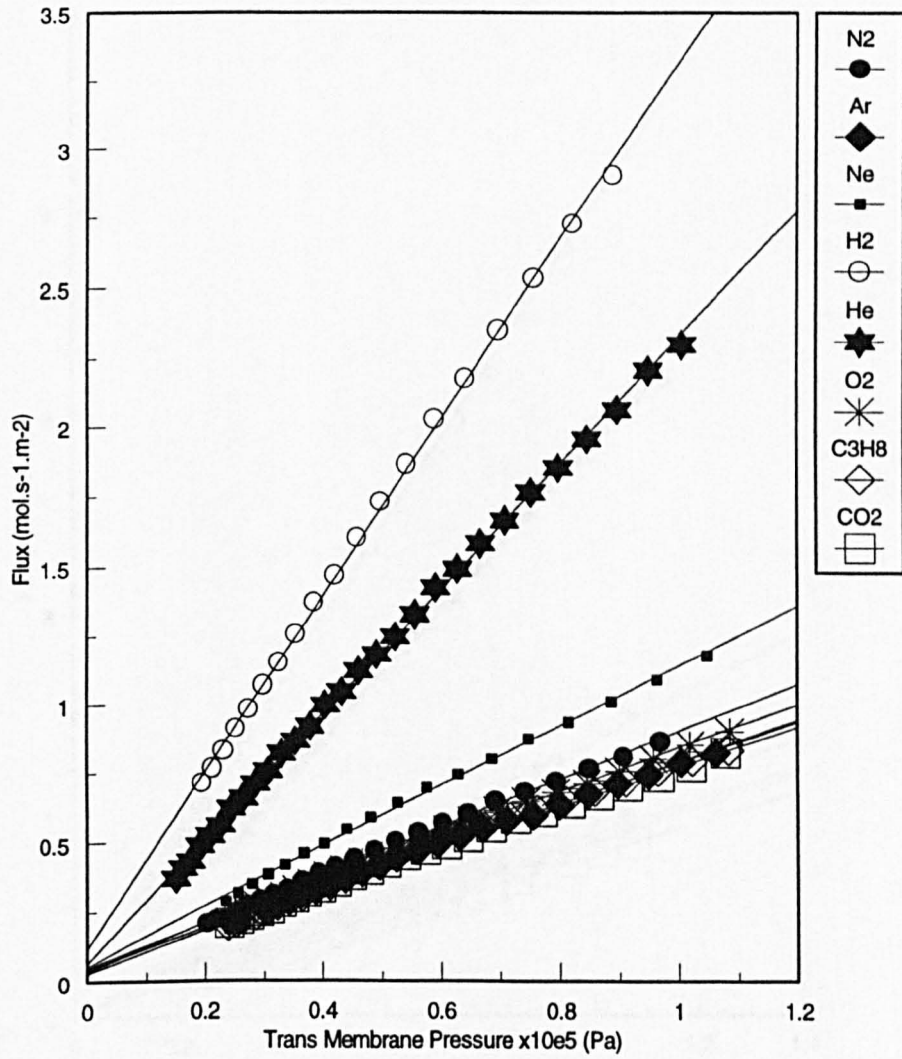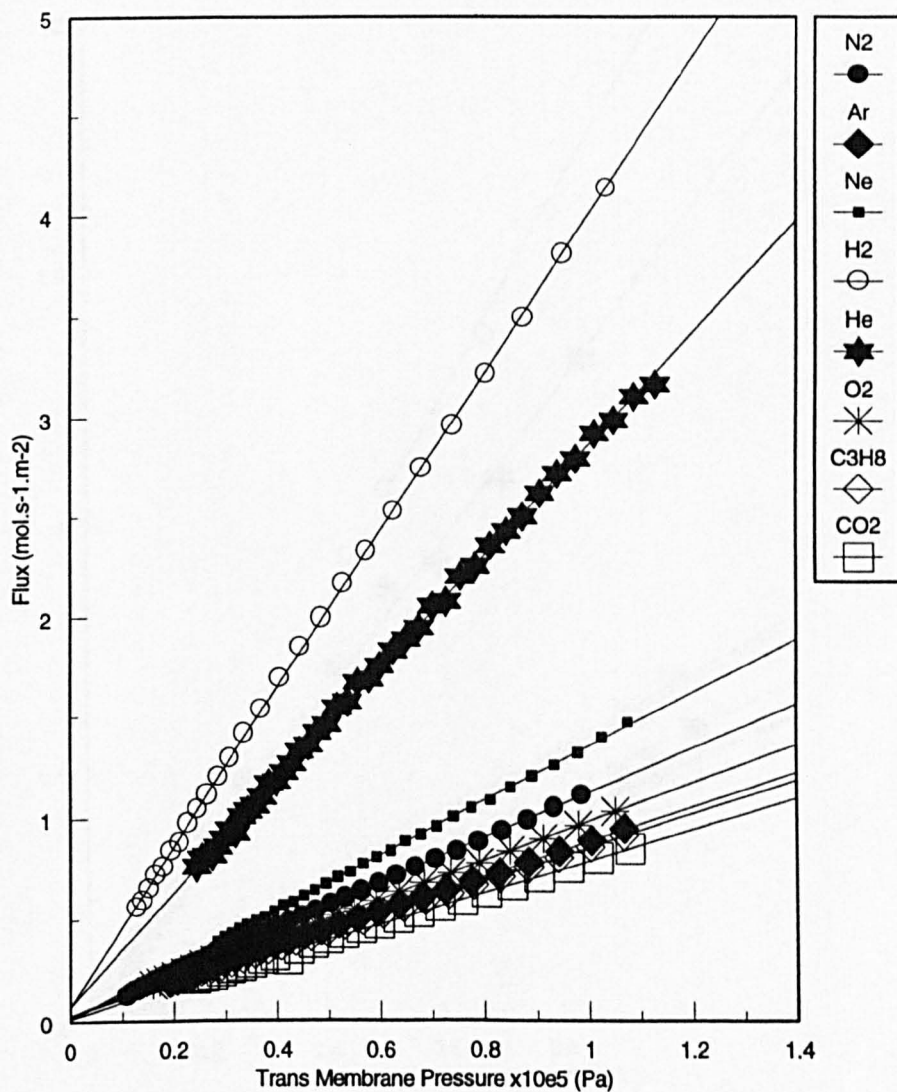
Fig. 5.6 - Gas flux versus transmembrane pressure with different gases for the sample 40/5

Fig. 5.7 - Gas flux versus transmembrane pressure with different gases for the sample 72/1/10/16
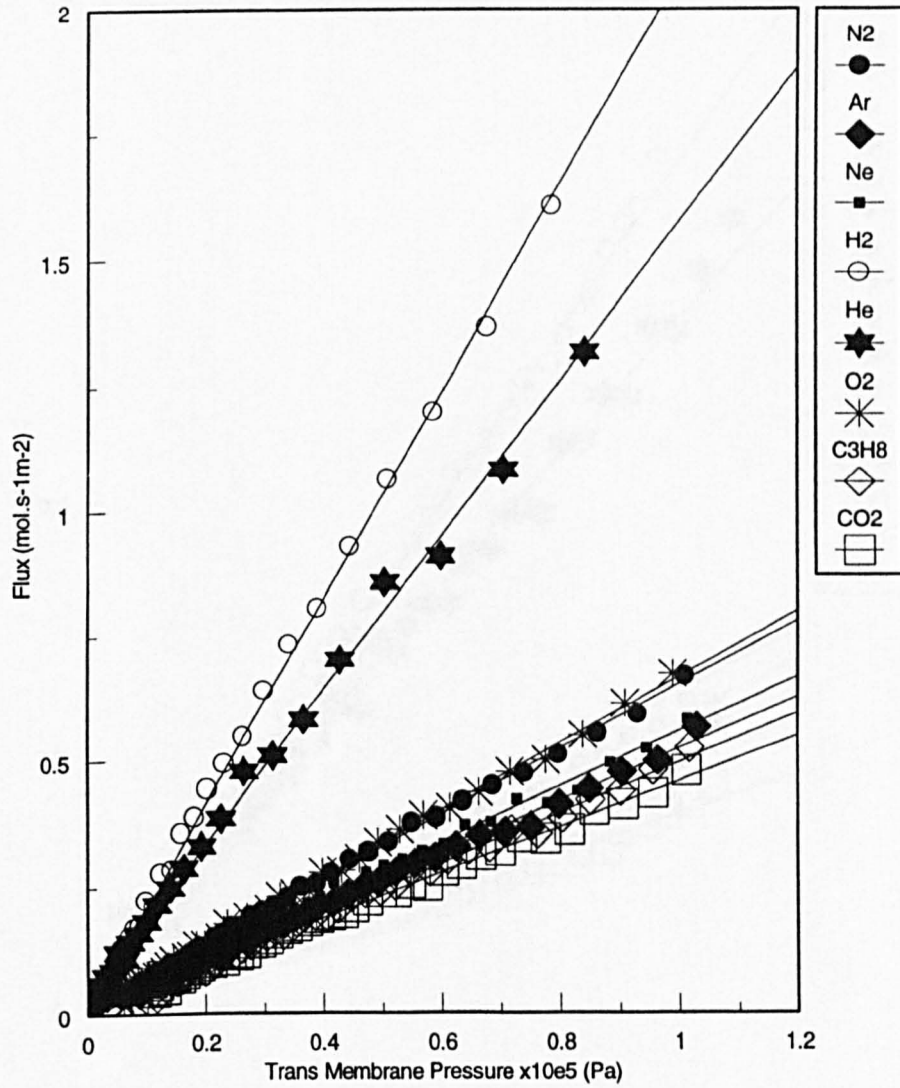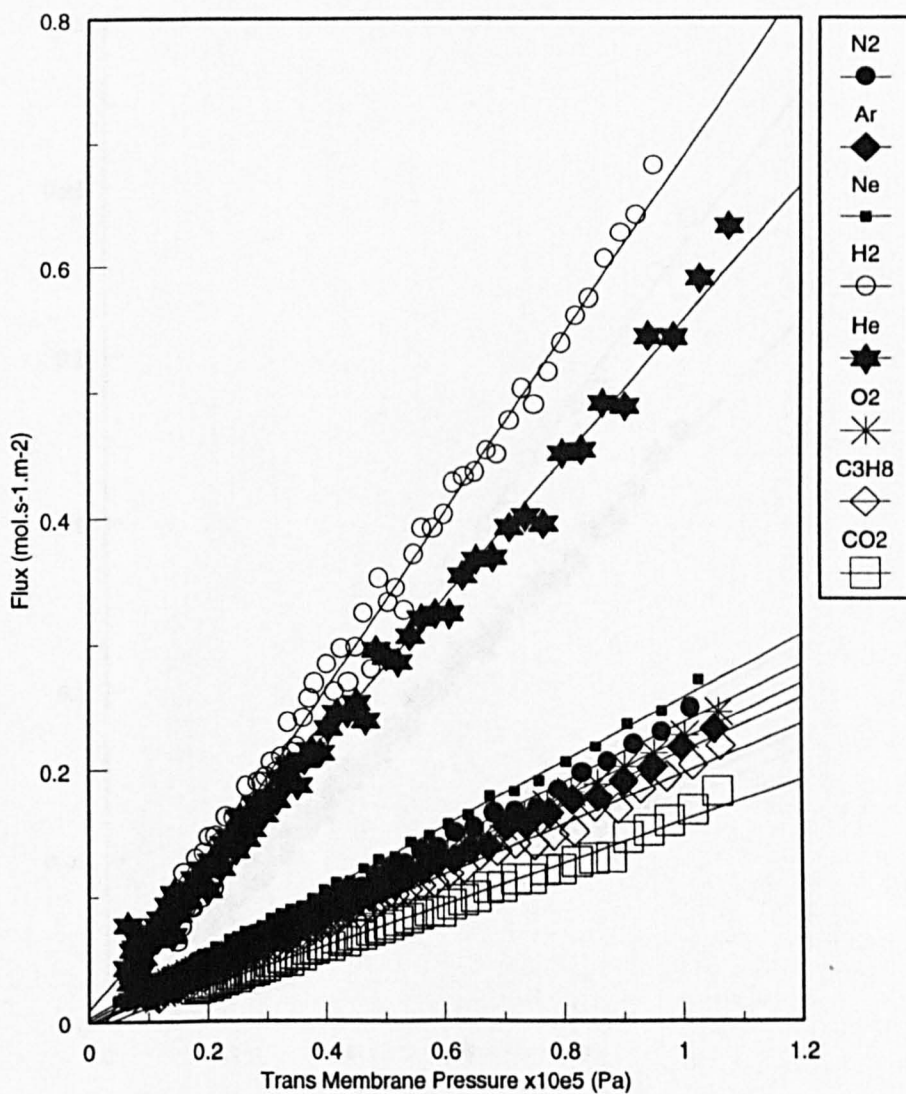
Fig. 5.8 - Gas flux versus transmembrane pressure with different gases for the sample 72/1/5/20
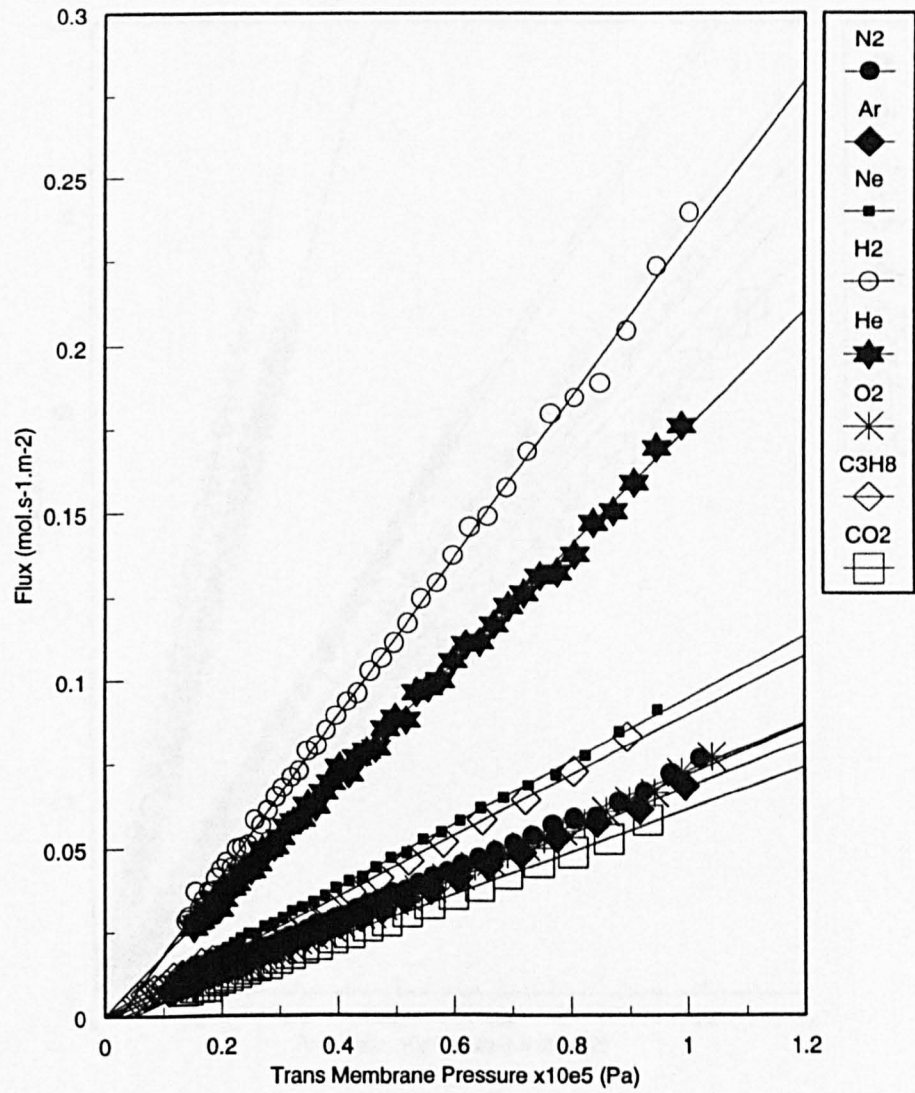
Fig. 5.9 - Gas flux versus transmembrane pressure with different
gases for the sample 72/1/5/40
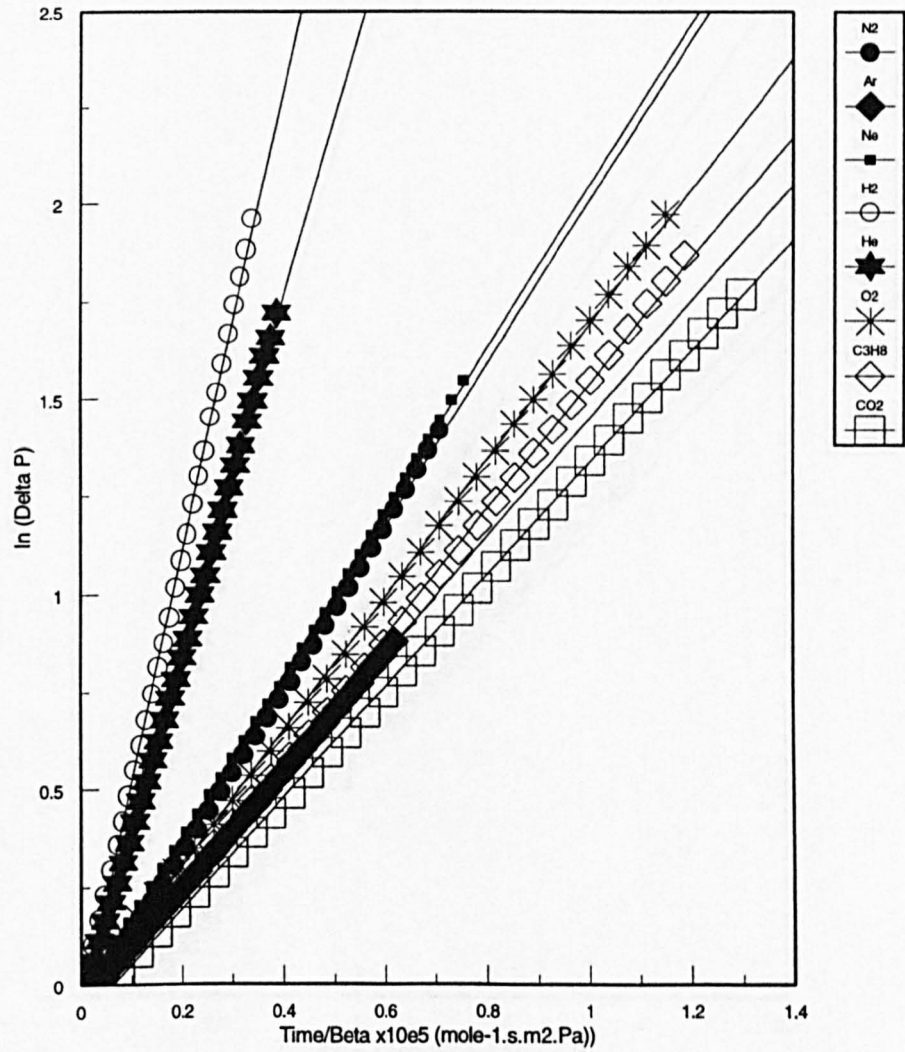
Fig. 5.10- Logarithm of pressure difference versus time with different gases for the sample 72/1
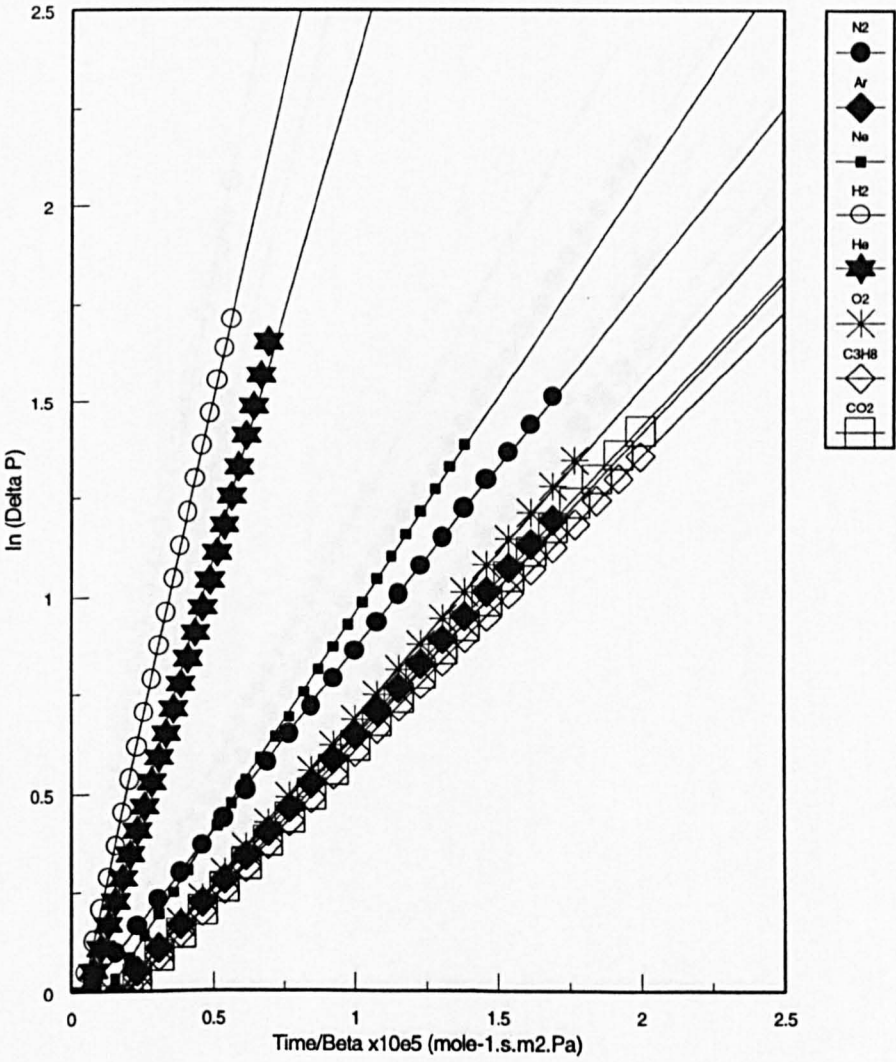
Fig. 5.11- Logarithm of pressure difference versus time with different gases for the sample 60/3
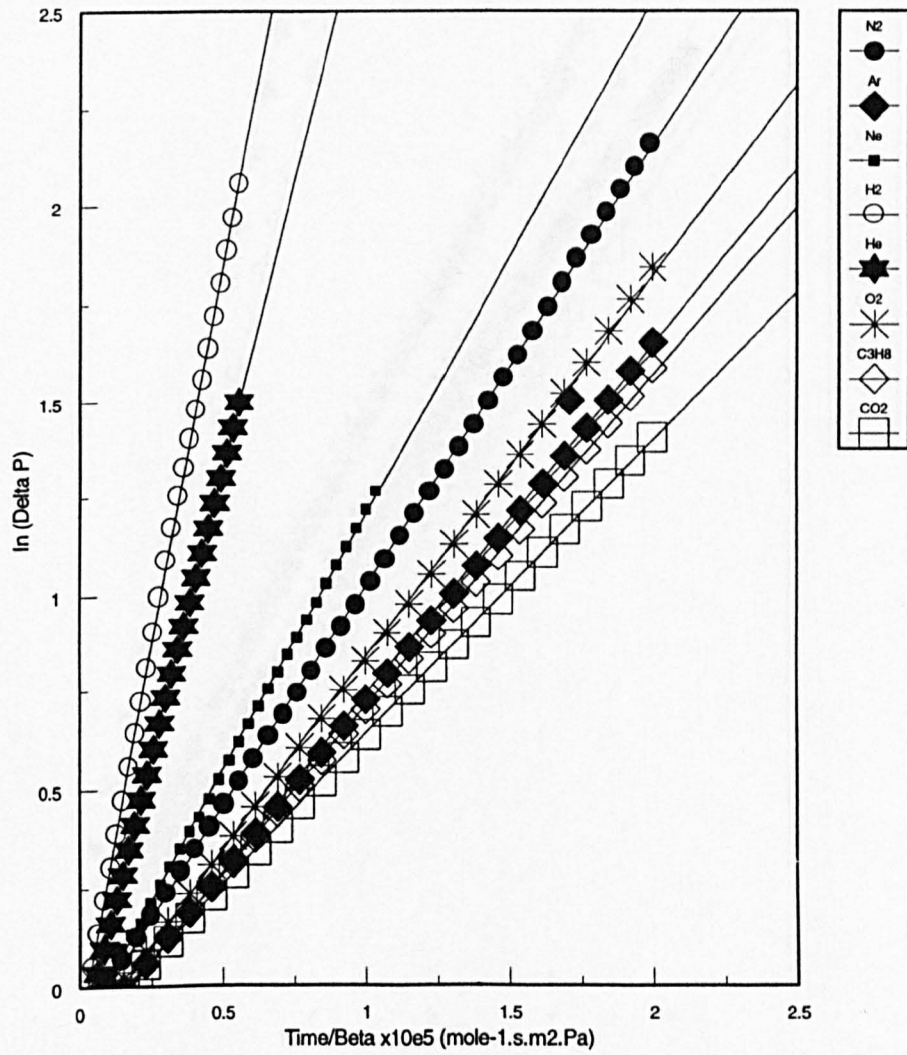
Fig. 5.12- Logarithm of pressure difference versus time with different gases for the sample 40/5
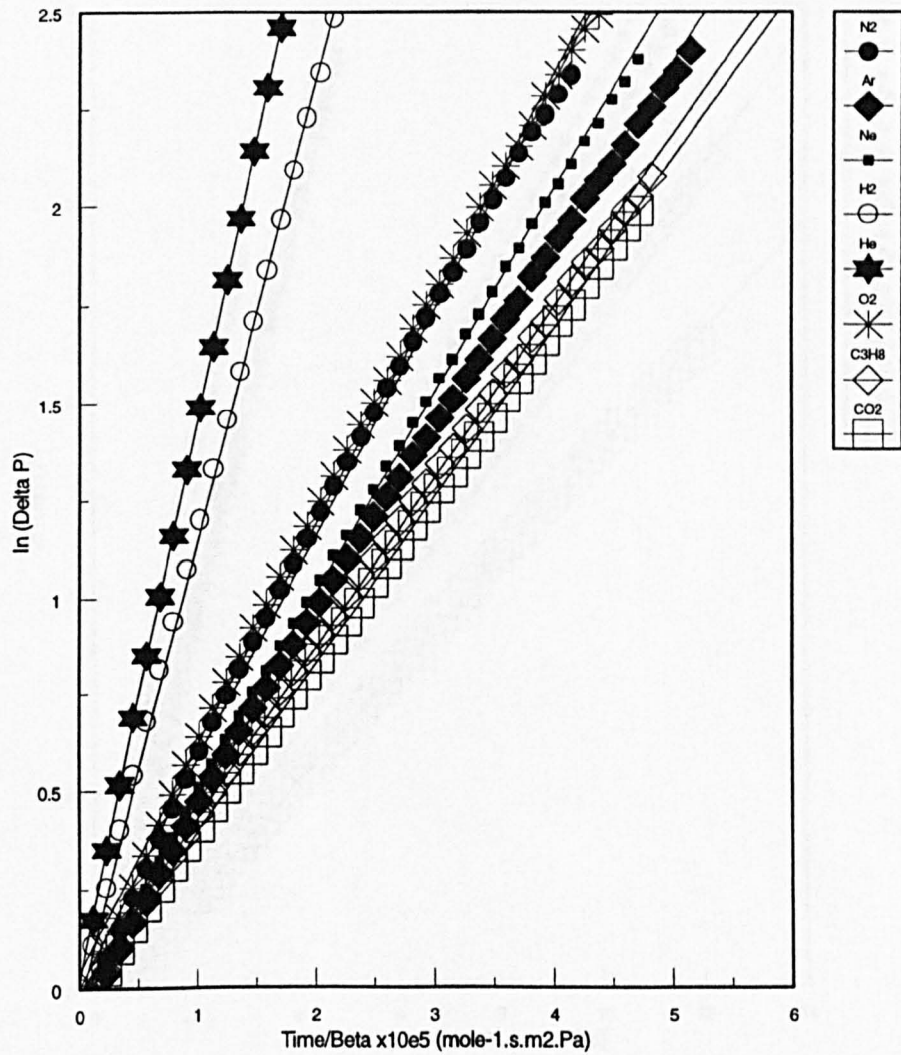
Fig. 5.13- Logarithm of pressure difference versus time with different gases for the sample 72/1/10/16
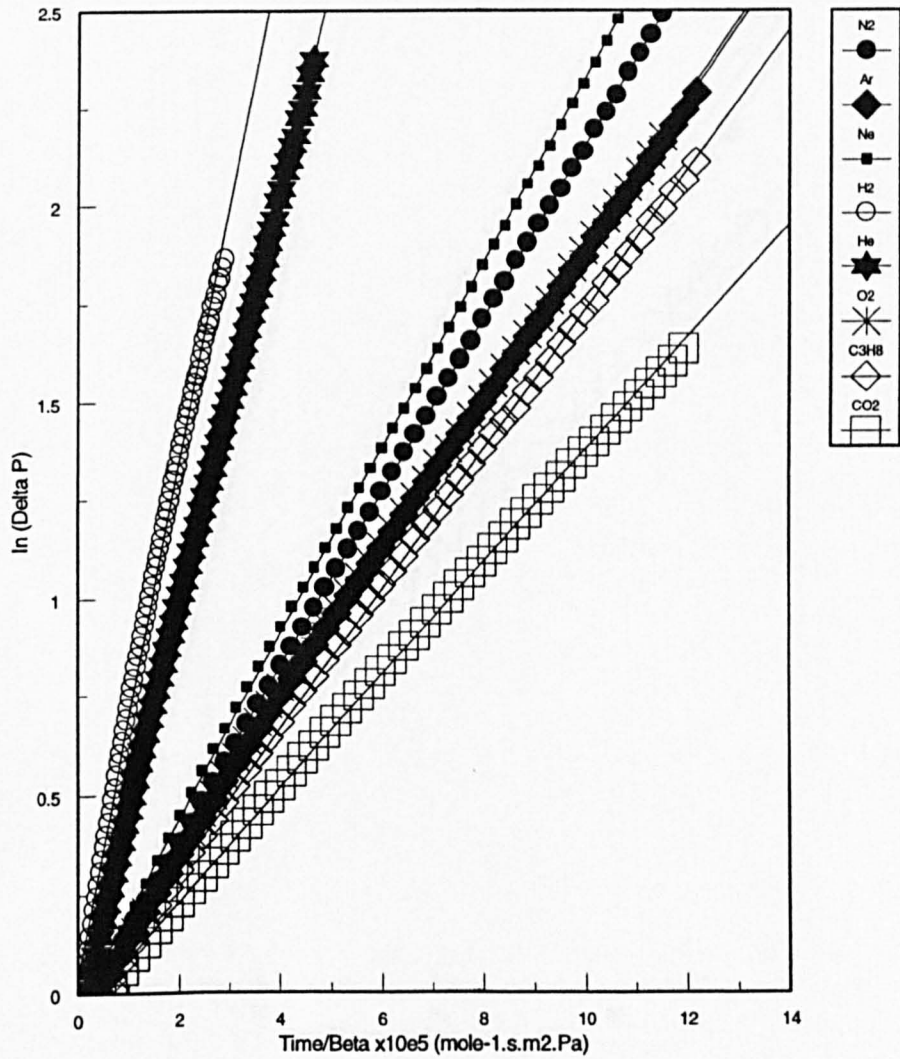
Fig. 5.14- Logarithm of pressure difference versus time with different
gases for the sample 72/1/5/20
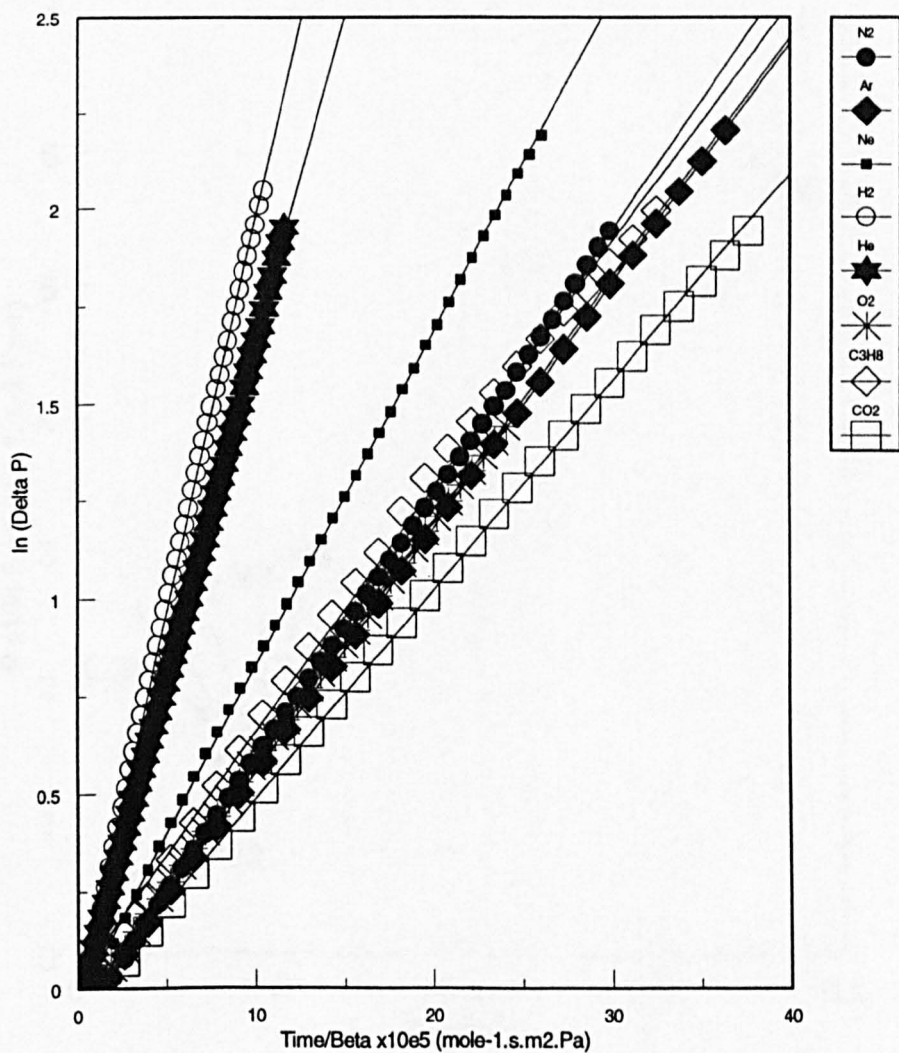
Fig. 5.15- Logarithm of pressure difference versus time with different gases for the sample 72/1/5/40
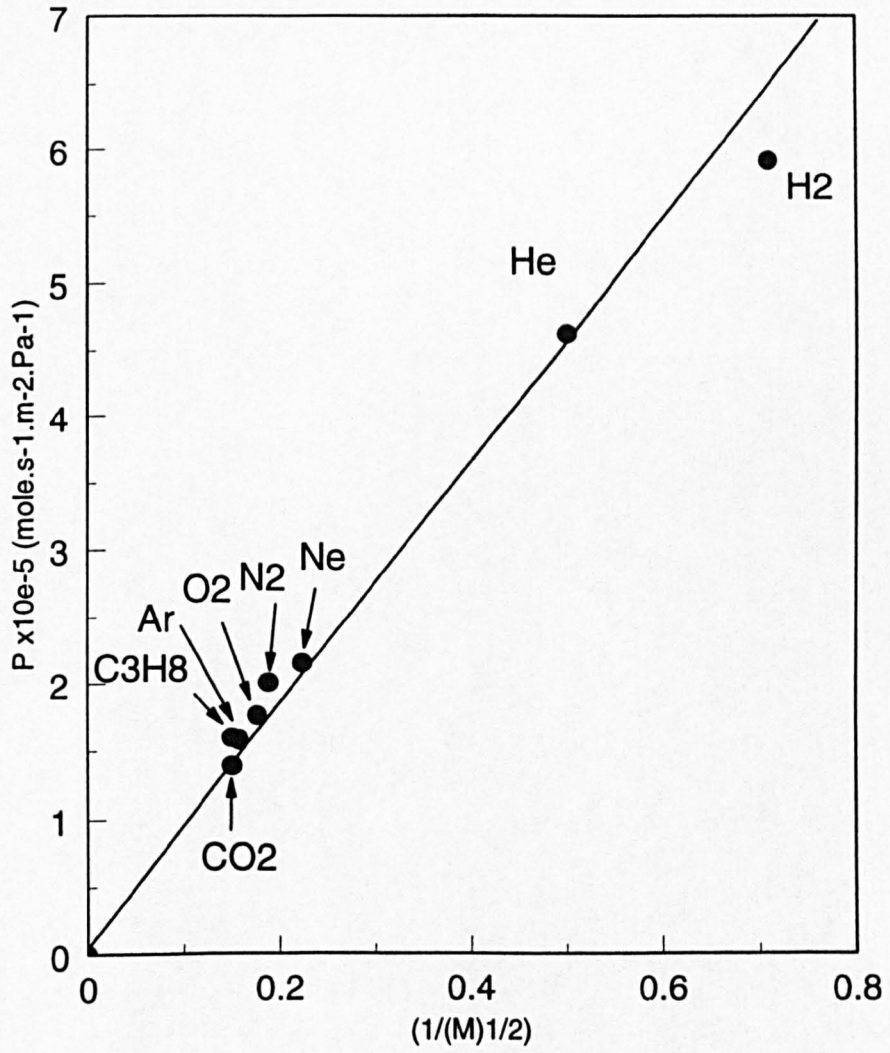
Fig. 5.16 - Variation of the permeation flux with the inverse of the square root of the molecular weight of the gases for the sample 72/1
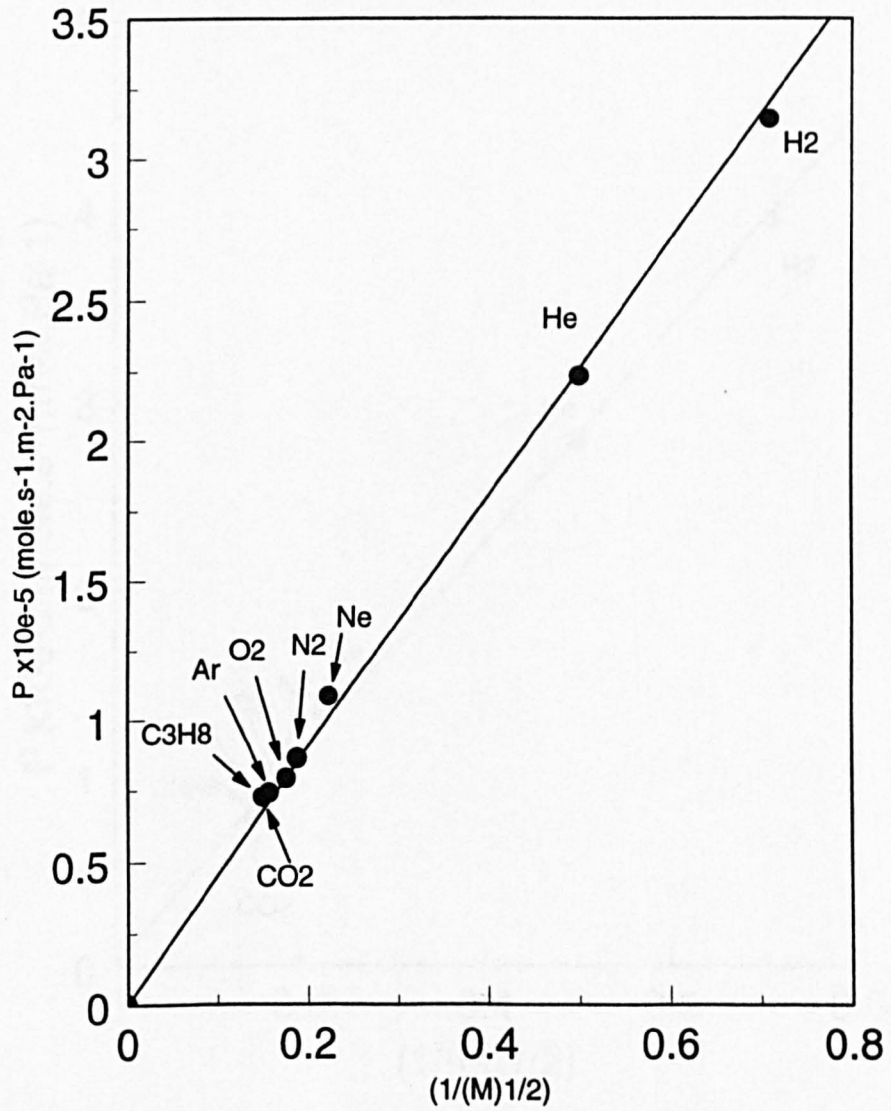
Fig. 5.17 - Variation of the permeation flux with the inverse of the square root of the molecular weight of the gases for the sample 60/3
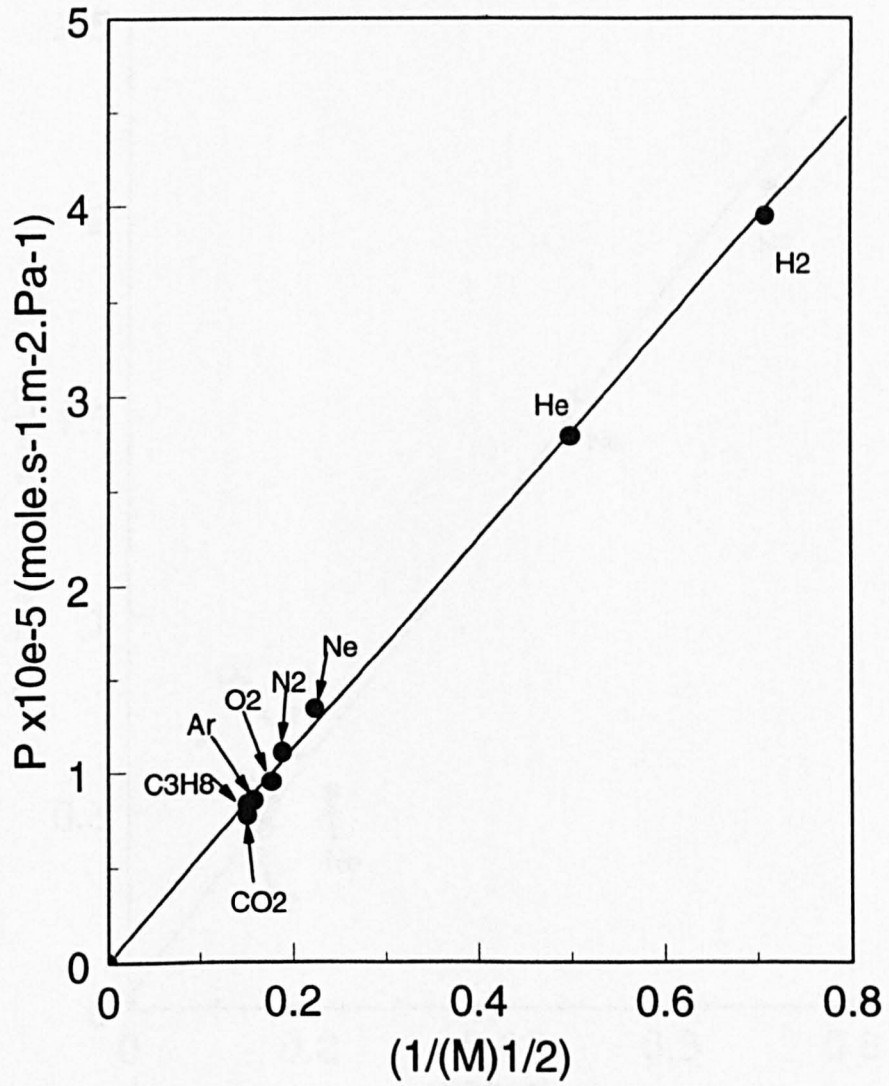
Fig. 5.18 - Variation of the permeation flux with the inverse of the square root of the molecular weight of the gases for the sample 40/5
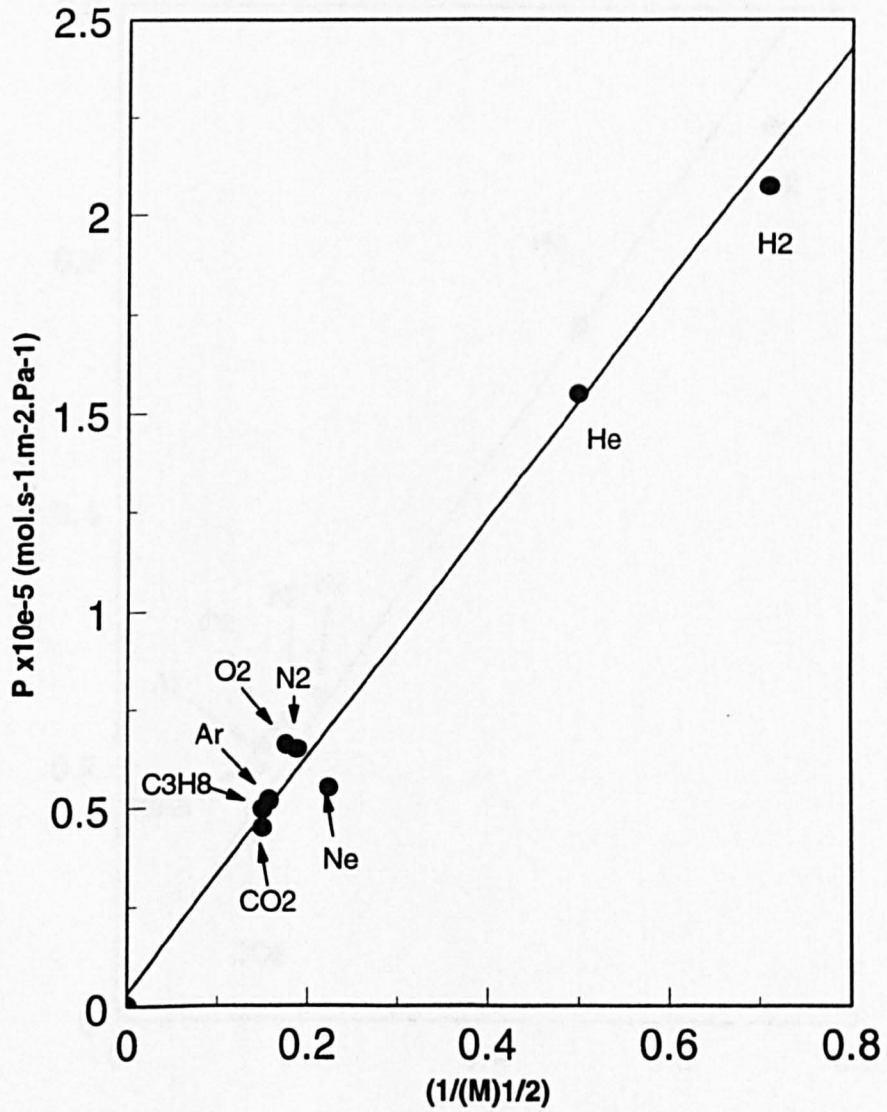
Fig. 5.19 - Variation of the permeation flux with the inverse of the square root of the molecular weight of the gases for the sample 72/1/10/16
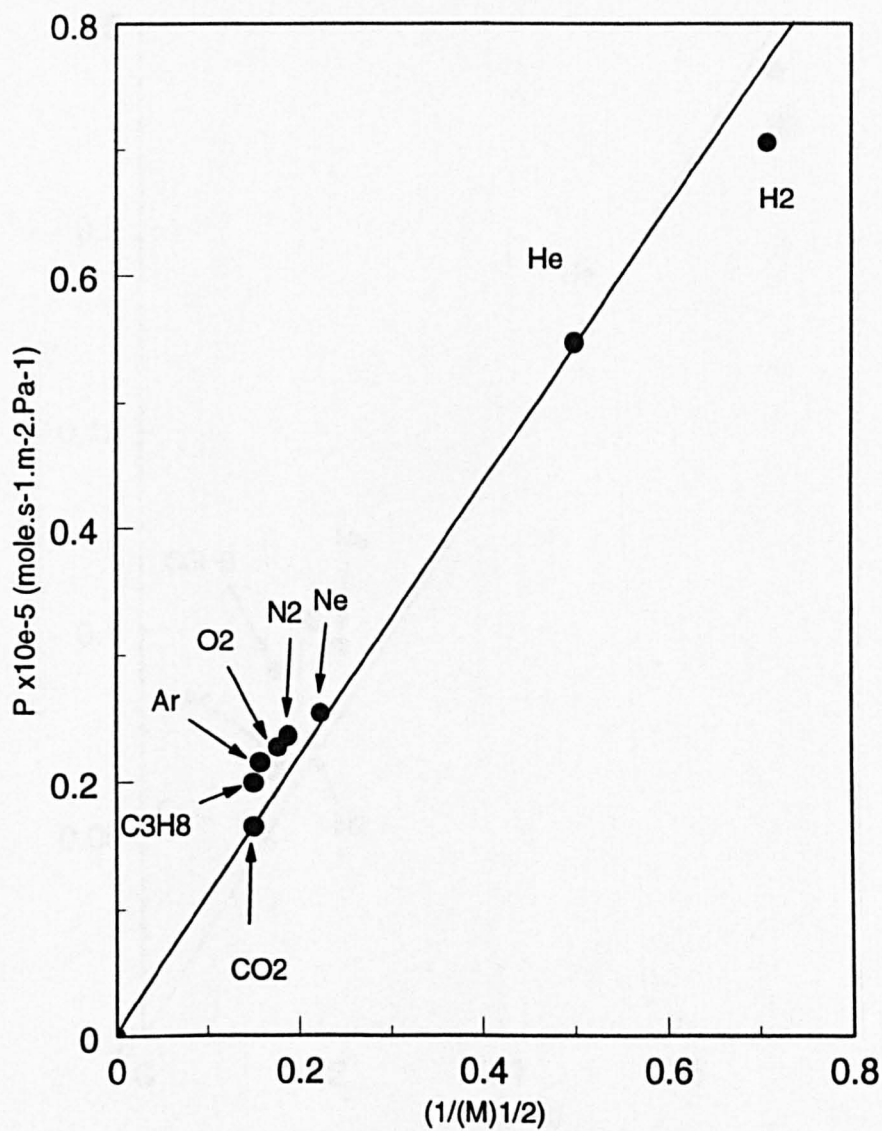
Fig. 5.20- Variation of the permeation flux with the inverse of the square root of the molecular weight of the gases for the sample 72/1/5/20
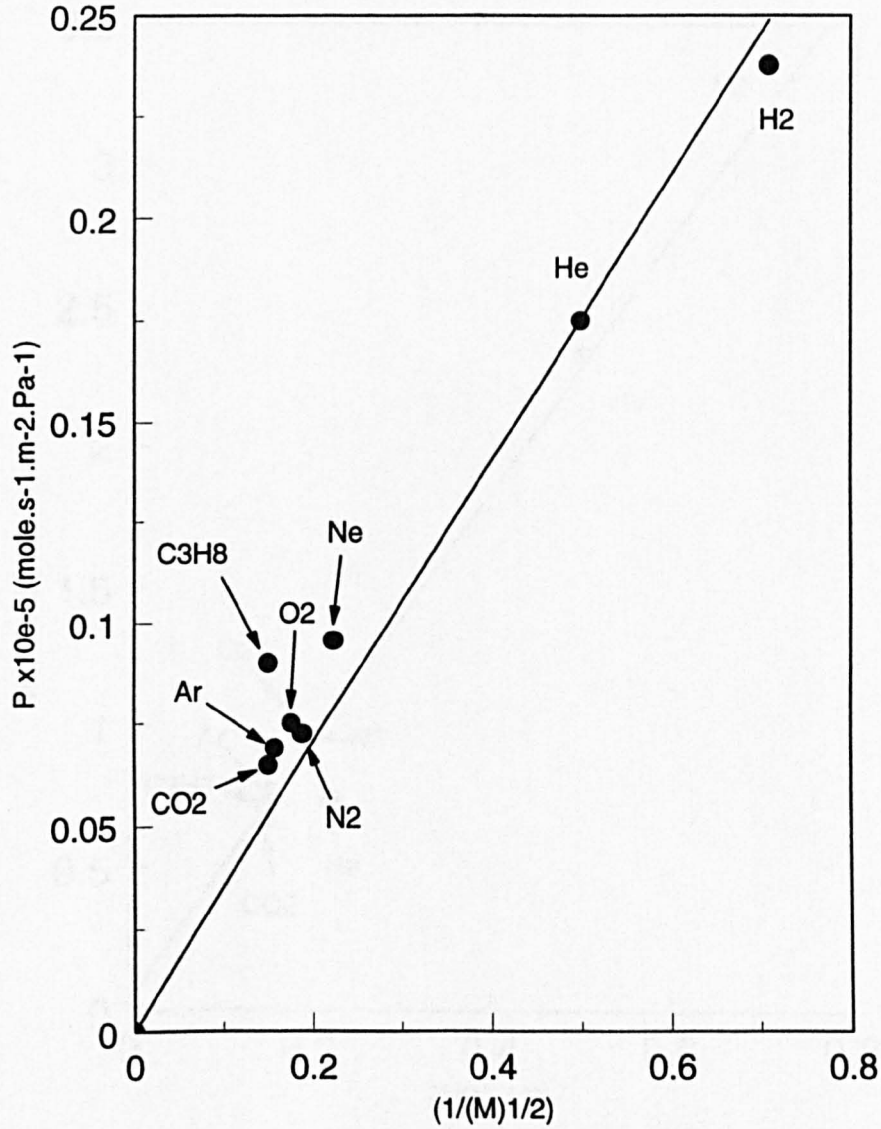
Fig. 5.21- Variation of the permeation flux with the inverse of the square root of the molecular weight of the gases for the sample 72/1/5/40
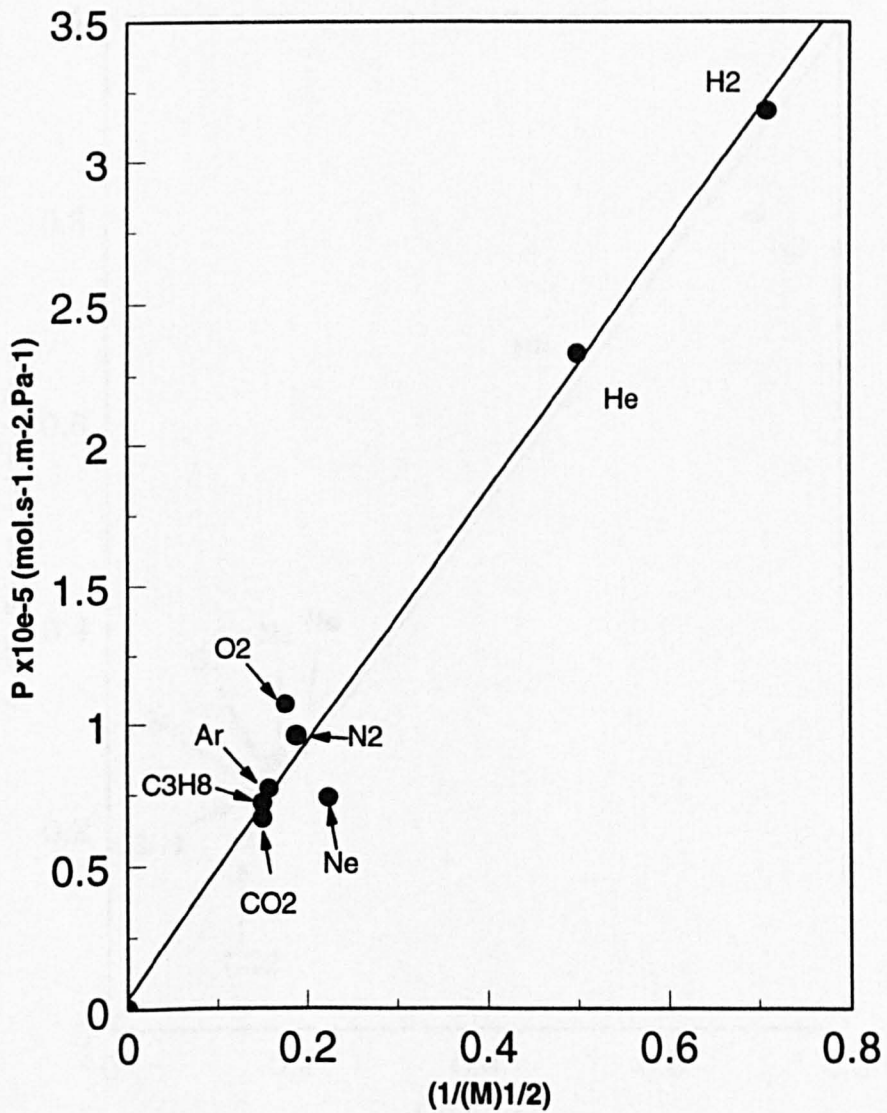
Fig. 5.22 - Variation of the permeation flux with the inverse of the square
root of the molecular weight of the gases for the active layer of
the sample 72/1/10/16
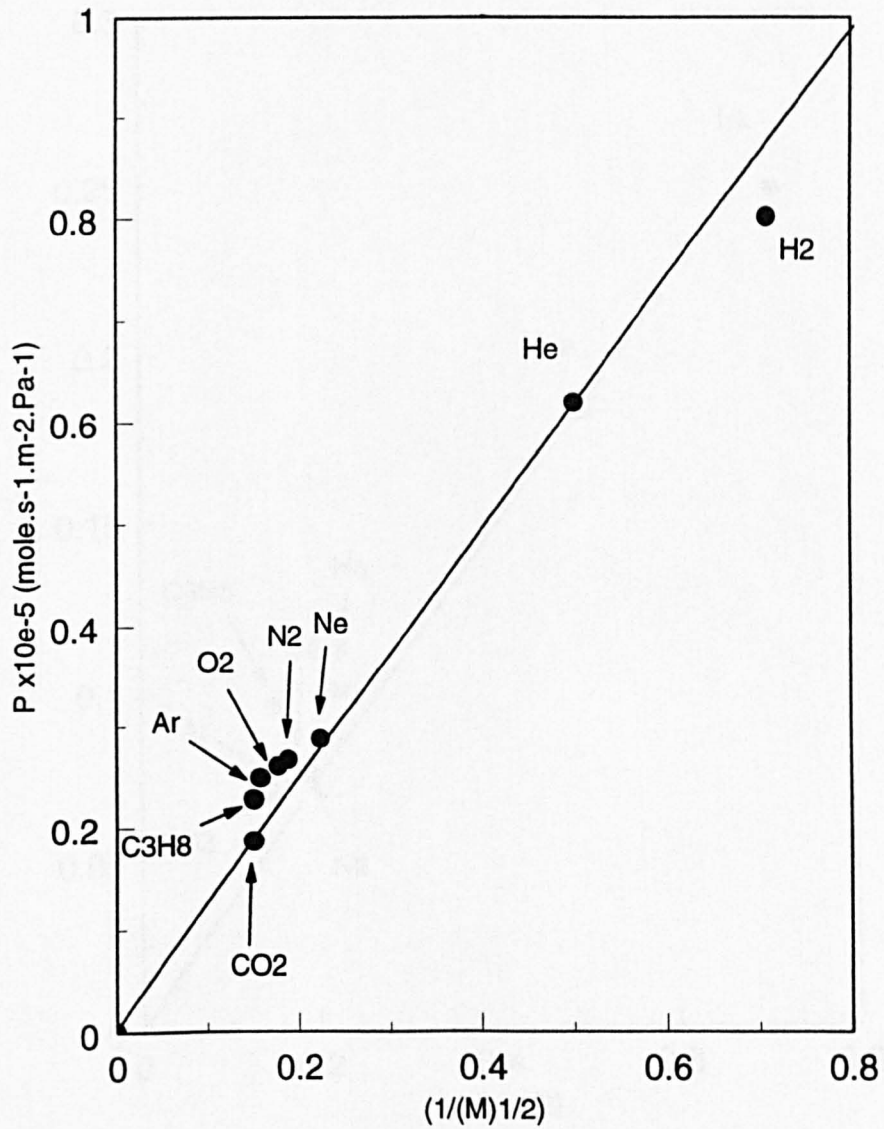
Fig. 5.23- Variation of the permeation flux with the inverse of the square
root of the molecular weight of the gases for the active layer of
the sample 72/1/5/20
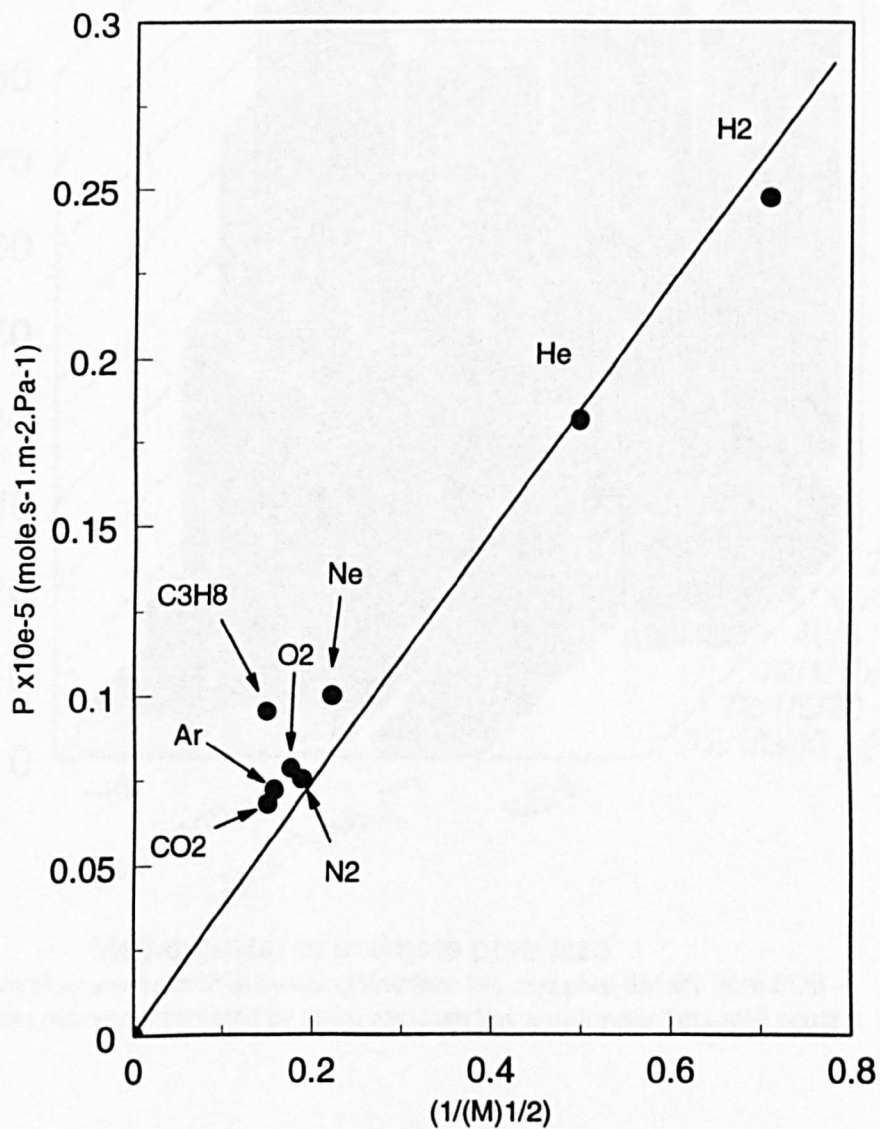
Fig. 5.24- Variation of the permeation flux with the inverse of the square
root of the molecular weight of the gases for the active layer of
the sample 72/1/5/40
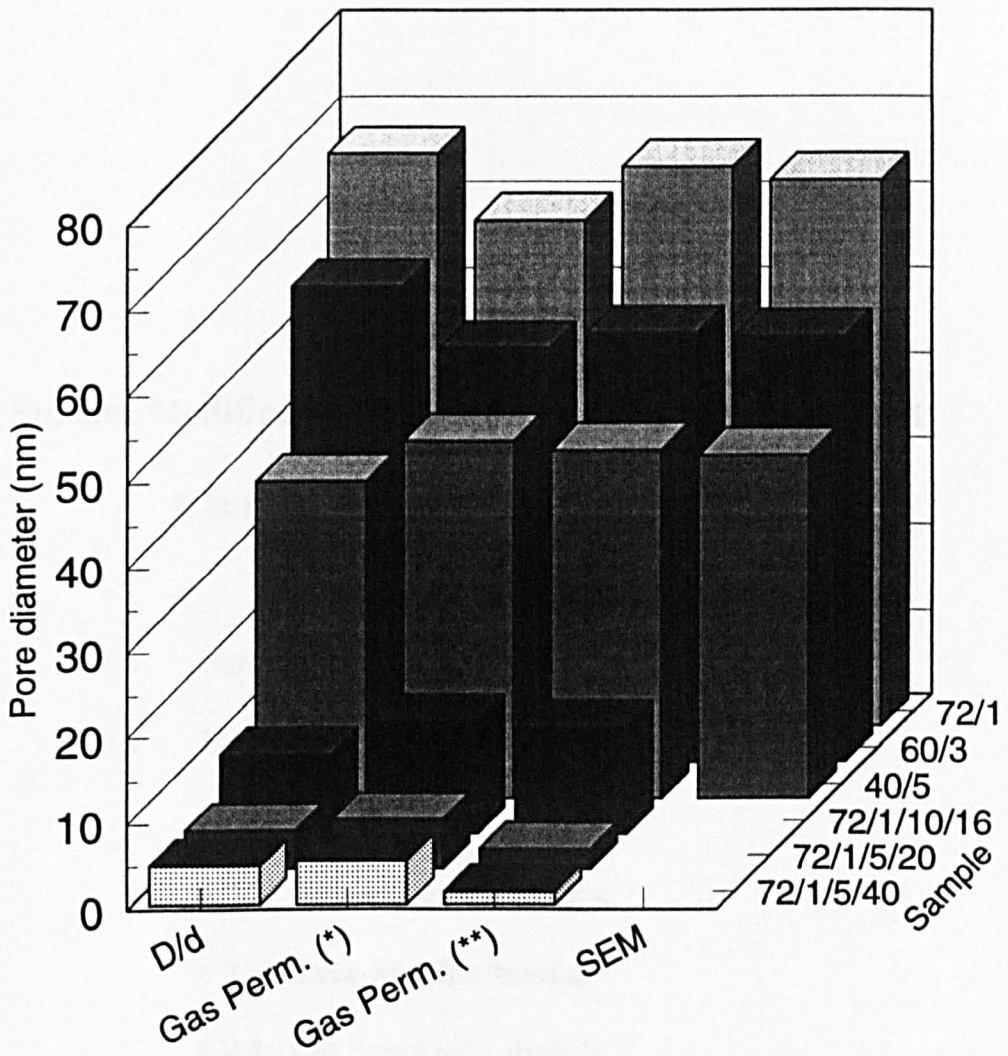
Fig. 5.25- Comparison of pore diameter of anodic alumina membranes estimated by different methods.

Chapter 6

Surface Modification of Anodic Alumina Membrane and

Characterisation by Gas Permeation

6.1 Introduction

Anodic alumina membranes with a narrow pore size distribution and with average pore diameter between 5 and 70 nm were prepared in Chapter 3 and characterised in Chapters 4 and 5. The mechanism for gas transport with these membranes is shown to be Knudsen diffusion. The permselectivity therefore is defined by the square root of the molecular masses of the gases, as discussed in Chapter 5. However, for most gas separation applications this is not effective enough. One method for increasing the separation factor can be the modification of the active layer with chemical compounds. Using techniques developed for surface modifications of ceramic membranes, functional molecules can be bonded to the ceramic membrane surfaces [1].

The surfaces of porous ceramic membranes have been modified to obtain improved separation or catalytic activity [2-9]. This surface modification can improve the permeability of a specific component and it may control the pore size of the membrane. In general, the modification of the surface of the membrane is often associated with a significant reduction of the permeability. This is partially compensated by increased selectivity.

As shown in Chapters 3 and 4, porous anodic alumina membranes, which are formed under certain electrolytic conditions, provide a unique basis for the preparation of a range of ceramic membranes sieves. This type of ceramic membrane has many advantages, such as, ideal geometric regularity of the pore structures, fully controllable pore morphology and unparalleled control of active layer thickness. This allows us to use many of the chemical and physical techniques for modification of the membrane

surface or for creation of active layers. Varying the anodisation voltage at the final stage of anodic alumina preparation, membranes with asymmetrical pore structures can be prepared and membranes with pore diameter around 5 nm are produced. However a membrane with this pore size is still not good enough to use for gas separation. The separation is still limited to the Knudsen factor (Chapter 5). In order to improve the gas separation some modification on the surface can be done.

This chapter will deal with surface modification of anodic alumina membranes by organo phosphate compounds and characterisation by a gas permeation method. The measurements will be performed using flat anodic alumina membranes after chemical surface modification by n-dodecylphosphate and octadecylphosphate. The permeation mechanism for untreated and treated membranes will be analysed and applied to estimate the pore diameter of the anodic alumina.

6.2 Experimental

6.2.1 Materials

n-dodecyl-phosphate (nDP) [11941] was purchased from Lancaster Chemicals (UK). Octadecyl-phosphate (ODP) was prepared according to method describe by Maya and Danis [10]. The preparation can be summarised as follows: 20 mmol of octadecyl alcohol dissolved in 75 ml of dry toluene was added dropwise to a solution of 60 mmol of $POCl_3$ in dry toluene over a 2 hours period. The HCl formed in the reaction was neutralised by pyridine. In order to isolate the compound and deactivate $POCl_3$ in excess, was the solution NaOH 1M added until pH 12. The sodium salt formed was washed until the pH of the filtrate was neutral. Finally, the powder was recristallised in acetic acid 99%. The reactions are:

a) $n\text{-}C_{18}H_{37}OH + POCl_3 \rightarrow n\text{-}C_{18}H_{37}OP(O)Cl_2 + HCl$

b) $n\text{-}C_{18}H_{37}OP(O)Cl_2 + 4\ NaOH \rightarrow n\text{-}C_{18}H_{37}OP(O)(ONa)_2 + 2\ NaCl$

c) $n\text{-}C_{18}H_{37}OP(O)(ONa)_2 + HCl \rightarrow n\text{-}C_{18}H_{37}OP(O)(OH)_2 + 2NaCl$
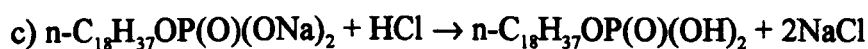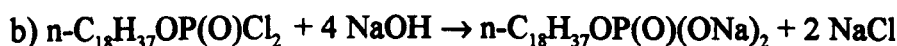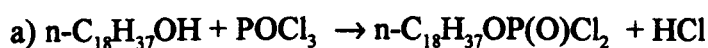
6.2.2 Membrane Modifications

Anodic alumina membrane were prepared by anodising aluminium 99.999% purity in an oxalic acid electrolyte. The details of preparation have been discussed in Chapter 2. From these developments the asymmetric membrane sample 72/1/10/16, was selected for testing these surface modifications. According to the characterisation discussed in

Chapters 4 and 5 this membrane has a pore diameter close to 11 nm and is suitable to treat with organic compound with chain length between 1- 3 nm.

The membrane was dried at room temperature before each modification. In the treatments with n-dodecyl-phosphate (nDP) and octadecylphosphate (ODP), anodic alumina membrane was dipped in 10 mmol of nDP (or ODP) dissolved in 40 ml of dry toluene with constant stirring for 2 hours at room temperature. After this reaction, the excess of unbound compound was removed in an soxhlet extractor with toluene for 24 hours. Before any test, the membrane was dried under vacuum (0.1 mmHg) at room temperature for 2 hours.

6.2.3 Infra-Red Spectroscopy

Infra-Red spectroscopy is a powerful technique to study how hydrocarbon chains are grafted onto the oxide surface. In order to check for the modifications on the membrane spectra were taken of an anodic alumina membrane untreated, treated by nDP and treated by ODP. The FTIR spectra were recorded on a Perkin Elmer FTIR-16PC (4000-400 cm^{-1}, resolution 2 cm^{-1}).

6.2.4 Gas Permeation System

Gas permeation properties were investigated using the system described in detail in Chapter 5.

6.3 Results and discussion

6.3.1 Infra-Red Spectroscopy

Infra-red spectroscopy was used in the course of this work to characterise the membrane surface modification by alkyl phosphated. Fig. 6.1 shows the Infra-red spectra of the untreated anodic membrane (curve 1), treated with nDP (curve 2) and treated with ODP (curve 3). In the spectra of the untreated anodic alumina only the broad peak for adsorbed water between 3700 and 2750 cm^{-1} can be seen as a distinguishing feature. Although the reactions on the oxide surface occur by phosphate molecules, the interpretation of the spectra for P=O and P-O-H between 1250 and 940cm^{-1} range is very difficult due to the very broad absorption band of aluminium oxide in this region. However, upon modifications of the surface with nDP and ODP, the distinct C-H stretching frequency appears in the region between 3000 and 2800cm^{-1}. This suggest that an effective grafting exist on the surface of the membrane. Indeed the intensity of the bands in the curve 2 for nDP with 12 C and curve 3 for ODP with 18 C can demonstrate the validation of the reaction. Similar results was observed by Pesek [11] with hydride alumina and hydride alumina treated with 1-octadecene. The reactivity of the surface hydroxide groups has been recently used to link organo-phosphate molecules to the zirconia oxide [1]. Analogous to the reaction between a zirconia surface and phosphate groups, the anodic alumina surface can react according to the reaction below:
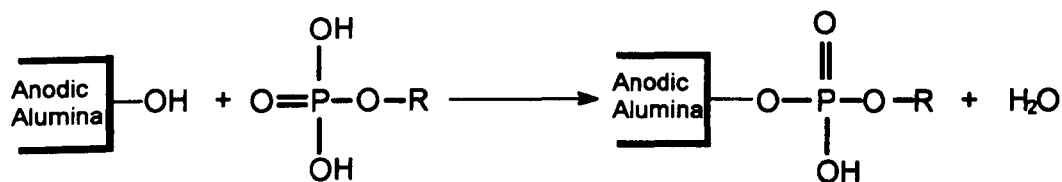
However the symmetry of the three oxygen atoms of the phosphate head linked to the oxide surface has not been elucidate yet, and at least three types of reaction could be expected:
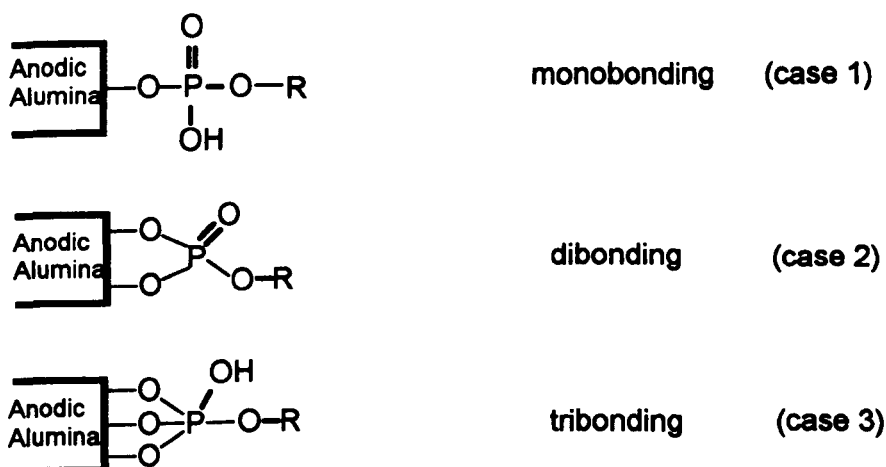
Additional to this study, anodic alumina membranes were treated with dimethyl octadecyl chlorosilane but no reaction was observed in this case. This effect will be discussed in detail in Chapter 8.

6.3.2 Gas Permeability

Figures 6.2 and 6.3 show the transmembrane pressure dependence of the flux of various gases at a constant temperature (20 °C) for an anodic alumina membrane treated by nDP and ODP, respectively. Similar to the untreated membrane (sample

72/1/10/16, Fig. 5.6, Chapter 5) the observed fluxes were perfectly linear with the upstream transmembrane pressure, indicating that the permeabilities were constant at given temperature. The Table 6.1 shows a compilation of the permeabilities obtained for the gases studied from the slope of the curves in Figs. 6.2 and 6.3. Comparison of these results show that the permeability of the gases are close to 4 times smaller in the nDP treated membrane compared to the untreated sample (Table 5.2, Chapter 5) and close to 60 times smaller in the ODP treated membrane, with the exception of propane and carbon dioxide. This shows that a pore size reduction occurs during the modification with nDP and ODP. For propane and carbon dioxide the decrease in the permeability for the ODP treated membrane was less than for other the gases and was reduced by close to 12 and 16 times, respectively, in relation to untreated membrane. This effect can be explained mainly by the solubility of these gases in a long carbon chain. The mole fraction solubilities [12, 13] of C_3H_8 and CO_2 in dodecane at a partial pressure of 1.013 bar and 298.2 K are 0.127 and 0.01089, respectively. These values are 2 and 1 order of magnitude higher then for N_2 (0.00123) and H_2 (0.00073), respectively. For ODP treated membrane the results suggest that the mechanism in the case of C_3H_8 and CO_2 permeation are not only by diffusion in a open pore but also due to a solubility effect.

The reciprocal of the square root of the molecular weights of these gases versus the permeabilities obtained are plotted in the Figs. 6.4 and 6.5. The results show markedly different behaviour between the untreated membrane (Fig. 5.18, Chapter 5), nDP treated membrane and ODP treated membrane. For both untreated and nDP treated

membranes the permeabilities of the gases are closed to the hypothetical line of Knudsen diffusion. Even for the ODP treated membrane (Fig. 6.5) some gases like H_2, He, N_2 and Ne show some evidence of Knudsen diffusion. However, the significant reduction of pore size with organic chain suggests some other form of permeation mechanism, such as, solubility and/or multilayer adsorption, mainly for C_3H_8 and CO_2, as discussed previously.

A separation factor α is obtained by the relation between the permeabilities of the used gases in relation to the He permeation and this is displayed in Table 6.3. In general, the separation factors of untreated membranes are very close to ideal Knudsen separation factors, given in the equation below;

$$\alpha = \sqrt{\frac{Mw_a}{Mw_b}} \qquad (6.1)$$

where α is the ideal Knudsen separation factor, Mw_a is the molecular weight of the used gas and Mw_b is the molecular weight of helium.

Although some gases (H_2, Ne, N_2 and Ar) show values of the Knudsen separation factor for nDP treated membrane close to ideal (Table 6.4) is not clear that the mechanism of gas permeation is due only to Knudsen diffusion. C_3H_8, CO_2, for instance, show values of 1.46 and 1.30 of deviation in relation to ideal Knudsen separation factor. In these case it is clear that there is a contribution of solubility of these gases in a C-C chain, of nDP, although this effect is small. On the other hand, for ODP treated membrane the values obtained for deviation of the ideal Knudsen are very larger and C_3H_8 and CO_2, shown values more than 9 and 6 times larger than the

ideal Knudsen coefficient, respectively. In this case the surface modification by ODP

gives not only pore size reduction but also contributes to an relative increase in

permeability of C_3H_8 and CO_2 in relation to other gases, due to solubilisation in a long

C-C chain, resulting in a higher separation factors for these gases.

6.3.3 Pore size characterisation by surface modification and gas permeation

In Chapter 5 the pore diameter of anodic alumina membranes was estimated by gas

permeation. In this chapter an alternative method to measure the pore size can be

applied using surface modification and gas permeation measurements. The basic idea is

to reduce the original pore diameter of the sample by grafting an organo phosphate

compound with a well known length and to measure the permeability before and after

the modification, Fig. 6.6 illustrates the general idea.

As the sample 72/1/10/16 is an asymmetric membrane (see Plate VIII and IX, Chapter

3) the chemical modification will reduce not only the pore size of the active layer but

also the support layer of the membrane. In this case it is necessary to calculate and

separate the reduction on the permeability in the different layers to estimate the pore

diameter of the active layer. Table 6.2 shows the compilation of the permeability in

each layer. In this case the experimental value of the membrane 72/1 from Chapter 5,

Table 5.2, is used to calculate the permeability of the active layer before and after

treatment with nDP and ODP, respectively.

To calculate the pore diameter it was assumed that the mechanism of gas permeation

follows Knudsen's law, although as discussed before other mechanisms, such as,

solubility and/or multilayer adsorption can be present. In this case from the equation

5.4a, Chapter 5, and taking into account that the porosity ($\varepsilon=n\pi r^2$) of the membrane is reduced by a monolayer of the phosphate compound, we can have the relation:

$$\frac{P_0}{P_1} = \left(\frac{r_0}{r_1}\right)^3 \qquad (6.2)$$

where P_0 and P_1 are the permeability of the active layer of the membrane before and after the treatment, respectively and r_0 and r_1 is the radius of the pore before and after treatment, respectively. If the length of the compound is known and equal to l, then the reduction on the initial radius will be, $r_1=r_0-l$, and the value of r_0 can be calculated from the equation 6.2. The length of the compound used in this study was calculated from the reference [14], and the values used were 1.77 nm for n-dodecyl-phosphate and 2.52 nm for octadecyl-phosphate. Table 6.4 shows a compilation of the values of pore diameter using different gases and treatments, nDP and ODP, respectively. The values of the pore diameter based on the nDP treatment are smaller than those estimated in Chapter 5, Tables 5.6 and 5.7 and the average value of 8.30nm (CO_2 and C_3H_8 is not included in this calculation) is close to the predicted values (9.3 nm) estimated by geometrical considerations, in Chapter 4. On the other hand the values calculated based on the ODP treatment are much smaller than for the nDP treated membrane. One explanation for these results can be due to a significant reduction of the initial pore size as the length of nDP is 1.77 nm and ODP is 2.52 nm and a decrease in the pore diameter between 3.5 and 5.0 nm was expected. In this case other mechanisms become important, for example, multilayer adsorption in the small pore,

consequently decreasing the permeability. Additionally, the equation 6.2 show a cubic relation between the radius and the permeabilities and the estimation of the pore diameter by this method become very sensitive for any small variation in the permeability.

6.4 Conclusion

In this chapter it has been shown that anodic alumina membranes can be easily modified by grafting organo phosphate molecules. The analysis made by FTIR showed n-dodecyl-phosphate and octadecyl-phosphate, used in this study, formed a stable monolayer on the surface of anodic the alumina membrane. In addition the gas permeation studies showed that the modification effectively reduces the pore size of the membrane and the permeability of the tested gases decreases by a factor of 4 times, approximately, for nDP treatment and 60 times, approximately, for the ODP treatment. The modification with ODP shows a high separation factor for CO_2 and C_3H_8 when compared with helium and this results is of interest for the potential use in the separation of these gases.

Also this research shows that the pore diameter of the anodic alumina can be estimated by gas permeation combined with surface modification. In this study the results obtained for pore diameter of the sample 72/1/10/16, using nDP and ODP modifications are smaller than the results obtained in Chapter 5. The values obtained from the nDP and ODP treatments are underestimate probably due to multilayer adsorption.

6.5 References

[1] J. Randon, P. Blanc, R. Paterson, Modification of ceramic membrane surfaces using phosphoric acid and alkyl phosphonic acids and its effect on ultrafiltration of BSA protein, J. Membr. Sci., 98 (1995) 119-129.

[2] T. Okubu and H. Inoue, Surface diffusion on modified surface of porous glass, J. Chem. Eng. Jpn., 20 (1987) 590.

[3] T. Okubu and H. Inoue, Introduction of gas specificity to porous glass membranes by treatment with tetraethoxysilane, J. Membr. Sci., 42 (1989) 109.

[4] S. Sugawara, M. Konno and S. Saito, Gas permeation through siloxane-anodic aluminum oxide composite membranes at temperatures up to 200 °C, J. Membr. Sci., 44 (1989) 151-160

[5] R. P. Castro, Y. Cohen and H. G. Monbouquette, The permeability behaviour of polyvinylpyrrolidone-modified porous silica membranes, J. Membr. Sci., 84 (1993) 151-160.

[6] T. Baba, M. Matsuda and C. Kamizawa, Lipid layer-immobilized membranes prepared by ultrafiltration and their gas permeation properties, J. Colloid Interface Sci., 163 (1994) 259-261.

[7] K. Kusakabe, Z. Y. Li, H. Maeda and S. Morooka, Preparation of supported composite membrane by pyrolysis of polycarbosilane for gas separation at high temperature, J. Membr. Sci., 103 (1995) 175-180.

[8] S. Nehlsen, T. Hunte and J. Müller, Gas permeation properties of plasma polymerized thin film siloxane-type membranes for temperatures up to 350 °C, J. Membr. Sci., 106 (1995) 1-7.

[9] F. Suzuki, K. Nakane and Y. Hata, Grafting of siloxane of poly(styrene-co-maleic acid) and application of this grafting technique to a porous membrane for gas separation, J. Membr. Sci., 104 (1995) 283-290.

[10]L. Maya and P. O. Danis, Bis(octadecyl phosphate)zirconium (IV). Novel support for reversed-phase chromatography, J. Chromatogr., 190 (1980) 145-149

[11]J. J. Pesek, Conversion of oxide surfaces to hydride surfaces, in Chemically Modified Surfaces, Ed. J. J. Pesek and I. Leigh, The Royal Society of Chemistry (1994), 1-23.

[12]P. G. T. Fogg and W. Gerrard, Solubility of Gases in Liquids, Ed. John Wiley & Sons Ltd, Chichester, 1991

[13]W. Hayduk, Solubility Data Series Volume 24, Propane, Butane and 2-Methylpropane, Pergamon Press, Oxford, 1986.

[14]CRC, Handbook of chemistry and physics, Editor-in-chief D. R. Lide, 76th edition, CRC Press Inc., 1995.

Table 6.1- Permeability of gases for an untreated anodic alumina membrane 72/1/10/16, treated with nDP and treated with ODP.

Gas	Permeability $(mole.s^{-1}.m^{-2}.Pa^{-1})x10^7$		
	Untreated membrane	Membrane treated with nDP	Membrane treated with ODP
H_2	207.00	53.60	2.08
He	154.90	35.50	1.54
Ne	54.80	16.50	1.02
N_2	64.80	15.10	9.70
O_2	66.60	15.10	1.30
Ar	51.70	13.40	1.23
CO_2	45.00	13.90	2.85
C_3H_8	49.50	15.60	4.20

Table 6.2- Gas permeability of each layer of membrane 72/1/10/16 before and after treatment with nDP and ODP

Gas	Permeability $(mole.s^{-1}.m^{-2}.Pa^{-1}).10^{-3}$					
	Untreated membrane		Membrane treated with nDP		Membrane treated with ODP	
	72/1(*)	10/16(**)	72/1	10/16(**)	72/1	10/16(**)
H_2	592.30	318.21	500.70	37.86	464.93	6.88
He	463.50	232.65	363.83	39.34	363.83	6.54
Ne	215.60	73.48	201.02	17.98	169.24	7.15
N_2	200.80	95.68	200.80	16.33	157.62	6.98
O_2	176.10	107.11	176.10	16.52	138.23	7.26
Ar	158.10	76.82	158.10	14.64	124.10	7.50
CO_2	138.70	66.61	138.70	15.45	108.87	9.08
C_3H_8	159.40	71.80	130.71	17.71	125.12	9.68

(*)Experimental value of the sample 72/1 from Chapter 5, Table 5.2.

(**)This notation is used to refer to the active layer of the membrane, in this case sample 72/1/10/16 as described in Chapter 3, 4 and 5.

Table 6.3- Knudsen separation factor in anodic alumina membrane, untreated, treated

with nDP and treated with ODP.

Gas relation	Separation factor α			
	Ideal Knudsen separation factor	Untreated membrane	Membrane treated with nDP	Membrane treated with ODP
H_2/He	1.41	1.37	1.51	1.35
Ne/He	0.45	0.35	0.46	0.66
N_2/He	0.38	0.42	0.43	0.63
O_2/He	0.35	0.43	0.43	0.84
Ar/He	0.32	0.33	0.38	0.80
CO_2/He	0.30	0.29	0.39	1.85
C_3H_8/He	0.30	0.32	0.44	2.73

(*) Ideal Knudsen separation factor was calculated by the relation, $\alpha = \sqrt{\frac{Mw_b}{Mw_a}}$, where

Mw_a is the molecular weight of different gas and Mw_b is the molecular weight of

Helium.

Table 6.4- Deviation of the ideal Knudsen separation factor for anodic alumina membrane untreated, treated with nDP and treated with ODP in relation to helium.

	Deviation of the ideal Knudsen separation factor(*)			
Gas relation	Ideal Knudsen separation factor	Untreated membrane	Membrane treated with nDP	Membrane treated with ODP
H_2/He	1.41	0.97	1.07	0.96
Ne/He	0.45	0.79	1.04	1.48
N_2/He	0.38	1.11	1.13	1.67
O_2/He	0.35	1.22	1.20	2.39
Ar/He	0.32	1.06	1.19	2.53
CO_2/He	0.30	0.96	1.30	6.14
C_3H_8/He	0.30	1.06	1.46	9.05

(*)The deviation separation factor was calculated by the relation between experimental Knudsen factor and ideal Knudsen separation factor.

6.17

Table 6.5- Calculated pore diameter of the active layer for anodic alumina sample 72/1/10/16 based on chemical treatments.

Gas	Pore diameter (nm)	
	Based on nDP(*) treatment/untreated membrane	Based on ODP(*) treatment/untreated membrane
H_2	8.31	5.77
He	7.90	5.82
Ne	9.51	5.97
N_2	8.00	5.99
O_2	7.69	6.16
Ar	8.41	6.20
CO_2	9.29	7.03
C_3H_8	9.47	7.56
Average value (**)	8.30	6.46
Standard Deviation(**)	0.59	0.21

(*) Calculation based on nDP and ODP lengths 1.77 nm and 2.52 nm, respectively. It also used the relation $\frac{P_0}{P_1} = \left(\frac{r_0}{r_1}\right)^3$, from Knudsen Law, to take into account that the porosity ($\varepsilon = n\pi r^2$) was reduced with the chemical treatment.

(**) These calculations do not include the values for CO_2 and C_3H_8, due to solubility effect.
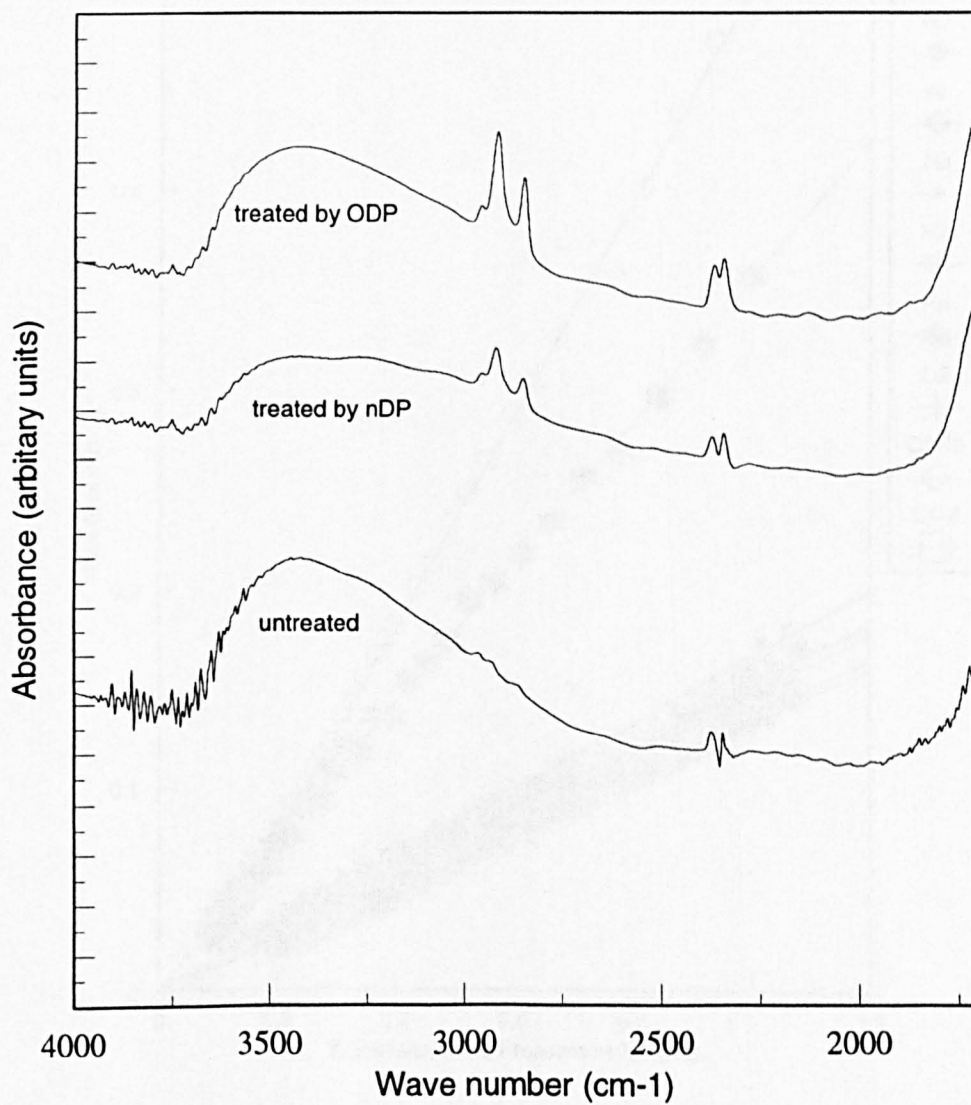
Fig. 6.1 - FTIR spectra of anodic alumina before and after treatment with
       nDP and ODP
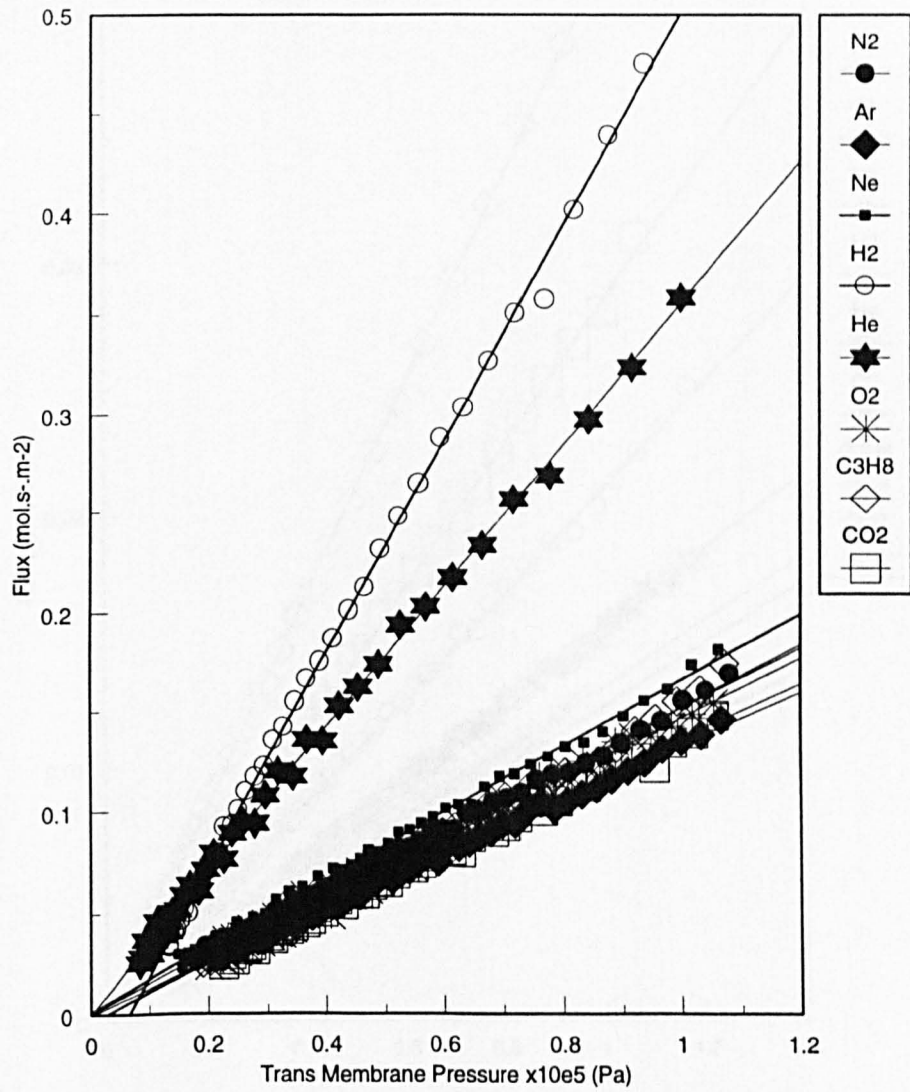
Fig. 6.2 - Gas flux versus transmembrane pressure with different
gases for the sample 72/1/10/16 treated by nDP
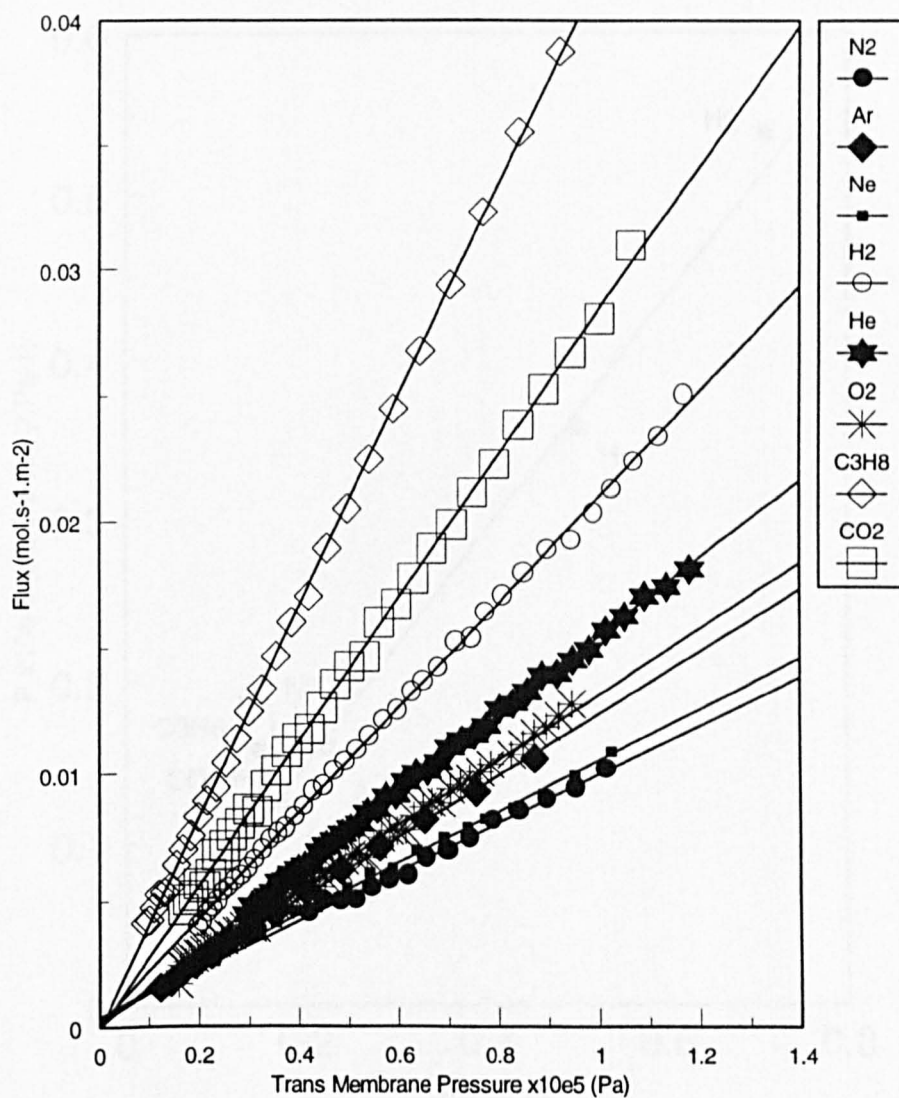
Fig. 6.3 - Gas flux versus transmembrane pressure with different
gases for the sample 72/1/10/16 treated by ODP
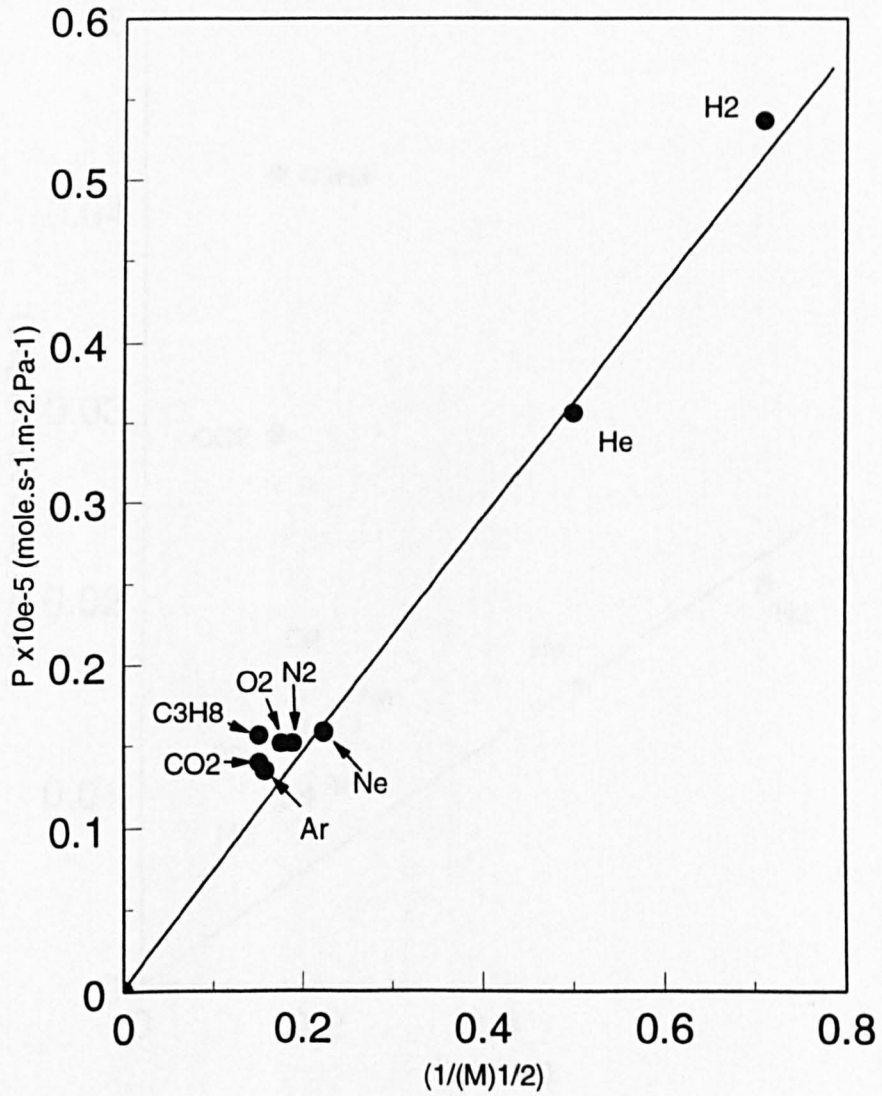
Fig. 6.4 - Variation of the permeation flux with the inverse of the square root of the molecular weight of the gases for the sample 72/1/10/16 treated by nDP

Fig. 6.5 - Variation of the permeation flux with the inverse of the square
root of the molecular weight of the gases for the sample 72/1/10/16
treated by ODP

untreated   phosphate compound treated

anodic
alumina

anodic   monomolecular layer of
alumina   phosphate compound chain

pore
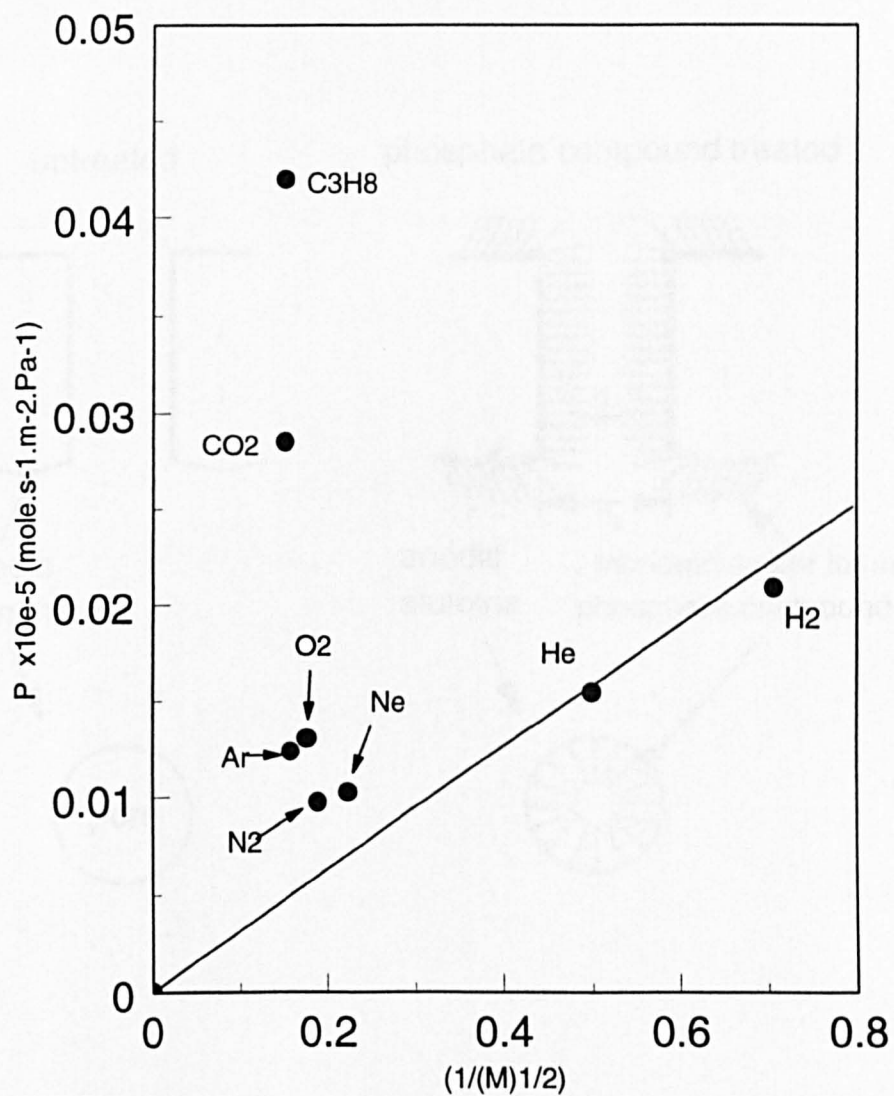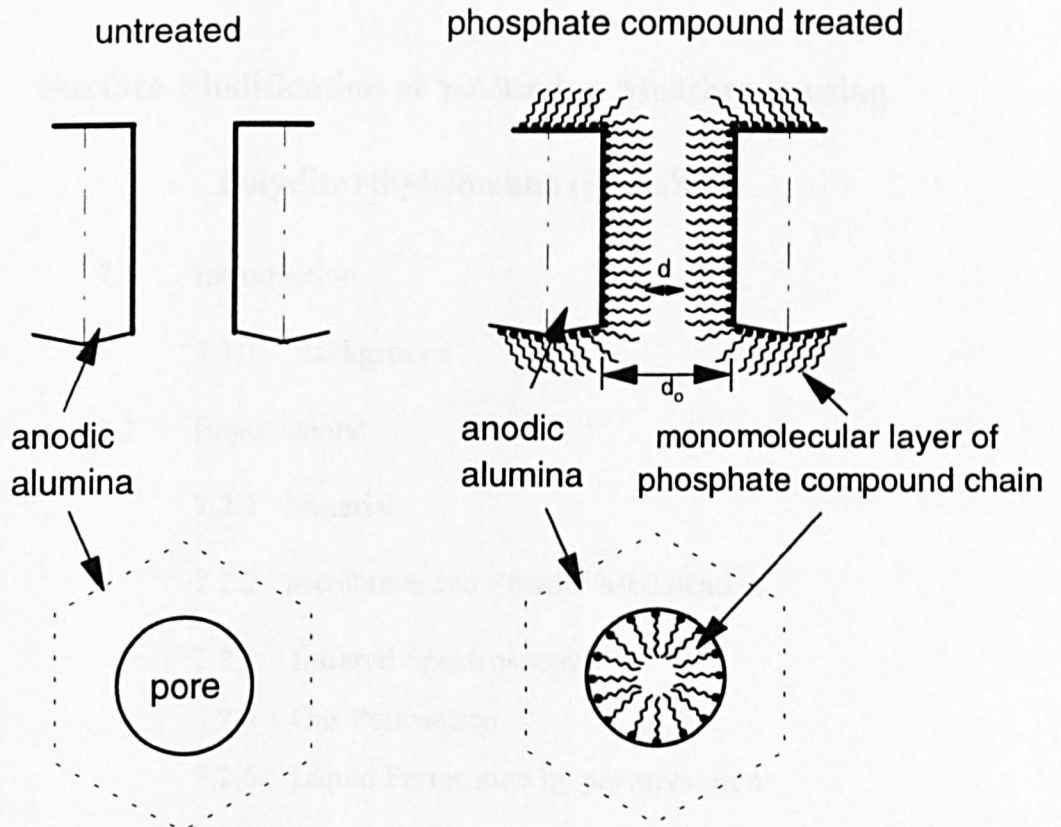
Fig. 6.6 Schematic hypothesis of the membrane morphology before
and after phosphate compound modification

Chapter 7

Surface Modification of γ-Alumina Membrane using Polydimethylsiloxane (PDMS)

7.1   Introduction

      7.1.1   Background

7.2   Experimental

      7.2.1   Material

      7.2.2   Membrane and Powder Modification

      7.2.3   Infrared Spectroscopy

      7.2.4   Gas Permeation

      7.2.5   Liquid Permeation by pervaporation

7.3   Results and Discussion

      7.3.1   Chemical Modification

      7.3.2   Pervaporation of pure liquids

      7.3.3   Gas permeability

      7.3.4   Separation by pervaporation

7.4   Conclusion

7.5   References

7.1 Introduction

Although the preparation of inorganic porous membranes by sol-gel process has been improved during the last decade, these types of membranes commercially available is still largely limited to four oxides, silica, zirconia, titania and alumina. Moreover, commercial membranes, having a pore diameter equal to or larger than 5nm, are unable to fractionate mixtures of low molecular weight liquids and are not efficient in separating gas mixtures. It is the aim of this chapter to investigate the potential of chemical modifications to obtain membranes with unique chemical properties. The approach considered here is surface bonding of organic molecules in a monolayer on the ceramic surface. This bonding can, in specific cases, increase the performances of the membrane by, on one hand reducing the pore size, and on the other hand, by promoting an eventual specific interaction between the membrane surface and the permeating molecules to improve separations. Several types of compounds can achieve the modification as, for instance, phosphate derivatives discussed in Chapter 6, chlorosilane derivatives [2], or triethoxysilicon compounds [3]. All of these products can be easily, covalently, bonded on silica, alumina, zirconia, and titania surfaces. They are often difficult to synthesise and to handle. An easier and less hazardous procedure is considered here. Its principle is to bond a silicone oil molecules to an alumina surface. This process has been demonstrated successfully on glass [4, 5] to obtain a hydrophobic glass. Any common commercial silicone oil can be used. If a polysiloxane as common as the polydimethylsiloxane (PDMS) can used to bind to the internal surfaces of a membrane with pores of a few nanometer diameter a membrane

having a ceramic morphology with its pores filled with immobilised silicone oil would be expected.. such a membranes might be considered to be similar to a supported liquid membrane, because of the high mobility of the siloxane chains, but the silicone would be unleacheable since it is covalently bonded to the walls of the porous ceramic. A very permeable membrane having hydrophobicity properties close to those of the silicone oil itself is expected, but which would have the dimensional stability and rigid morphology of the ceramic. This type of hybrid organo-ceramic might be very interesting and valuable on an industrial level.

This study is concerned specifically with the effect of siliconising the pores of a 5nm pore membrane and so the silicone molecules were expected to partly or completely fill the pores of the active layer of the alumina membrane. Such coating, as will be described here, applied on microporous or macroporous membranes or filters would be effective in a different way, rendering the surface hydrophobic, oleophilic, and having a major effect upon fouling surface tension and other properties.

7.1.1 Background

It is well known that siloxane derivatives can be cleaved by the action of aqueous alkaline solutions [6, 7]. Si-O bonds are broken to become Si-OH (silanol) ones. The formation of these silanol compounds has been studied by Voronkov [8], using phenol derivatives and Sprung [9] using alcohols, as hydrolysis agent.

Depending on the hydrolysis agent used either alkyl- or aryl- silicone compounds could be obtained. The reactions involved are shown below :

where Ar is an aromatic residue and R an aliphatic one.

The reactions take place in an apolar solvent (such as toluene or xylene) generally using a catalyst: benzene sulfonic acid for aryl derivatives [8] and para-toluene sulfonic acid or sodium methanolate for alkyl derivatives [9]. The question arises as to whether the hydroxyl groups on the surface of a ceramic oxide would react similarly. Although no mechanism was discussed it appears that a very similar process was used some forty years ago to make glass surfaces permanently hydrophobic [4]. The glass surface lightly coated with commercial silicone oil was heated to 180°C. If the hydroxyl groups of the glass surface (more generally the SiO_2 surfaces) react, under high temperature conditions, with siloxane derivatives, it was expected other type of oxides which retained hydroxylated surfaces would react similarly. In particular the membrane oxides alumina, zirconia, silica or titania which have hydroxyl groups on their surfaces might then be grafted to a siloxane derivative. It was considered that this reaction could be an interesting way to modify oxide porous membrane surfaces.

The study presented in this chapter will be focused on the modification of γ-alumina surfaces, mainly because alumina membranes are commercially available with a very small pore diameter (5 nm) and are thus, the best candidates to record the modification effects. The objective here was to attempt to fill the nanometer pores of the host alumina membrane with silicone molecules attached only to the surface of the oxide

and not themselves polymerised. The properties of such membranes would fundamentally altered in a way that is not entirely predictable. The alkyl phosphate treatment described in Chapter 6 on a 11nm anodic alumina membrane altered the pore surfaces and reduced the pore diameter, this treatment is expected to effectively fill the ceramic pores.

The reaction expected consists of a cleavage of the Si-O bond of the silicone polymer with recombination on the hydroxylated alumina surface, as shown below :

The ceramic alumina membranes are prepared industrially by a sol-gel process [10], using a colloidal suspension of metal alkoxides or hydrous metal oxide precursors, a peptising agent or an organic binder, a solution casting on a ceramic support and finally a thermal treatment. Exactly the same method, without casting step, can be used to prepare industrial alumina powders which can then, be considered, to be morphologically identical to the membrane itself. The chemical membrane surface modification can then be easily studied, merely by examining a modified powder on which the modification has been carried out in exactly the same conditions as for the membrane. The best way to study chemical changes on the active layer was to use infra-red spectroscopy on the chemically modified alumina powder. The effect of

chemical modification on the membrane itself can be studied by gas and liquid

permeation measurements.

7.2 Experimental

7.3.1 Materials

The siloxane oil used (Fluka Catalogue ref. 85421) is a polydimethylsiloxane (PDMS) type oil, having a typical viscosity of 545mPa.s at 20°C. This kind of polymer is very stable and no degradation reaction occurs up to 300°C [11, 12] when the polymer is not in the presence of hydroxyl group sources.

The ceramic porous membrane used, an gama alumina membrane in conventional tube format, external diameter 1cm, was donated by Societe des Ceramiques Techniques (SCT) who estimated it as having a pore diameter of 5nm.

The alumina powder, also supplied by SCT, was obtained from the sol used in preparing the membrane and was chemically and morphologically equivalent to the alumina of the active layer of the test membrane.

7.2.2. Membrane and powder modification process

The chemical treatment of the membrane and powder were identical, as follows: the alumina membrane (or powder) was washed, for 12 hours, by a continuous flow of cold distilled water to remove soluble impurities from the oxide surface. The membrane (or powder) was dried for 24 hours at 65 °C and then immersed in the pure dry silicone oil. The resulting preparation was placed under vacuum (~1 mmHg), until no more bubbles can be observed. This process was used to fill the pores of the membrane and to remove gas absorbed on the membrane (or powder) surface. The preparation was baked at 180°C for 2 hours under nitrogen. The membrane (or

powder) was then extracted by hot toluene in a Soxhlet extractor for 48 hours to remove unbound silicone oil molecules. Thereafter it was dried, first at 65 °C for 24 hours, and then at ambient temperature but under vacuum (~1 mmHg) for 2 hours. The membrane (or powder) was then ready for investigations.

7.2.3. Infrared Spectroscopy

In Chapter 6 the surface modification on the anodic alumina membrane was proved by using a self supported treated thin membrane and FTIR. In this study the dry powder is prepared as KBr disks and infrared spectra are recorded on the same instrument described in Chapter 6, a Perkin-Elmer FTIR 16PC spectrometer in the 4000-600 cm^{-1} area, with a 2 cm^{-1} resolution.

7.2.4 Gas permeation measurements

The permeability of pure gases was measured by monitoring pressure in both high and low pressure sides of a permeation cell. The system used was similar to one described in detail in a Chapter 5, except for the membrane cell, in this case, a tubular membrane was placed in a cell shown in Fig. 7.1. Its principle can be summarised as follows : the high pressure side was maintained at a constant 2 bars (absolute pressure), whereas the initial pressure on the low pressure side was initially 1 bar (absolute). This latter side was constituted by a fixed volume cylinder filled with the permeant gas. As the gas permeates, the pressure increase in this collecting volume was monitored. The pressure difference across the membrane, initially one atmosphere, decreased with

time, approaching zero as the system approached equilibrium. From these data the permeabilities of a series of gases were obtained. All the measurements were conducted at 20° C, using a geometrical area of test membrane of 4.98×10^{-4} m^2.

7.2.5 Liquid permeation by Pervaporation

The experimental technique, as described below, is termed pervaporation [14-16], if the membrane has a dense active layer, and membrane distillation if the membrane is merely porous.

The permeability of pure liquids or binary liquid mixtures was measured by weighing the amount of compound transferred through the membrane as a function of time. The schematic diagram of pervaporation system is shown in Fig. 7.2. The upstream side of the membrane was in contact with the circulating liquid feed at atmospheric pressure whereas the downstream face of the membrane was maintained at a very low pressure (~1mmHg). The vapours transferred through the membrane to the downstream side were collected by condensation in a cold trap cooled by liquid nitrogen. The membrane flux was measured as a mass flow (kg.h^{-1}.m^{-2}), as commonly in pervaporation literature [16].

When a binary liquid mixture is used as the feed, the measured flux is the sum of the individual fluxes. Under steady state conditions the separate fluxes are obtained by analysis of the permeate. From the concentrations of each species in the feed and in the permeate the membrane selectivity α was obtained. Concentrations were determined by measuring the refractive index of the mixtures at 25°C.

The two main parameters used to characterise the membrane were: the total flux J in

kg.h^{-1}.m^{-2} and the membrane selectivity α (undimensional parameter) defined below in

the Equation (7.1) :

$$\alpha = \frac{W'}{(1 - W')} \frac{(1 - W)}{W} \qquad (7.1)$$

where   W' is the weight fraction of the preferentially transferred species, in the

permeate and W is the weight fraction of the preferentially transferred species, in the

feed.

7.3 Results and discussion

7.3.1. Chemical modification

Infra-red spectroscopy is particularly suitable for detecting the presence of siloxane

compounds on the alumina surface because the silicone oil absorption bands can easily

be isolated. As shown in Fig. 7.3, the strong broad bands between 1000 and $1100cm^{-1}$,

characteristic of the Si-O vibration bond, and the strong sharp band near $1250\ cm^{-1}$,

characteristic of Si-CH_3 bond, appear on the treated alumina spectrum, giving clear

evidence of siloxane derivative presence, on the alumina surface. Because the alumina

powder was extracted for a long time (48 hours) in a Soxhlet extractor, using toluene

(which is an excellent solvent for silicone oil even at low temperatures), it can be

assumed that the absorption bands recorded, come from siloxane molecules covalently

grafted to the alumina surface. Moreover this grafted layer can only be a

monomolecular, because only the hydroxyl groups of the alumina surface can react

with the siloxane groups. There is little likelihood of other reactions since the PDMS

oil is stable at temperatures up to 300°C [11,12], the decomposition temperature of

the PDMS chains, and the grafting process was performed at 180°C. The siliconised

membrane had high chemical and thermal stability and the silicone layers were not

altered or removed by solvent or by the liquids and gases used for the permeation tests

performed in this research. As observed by Randon *et al* [1], hydrophobic material in a

surface coating, is impermeable to water and ions which can lead to the hydrolysis of

the alumina-silicone oil bond. This stability was monitored by studying the permeation,

under pervaporation conditions, of very polar molecules through the membrane. The

results are shown in Table 7.1. The exceptional hydrophobicity is shown by total membrane impermeability to water. Low molecular weight alcohols pass through the modified alumina membrane and always reach a reproducible steady state. This indicates that even the lighter alcohols such as methanol or ethanol are unable to hydrolyse the alumina-PDMS bond. In these two cases, it can be concluded that such a membrane is very stable in relatively mild conditions. Under aggressive conditions, as for example, exposure to concentrated alkaline solutions, the membrane layer is hydrolysed not least by cleavage of the siloxane bonds themselves [6, 7]. Nevertheless, it seems that the modified PDMS-membranes can resist easily to most of the usual organic solvents, leading to stable performances in time, shown in the Fig. 7.4.

7.3.2 Pervaporation of pure liquids

The pervaporation results of a series of simple organic molecules and water are shown in Fig. 7.4. In broad terms we may conclude that the permeability of the treated membrane increases for molecules as they become less polar, although there are obvious exceptions, particularly the low permeability of toluene. It is not immediately clear from these measurements whether the membrane retains open pores. The question seems to be settled by the results concerning the permeation of a homologous series of low molecular weight alcohols through the modified membrane (Fig. 7.5). The permeability series is EtOH >> nPrOH> MeOH> nBuOH, and it is clear that the process is not membrane distillation. It rather seems that the permeability is caused by a combination of solubility and diffusivity in the siloxane material. The maximum flux

obtained for ethanol might be due to the best combination of these two parameters. In this latter case the transfer mechanism appears to be a solution-diffusion mechanism [15, 16], meaning that the grafted PDMS chains formed a dense layer on the ceramic surface. An objection to the solution/diffusion hypothesis might be that the real size of the diffusing species in the methanol case might be larger than in the ethanol one, because methanol can be associated in a cluster form due to self-association by strong intermolecular hydrogen bonds. The concept of cluster formation and behaviour inside a membrane is a controversial subject. Most studies in this area suggest that clusters exists in a membrane, but that the diffusion process occurs by cluster desaggregation and single molecule diffusion [17, 18]. According to this latter hypothesis, the results recorded for the alcohol permeation suggest a solution/diffusion mechanism, certainly not a simple open pore diffusion. In this case, the PDMS-modified alumina membrane can be seen as a composite membrane in which a monomolecular dense PDMS layer is grafted on a porous alumina support having very small average pore diameter. Results obtained with other solvents are similar. Indeed, toluene and chloroform which are larger than water or methanol, but much more soluble in the siloxane polymer, pass through the membrane much faster. However, an objection can be formulated: the highest fluxes are obtained for the compounds having the highest vapour pressure at the experiment temperature (20°C). In this case, the difference in flux from one solvent to an other could be due merely by the difference of vapour pressure, assuming that the membrane is still porous and that an evaporation takes place through it. It is clear from Fig.7.6, that there is no correlation between the steady state permeation fluxes

of the test compounds (Figs. 7.3 and 7.4) and their saturated vapour pressures at 20°C. This suggests once more that the ceramic pores of the PDMS-modified membrane are completely blocked by the polymer. It is easy seen that the original untreated alumina membrane behaves very differently, under the same experimental conditions. Compared to the PDMS-modified membrane, the permeation fluxes are huge, and in the specific case of water, liquid water can be observed very quickly in the downstream cell side, before the cold trap. In this case the transfer is through open pores and the process a simple membrane distillation.

The morphology of the porous alumina membrane and of the PDMS modified one, and their respective transfer mechanism are represented diagrammatically in Fig. 7.7. The representation is schematic and makes no attempt to represent the tortuous pore structure of the alumina.

7.3.3 Gas permeability

To investigate further the properties of the PDMS-treated membrane, gas permeation experiments were carried out on it and on the original untreated membrane. The results are presented in the Table 7.2 and Figs. 7.8 and 7.9. Good linearity between flux and transmembrane pressure showed that the gas permeabilities in both membrane were constant over the experimental conditions. A comparison of Figs. 7.8 and 7.9. shows that the permeability of gases studied are smaller in the treated membrane by between 4 and five orders of magnitude. Such a reduction in a membrane in which the diameter of the untreated pores is 5 nm is clear evidence that diffusion occurs no

longer in open pores but by molecular diffusion through the silicone layer as concluded

previously from pervaporation results. The transport behaviour of a range of common

gases across the untreated membrane was measured (Table 7.2). The permeabilities

plotted against the reciprocal of the square root of the molecular weights of the gases

is not linear and so, even in this case, the mechanism of gas permeation is not simple

Knudsen flow (Fig. 7.10), as shown by anodic alumina membrane, Chapter 5. This

suggests adsorption and condensation effects influence the transport of many of the

gases. As discussed in Chapter 5, Section 5.3.1, the gas least likely to be affected is

helium, and on this basis a tentative ideal Knudsen line was drawn, Fig. 7.10. Of the

remaining gases the only other gas on the 'theoretical' line was neon, which, would

also be expected to show minimum condensation or adsorption tendencies. For the

others, the permeabilities are much larger than Knudsen mechanism would predict.

Concerning the treated membrane, as expected, there is no evidence for Knudsen flow.

The treated membrane seems to exhibit some similarities and some differences to the

transport properties of PDMS dense film for certain gases. For example the ratio of

permeabilities for CO_2/N_2 is 11.4 for a dense PDMS film [20], and 10.2 for the

alumina PDMS-modified membrane which is a very similar value. In the same

reference, however the CH_4/N_2 permeability ratio, was 3.4 for the dense PDMS film,

but for the alumina-PDMS membrane the ratio was 16.7 which is very different. It

seems then, that the alumina PDMS-modified membrane is not equivalent merely to a

dense PDMS layer cast on a porous surface. This result is interesting because it shows

that ceramic/polymer composite membranes (as prepared in this work) constitute an

alternative to purely polymeric or purely inorganic membranes. The composite retains

the rigidity and pore morphology of the host ceramic, while the polymer grossly alters

the ceramic membrane functionality. The functionality of the polymer will also be

modified by the fact that the polymer within the pores of the ceramic structure is

physically restricted, affecting the solubility and path tortuosity of permeants, and

selectivity as compared with the free polymer. To complete the assessment, it is to be

reported that correlation cannot be found between the molecular weight or the kinetic

diameter (Table 5.1, Chapter 5) of the diffusing gas molecule, and its permeability

through the treated membrane. All evidence confirms that the transfer mechanism

through the PDMS-alumina membrane occurs by a solubility/diffusion mechanism, in

other words by gas dissolution and gas diffusion in the membrane.

7.3.4 Separation by pervaporation

One of the most promising industrial application of hydrophobic membranes is the

extraction of organic compounds from water [16, 21]. Indeed, it can be interesting, for

ecological or economical reasons to extract volatile organic compounds (VOC) from

water [22] or alcohol from aqueous fermentation broths [23]. In these cases, a ceramic

membrane grafted by PDMS could be valuable because the hydrophobic layer being

very thin (monomolecular layer), must lead to a very permeable membranes. In order

to evaluate the behaviour of the modified alumina membrane during a real liquid

mixture separation experiment, the membrane is placed in the liquid permeation device

and pure liquid feed is replaced by a liquid aqueous organic mixture of controlled

composition. An aqueous mixture containing 10 wt% of tetrahydrofurane (THF) was chosen as first test mixture because THF and water are soluble in all proportions and then the measure of the refractive index is easy. This first attempt shows clearly that the membrane is selective to the organic compounds (Table 7.3). Indeed, at 20°C, the permeate becomes richer in THF than the feed and the selectivity α is 20 in favour of THF. This promising result leads the study toward a more interesting separation on the industrial angle. Alcohols, especially 1-butanol (nBuOH), are produced during fermentation reactions. The nBuOH is proved to be toxic to the micro-organism performing fermentation when it reaches a concentration of only 2 wt%, in the fermentation broth [23]. A method for continuously removing nBuOH from dilute fermentation both is of great industrial interest. In a pervaporation test 5 wt% nBuOH aqueous solution was used. The experiments are carried out at 40°C for comparison with the literature data on polymer membranes. The results are shown in Table 7.3. It is shown that the PDMS modified alumina membrane is very permeable, compared to a dense PDMS membrane. On the other hand, nevertheless, its selectivity is still relatively low (α=20 against 82 for dense PDMS). In fact, the difference of selectivity between these two membranes may not be as these values suggest, since the silicone modification membrane was tested with a feed containing 5 wt% of nBuOH whereas the literature data refer to a feed containing 6.1 wt% of nBuOH. It is well known that the selectivity of a membrane generally decreases when the organic compound concentration decreases in the feed [24]. Although, it seems obvious that the alumina PDMS-modified membrane is not as selective as a dense PDMS membrane, even if the

7.16

selectivity values must be closer to each other that those obtained. Nevertheless, the

much higher flux exhibited by the alumina modified membrane, is really a valuable

advantage over the pure polymeric membranes, for certain kinds of applications where

the permeation flux is a vital parameter.

7.4 Conclusion

A new way to prepare hydrophobic membranes is reported. It has been shown that polydimethylsiloxane oil (and any other silicone oil molecules) can be grafted onto a porous alumina membrane (or any hydroxylated ceramic or glass) merely by heating, to 180°C, producing a covalently grafted monolayer of silicone oil, almost certainly monomolecular. This kind of membrane is chemically and thermally stable, unaffected by organic solvents (as shown by its stability under prolonged extraction by toluene in a Soxhlet extractor) but susceptible to alkali attack (as is the silicone oil itself). The membrane is totally impermeable to pure water, and organic solvents may be extracted from water mixtures by pervaporation. Very high permeation fluxes were obtained, suggesting possible use of these silicone/ceramic membranes in extraction of volatile organic compounds. Both treated and untreated membranes were gas permeable and neither exhibited Knudsen diffusion. The results of all permeation experiments with liquids and gases are consistent with the hypothesis that the treated membrane is no longer porous and that permeant molecules are transported by a solution/diffusion mechanism, as in a dense polymer film. There is evidence however, that the properties of the grafted polymer molecules in the porous ceramic matrix are no longer analogous to those of the polymer films of the same material. This easy modification method can be applied to macroporous membranes modifying surface properties and increasing hydrophobiticy without pore blocking. Such treated membranes may have particular applications in organic filtrations and in aqueous separation procedure as an anti-fouling coating.

7.5 References

[1] J. Randon, P. Blanc, R. Paterson, Modification of ceramic membrane surfaces using phosphoric acid and alkyl phosphonic acids and its effect on ultrafiltration of BSA protein, J. Membr. Sci., 98 (1995) 119-129.

[2] J. J. Pesek, Conversion of oxide surfaces to hydride surfaces, in Chemically Modified Surfaces, Ed. J. J. Pesek and I. Leigh, The Royal Society of Chemistry, (1994) 1-23.

[3] R. E. Johnson and D. I. Ford, Stability and reactivity of dimethylethoxysilane, in Chemically Modified Surfaces, Ed. J. J. Pesek and I. Leigh, The Royal Society of Chemistry, (1994) 164-184.

[4] G. J. Hills and D. J. G. Ives, The calomel electrode and other mercury-mercurous salt electrodes, in Reference Electrodes : theory and practice, edited by D.J.G Ives and G.J. Janz, New York Academic Press, (1961) 135-136.

[5] G.J. Hills, D.J.G. Ives, The hydrogen-calomel cell - Part II - The calomel electrode, J. Chem. Soc., (1951) 311.

[6] F. M. Lewis, Chemistry of silicone elastomers, in Polymer Chemistry of Synthetic Elastomers - Part II, edited by J.P. Kennedy and E.G.M. Tornqvist, Interscience Publishers, (1969) 791.

[7] W. J. Bobear, Behaviour of silicone rubber in sealed systems at high temperatures, Rubber Age, 84 (1958) 448.

[8] M. G. Voronkov, Z. I. Shabarova, Cleavage of hexaalkyldisiloxanes by phenols, Zhur. Obshchei Khim., 30 (1960) 1955-1958.

[9] M. M. Sprung and F. O. Guenther, The reaction of some silanols and siloxanes with n-octyl alcohol, J. Org. Chem., 26 (1961) 552-557.

[10] A. Larbot, J. P. Fabre, C. Guizard and L. Cot, New inorganic ultrafiltration membranes, J. Am. Ceram. Soc., 72, (1989), 257.

[11] F. M. Lewis, Chemistry of silicone elastomers, in Polymer Chemistry of Synthetic Elastomers - Part II, edited by J. P. Kennedy and E. G. M. Tornqvist, Interscience Publishers (1969) 769.

[12] W. J. Bobear, Heat-aging studies on silicone rubber stocks, Rubber Age, 95 (1964) 31.

[13] J. Randon, R. Paterson, Composite ceramic-organic membranes for gas separation, in press.

[14] J. Neel, Introduction to pervaporation, in Pervaporation Membrane Separation Processes, Ed. R. Y. M. Huang, Elsevier (1991), 1-110.

[15] J. Neel, P. Aptel, La pervaporation : principe de la technique. Entropie 104, (1982), 15.

[16] S. Zhang and E. Drioli, Pervaporation membranes, Sep. Sci. Technol., 30 (1995), 1-31.

[17] J. A. Barrie, B. Platt, The diffusion and clustering of water vapors in polymers, Polymer, 4 (1966) 303.

[18] J. A. Barrie, Diffusion of methanol in polydimethylsiloxane, J. Polym. Sci., 4 (1966) 3081.

[19] M. Mulder, Membrane processes, in Basic Principle of Membrane Technology, Ed. Kluwer Academic Publishers, (1991), 221-222.

[20] M. Mulder, Membrane processes, in Basic Principles of Membrane Technology, Ed. Kluwer Academic Publishers, (1991), 228.

[21] National Research Council : Separation & Purification. National Academy Press, Washington (1987).

[22] W. A. Telliard, G. S. Goldberg, Sampling and analysis procedure for screening industrial effluents for priority pollutants, Symp. Proc. Process Meas. Environ. Assess., (1978) 104-107.

[23] M. J. Spivey, The acetone/butanol/ethanol fermentation, Process Biochem. (1978), 2.

[24] J. Neel, Introduction to pervaporation, in Pervaporation Membrane Separation Processes, Ed. R.Y.M. Huang, Elsevier (1991), 27-31.

Table 7.1 Pure liquid solvent permeation experiments. T= 20 °C with a downstream pressure of 1mmHg.

Solvent	Flux through untreated alumina membrane $(kg.h^{-1}.m^{-2})$	Flux through PDMS-treated alumina membrane $(kg.h^{-1}.m^{-2})$
H_2O	18.00	trace
MeOH	-	0.21
EtOH	-	0.82
nPrOH	-	0.23
nBuOH	-	0.16
Et_2O	-	4.20
THF	-	1.80
acetone	-	2.32
$CHCl_3$	110.00	4.60
toluene	-	2.17

Table 7.2 Pure gas permeation experiments for γ-alumina membrane. T=20°C.

Gas	Permeability untreated membrane $(mole.s^{-1}.m^{-2}.Pa^{-1}).10^{7}$	Permeability PDMS-treated membrane $(mole.s^{-1}.m^{-2}.Pa^{-1}).10^{11}$
He	92.01	110.00
CH_4	84.52	100.00
Ne	43.35	70.00
N_2	55.12	6.00
Ar	42.91	90.00
CO_2	46.46	61.00
C_3H_8	73.24	83.00

Table 7.3 Aqueous mixture pervaporation experiments. Down stream pressure, 1mmHg

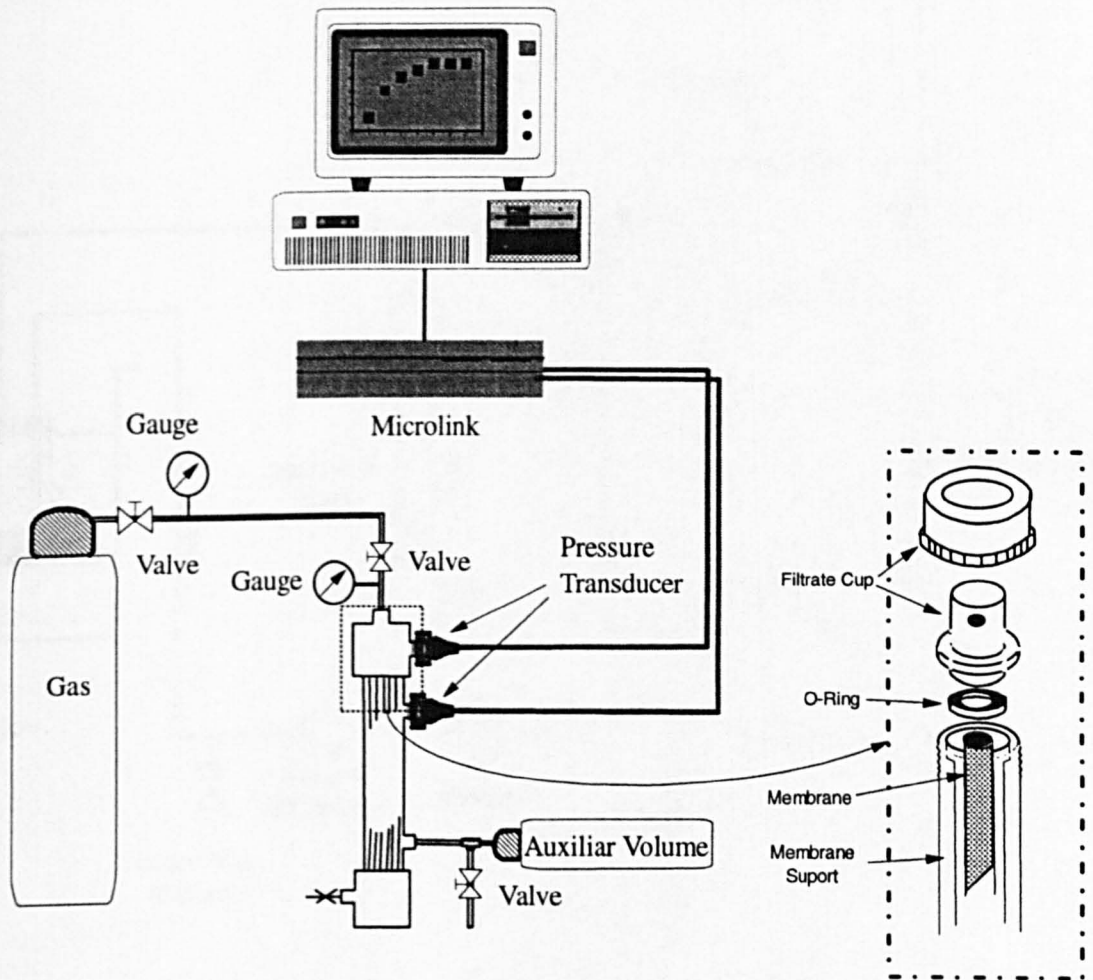| Aqueous liquid mixture feed	Membrane nature	Temperature (°C)	Total flux (kg.h^{-1}.m^{-2})	Selectivity α (dimensionless)
10 wt% THF	PDMS-alumina treated	20.00	0.10	20.00
5 wt% nBuOH	alumina untreated	40.00	25.00	1.00
5 wt% nBuOH	PDMS-alumina treated	40.00	0.31	20.00
6.1 wt% nBuOH	pure dense PDMS[12]	40.00	0.17	82.00

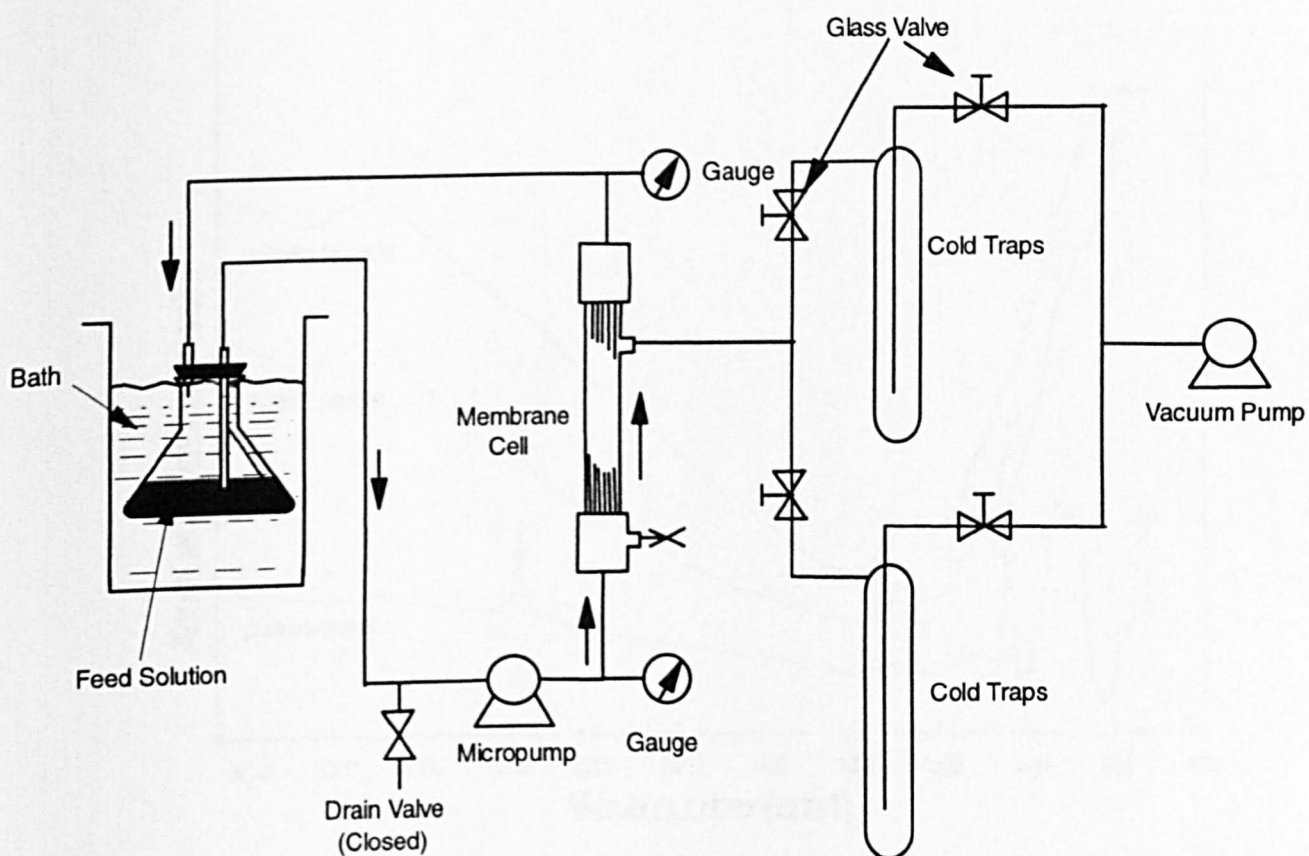Fig.7.1 Schematic diagram of gas permeation sysytem for tubular membrane.

Fig.7.2 Schematic diagram of pervaporation system.
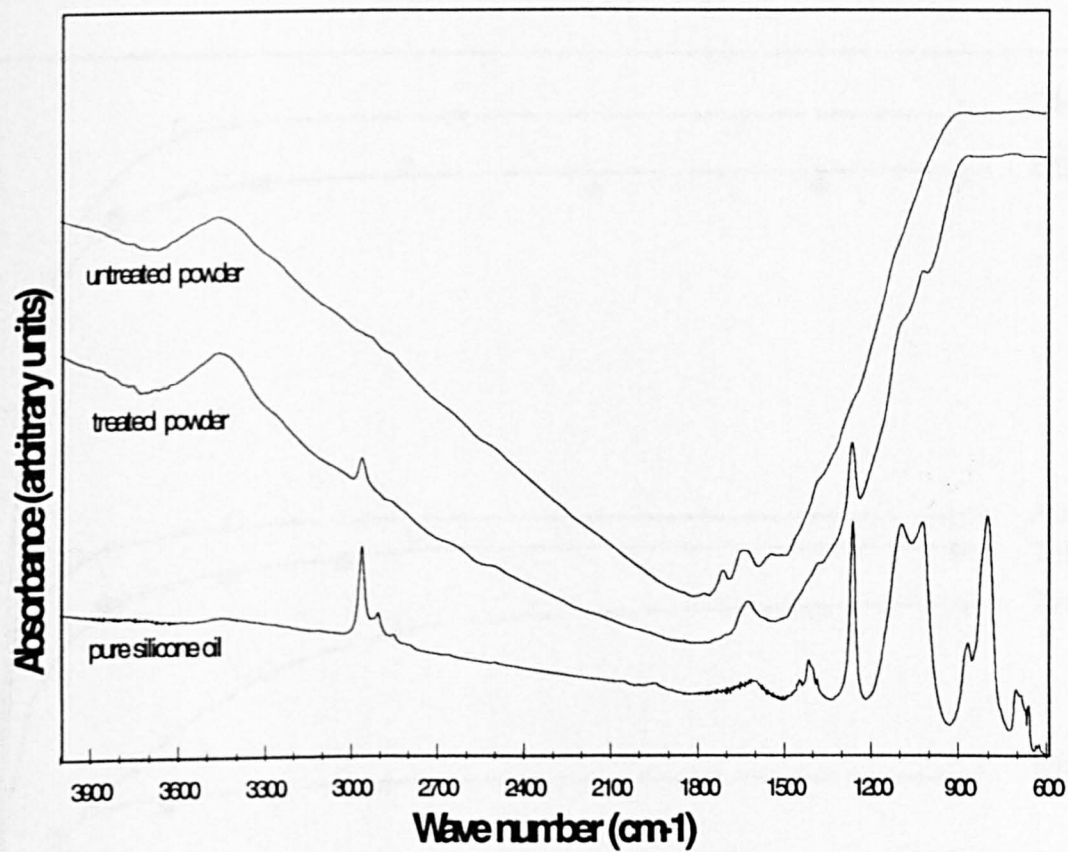
Fig.7.3 FTIR spectra of an alumina powder before and after silicone oil treatement.

Fig.7.4 Permeation measurements of pure solvents through a 5 nm Al2O3 PDMS-modified membrane. T= 20 °C, with a downstream pressure of 1 mmHg.
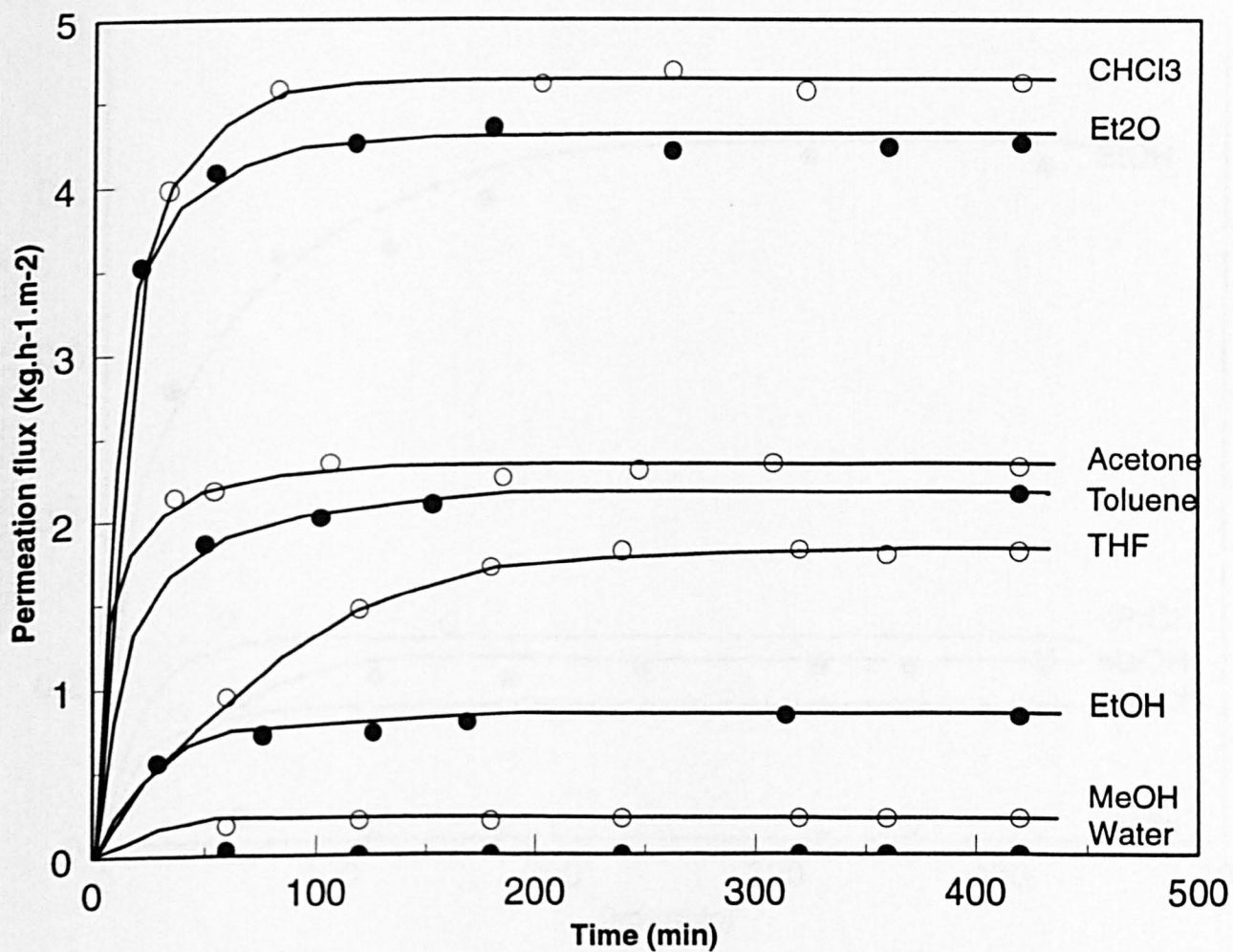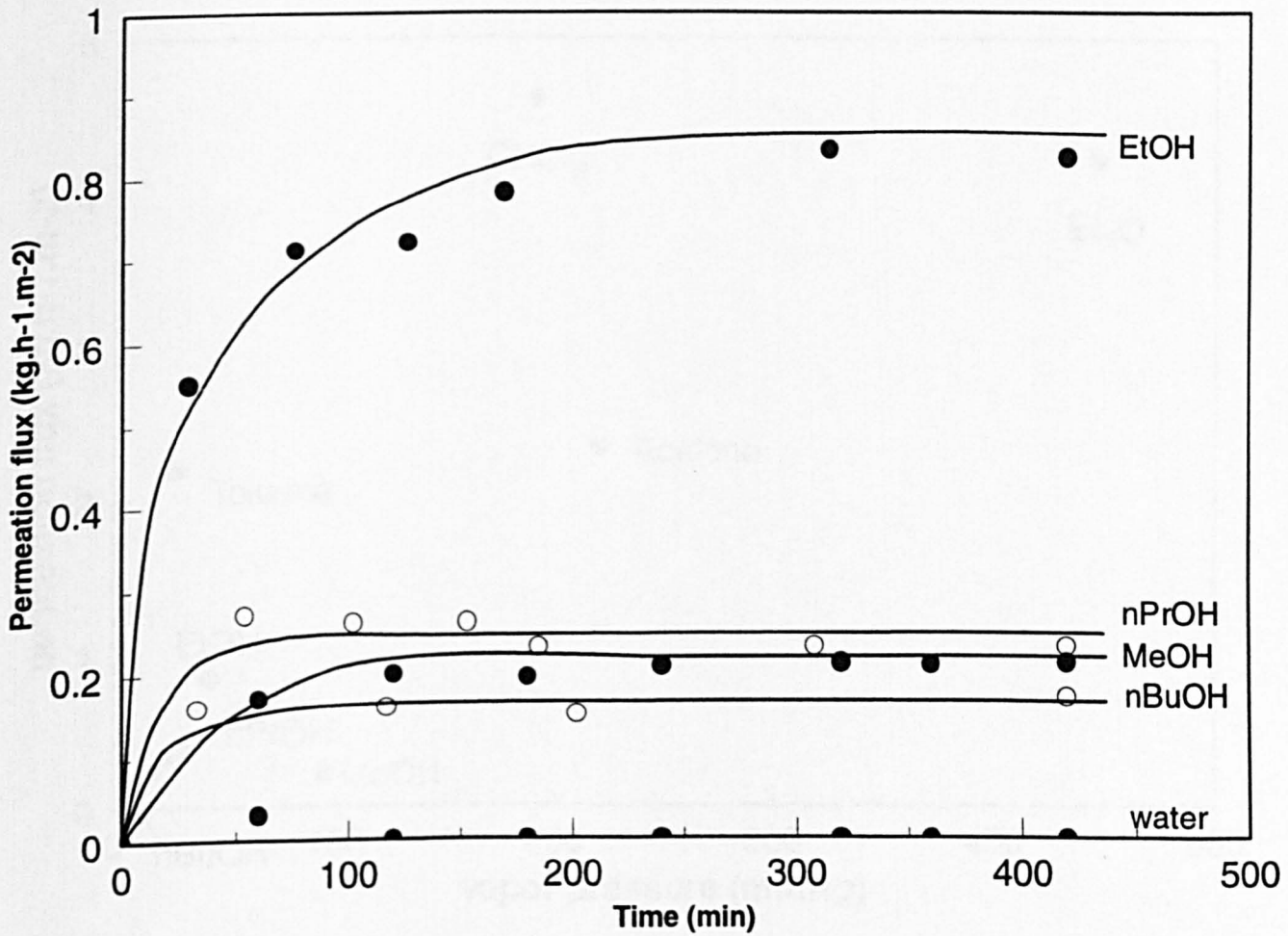
Fig.7.5 Permeation measurements of pure polar solvents through a 5 nm Al2O3 ODMS-modified membrane. T=20℃, with a downstream pressure of 1 mmHg.
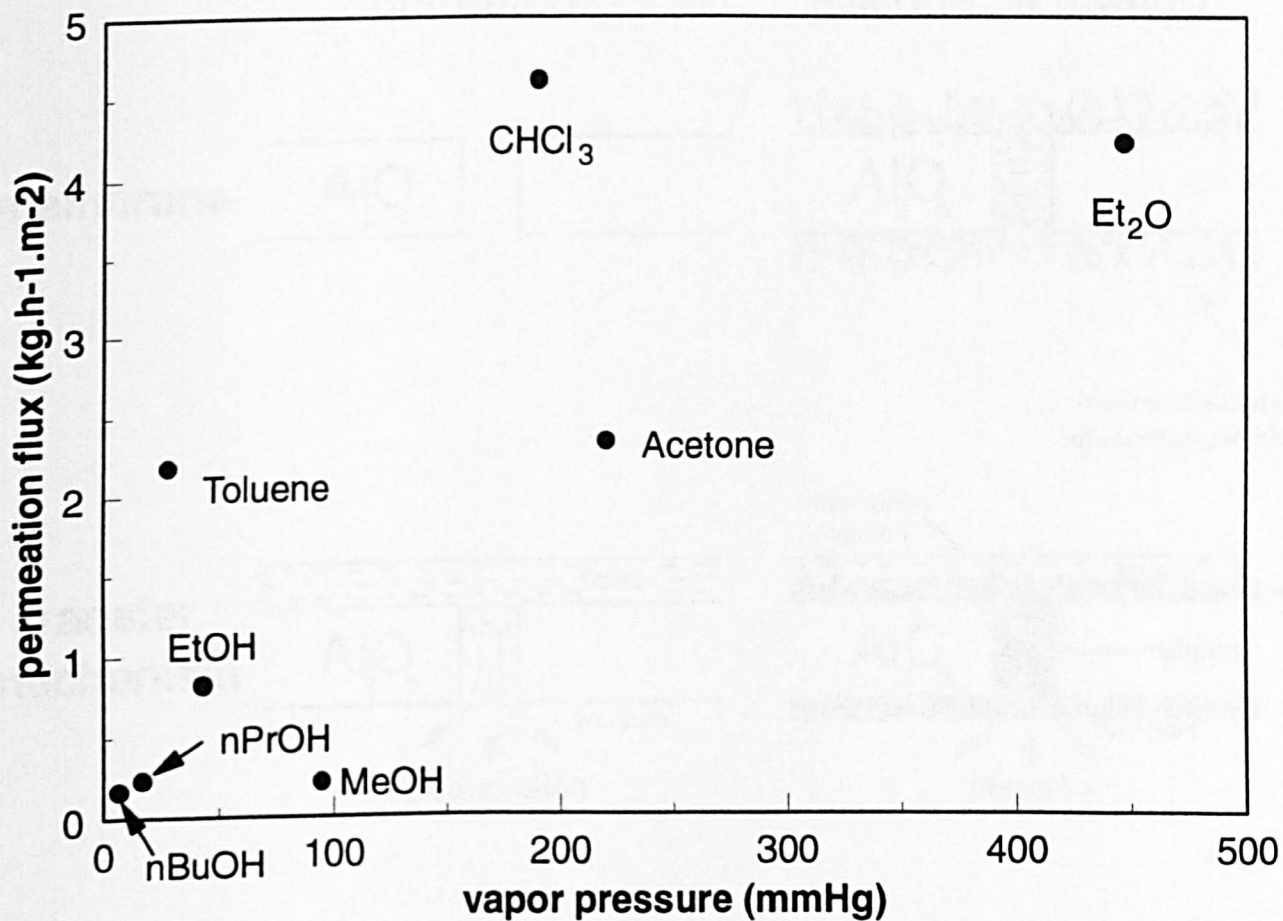
Fig.7.6 Variation of the permeation flux with the vapor pressure of the transferred compounds at 20℃, through the Al2O3 PDMS-modified membrane..

untreated   silicone oil treated

membrane

$AlO_{2}{}_{3}$

$AlO_{2}{}_{3}$

monomolecular layer
of polysiloxane chains

**transfer
mechanism**

liquid

$AlO_{2}{}_{3}$

vacuum

evaporation

dissolution
(sorption)

liquid

$AlO_{2}{}_{3}$

diffusion

vacuum

desorption
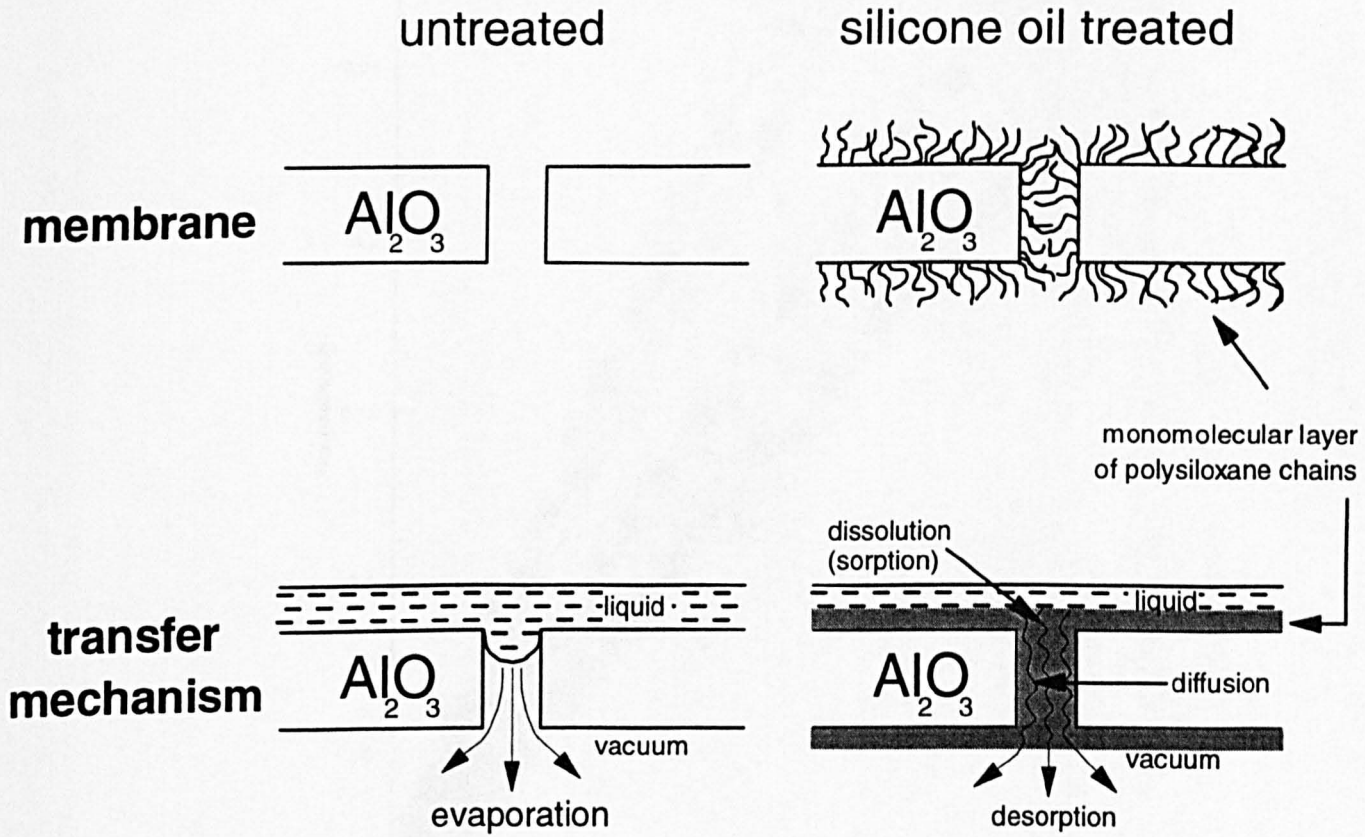
Fig.7.7 Schematic hypothesis of the membrane morphology and of the transfer mechanism
occurring through it, before and after silicone oil.
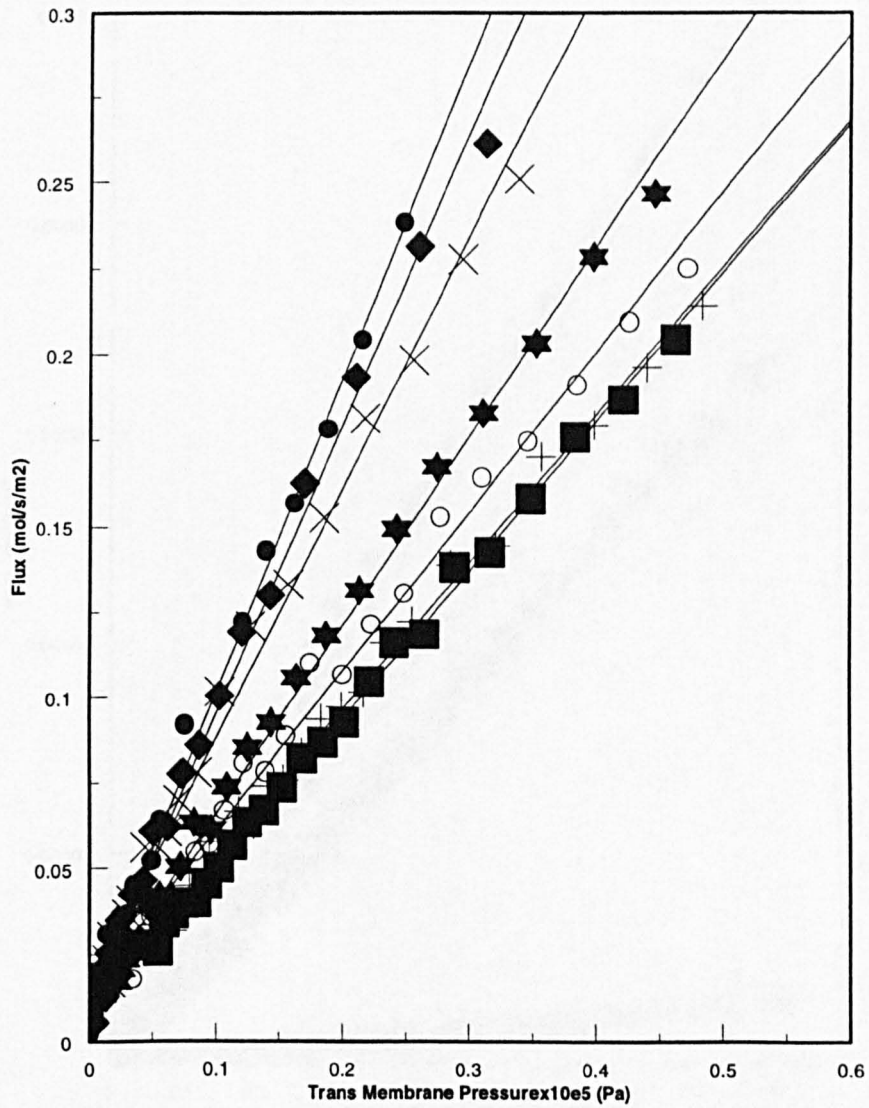
Fig.7.8 Gas permeability properties of the 5 nm alumina membrane at 20 C, before
modification. He,●; Ne,■; Ar,+ ;N2,★; CO2,○; CH4,◆; C3H8,×. Permeabilities
are listed in Table 7.2.
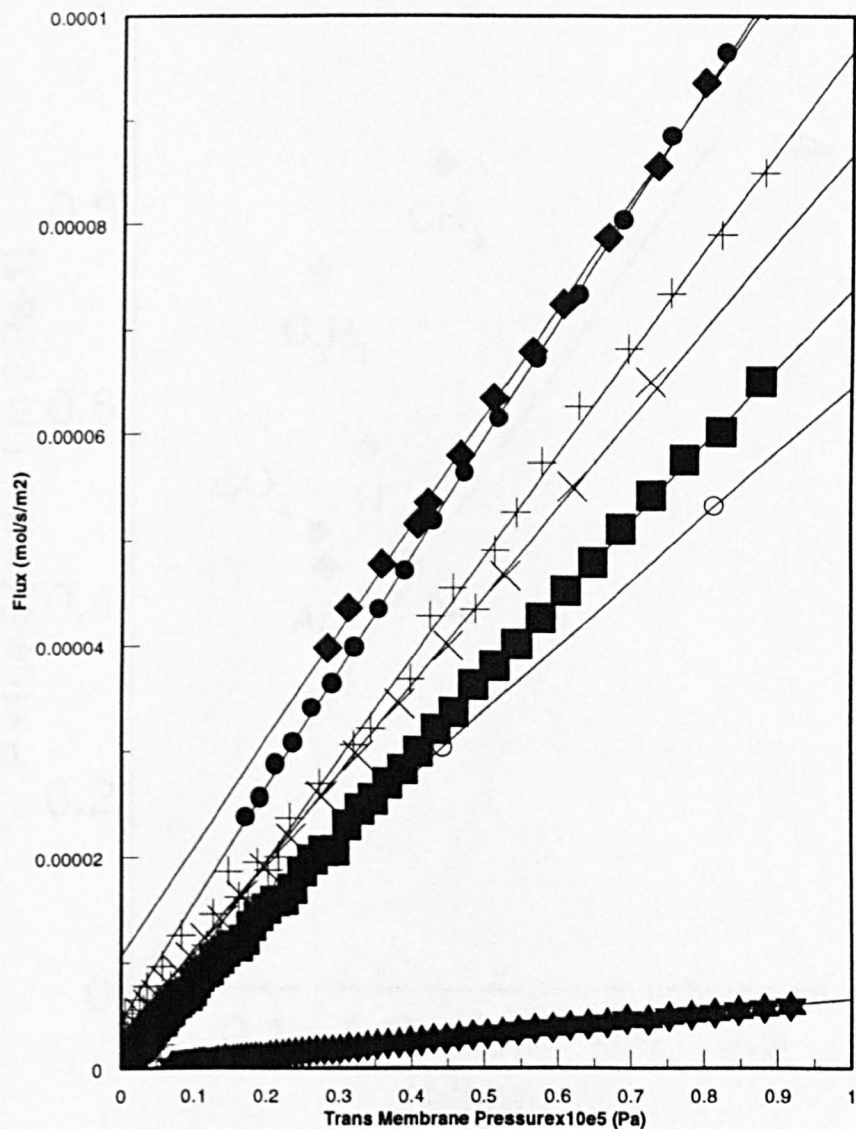
Fig.7.9 Gas permeability properties of the 5 nm alumina membrane at 20 C, after silicone oil (PDMS) treatmente modification. He,●; Ne,■; Ar,+ ;N2,★; CO2,○; CH4,◆; C3H8,×. Permeabilities are listed in Table 7.2.
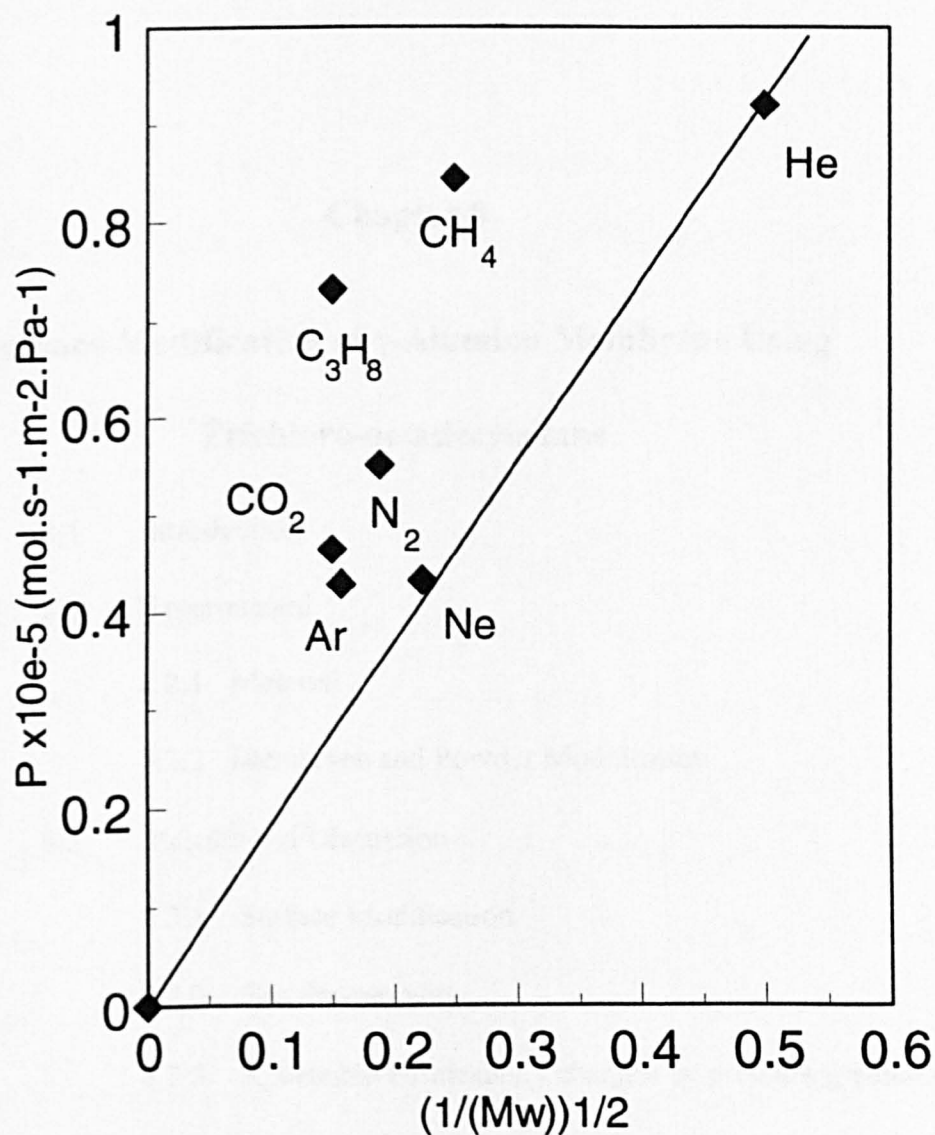
Fig.7.10 Variation of the permeability (at 20 C) of several pure gases with their respective molecular weights, through the untreated 5 nm alumina membrane. Comparasion of the real gas permeability with a straight line corresponding the Knudsen flow through the membrane.

Chapter 8

Surface Modification of γ-Alumina Membrane Using

Trichloro-octadecylsilane

8.1 Introduction

As show in Chapters 6 and 7, surface modification of ceramic membranes by covalently bonded molecular monolayers is a convenient way to alter membrane performance. A monolayer, according to its thickness and functionality, will reduce the effective pore size (even filling the pores as shown in Chapter 7) and alter the chemistry of both external and internal surfaces of the membrane and so modify (often dramatically) membrane selectivity, permeability and fouling characteristics [1]. Commercially available porous ceramic membranes, as yet, have pores which are too large to be used, for applications such as gas separations, although research membranes are now under development which have pore size ~ 1nm which will be of considerable interest. For membranes with pores < 10nm, bonding organic compounds covalently to pore surfaces is probably the most flexible and controllable method for modification. Phosphate derivatives (as described in Chapter 6), triethoxysilicon compounds [2], chlorosilane derivatives [3], or even polysiloxanes, in Chapter 7, have been successfully used to modify ceramic surfaces as alumina, zirconia, silica, titania, or thoria. They were used mainly to prepare new chromatographic stationary phases seldom in the membrane applications. In this chapter octadecyl-silane derivatives will be investigated as potentially interesting candidates to modify a ceramic surface, despite of their high moisture sensitivity, which results in handling difficulties. Chlorosilanes easily react with the surface hydroxyl groups, generating only hydrochloric acid as a by-product, which is easily removed from the reaction medium. A broad range of chlorosilanes are commercially

available, increasing the diversity of the potential modifications. In this Chapter the same commercial available alumina membranes with 5nm pores described in Chapter 7 will be used to be modified using octadecylchlorosilanes and the gas permeation properties will be investigated.

8.1.2 Background

It is well known that chlorosilane compounds are very reactive on any kind of hydroxyl groups, generating hydrochloric acid [5]. This property has been extensively exploited to modify silica surfaces to prepare new stationary phases for chromatography [6]. Other hydroxylated inorganic oxides such as zirconia, alumina, or titania might equally well be used. The chemical reaction involved in this type of reaction can be described as follows:
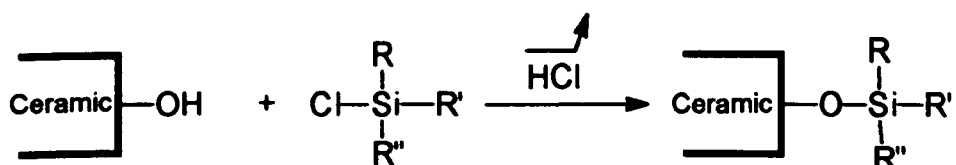
The basic concept is to graft on a ceramic membrane surface (γ-alumina in this case) a chlorosilane derivative with a substituent hydrocarbon chain long enough to significantly reduce the membrane pore size or even block the pores and examine the consequences for gas diffusion.

The first part of this chapter will deal with the grafting reaction, the second will describe the effects of this modification on gas permeation.

To study the reaction between the alumina and the chlorosilane, alumina powder was used rather the membrane itself. Alumina powder, which can be considered as morphologically equivalent to the membrane as described in Chapter 7.

8.2 Experimental

8.2.1 Powder and membrane modification

The same tubular gamma alumina membranes, with 10mm external diameter, described in Chapter 7 were used. The active layer was a thin layer of porous alumina (pore size 5nm) deposited on the inner tube surface, deposited by a sol-gel process. Also the chemical reaction experiments were performed on the same gamma alumina powder. A typical modification of the alumina powder (or membrane) by a chlorosilane derivative was as follows: 0.5g of alumina powder (or membrane) was mixed with 10 ml of dry toluene in a two-necked reaction flask fitted with a dropping funnel and a reflux condenser. The reflux condenser was connected to a vacuum pump. Using a controlled leak, the reaction vessel was maintained under a moderate vacuum (roughly 400 mmHg). The toluene/alumina suspension was gently refluxed without significant solvent losses. 10 mmole of a chlorosilane derivative, dissolved in 10 ml of dry toluene, were then added relatively quickly to the suspension. A further 10 ml of dry toluene was added to the reaction mixture rinsing the dropping funnel. The reaction mixture was refluxed for a further 2 hours, the HCl formed being pumped out of the reactor. After this reaction step, the powder (or membrane) was quickly transferred in a Soxhlet apparatus and extracted with toluene, for 12 hours, to remove unbound siloxane molecules from the alumina surface. The powder was then dried for 24 hours at 65 °C, over silica gel, followed by 1 hour at ambient temperature under vacuum (0.1 mmHg).

The chlorosilanes compounds used were dimethyl octadecyl chlorosilane and octadecyl trichlorosilane, both purchased from Fluka (catalogue ref.: 40950 and 74762) and used without further purification.
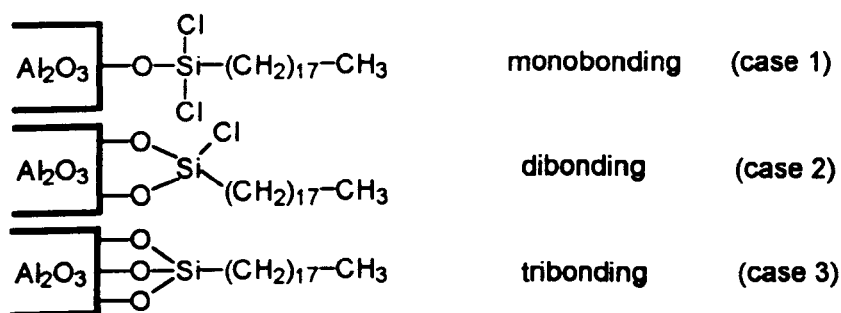
8.2.2 Infrared spectroscopy measurements

Similarly to Chapters 6 and 7, it were used FTIR spectra and the modified powders prepared as KBr discs to prove an effective grafting of hydrocarbon chains on the alumina surface, since the C-H absorption are easily detected on 2900 - 3000 cm^{-1} bands.

8.3 Results and discussion

8.3.1 Surface Modification

The infrared spectroscopy is a particularly suitable technique to detect the presence of hydrocarbon chains on the alumina surface. Indeed, the C-H absorption band due to a stretching of the chemical bond itself, can easily be isolated between 2900 and 3000 cm^{-1}. Octadecylsilanes were used in this study because their chains would be some 2.5 nm fully extended approximately equal to the membrane pore radius. (The manufacturer's estimate of pore diameter is 5nm.) For such long chain aliphatics the intensity of the C-H absorption band is relatively high and thus the detection of successful grafting becomes easier.

When dimethyl octadecyl chlorosilane was used as a reactant no C-H bonds were detected on the alumina surfaces and so no reaction takes place between the chlorosilane and the hydroxyl group of the alumina. The same result was observed in anodic alumina membrane. This lack of reactivity could be due to the steric effect of the octadecyl chain and the two methyl groups limiting the access of the Si-Cl bond to hydroxyl groups of the alumina surface. With octadecyl trichlorosilane the steric effect is reduced and three Si-Cl bonds are available to react with the surface and the grafting reaction is successful as shown by the infrared spectra of Fig. 8.1. This reaction was expected to produce a permanent modification because the chemical grafting is by a very stable Si-O bond. The precise structure of the bonding on the surface is still unresolved, although the reaction mechanism is clear. Three possibilities exist:

Al_2O_3 —O—Si(Cl)(Cl)—(CH$_2$)$_{17}$—CH$_3$	monobonding	(case 1)
Al_2O_3 —O,O—Si(Cl)—(CH$_2$)$_{17}$—CH$_3$	dibonding	(case 2)
Al_2O_3 —O,O,O—Si—(CH$_2$)$_{17}$—CH$_3$	tribonding	(case 3)

Membrane treated in this way are extremely hydrophobic. For this reason it is not clear in case 1 and case 2 whether Si-Cl bonds will hydrolyse. Hydrolysis must generate hydrochloric acid, however on exposure to water over a long period no change in pH was detected. On this basis tribonding (case 3) is most probable.

8.3.2 Gas permeability

Gas permeabilities of seven common gases were determined for the gamma alumina membrane before and after treatment with octadecyl trichlorosilane. The results, in Table 8.1 and Figs. 7.8 (Chapter 7) and 8.2, show that the gas permeabilities of the octadecylsilanised (ODS) membrane are three orders of magnitude smaller than for the untreated membrane. It is clear that the pores of the ODS membrane are effectively obstructed by the octadecyl aliphatic chains. There can be no concept of an open pore remaining. The permeabilities of test gases are however, on average 4 times larger by than for the silicone treated membrane in Chapter 7. Permeant gases must therefore pass through the hydrocarbon chains, but an element of openness or fluidity may remain perhaps because the total length of the extended graft chain can be estimated to be about 2.5-2.6nm. If the pore shape is assumed to be circular a

complete ODS monolayer could just fill a 5nm pore but might retain a degree chain mobility (fluidity) in the pore centres. Gas permeation data reported in a previous chapter, show clearly that the transfer mechanism in the open pores of the untreated membrane is not a simple Knudsen flow, Fig. 7.10. Deviations from a simple kinetic model for the ODS-modified membrane are even larger, Fig. 8.3. A feature of the ODS-membrane is the near constancy of the permeabilities. The seven gases, although ranging widely in mass (from He (MW, 4) to propane and carbon dioxide (MW, 44)) and in chemical properties, all have permeabilities in the range $\pm 10\%$ of the average value of 360×10^{-11} mole $s^{-1} m^{-2} Pa^{-1}$, except methane which has the highest permeability of the group, 481×10^{-11} mole $s^{-1} m^{-2} Pa^{-1}$. Although the gases differ widely in mass and chemical properties methane has a higher permeability than helium suggesting a solubility/diffusion mechanism. The interplay of diffusion (mobility) and solubility cannot be resolved without further research but the two factors appear to largely cancel for the gases studied: gases with high mobility have a low solubility (e.g. He) and those with high solubility have low mobility (e.g. propane).

8.3.3 Reversible permeability changes produced by pressure gradients

In Chapter 7, a monolayer of low molecular weight polydimethylsiloxane (silicone) was bound to the γ-alumina membrane and so the monolayer molecules are internally cross-linked polymers. In this case the monolayer has octadecyl chains each linear molecule with a potential for chain mobility increasing from its point of attachment on the surface, towards the centre of the pore. Direct evidence of reversible chain

movements was obtained quite unexpectedly in a series of experiments described below for nitrogen permeation.

In these γ-alumina membranes the thin active layer of gamma alumina (pore size 5nm) is located on the inner surface of the microporous tubular membrane (designated face 1) the outer face (shell side) will be designated as face 2, shown diagrammatically in Fig. 8.5. It was observed that when the membrane was under a nitrogen pressure of 1atmosphere on the inner tube surface (face 1) and the shell side (face 2) was evacuated for 10 minutes the ODS membrane nitrogen gas permeabilities was reduced by a five times to from 322×10^{-11} to 62×10^{-11} mole s^{-1} m^{-2} Pa^{-1}. This change was metastable, the membrane remaining in its modified state during normal handling and during repeated gas permeation experiments. The permeability plots of flux against pressure difference across the tube were linear and reproducible, Fig. 8.4.

In this research it proved to be significant that gas permeabilites were obtained in all cases for transport across a membrane from tube to shell side (face 1 to face 2) with initial pressure difference of 1 bar, (face 1, 2 bar and face 2, 1 bar). The high pressure side was maintained constant and the flow of gas computed from the rise in pressure of the low pressure side at 20 °C. As shown in Figs 7.8 (from Chapter 7), 8.2 and 8.4, permeation was followed until the pressure differential equalised in most cases.

In Fig. 8.5 the permeability changes induced by a series of conditioning treatments are summarised and the data for each permeability experiment shown in Fig. 8.4. When the conditions were reversed (face 2, 1atm, face 1 evacuated for 10 minutes) the

membrane returned to its original nitrogen permeability (299×10^{-11} mole s^{-1} m^{-2} Pa^{-1}). This reversal was reproducible in cyclical experiments. A membrane in the low permeability state was stable and had a reproducible permeability over the several hours of experimentation. This form is not stable over a longer period. A membrane in the low permeability state left for 16 days at ambient 20°C recovered its original high permeability (337×10^{-11} mole s^{-1} m^{-2} Pa^{-1}). This is explicable if the low permeability state is due to a packing of chains under the stress induced by the pressure treatment. Under uniform pressure, the chains would tend to relax toward the more stable, high flux morphology.

Applying the standard conditions (face 1, 1 atm: face 2, evacuated) for 12 hours rather than the normal 10 minutes caused an additional 39 % reduction in the low permeability state (from 62×10^{-11} to 38×10^{-11} mole s^{-1} m^{-2} Pa^{-1}). The high permeability state could not be recovered by back pressure (face 2, 4 atm; face 1, 1 atm) for 45 minutes: the permeability rose only from 38×10^{-11} to 82×10^{-11} mole s^{-1} m^{-2} Pa^{-1}. The high permeability state was achieved by a reverse pressure gradient (face 1, 1 atm; face 2, 2 atm) but only after 15 hours. Under standard conditions (face 1, 1 atm: face 2, evacuated) for 1 hour gave a permeability of 40×10^{-11} mole s^{-1} m^{-2} Pa^{-1} almost identical to that achieved previously after 12 hours, indicating that the change to the lowest permeability state is largely (90 %) achieved after 10 minutes and 99 % after 1 hour. There is no reasonable explanation for such reversible and reproducible changes other than by changes in the morphology or packing of the octadecyl chains of the bound monolayer, the potential for chain reorientation increasing progressively from its

point of attachment on the surface, towards the centre of the pore. The relaxation period was long, full recovery being observed after 16 days, under ambient conditions. No changes in permeability were observed during the first 24 hours. It is clear that the hydrocarbon chains are not liquid at the experimental temperature, 20 °C, otherwise the monolayer would recover rapidly from any mechanical distortion to a randomised fluidity. Packing of the hydrocarbon chains due to a pressure difference of 1atm against vacuum can be envisaged as a one-sided molecular bombardment by nitrogen molecules moving the mobile ends of the octadecyl chains in the direction of the evacuated side. If this were so we might expect that chains would bend towards the pore wall towards the evacuated side. Using a simple pore model with a molecular monolayer attached to the walls of a pore, such movements would be expected to pack the octadecyl chains more closely against the pore wall, open the pores and increase the permeability. The reverse is observed, a low permeability state is obtained.

A tentative explanation might be that the octadecyl chains on the surface of the active layer on the tube side (face 1, above) are partly forced into the pores which are already partly or completely covered by a ODS monolayer, Fig 8.6. In this way chain movement would lower rather than raise permeabilities, by further obstructing molecular flow. If this is so then the active layer must be asymmetrical since reversal of this treatment (1 atm pressure applied from the shell side against a vacuum on the tube side) does not (also) create a low permeability state once more, but merely restores the high permeability (relaxed) state. This implies that there is no mechanism

by which octdecyl chains may block the pores of the active layer at its interface with microporous support. This may be because at this interface there is no free external surface to provide the excess of hydrocarbon chains capable of entering the pores, but only a transition to the much wider pores of the support. Alternatively, one might imagine that or that efficient silanisation of the active layer is largely confined to outer surface of the tube side (face 1) and immediately adjacent pore surfaces. This latter hypothesis might be justified, firstly, if the octadecyl trichlorosilane, which is large relative to the pore dimensions, may not easily diffuse through the pores, and secondly, because each molecule which reacts with a hydroxylated site within porous active layer will further obstruct the access of following molecules to sites deeper in the porous structure.

A further factor in this phenomenon is the observation that the creation of the low permeability state and restoration of the original high permeability state is quickly and easily achieved by ten minute application of a pressure of 1atm against a vacuum (here 1 mmHg). An equal applied pressure difference of 2 bar against 1 bar (the experimental conditions for measuring permeation) neither creates the low permeability form as evidenced by the constancy and reproducibility of all the original permeability data of Fig. 8.2, nor, in reverse, restores the high permeability form, as seen in Fig. 8.4. Even pressure difference of 4 bar versus 1bar have little effect, Fig. 8.5.

The reasons for this are not clear. Under standard permeation conditions (face 1, 2 atm, face 2, 1 atm) nitrogen permeability of the membrane in its low permeability state

8.12

is constant and reproducible over many hours. Its was of interest to measure the permeability of propane in this membrane since it is very soluble in hydrocarbons and so might be expected to cause a relaxation of the octadecyl chains and consequently have a high permeability. Contrary to this expectation, the permeablitity of propane was low (35×10^{-11} mol.s^{-1}.m^{-2}.Pa^{-1}), stable and very similar to that of nitrogen (40×10^{-11} mol.s^{-1}.m^{-2}.Pa^{-1}). Therefore, it seems that propane is not able, by itself, to induce a fast membrane morphology modification. However, when the membrane, in its low permeability state, was dipped in toluene (solvent) for 10 min and air dried, its nitrogen permeability measured immediately thereafter was 315×10^{-11} mol.s^{-1}.m^{-1}.Pa^{-1} (Fig. 8.5). This indicates that solubilisation of the octadecyl chains causes a return to the fully relaxed high permeability state.

8.4 Conclusion

The alumina membrane can be easily modified by grafting a monolayer of organic trichlorosilane molecules. Octadecyltrichlorosilane, used in this study, formed a chemically stable monolayer on an alumina membrane. The modification was permanent blocked the original 5 nm pores effectively and reduced the gas permeability of the membrane for the test gases (He, Ne, Ar, N_2, CO_2, CH_4, C_3H_8) by three orders of magnitude. All have permeabilities in the range 10 % of the average value of 360×10^{-11} mole $s^{-1} m^{-2} Pa^{-1}$, except methane which has the highest permeability, 481×10^{-11} mole $s^{-1} m^{-2} Pa^{-1}$. This membrane is not of obvious use for separation of these gases on the basis of this study.

This research shows that the octadecyl chains on the γ-alumina surface may be rearranged changing the permeability characteristics of the membrane. A pressure difference of 1 atm against vacuum applied on the tube side produced a metastable form in which the permeabilites of the test gases were an order of magnitude smaller. The membrane could be easily and reversibly switched between its high (original) and low permeability states by reversal of the pressure treatment. Evidence is presented to show that the low permeability state is caused by movement of the surface hydrocarbon chains on the tube side moving into the pores (a self fouling phenomenon). This state is metastable and gas permeabilities are easily measured. The membrane however relaxes slowly into its original high permeability state after several days storage, or immediately if treated by a hydrocarbon solvent (toluene). This unexpected and novel effect, due to a mild pressure, suggests that useful rectification

effects (gated transport) might be easily achieved, as here with pressure, but also with suitable functionalisation of chain substituents by electric or other forces.

8.5 References

[1] J. Randon, P. Blanc, R. Paterson, Modification of ceramic membrane surfaces using phosphoric acid and alkyl phosphonic acids and its effect on ultrafiltration of BSA protein, J. Membr. Sci., 98 (1995) 119-129.

[2] R.E. Johnson and D.I. Ford, "Stability and reactivity of dimethylethoxysilane, in Chemically Modified Surfaces" , Ed. J.J. Pesek and I. Leigh, The Royal Society of Chemistry, (1994) 164-184.

[3] J.J. Pesek, Conversion of oxide surfaces to hydride surfaces, in Chemically Modified Surfaces, Ed. J.J. Pesek and I. Leigh, The Royal Society of Chemistry, (1994) 1-23.

[4] C. Leger, H. L. Lira, and R. Paterson, Preparation and properties of surface modified ceramic membranes. Part II. Gas and liquid permeabilities of 5 nm alumina membranes modified by a monolayer of bond polydimethylsiloxane (PDMS) silicone oil, J. Membr. Sci., 120 (1996) 135-146.

[5] A.R. Bassindale and P.G. Taylor, Reaction mechanisms of nucleophilic attack at silicon, in The Chemistry of Organic Silicon Compounds, Part I, Edited by S. Patai and Z. Rappoport, Interscience Publication, (1989) 839-892.

[6] M.J. Wirth and H.O. Fatunmbi, Spectroscopic and chromatographic characterization of a self-assembled monolayer as a stationary phase, in Chemically Modified Surfaces, Ed. J.J. Pesek and I. Leigh, The Royal Society of Chemistry, (1994) 203-209.

[7] A. Larbot, J.P. Fabre, C. Guizard and L. Cot, New inorganic ultrafiltration membranes, J. Am. Ceram. Soc., 72, (1989), 257.

[8] J. Randon, R. Paterson, Composite ceramic-organic membranes for gas separation, in preparation.

Table 8.1 Gas permeability, at 20°C, of several gases. through a 5nm SCT membrane, untreated, and octadecyl trichlorosilane modified.

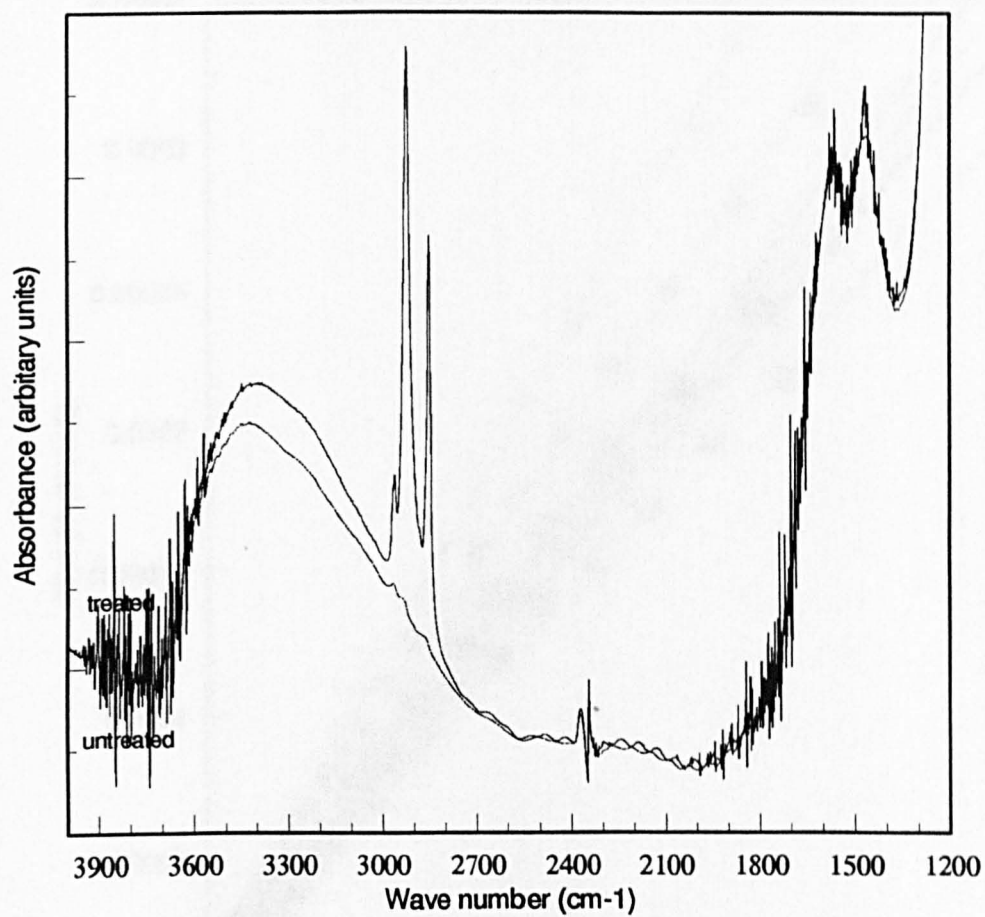| Gas	Untreated membrane permeability(mole.s^{-1}.m^{-2}.Pa^{-1})x10^8	Treated membrane permeability(mole.s^{-1}.m^{-2}.Pa^{-1})x10^{11}
He	920	390
CH_4	845.00	481
Ne	433.00	323
N_2	551	335
Ar	429	294
CO_2	465.00	353
C_3H_8	732.00	350

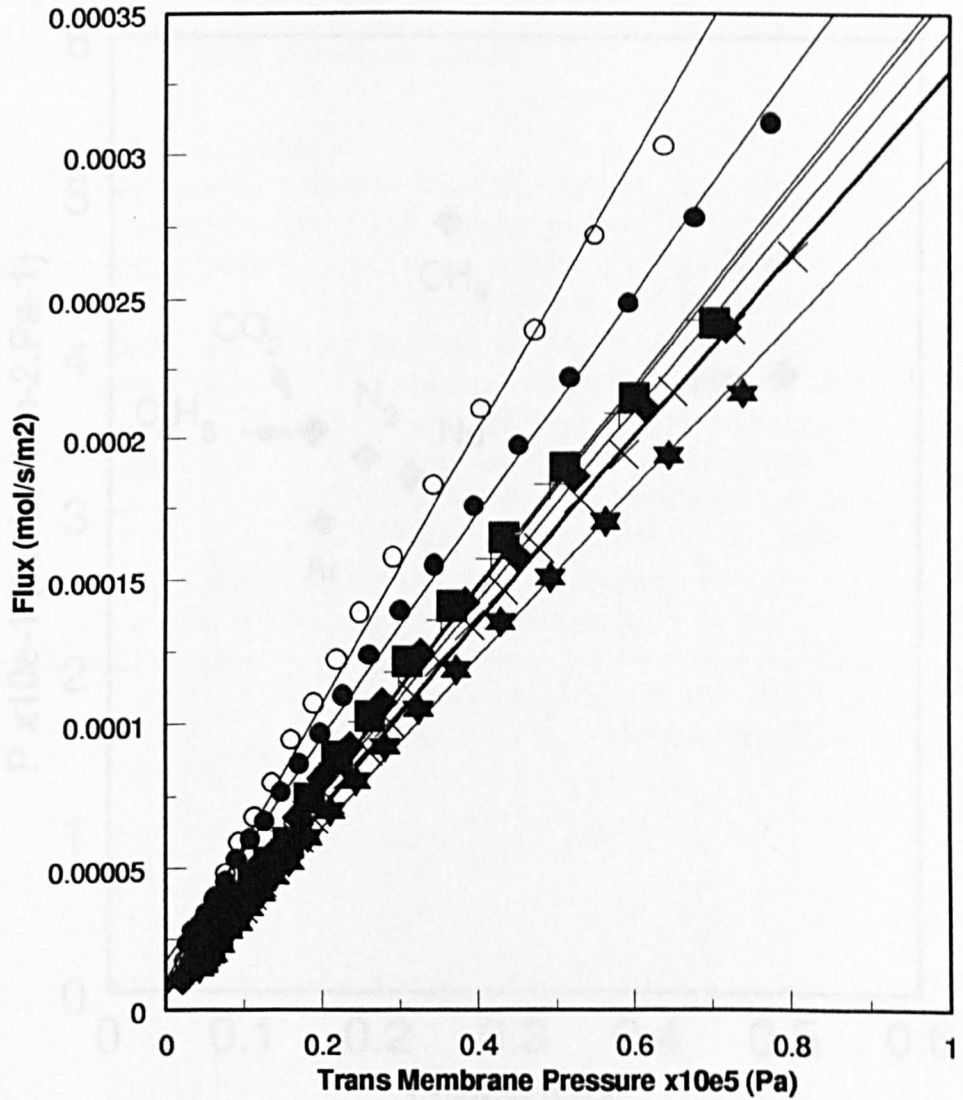Fig.8.1 FTIR spectra of an alumina powder before and after octadecyl trichlorosilane treatement.

Fig.8.2 Gas permeability properties of the 5 nm alumina membrane at 20 C, after octadecyl trichlorosilane treatment modification. He,●; C3H8,■; CO2,+ ;Ar,★; CH4,O; N2,◆; Ne,×. Permeabilities are listed in Table 1.
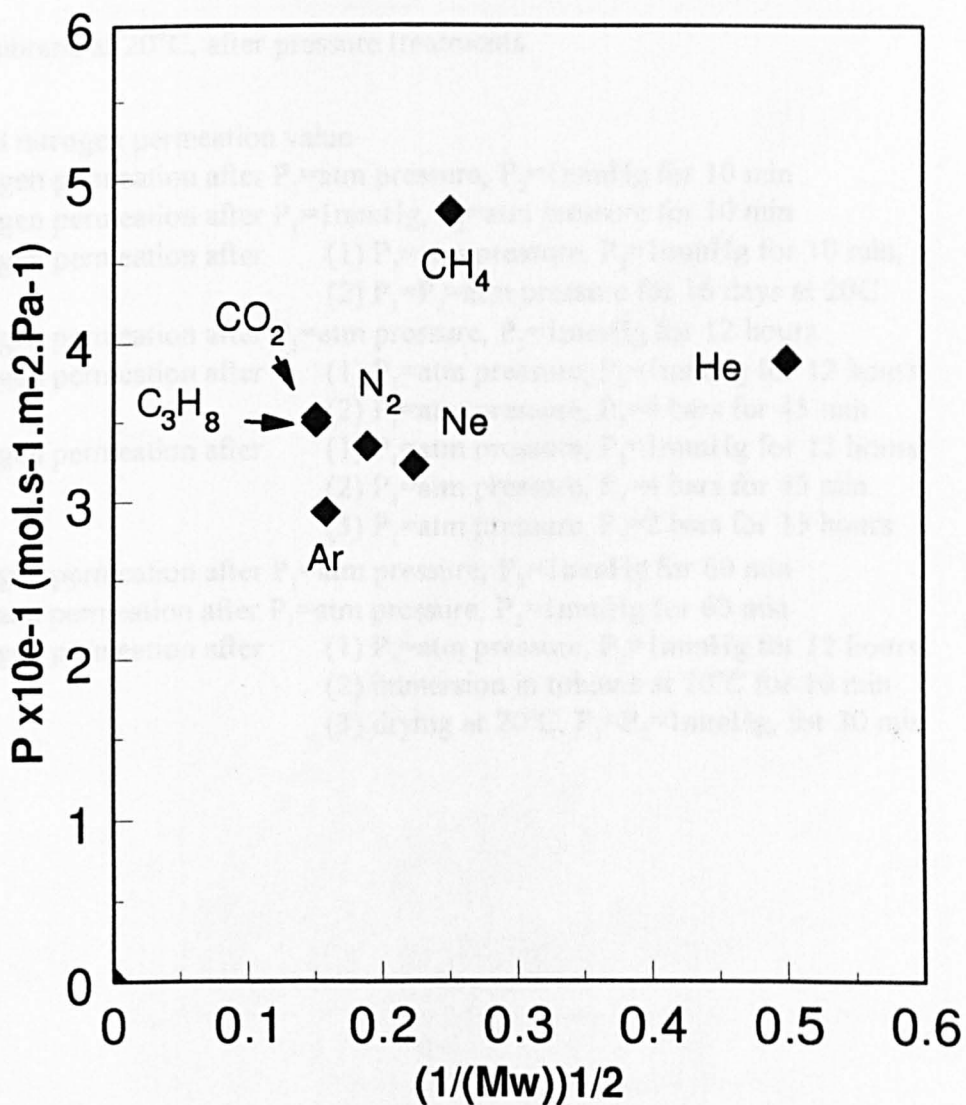
Fig.8.3 Variation of the permeability (at 20 C) of several pure gas with their respective molecular weight, through the octadecyl thrichlorosilane modified 5 nm alumina membrane.

Fig. 8.4 Gas permeability properties of the modified octadecyl trichlorosilane 5nm

alumina membrane at 20°C, after pressure treatments.

◆   initial nitrogen permeation value
●   nitrogen permeation after P_1=atm pressure, P_2=1mmHg for 10 min
✱   nitrogen permeation after P_1=1mmHg, P_2=atm pressure for 10 min
○   nitrogen permeation after   (1) P_1=atm pressure, P_2=1mmHg for 10 min,
                                    (2) P_1=P_2=atm pressure for 16 days at 20C
    nitrogen permeation after P_1=atm pressure, P_2=1mmHg for 12 hours
□   nitrogen permeation after   (1) P_1=atm pressure, P_2=1mmHg for 12 hours
                                    (2) P_1=atm pressure, P_2=4 bars for 45 min
■   nitrogen permeation after   (1) P_1=atm pressure, P_2=1mmHg for 12 hours
                                    (2) P_1=atm pressure, P_2=4 bars for 45 min
                                    (3) P_1=atm pressure, P_2=2 bars for 15 hours
+   nitrogen permeation after P_1=atm pressure, P_2=1mmHg for 60 min
✕   propane permeation after P_1=atm pressure, P_2=1mmHg for 60 min
    nitrogen permeation after   (1) P_1=atm pressure, P_2=1mmHg for 12 hours
                                    (2) immersion in toluene at 20°C for 10 min
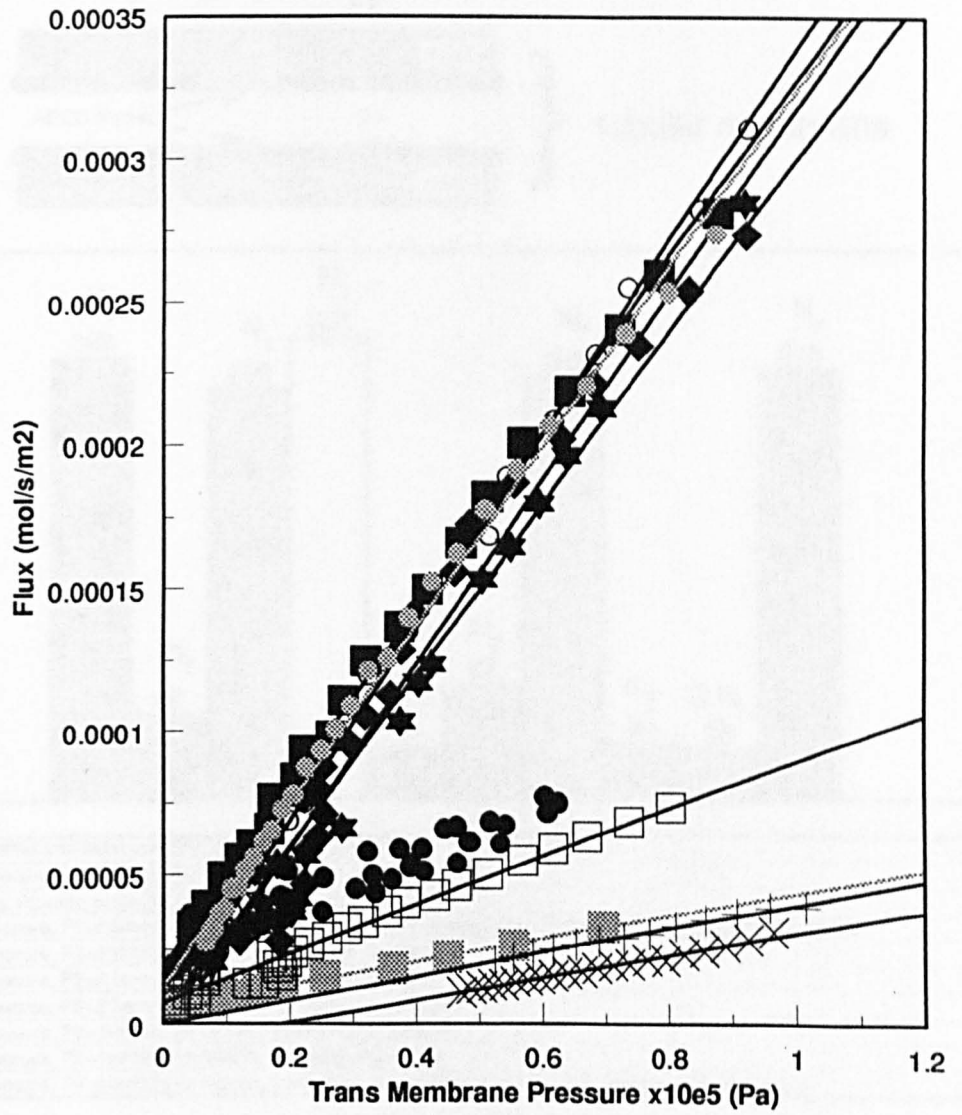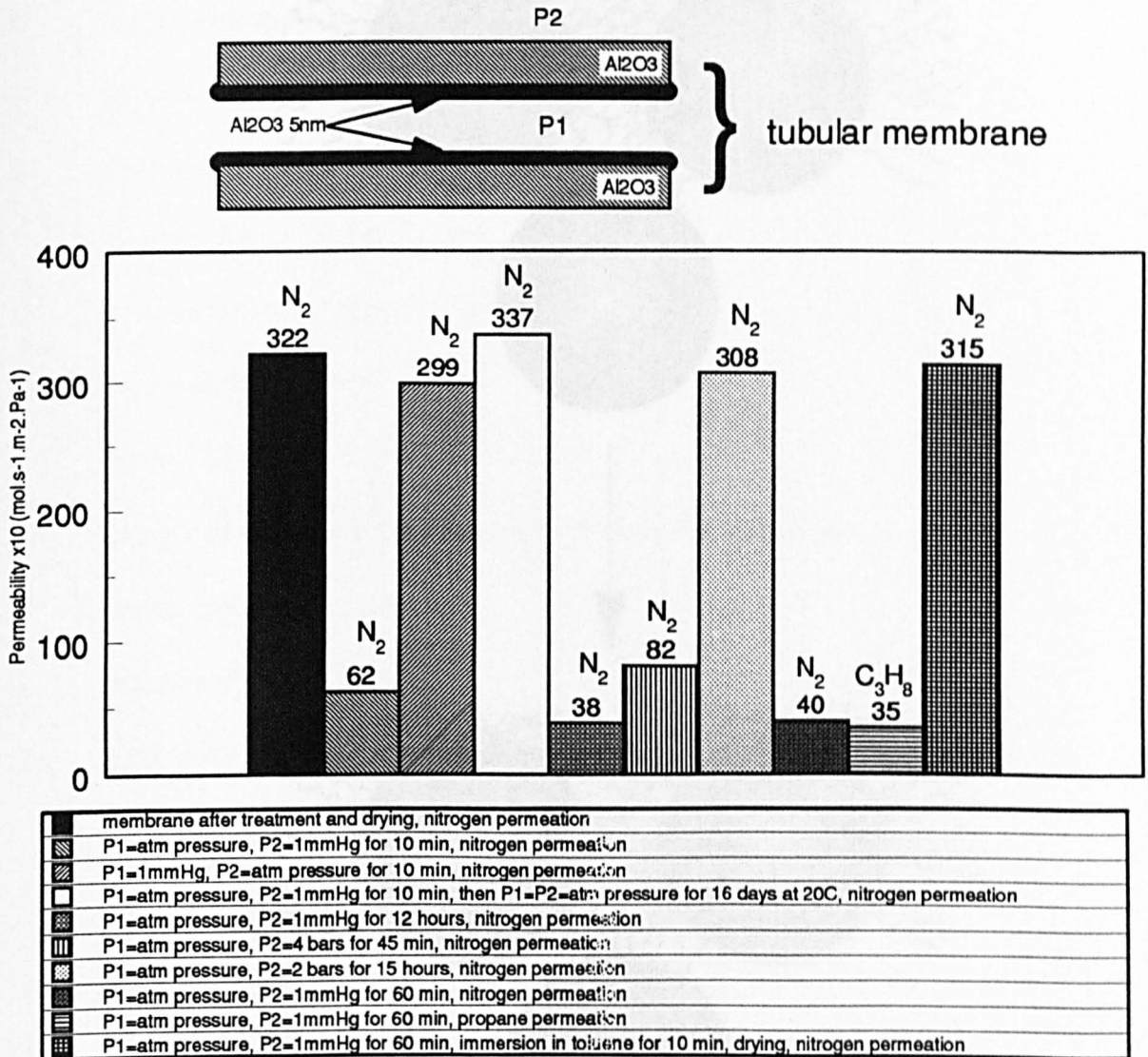   (3) drying at 20°C, P_1=P_2=1mmHg, for 30 min

Fig.8.5 Gas permeability properties of the modified octadecyl trichlorosilane 5 nm alumina membrane at 20 C, after pressure treatments.

Fig.8.6 Hypothesis of the morphology change, induced by the pressure treatments.

List of symbols

A   surface area of membrane (m^2)

D   surface diffusion coefficient ($m^2.s^{-1}$)

D   cell diameter of anodic alumina film (m)

d   pore size diameter (m)

J   gas flux density ($mole.s^{-1}.m^{-2}$)

M   molecular mass of the gas ($Kg.mol^{-1}$)

N   Avogrado's number

n   number of pores per m^2

n   amount of moles of the gas permeate through the membrane

P   permeability ($mole.s^{-1}.m^{-2}.Pa^{-1}$)

p   pressure (Pa)

R   gas constant ($J.mol^{-1}.K^{-1}$)

r   mean pore radius (m)

T   absolute temperature (K)

t   time (s)

U   voltage of anodisation (V)

V   volume of the low pressure side in the cell (m^3)

W weight fraction of the preferentially transferred species, in the feed (g)

W'' weight fraction of the preferentially transferred species, in the permeate (g)

x   fractional occupation of the surface coverage in relation to a monolayer

Greek symbols

α membrane selectivity

β cells constant (V/ART)

δ thickness of the membrane (μm)

ε porosity

λ mean free path (nm)

η viscosity of the gas (Pa.s)

μ shape factors

ν average velocity (m.s^{-1})

σ minimum kinetic diameter (Å)

Published Papers

Preparation and properties of surface modified ceramic membranes. Part II [1]. Gas and liquid permeabilities of 5 nm alumina membranes modified by a monolayer of bound polydimethylsiloxane (PDMS) silicone oil

Christian Leger, Helio De L. Lira, Russell Paterson [*]

Colloid and Membrane Science Research Group, Chemistry Department, University of Glasgow, Glasgow G12 8QQ, UK

Abstract

A new way to prepare hydrophobic membranes is reported. Polydimethylsiloxane oil (and any other silicone oil molecules) was grafted onto a porous alumina membrane (or any hydroxylated ceramic or glass) by heating, to 180°C, producing a covalently grafted monolayer of silicone oil, chemically and thermally stable, unaffected by organic solvents but susceptible to alkali attack (as is the silicone oil itself). The membrane is totally impermeable to pure water, and organic solvents may be extracted from water mixtures by pervaporation. Very high permeation fluxes were obtained, suggesting possible use of these silicone/ceramic membranes in extraction of volatile organic compounds (VOCs). This simple modification can be applied to macroporous membranes increasing hydrophobicity without pore blocking.

Keywords: Surface modification; Silicone; Ceramic membrane; Gas permeation; Liquid permeation; Pervaporation

1. Introduction

Although the preparation of inorganic porous membranes has been improved during the last decade, the types of ceramic membranes commercially available is still largely limited to four oxides, silica, zirconia, titania and alumina. Moreover, commercial membranes, having a pore diameter equal to or larger that 5 nm, are unable to fractionate mixtures of low molecular weight liquids and are not efficient

in separating gas mixtures. It is the aim of these papers to investigate the potential of chemical modifications to obtain membranes with unique chemical properties. The approach considered here is surface bonding of organic molecules in a monolayer on the ceramic surface. This bonding can, in specific cases, increase the performances of the membrane by, on one hand reducing the pore size, and on the other hand, by promoting an eventual specific interaction between the membrane surface and the permeating molecules to improve separations. Several types of compounds can achieve the modification as, for instance, phosphate derivatives [1], chlorosilane derivatives [2], or triethoxysilicon compounds [3]. All of

---

[*] Corresponding author.

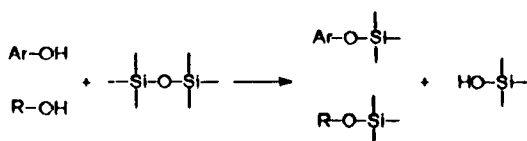[1] Ref. [1] is designated Part 1 of this series.

these products can be easily, covalently, bonded on silica, alumina, zirconia, and titania surfaces. They are often difficult to synthesise and to handle. An easier and less hazardous procedure is considered here. Its principle is to bond a silicone oil molecules to an alumina surface. This process has been demonstrated successfully on glass [4,5] to obtain a hydrophobic glass. Any common commercial silicone oil can be used. If a polysiloxane as common as the polydimethylsiloxane (PDMS) can used to bind to the internal surfaces of a membrane with pores of a few nanometer diameter. a membrane having a ceramic morphology with its pores filled with immobilised silicone oil would be expected. Such a membrane might be considered to be similar to a supported liquid membrane, because of the high mobility of the siloxane chains, but the silicone would be unleacheable since it is covalently bonded to the walls of the porous ceramic. A very permeable membrane having hydrophobicity properties close to those of the silicone oil itself is expected, but which would have the dimensional stability and rigid morphology of the ceramic. This type of hybrid organo-ceramic might be very interesting and valuable on an industrial level.

This study is concerned specifically with the effect of siliconising the pores of a 5 nm pore membrane and so the silicone molecules were expected to partly or completely fill the pores of the active layer of the alumina membrane. Such coating, as will be described here, applied on microporous or macroporous membranes or filters would be effective in a different way, rendering the surface hydrophobic, oleophilic, and having a major effect upon fouling surface tension and other properties.

2. Background

It is well known that siloxane derivatives can be cleaved by the action of aqueous alkaline solutions [6,7]. Si–O bonds are broken to become Si–OH (silanol) ones. The formation of these silanol compounds has been studied by Voronkov and Shabarova [8] using phenol derivatives and Sprung and Guenther [9] using alcohols as hydrolysis agent.

Depending on the hydrolysis agent used either alkyl- or aryl-silicone compounds could be obtained. The reactions involved are shown below:
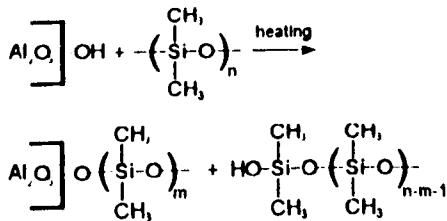

where Ar is an aromatic residue and R an aliphatic one.

The reactions take place in an apolar solvent (such as toluene or xylene) generally using a catalyst: benzene sulfonic acid for aryl derivatives [8] and para-toluene sulfonic acid or sodium methanolate for alkyl derivatives [9]. The question arises as to whether the hydroxyl groups on the surface of a ceramic oxide would react similarly. Although no mechanism was discussed, it appears that a very similar process was used some forty years ago to make glass surfaces permanently hydrophobic [4]. The glass surface lightly coated with commercial silicone oil was heated to 180°C. If the hydroxyl groups of the glass surface (more generally the SiO$_2$ surfaces) react, under high temperature conditions, with siloxane derivatives, it was expected other type of oxides which retained hydroxylated surfaces would react similarly. In particular the membrane oxides alumina, zirconia, silica or titania which have hydroxyl groups on their surfaces might then be grafted to a siloxane derivative. It was considered that this reaction could be an interesting way to modify oxide porous membrane surfaces.

The study presented in this paper will be focused on the modification of alumina surfaces, mainly because alumina membranes are commercially available with a very small pore diameter (5 nm) and are thus, the best candidates to record the modification effects. The objective here was to attempt to fill the nanometer pores of the host alumina membrane with silicone molecules attached only to the surface of the oxide and not themselves polymerised. The properties of such membranes would fundamentally altered in a way that is not entirely predictable. The alkyl phosphate treatment described in Part I [1] on a 20 nm pore altered the pore surfaces but only reduced

the pore diameter by a few percent, this treatment was expected to effectively fill the ceramic pores.

The reaction expected consists of a cleavage of the Si–O bond of the silicone polymer with recombination on the hydroxylated alumina surface, as shown below:

$$\left[Al_2O_3\right]OH + -\left(\underset{CH_3}{\overset{CH_3}{Si}}-O\right)_n \xrightarrow{heating}$$

$$\left[Al_2O_3\right]O\left(\underset{CH_3}{\overset{CH_3}{Si}}-O\right)_m + HO-\underset{CH_3}{\overset{CH_3}{Si}}-O-\left(\underset{CH_3}{\overset{CH_3}{Si}}-O\right)_{n-m-1}$$

The ceramic alumina membranes are prepared industrially by a sol–gel process [10], using a colloidal suspension of metal alkoxides or hydrous metal oxide precursors, a peptising agent or an organic binder, a solution casting on a ceramic support and finally a thermal treatment. Exactly the same method, without casting step, can be used to prepare industrial alumina powders which can then, be considered, to be morphologically identical to the membrane itself. The chemical membrane surface modification can then be easily studied, merely by examining a modified powder on which the modification has been carried out in exactly the same conditions as for the membrane. The best way to study chemical changes on the active layer was to use to use infra-red spectroscopy on the chemically modified alumina powder. The effect of chemical modification on the membrane itself can be studied by gas and liquid permeation measurements. Alumina membranes, with a pore diameter 5 nm and the active layer in powder form in gram quantities, used in these studies, were kindly donated by the Societe des Ceramiques Techniques (SCT), Division Membranes (France).

3. Experimental

3.1. Raw materials

The siloxane oil used (Fluka Catalogue ref. 85421) is a polydimethylsiloxane (PDMS) type oil, having a typical viscosity of 545 mPa s at 20°C. This kind of

polymer is very stable and no degradation reaction occurs up to 300°C [11,12] when the polymer is not in the presence of hydroxyl group sources.

The ceramic porous membrane used, an alumina membrane in conventional tube format, external diameter 1 cm, was donated by Societe des Ceramiques Techniques (SCT) who estimated it as having a pore diameter of 5 nm.

The alumina powder, also supplied by SCT, was obtained from the sol used in preparing the membrane and was chemically and morphologically equivalent to the alumina of the active layer of the test membrane.

3.2. Membrane and powder modification process

The chemical treatment of the membrane and powder were identical, as follows: the alumina membrane (or powder) was washed, for 12 h, by a continuous flow of cold distilled water, to remove soluble impurities from the oxide surface. The membrane (or powder) was dried for 24 h at 65°C and then immersed in the pure dry silicone oil. The resulting preparation was placed under vacuum (~ 1 mmHg), until no more bubbles can be observed. This process was used to fill the pores of the membrane and to remove gas absorbed on the membrane (or powder) surface. The preparation was baked at 180°C for 2 h under nitrogen. The membrane (or powder) was then extracted by hot toluene in a Soxhlet extractor for 48 h to remove unbound silicone oil molecules. Thereafter it was dried, first at 65°C for 24 h, and then at ambient temperature but under vacuum (~ 1 mmHg) for 2 h. The membrane (or powder) was then ready for investigations.

3.3. Infra-red measurements

The dry powder is prepared as KBr disks and FTIR spectra are recorded on a Perkin-Elmer FTIR 16PC spectrometer in the 4000–600 cm^{-1} area, with a 2 cm^{-1} resolution.

3.4. Gas permeation measurements

The permeability of pure gases was measured by monitoring pressure in both high and low pressure sides of a permeation cell. The system used was

described in detail in a previous paper [13]. Its principle can be summarised as follows: the high pressure side was maintained at a constant 2 bar (absolute pressure), whereas the initial pressure on the low pressure side was initially 1 bar (absolute). This latter side was constituted by a fixed volume cylinder filled with the permeant gas. As the gas permeates, the pressure increase in this collecting volume was monitored. The pressure difference across the membrane, initially 1 atm, decreased with time, approaching zero as the system approached equilibrium. From these data the permeabilities of a series of gases were obtained. All the measurements were conducted at 20°C, using a geometrical area of test membrane of 4.98×10^{-4} m^2.

3.5. Liquid permeation measurements by pervaporation / membrane distillation

The experimental technique, as described below, is termed pervaporation [14], if the membrane has a dense active layer, and membrane distillation if the membrane is merely porous.

The permeability of pure liquids of binary liquid mixtures was measured by weighing the amount of compound transferred through the membrane as a function of time. The upstream side of the membrane was in contact with the rapidly circulating liquid feed at atmospheric pressure whereas the downstream face of the membrane was maintained at a very low pressure (~ 1 mmHg). The vapours transferred through the membrane to the downstream side were collected by condensation in a cold trap cooled by liquid nitrogen. The membrane flux was measured as a mass flow (kg h^{-1} m^{-2}), as commonly in pervaporation literature. When a binary liquid mixture is used as the feed, the measured flux is the sum of the individual fluxes. Under steady state conditions the separate fluxes are obtained by analysis of the permeate. From the concentrations of each species in the feed and in the permeate the membrane selectivity α was obtained. Concentrations were determined by measuring the refractive index of the mixtures at 25°C.

The two main parameters used to characterise the membrane were: the total flux J in kg h^{-1} m^{-2} and

the membrane selectivity α (dimensionless parameter) defined below:

$$\alpha = \frac{W'}{(1 - W')} \frac{(1 - W)}{W}$$

where W' is the weight fraction of the preferentially transferred species, and in the permeate W is the weight fraction of the preferentially transferred species, in the feed.

4. Results and discussion

4.1. Chemical modification

Infra-red spectroscopy is particularly suitable for detecting the presence of siloxane compounds on the alumina surface because the silicone oil absorption bands can easily be isolated. As shown in Fig. 1, the strong sharp band near 1250 cm^{-1}, characteristic of Si-CH$_3$ bond, appear on the treated alumina spectrum, giving clear evidence of siloxane derivative presence, on the alumina surface. Because the alumina powder was extracted for a long time (48 h) in a Soxhlet extractor, using toluene (which is an excellent solvent for silicone oil even at low temperatures), it can be assumed that the absorption bands recorded, come from siloxane molecules covalently grafted to the alumina surfaces, both external and internal, within the pore structure. Moreover this grafted layer can only be a monomolecular, because only the hydroxyl groups of the alumina surface can react with the siloxane groups. There is little likelihood of other reactions since the PDMS oil is stable at temperatures up to 300°C [11,12], the decomposition temperature of the PDMS chains, and the grafting process was performed at 180°C. The siliconised membrane had high chemical and thermal stability and the silicone layers were not altered or removed by solvent or by the liquids and gases used for the permeation tests performed in this research. As observed in Part I, hydrophobic material in a surface [2] coating, is impermeable to water and ions which can

---

[2] This includes all surfaces of the alumina structure, both external and internal, which are accessible to the PDMS molecules.
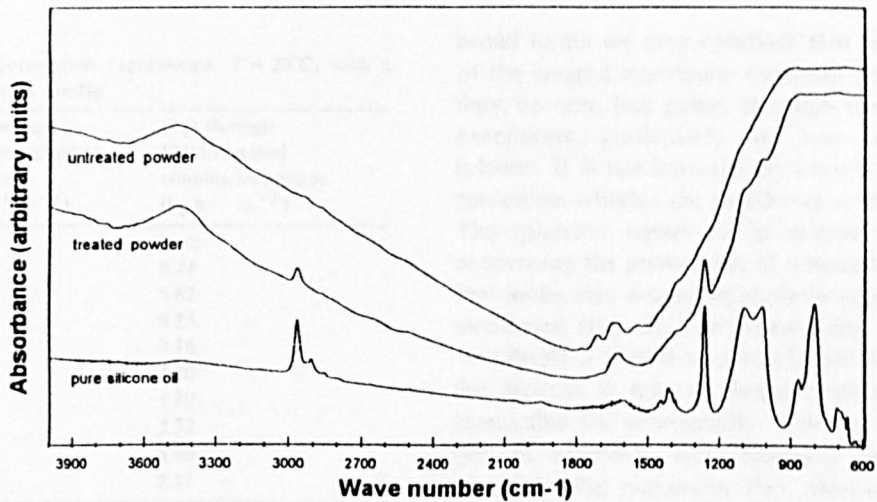
Fig. 1. FTIR spectra of an alumina powder before and after silicone oil treatment.

lead to the hydrolysis of the alumina–silicone oil bond. This stability was monitored by studying the permeation, under pervaporation conditions, of very polar molecules through the membrane. The results are shown in Table 1. The exceptional hydrophobicity is shown by total membrane impermeability to water. Low molecular weight alcohols pass through the modified alumina membrane and always reach a reproducible steady state. This indicates that even the

lighter alcohols such as methanol or ethanol are unable to hydrolyse the alumina–PDMS bond. In these two cases, it can be concluded that such a membrane is very stable in relatively mild conditions. Under aggressive conditions, as for example, exposure to concentrated alkaline solutions, the membrane layer is hydrolysed not least by cleavage of the siloxane bonds themselves [6,7]. Nevertheless, it seems that the modified PDMS-membranes can
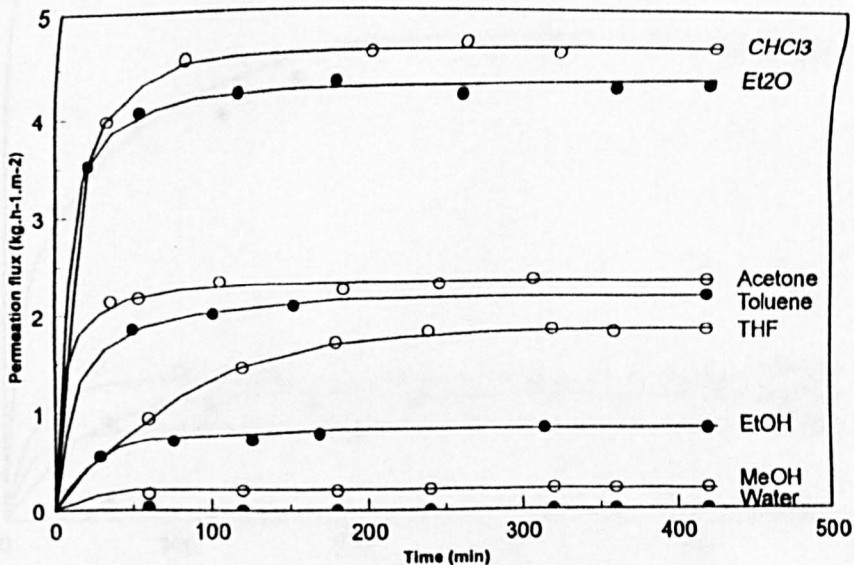

Fig. 2. Permeation measurements of pure solvents through a 5 nm Al_2O_3 PDMS-modified membrane. $T = 20°C$, with a downstream pressure of 1 mmHg.

Table 1
Pure liquid solvent permeation experiments. $T = 20°C$, with a downstream pressure of 1 mmHg

Solvent	Flux through untreated alumina membrane (kg h^{-1} m^{-2})	Flux through PDMS-treated alumina membrane (kg h^{-1} m^{-2})
H$_2$O	18	trace
MeOH		0.21
EtOH		0.82
nPrOH		0.23
nBuOH		0.16
Et$_2$O		4.20
THF		1.80
Acetone		2.32
CHCl$_3$	110	4.60
Toluene		2.17

resist easily to most of the usual organic solvents, leading to stable performances in time, shown in Fig. 2.

4.2. Pervaporation of pure liquids

The pervaporation results of a series of simple organic molecules and water are shown in Fig. 2. In broad terms we may conclude that the permeability of the treated membrane increases for molecules as they become less polar, although there are obvious exceptions, particularly the low permeability of toluene. It is not immediately clear from these measurements whether the membrane retains open pores. The question seems to be settled by the results concerning the permeation of a homologous series of low molecular weight alcohols through the modified membrane (Fig. 3). The permeability series is EtOH $\gg$ nPrOH > MeOH > nBuOH, and it is clear that the process is not membrane distillation. It rather seems that the permeability is caused by a combination of solubility and diffusivity in the siloxane material. The maximum flux obtained for ethanol might be due to the best combination of these two parameters. In this latter case the transfer mechanism appears to be a solution-diffusion mechanism [15], meaning that the grafted PDMS chains formed a dense layer on the external and internal ceramic surfaces. An objection to the solution/diffusion hypothesis might be that the real size of the diffusing species in the methanol case might be larger than in the ethanol one, because methanol can be associated in a cluster form due to self-association by strong
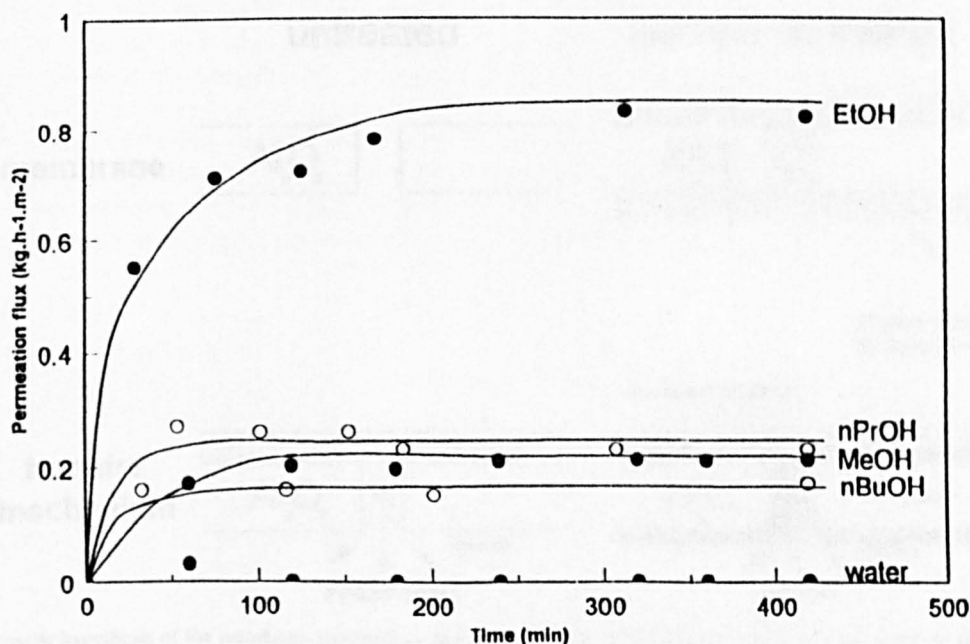

Fig. 3. Permeation measurements of pure polar solvents through a 5 nm Al$_2$O$_3$ PDMS-modified membrane. $T = 20°C$, with a downstream pressure of 1 mmHg.
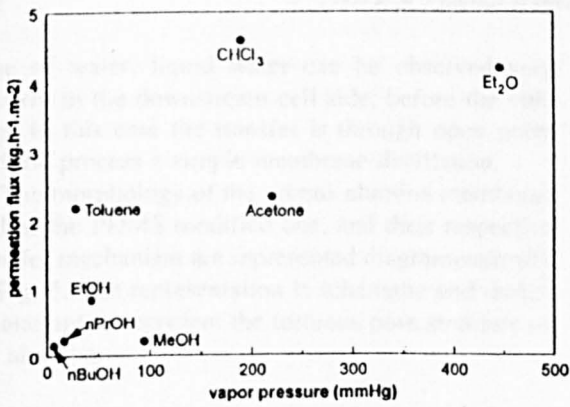
Fig. 4. Variation of the permeation flux with the vapor pressure of the transferred compounds at 20°C, through the Al_2O_3 PDMS-modified membrane.

intermolecular hydrogen bonds. The concept of cluster formation and behaviour inside a membrane is a controversial subject. Most studies in this area suggest that clusters exists in a membrane, but that the diffusion process occurs by cluster disaggregation and single molecule diffusion [16,17]. According to this latter hypothesis, the results recorded for the alcohol permeation suggest a solution/diffusion mechanism, certainly not a simple open pore diffu-

sion. In this case, the PDMS-modified alumina membrane can be seen as a composite membrane in which a monomolecular dense PDMS layer is grafted on a porous alumina support having very small average pore diameter. Results obtained with other solvents are similar. Indeed, toluene and chloroform which are larger than water or methanol, but much more soluble in the siloxane polymer, pass through the membrane much faster. However, an objection can be formulated: the highest fluxes are obtained for the compounds having the highest vapour at the experiment temperature (20°C). In this case, the difference in flux from one solvent to an other could be due merely by the difference of vapour pressure, assuming that the membrane is still porous and that an evaporation takes place through it. It is clear from Fig. 4, that there is no correlation between the steady state permeation fluxes of the test compounds (Figs. 1 and 2) and their saturated vapour pressures at 20°C. This suggests once more that the ceramic pores of the PDMS-modified membrane are completely blocked by the polymer. It is easy seen that the original untreated alumina membrane behaves very differently, under the same experimental conditions. Compared to the PDMS-modified membrane, the permeation fluxes are huge, and in the specific
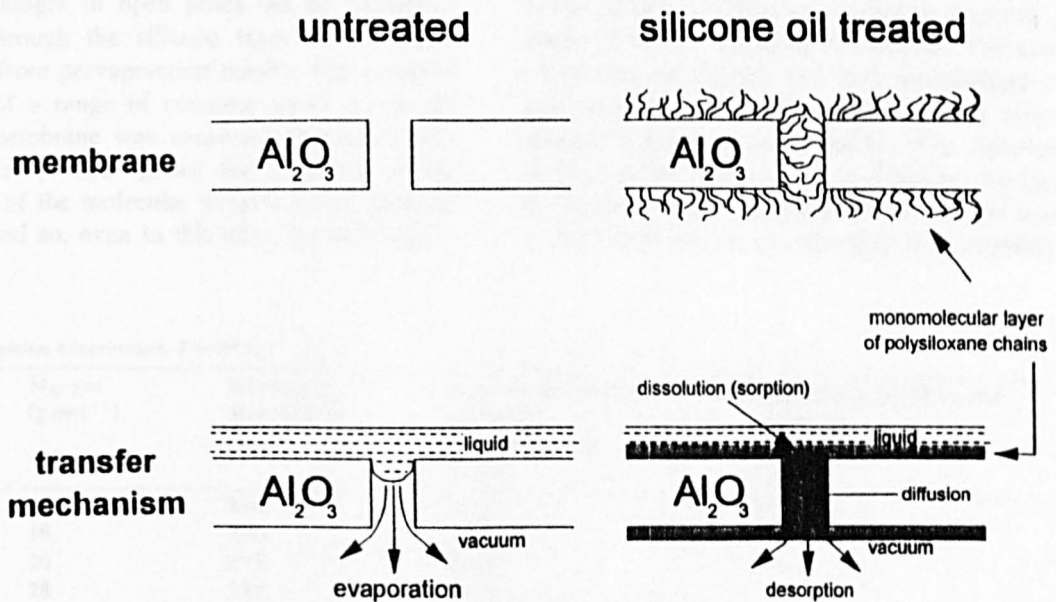

Fig. 5. Schematic hypothesis of the membrane morphology and of the transfer mechanism occurring through it, before and after silicone oil modification.

case of water, liquid water can be observed very quickly in the downstream cell side, before the cold trap. In this case the transfer is through open pores and the process a simple membrane distillation.

The morphology of the porous alumina membrane and of the PDMS modified one, and their respective transfer mechanism are represented diagrammatically in Fig. 5. The representation is schematic and makes no attempt to represent the tortuous pore structure of the alumina.

4.3. Gas permeation

To investigate further the properties of the PDMS-treated membrane, gas permeation experiments were carried out on it and on the original untreated membrane. The results are presented in Table 2 and Figs. 6 and 7. Good linearity between flux and transmembrane pressure showed that the gas permeabilities in both membrane were constant over the experimental conditions. A comparison of Figs. 6 and 7. shows that the permeability of gases studied are smaller in the treated membrane by between 4 and 5 orders of magnitude. Such a reduction in a membrane in which the diameter of the untreated pores is 5 nm is clear evidence that diffusion occurs no longer in open pores but by molecular diffusion through the silicone layer as concluded previously from pervaporation results. The transport behaviour of a range of common gases across the untreated membrane was measured (Table 2). The permeabilities plotted against the reciprocal of the square root of the molecular weights of the gases is not linear and so, even in this case, the mechanism

of gas permeation is not simple Knudsen flow (Fig. 8). This suggests adsorption and condensation effects influence the transport of many of the gases. The gas least likely to be affected is helium, and on this basis a tentative ideal Knudsen line was drawn, Fig. 8. Of the remaining gases the only other gas on the "theoretical" line was neon, which, would also be expected to show minimum condensation or adsorption tendencies. For the others, the permeabilities are much larger than Knudsen mechanism would predict.

Concerning the treated membrane, as expected, there is no evidence for Knudsen flow. The treated membrane seems to exhibit some similarities and some differences to the transport properties of PDMS dense film for certain gases. For example the ratio of permeabilities for CO_2/N_2 is 11.4 for a dense PDMS film and 10.2 for the alumina PDMS-modified membrane which is a very similar value [18,19]. In the same reference, however the CH_4/N_2 permeability ratio, was 3.4 for the dense PDMS film, but for the alumina-PDMS membrane the ratio was 16.7 which is very different. It seems then, that the alumina PDMS-modified membrane is not equivalent merely to a dense PDMS layer cast on a porous surface. This result is interesting because it shows that ceramic/polymer composite membranes (as prepared in this work) constitute an alternative to purely polymeric or purely inorganic membranes. The composite retains the rigidity and pore morphology of the host ceramic, while the polymer grossly alters the ceramic membrane functionality. The functionality of the polymer will also be modified by the fact that the polymer within the pores of the ceramic structure is physically restricted, affecting the solubility and

Table 2
Pure gas permeation experiments. $T = 20°C$

Gas	M_w gas (g mol^{-1})	Kinetic gas diameter [16] (Å)	Permeability untreated membrane (mol s^{-1} m^{-2} bar^{-1}) $\times 10^2$	Permeability PDMS-treated membrane (mol s^{-1} m^{-2} bar^{-1}) $\times 10^6$
He	4	2.60	92.01	110
CH_4	16	3.80	84.52	100
Ne	20	2.75	43.35	70
N_2	28	3.62	55.12	6
Ar	40	3.40	42.91	90
CO_2	44	3.30	46.46	61
C_3H_8	44	4.30	73.24	83

path tortuosity of permeants, and selectivity as compared with the free polymer. To complete the assessment, it is to be reported that correlation cannot be found between the molecular weight or the kinetic diameter of the diffusing gas molecule, and its permeability through the treated membrane. All evidence confirms that the transfer mechanism through the PDMS-alumina membrane occurs by a solubility/diffusion mechanism, in other words by gas dissolution and gas diffusion in the membrane.

4.4. Separation by pervaporation

One of the most promising industrial application of hydrophobic membranes is the extraction of organic compounds from water [20]. Indeed, it can be interesting, for ecological or economical reasons to extract volatile organic compounds (VOC) from water [21] or alcohol form aqueous fermentation broths [22]. In these cases, a ceramic membrane grafted by PDMS could be valuable because the hydrophobic
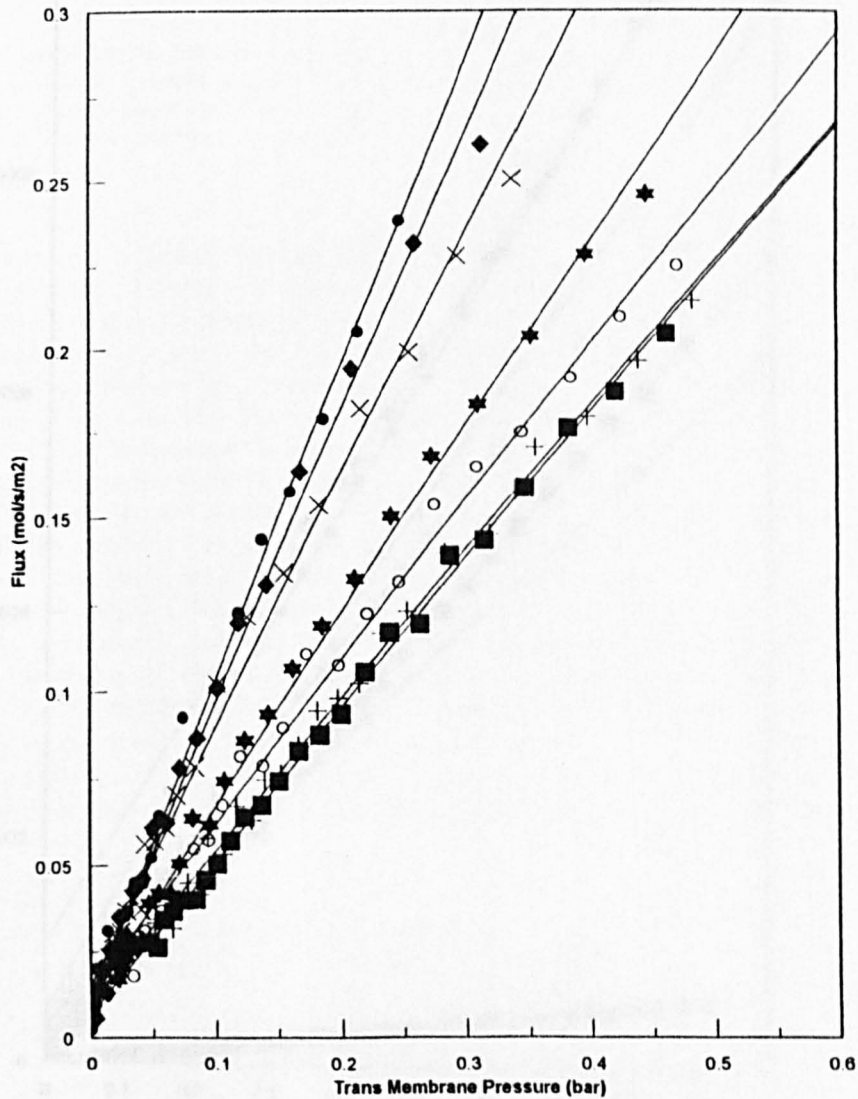

Fig. 6. Gas permeability properties of the 5 nm alumina membrane at 20°C, before modification. He, ●; Ne, ■; Ar, +; N_2, ★; CO_2, O; CH_4, ◆; C_3H_8, ×. Permeabilities are listed in Table 2.

layer being very thin (monomolecular layer), must lead to a very permeable membranes. In order to evaluate the behaviour of the modified alumina membrane during a real liquid mixture separation experiment, the membrane is placed in the liquid permeation device and pure liquid feed is replaced by a liquid aqueous organic mixture of controlled composition. An aqueous mixture containing 5 wt%

of tetrahydrofuran (THF) was chosen as first test mixture because THF and water are soluble in all proportions and then the measure of the refractive index is easy. This first attempt shows clearly that the membrane is selective to the organic compounds (Table 3). Indeed, at 20°C, the permeate becomes richer in THF than the feed and the selectivity α is 20 in favour of THF. This promising result leads us
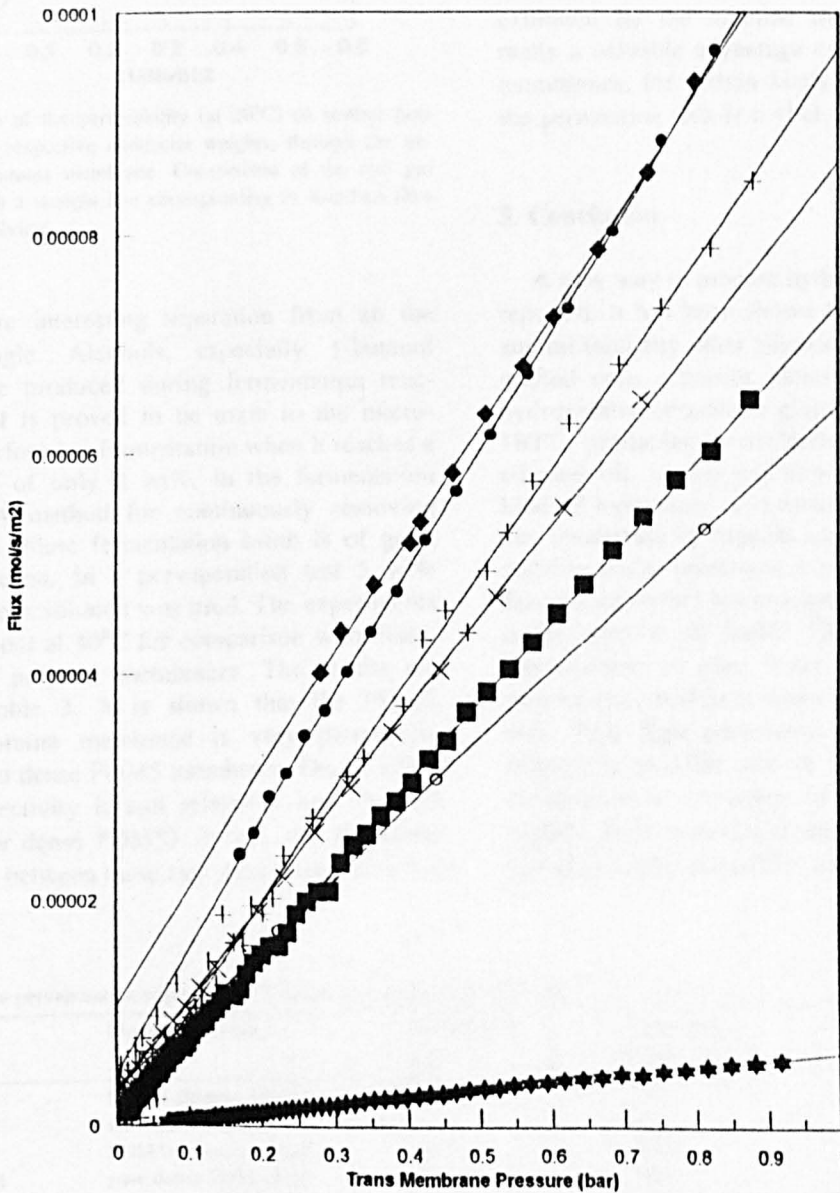

Fig. 7. Gas permeability properties of the 5 nm alumina membrane at 20°C, after silicone oil (PDMS) treatment. He, ●; Ne, ■; Ar, +; N₂, ★; CO₂, ○; CH₄, ♦; C₃H₈, ×. Permeabilities are listed in Table 2.
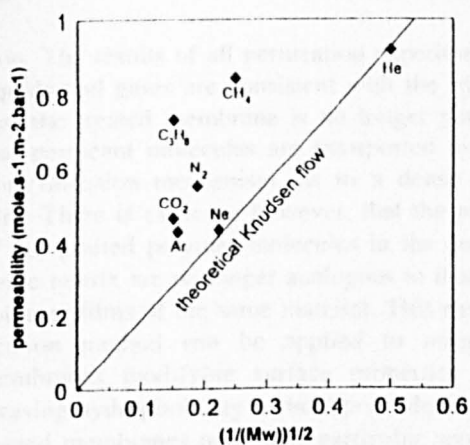
Fig. 8. Variation of the permeability (at 20°C) of several pure gases with their respective molecular weights, through the untreated 5 nm alumina membrane. Comparison of the real gas permeability with a straight line corresponding to Knudsen flow through the membrane.

to study more interesting separation from an the industrial angle. Alcohols, especially 1-butanol (nBuOH), are produced during fermentation reactions. nBuOH is proved to be toxic to the microorganisms performing fermentation when it reaches a concentration of only 2 wt%, in the fermentation broth [22]. A method for continuously removing nBuOH from dilute fermentation broth is of great industrial interest. In a pervaporation test 5 wt% nBuOH aqueous solution was used. The experiments were carried out at 40°C for comparison with literature data on polymer membranes. The results are shown in Table 3. It is shown that the PDMS modified alumina membrane is very permeable, compared to a dense PDMS membrane. On the other hand, its selectivity is still relatively low ($\alpha = 20$ against 82 for dense PDMS). In fact, the difference of selectivity between these two membranes may not

be as these values suggest, since the silicone modified membrane was tested with a feed containing 5 wt% of nBuOH whereas the literature data refer to a feed containing 6.1 wt% of nBuOH. It is well known that the selectivity of a membrane generally decreases when the organic compound concentration decreases in the feed [23]. Although, it seems obvious that the silica PDMS-modified membrane is not as selective as a dense PDMS membrane, even if the selectivity values must be closer to each other that those obtained. Nevertheless, the much higher flux exhibited by the alumina modified membrane, is really a valuable advantage over the pure polymeric membranes, for certain kinds of applications where the permeation flux is a vital parameter.

5. Conclusion

A new way to prepare hydrophobic membranes is reported. It has been shown that polydimethylsiloxane oil (and any other silicone oil molecules) can be grafted onto a porous alumina membrane (or any hydroxylated ceramic or glass) merely by heating, to 180°C, producing a covalently grafted monolayer of silicone oil, almost certainly monomolecular. This kind of membrane is chemically and thermally stable, unaffected by organic solvents (as shown by its stability under prolonged extraction by toluene in a Soxhlet extractor) but susceptible to alkali attack (as is the silicone oil itself). The membrane is totally impermeable to pure water, and organic solvents may be extracted from water mixtures by pervaporation. Very high permeation fluxes were obtained, suggesting possible use of these silicone/ceramic membranes in extraction of volatile organic compounds. Both treated and untreated membranes were gas permeable and neither exhibited Knudsen diffu-

Table 3
Aqueous mixture pervaporation experiments. Downstream pressure of 1 mmHg

Aqueous liquid mixture feed	Membrane nature	Temperature (°C)	Total flux (kg h^{-1} m^{-2})	Selectivity α (dimensionless)
10 wt% THF	PDMS-alumina treated	20	0.1	20
5 wt% nBuOH	alumina untreated	40	25	1
5 wt% nBuOH	PDMS-alumina treated	40	0.31	20
6.1 wt% nBuOH	pure dense PDMS [12]	40	0.17	82

sion. The results of all permeation experiments with liquids and gases are consistent with the hypothesis that the treated membrane is no longer porous and that permeant molecules are transported by a solution/diffusion mechanism, as in a dense polymer film. There is evidence however, that the properties of the grafted polymer molecules in the porous ceramic matrix are no longer analogous to those of the polymer films of the same material. This easy modification method can be applied to macroporous membranes modifying surface properties and increasing hydrophobicity without pore blocking. Such treated membranes may have particular applications in organic filtrations and in aqueous separation procedure as an anti-fouling coating.

Acknowledgements

References

[1] J. Randon, P. Blanc and R. Paterson, Modification of ceramic membrane surfaces using phosphoric acid and alkyl phosphonic acids and its effect on ultrafiltration of BSA protein, J. Membrane Sci., 98 (1995) 119–129.

[2] J.J. Pesek, Conversion of oxide surfaces to hydride surfaces, in J.J. Pesek and I. Leigh (Eds.), Chemically Modified Surfaces, The Royal Society of Chemistry, 1994, pp. 1–23.

[3] R.E. Johnson and D.I. Ford, Stability and reactivity of dimethylethoxysilane, in J.J. Pesek and I. Leigh (Eds.), Chemically Modified Surfaces, The Royal Society of Chemistry, 1994, pp. 164–184.

[4] G.J. Hills and D.J.G. Ives, The calomel electrode and other mercury-mercurous salt electrodes, in D.J.G. Ives and G.J. Janz (Eds.), Reference Electrodes: Theory and Practice, Academic Press, New York, 1961, pp. 135–136.

[5] G.J. Hills, D.J.G. Ives, The hydrogen–calomel cell. Part II. The calomel electrode, J. Chem. Soc., (1951) 311.

[6] F.M. Lewis, Chemistry of silicone elastomers, in J.P. Kennedy and E.G.M. Tornqvist (Eds.), Polymer Chemistry of Synthetic Elastomers, Part II, Interscience Publishers, London, 1969, p. 791.

[7] W.J. Bobear, Behavior of silicone rubber in sealed systems at high temperatures, Rubber Age, 84 (1958) 448.

[8] M.G. Voronkov and Z.I. Shabarova, Cleavage of hexaalkyldisiloxanes by phenols, Zhur. Obshchei Khim., 30 (1960) 1955–1958.

[9] M.M. Sprung and F.O. Guenther, The reaction of some silanols and siloxanes with n-octyl alcohol, J. Org. Chem., 26 (1961) 552–557.

[10] A. Larbot, J.P. Fabre, C. Guizard and L. Cot, New inorganic ultrafiltration membranes, J. Am. Ceram. Soc., 72, (1989), 257.

[11] F.M. Lewis, Chemistry of silicone elastomers, in J.P. Kennedy and E.G.M. Tornqvist (Eds.), Polymer Chemistry of Synthetic Elastomers, Part II, Interscience Publishers, London, 1969, p. 769.

[12] W.J. Bobear, Heat-aging studies on silicone rubber stocks, Rubber Age, 95 (1964) 31.

[13] J. Randon and R. Paterson, Composite ceramic–organic membranes for gas separation, in press.

[14] J. Neel, Introduction to pervaporation, in R.Y.M. Huang (Ed.), Pervaporation Membrane Separation Processes, Elsevier, Amsterdam, 1991, pp. 1–110.

[15] J. Neel and P. Aptel, La pervaporation: principe de la technique, Entropie, 104 (1982) 15.

[16] J.A. Barrie and B. Platt, The diffusion and clustering of water vapors in polymers, Polymer, 4 (1966) 303.

[17] J.A. Barrie, Diffusion of methanol in polydimethylsiloxane, J. Polym. Sci., 4 (1966) 3081.

[18] M. Mulder, Membrane processes, in Basic Principle of Membrane Technology, Kluwer Academic, Dordrecht, 1991, pp. 221–222.

[19] M. Mulder, Membrane processes, in Basic Principles of Membrane Technology, Kluwer Academic, Dordrecht, 1991, p. 228.

[20] National Research Council: Separation and Purification. National Academy Press, Washington, 1987.

[21] W.A. Telliard and G.S. Goldberg, Sampling and analysis procedure for screening industrial effluents for priority pollutants, Symp. Proc. Process Meas. Environ. Assess., (1978) 104–107.

[22] M.J. Spivey, The acetone/butanol/ethanol fermentation, Proc. Biochem., (1978) 2.

[23] J. Neel, Introduction to pervaporation, in R.Y.M. Huang (Ed.), Pervaporation Membrane Separation Processes, Elsevier, Amsterdam, 1991, pp. 27–31.

Preparation and properties of surface modified ceramic membranes. Part III. Gas permeation of 5 nm alumina membranes modified by trichloro-octadecylsilane

Christian Leger, Helio De L. Lira, Russell Paterson *

Colloid and Membrane Science Research Group, Chemistry Department, University of Glasgow, Glasgow G12 8QQ, UK

Abstract

Stable trichloro-octadecyl silane (ODS) derivatives of a 5 nm γ-alumina ceramic membrane were prepared. Gas permeabilities of the untreated membrane did not show Knudsen diffusion at 20°C. Gas permeabilities of the ODS membrane were three orders of magnitude lower; He, Ne, Ar, CO_2, C_3H_8 have near constant permeabilities 360 mol s^{-1} m^{-2} bar^{-1}, except methane which has the highest permeability of the group, 481 mol s^{-1} m^{-2} bar^{-1}. The mechanism of diffusion is solution/diffusion. Remarkably, permeabilities of ODS-alumina membrane were reduced by 5 × after exposure to a pressure difference of 1 atm (active layer side) against vacuum for only 10 min. The effect was metastable but could be reversed on standing for several hours, reversal of pressure difference or after washing with (hydrocarbon solvent) toluene. The mechanism was presumed to be due to movement of the octadecyl-hydrocarbon chains of the silane monolayer causing a partially blocked pore structure; perhaps a unique example of self-fouling.

Keywords: Ceramic membrane; Octadecylsilane modification; Gas permeabilities; Self-fouling

1. Introduction

Surface modification of ceramic membranes by covalently bonded molecular monolayers is a convenient way to alter membrane performance. A monolayer, according to its thickness and functionality, will reduce the effective pore size (even filling the pores as in Part II [4]) and alter the chemistry of both external and internal surfaces of the membrane and so modify (often dramatically) membrane selectivity, permeability and fouling characteristics (Part I [1]).
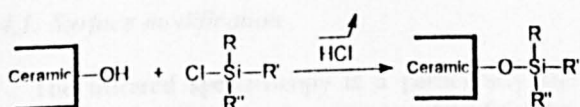
Commercially available porous ceramic membranes, as yet, have pores which are too large to be used, for applications such as gas separations, although research membranes are now under development which have pore size ~ 1 nm which will be of considerable interest. For membranes with pores < 10 nm, bonding organic compounds covalently to pore surfaces is probably the most flexible and controllable method for modification. Phosphate derivatives (Part I) [1], triethoxysilicon compounds [2], chlorosilane derivatives [3], or even polysiloxanes (Part II) [4] have been successfully used to modify ceramic surfaces as alumina, zirconia, silica, titania, or thoria. They were

* Corresponding author.

used mainly to prepare new chromatographic stationary phases seldom in the membrane applications. In this paper octadecylsilane derivatives were investigated as potentially interesting candidates to modify a ceramic surface, despite of their high moisture sensitivity, which results in handling difficulties. Chlorosilanes easily react with the surface hydroxyl groups, generating only hydrochloric acid as a by-product, which is easily removed from the reaction medium. A broad range of chlorosilanes are commercially available, increasing the diversity of the potential modifications. In this paper commercial available alumina membranes with 5 nm pores were modified using octdecylchlorosilanes. Gas permeation properties were investigated.

2. Background

It is well known that chlorosilane compounds are very reactive on any kind of hydroxyl groups, generating hydrochloric acid [5]. This property has been extensively exploited to modify silica surfaces to prepare new stationary phases for chromatography [6]. Other hydroxylated inorganic oxides such as zirconia, alumina, or titania might equally well be used. The chemical reaction involved in this type of reaction can be described as follows:

$$\text{Ceramic}\!-\!OH \ + \ Cl\!-\!\underset{R''}{\overset{R}{\underset{|}{\overset{|}{Si}}}}\!-\!R' \ \xrightarrow{\ HCl\ } \ \text{Ceramic}\!-\!O\!-\!\underset{R''}{\overset{R}{\underset{|}{\overset{|}{Si}}}}\!-\!R'$$

The basic concept was to graft on a ceramic membrane surface, (alumina in this paper) a chlorosilane derivative with a substituent hydrocarbon chain long enough to significantly reduce the membrane pore size or even block the pores and examine the consequences for gas diffusion.

The first part of this paper deals with the grafting reaction, the second describes the effects of this modification on gas permeation.

To study the reaction between the alumina and the chlorosilane, alumina powder was used rather the membrane itself. Alumina powder, which can be considered as morphologically equivalent to the membrane was used as in Part II [4].

3. Experimental

3.1. Powder and membrane modification

Tubular gamma alumina membranes, 10 mm external diameter, were used. The tube material was microporous gamma alumina. The active layer was a thin layer of porous alumina (pore size 5 nm) deposited on the inner tube surface by a sol–gel process. Chemical reaction experiments were performed on gamma alumina powder [7]. This powder was obtained from the same sol as that used to prepare the membrane and prepared under identical conditions. It may be considered to be chemically and morphologically equivalent to the material of the active layer of the membrane. Both the powder and the membrane were kindly donated by the Societe des Ceramiques Techniques (SCT).

A typical modification of the alumina powder (or membrane) by a chlorosilane derivative was as follows: 0.5 g of alumina powder (or membrane) was mixed with 10 ml of dry toluene in a two-necked reaction flask fitted with a dropping funnel and a reflux condenser. The reflux condenser was connected to a vacuum pump. Using a controlled leak, the reaction vessel was maintained under a moderate vacuum (roughly 400 mmHg). The toluene/alumina suspension was gently refluxed without significant solvent losses. 10 mmol of a chlorosilane derivative, dissolved in 10 ml of dry toluene, were then added relatively quickly to the suspension. A further 10 ml of dry toluene was added to the reaction mixture rinsing the dropping funnel. The reaction mixture was refluxed for a further 2 h, the HCl formed being pumped out of the reactor. After this reaction step, the powder (or membrane) was quickly transferred in a Soxhlet apparatus and extracted with toluene, for 12 h, to remove unbound siloxane molecules from the alumina surface. The powder was then dried for 24 h at 65°C, over silica gel, followed by 1 h at ambient temperature under vacuum (0.1 mmHg). The chlorosilanes compounds used were dimethyl octadecyl chlorosilane and octadecyl trichlorosilane, both purchased from Fluka (catalogue ref. 40950 and 74762) and used without further purification.

3.2. Infrared spectroscopy measurements

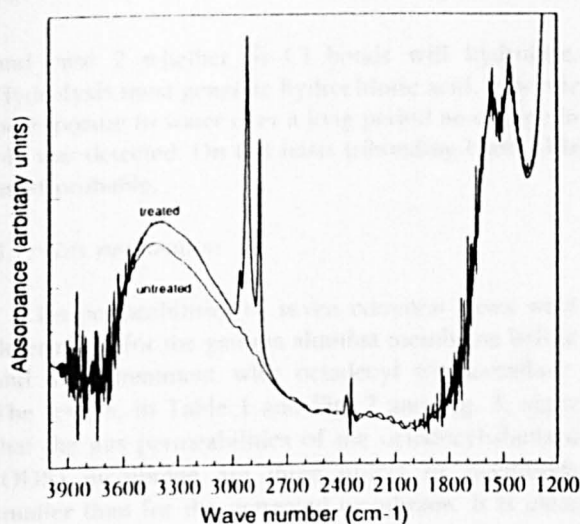Infrared spectroscopy is a powerful and convenient technique to prove an effective grafting of

Fig. 1. FTIR spectra of an alumina powder before and after octadecyl trichlorosilane treatment.

hydrocarbon chains on the alumina surface, because the C–H absorption bands (2900–3000 cm^{-1}) are easily detected. The samples, based on the modified powders, were prepared as KBr discs and spectra measured using a Perkin Elmer 16PC FTIR spectrometer.

4. Results and discussion

4.1. Surface modification

The infrared spectroscopy is a particularly suitable technique to detect the presence of hydrocarbon chains on the alumina surface. Indeed, the C–H absorption band due to a stretching of the chemical bond itself, can easily be isolated between 2900 and 3000 cm^{-1}. Octadecylsilanes were used in this study because their chains would be some 2.5 nm fully extended approximately equal to the membrane pore radius. (The manufacturer's estimate of pore diameter is 5 nm.) For such long chain aliphatics the intensity of the C–H absorption band is relatively high and thus the detection of successful grafting becomes easier. When dimethyl octadecyl chlorosilane was used as a reactant no C–H bonds were detected on the alumina surfaces and so no reaction takes place between the chlorosilane and the hydroxyl group of the alumina. This lack of reactivity could be due to the steric effect of the octadecyl chain and the two methyl groups limiting the access of the Si–Cl bond to hydroxyl groups of the alumina surface. With octadecyl trichlorosilane the steric effect is reduced and three Si–Cl bonds are available to react with the surface and the grafting reaction is successful as shown by the infrared spectra of Fig. 1. This reaction was expected to produce a permanent modification because the chemical grafting is by a very stable Si–O bond. The precise structure of the bonding on the surface is still unresolved, although the reaction mechanism is clear. Three possibilities exist:
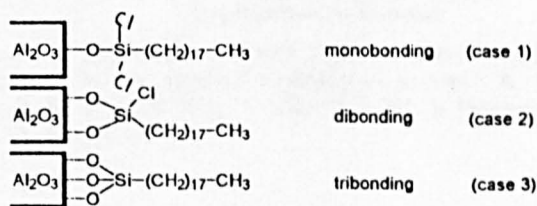
Membranes treated in this way are extremely hydrophobic. For this reason it is not clear in case 1

Table 1

Gas permeations, at 20°C, of several gases, through a 5 nm SCT membrane, untreated, and octadecyl trichlorosilane modified

Gas	Untreated membrane permeation (mol s^{-1} m^{-2} bar^{-1}) $\times 10^3$	Treated membrane permeation (mol s^{-1} m^{-2} bar^{-1}) $\times 10^6$
He	920	390
CH$_4$	845	481
Ne	433	323
N$_2$	551	335
Ar	429	294
CO$_2$	465	353
C$_3$H$_8$	732	350

and case 2 whether Si–Cl bonds will hydrolyse. Hydrolysis must generate hydrochloric acid, however on exposure to water over a long period no change in pH was detected. On this basis tribonding (case 3) is most probable.

4.2. Gas permeation

Gas permeabilities of seven common gases were determined for the gamma alumina membrane before and after treatment with octadecyl trichlorosilane. The results, in Table 1 and Fig. 2 and Fig. 3, show that the gas permeabilities of the octadecylsilanised (ODS) membrane are three orders of magnitude smaller than for the untreated membrane. It is clear that the pores of the ODS membrane are effectively
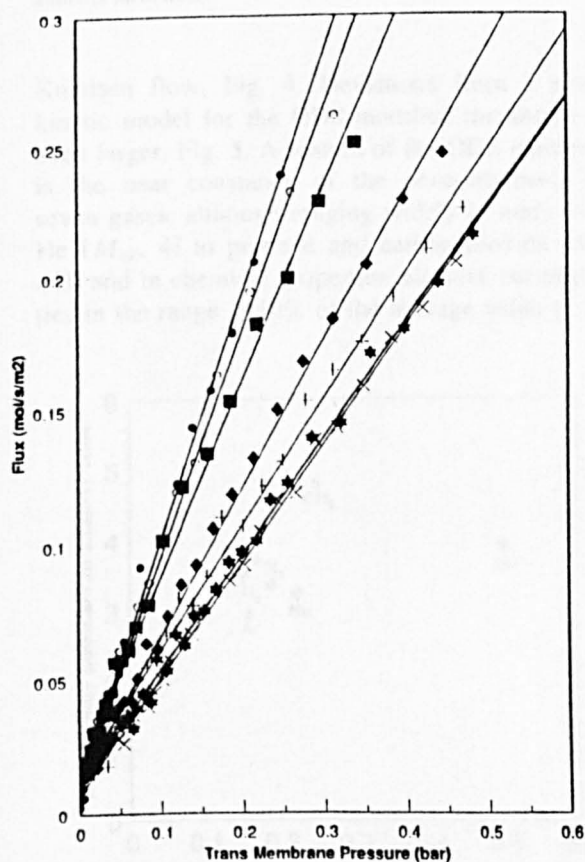
Fig. 2. Gas permeability properties of the 5 nm alumina membrane at 20°C, before modification. He, ●; Ne, ×; Ar, ★; N₂, ♦; CO₂, +; CH₄, O; C₃H₈, ■. Permeabilities are listed in Table 1.
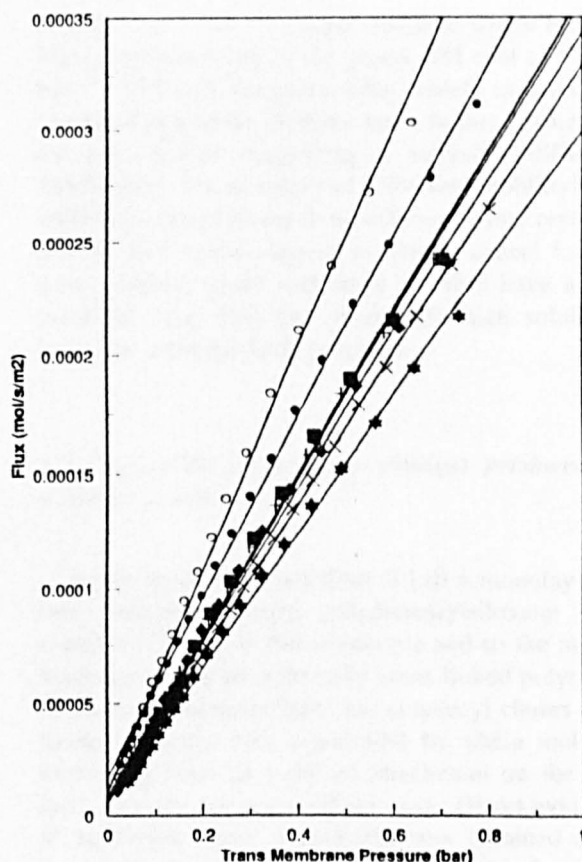
Fig. 3. Gas permeability properties of the 5 nm alumina membrane at 20°C, after octadecyl trichlorosilane treatment. He, ●; Ne, ×; Ar, ★; N₂, ♦; CO₂, +; CH₄, O; C₃H₈, ■. Permeabilities are listed in Table 1.

obstructed by the octadecyl aliphatic chains. There can be no concept of an open pore remaining. The permeabilities of test gases are however, on average 4 times larger by than for the silicon treated membrane (Part II [4]). Permeant gases must therefore pass through the hydrocarbon chains, but an element of openness or fluidity may remain perhaps because the total length of the extended graft chain can be estimated to be about 2.5–2.6 nm. If the pore shape is assumed to be circular a complete ODS monolayer could just fill a 5 nm pore but might retain a degree chain mobility (fluidity) in the pore centres. Gas permeation data reported in a previous paper [4], show clearly that the transfer mechanism in the open pores of the untreated membrane is not a simple
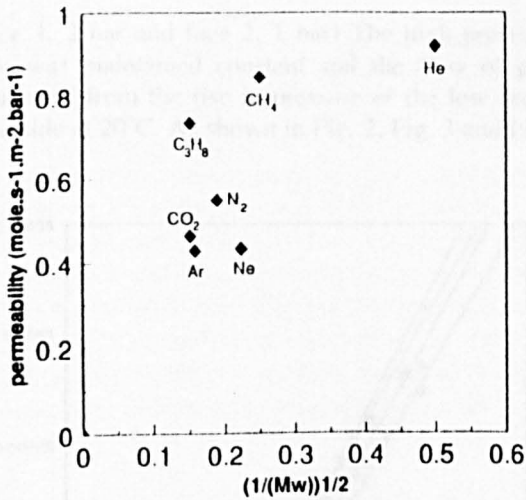
Fig. 4. Variation of the permeability (at 20°C) of several pure gas with their respective molecular weight, through the untreated 5 nm alumina membrane.

Knudsen flow, Fig. 4. Deviations from a simple kinetic model for the ODS-modified membrane are even larger, Fig. 5. A feature of the ODS-membrane is the near constancy of the permeabilities. The seven gases, although ranging widely in mass (from He (M_w, 4) to propane and carbon dioxide (M_w, 44)) and in chemical properties, all have permeabilities in the range ±10% of the average value of 360
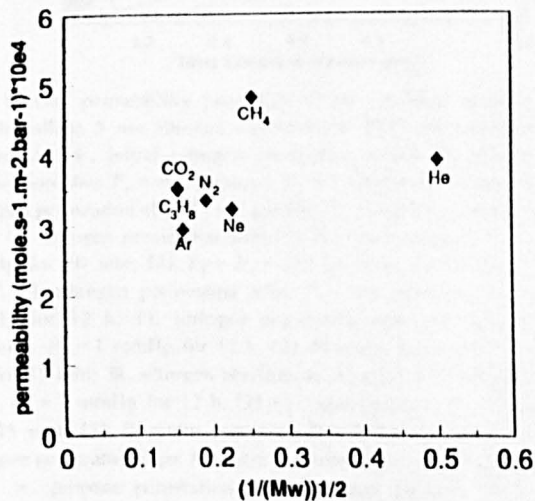

Fig. 5. Variation of the permeability (at 20°C) of several pure gas with their respective molecular weight, through the octadecyl trichlorosilane modified 5 nm alumina membrane.

mol s^{-1} m^{-2} bar^{-1}, except methane which has the highest permeability of the group, 481 mol s^{-1} m^{-2} bar^{-1}. Although the gases differ widely in mass and chemical properties methane has a higher permeability than helium suggesting a solubility/diffusion mechanism. The interplay of diffusion (mobility) and solubility cannot be resolved without further research but the two factors appear to largely cancel for the gases studied: gases with high mobility have a low solubility (e.g. He) and those with high solubility have low mobility (e.g. propane).

4.3. Reversible permeability changes produced by pressure gradients

In the previous paper (Part II [4]) a monolayer of low molecular weight polydimethylsiloxane (silicone) was bound to the membrane and so the monolayer molecules are internally cross-linked polymers. In this case the monolayer has octadecyl chains each linear molecule with a potential for chain mobility increasing from its point of attachment on the surface, towards the centre of the pore. Direct evidence of reversible chain movements was obtained quite unexpectedly in a series of experiments described below for nitrogen permeation. In these membranes the thin active layer of gamma alumina (pore size 5 nm) is located on the inner surface of the microporous tubular membrane (designated face 1) the outer face (shell side) will be designated as face 2, shown diagrammatically in Fig. 7. It was observed that when the membrane was under a nitrogen pressure of 1 atm on the inner tube surface (face 1) and the shell side (face 2) was evacuated for 10 min the ODS membrane nitrogen gas permeabilities was reduced by a five times to from 322 to 62 mol s^{-1} m^{-2} bar^{-1}. This change was metastable, the membrane remaining in its modified state during normal handling and during repeated gas permeation experiments. The permeability plots of flux against pressure difference across the tube were linear and reproducible, Fig. 6.

In this research it proved to be significant that gas permeabilities were obtained in all cases for transport across a membrane from tube to shell side (face 1 to face 2) with initial pressure difference of 1 bar,

(face 1, 2 bar and face 2, 1 bar) The high pressure side was maintained constant and the flow of gas computed from the rise in pressure of the low pressure side at 20°C. As shown in Fig. 2, Fig. 3 and Fig.
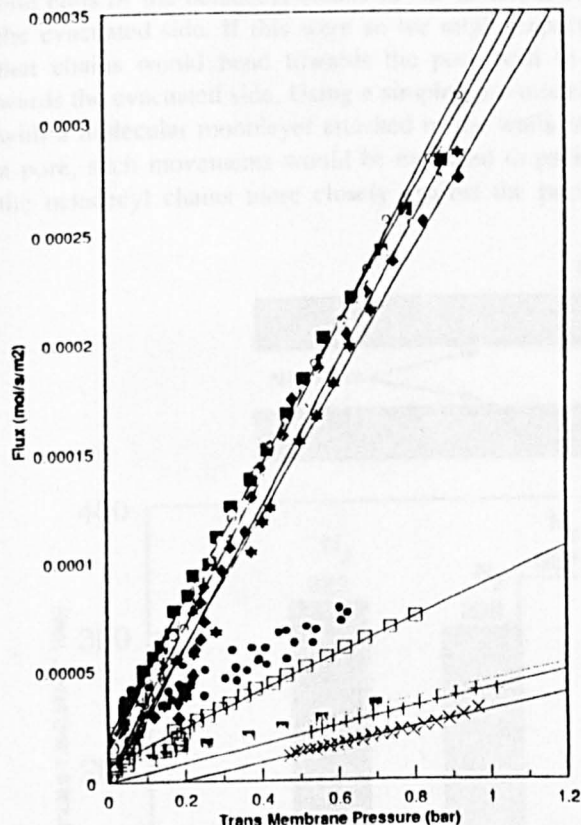

Fig. 6. Gas permeability properties of the modified octadecyl trichlorosilane 5 nm alumina membrane at 20°C, after pressure treatments: ♦, initial nitrogen permeation value; ●, nitrogen permeation after $P_1 =$ atm pressure, $P_2 = 1$ mmHg for 10 min; ★, nitrogen permeation after $P_1 = 1$ mmHg, $P_2 =$ atm pressure for 10 min; ○, nitrogen permeation after (1) $P_1 =$ atm pressure, $P_2 = 1$ mmHg for 10 min; (2) $P_1 = P_2 =$ atm pressure for 16 days at 20°C; □, nitrogen permeation after $P_1 =$ atm pressure, $P_2 = 1$ mmHg for 12 h; ◻, nitrogen permeation after (1) $P_1 =$ atm pressure, $P_2 = 1$ mmHg for 12 h; (2) $P_1 =$ atm pressure, $P_2 = 4$ bar for 45 min; ■, nitrogen permeation after (1) $P_1 =$ atm pressure, $P_2 = 1$ mmHg for 12 h; (2) $P_1 =$ atm pressure, $P_2 = 4$ bar for 45 min; (3) $P_1 =$ atm pressure, $P_2 = 2$ bar for 15 h; +, nitrogen permeation after $P_1 =$ atm pressure, $P_2 = 1$ mmHg for 60 min; ×, propane permeation after $P_1 =$ atm pressure, $P_2 = 1$ mmHg for 60 min; ○, nitrogen permeation after (1) $P_1 =$ atm pressure, $P_2 = 1$ mmHg for 12 h; (2) immersion in toluene at 20°C for 10 min; (3) drying at 20°C, $P_1 = P_2 = 1$ mmHg for 30 min.

6, permeation was followed until the pressure differential equalised in most cases.

In Fig. 7 the permeability changes induced by a series of conditioning treatments are summarised and the data for each permeability experiment shown in Fig. 5. When the conditions were reversed (face 2, 1 atm, face 1 evacuated for 10 min) the membrane returned to its original nitrogen permeability (299 mol s^{-1} m^{-2} bar^{-1}). This reversal was reproducible in cyclical experiments. A membrane in the low permeability state was stable and had a reproducible permeability over the several hours of experimentation. This form is not stable over a longer period. A membrane in the low permeability state left for 16 days at ambient 20°C recovered its original high permeability (337 mol s^{-1} m^{-2} bar^{-1}). This is explicable if the low permeability state is due to a packing of chains under the stress induced by the pressure treatment. Under uniform pressure, the chains would tend to relax toward the more stable, high flux morphology.

Applying the standard conditions (face 1, 1 atm; face 2, evacuated) for 12 h rather than the normal 10 min caused an additional 39% reduction in the low permeability state (from 62 to 38 mol s^{-1} m^{-2} bar^{-1}). The high permeability state could not be recovered by back pressure (face 2, 4 atm; face 1, 1 atm) for 45 min: the permeability rose only from 38 to 82 mol s^{-1} m^{-2} bar^{-1}. The high permeability state was achieved by a reverse pressure gradient (face 1, 1 atm; face 2, 2 atm) but only after 15 h. Under standard conditions (face 1, 1 atm; face 2, evacuated) for 1 h gave a permeability of 40 mol s^{-1} m^{-2} bar^{-1} almost identical to that achieved previously after 12 h, indicating that the change to the lowest permeability state is largely (90%) achieved after 10 min and 99% after 1 h.

There is no reasonable explanation for such reversible and reproducible changes other than by changes in the morphology or packing of the octadecyl chains of the bound monolayer, the potential for chain reorientation increasing progressively from its point of attachment on the surface, towards the centre of the pore. The relaxation period was long, full recovery being observed after 16 days, under ambient conditions. No changes in permeability were observed during the first 24 h. It is clear that the hydrocarbon chains are not liquid at the experimental

temperature, 20°C, otherwise the monolayer would recover rapidly from any mechanical distortion to a randomised fluidity. Packing of the hydrocarbon chains due to a pressure difference of 1 atm against vacuum can be envisaged as a one-sided molecular bombardment by nitrogen molecules moving the mobile ends of the octadecyl chains in the direction of the evacuated side. If this were so we might expect that chains would bend towards the pore wall towards the evacuated side. Using a simple pore model with a molecular monolayer attached to the walls of a pore, such movements would be expected to pack the octadecyl chains more closely against the pore

wall, open the pores and increase the permeability. The reverse is observed, a low permeability state is obtained.

A tentative explanation might be that the octadecyl chains on the surface of the active layer on the tube side (face 1, above) are partly forced into the pores which are already partly or completely covered by a ODS monolayer, Fig. 8. In this way chain movement would lower rather than raise permeabilities, by further obstructing molecular flow. If this is so then the active layer must be asymmetrical since reversal of this treatment (1 atm pressure applied from the shell side against a vacuum on the tube
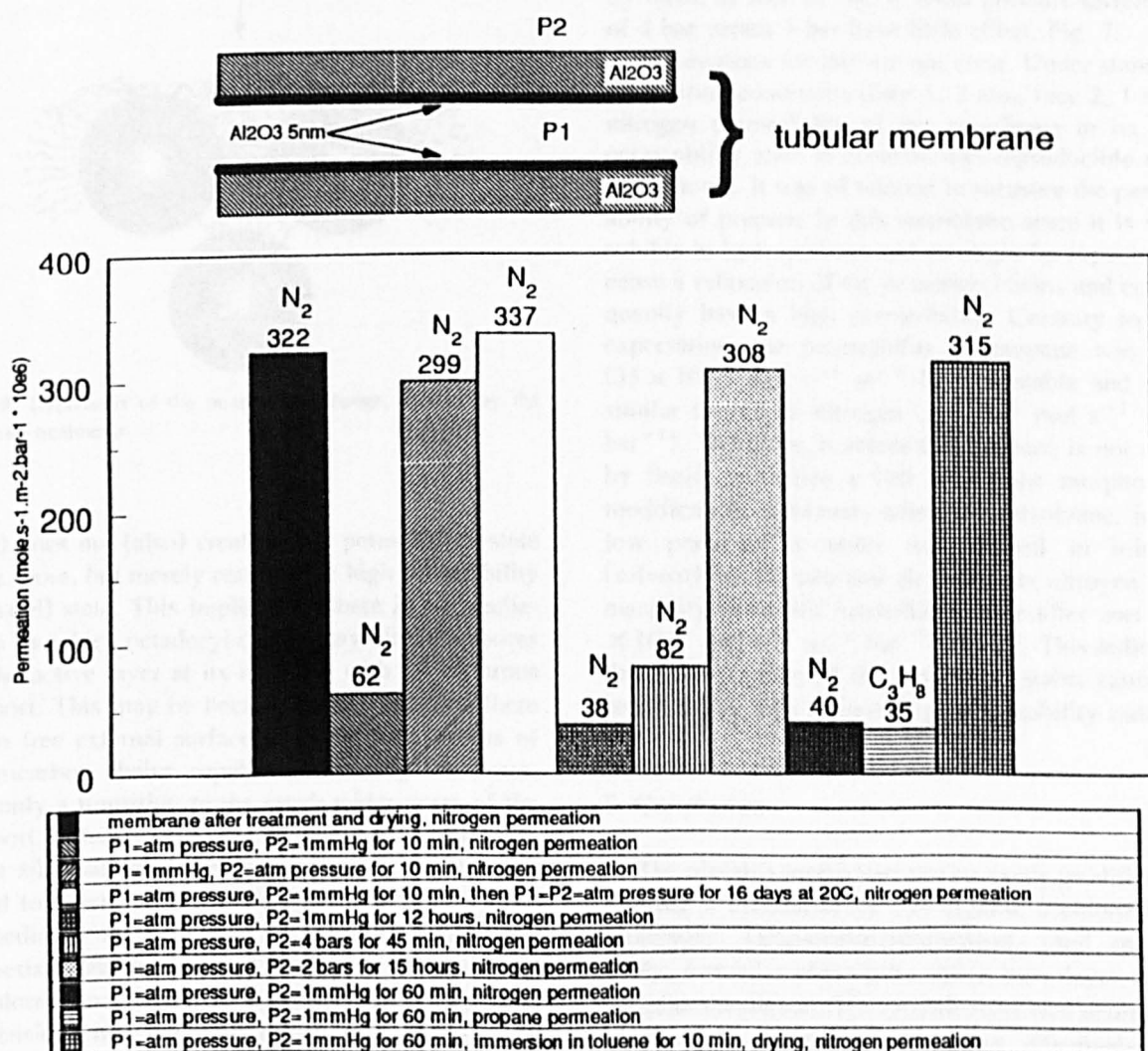

Fig. 7. Gas permeability properties of the modified octadecyl trichlorosilane 5 nm alumina membrane at 20°C, after pressure treatments.
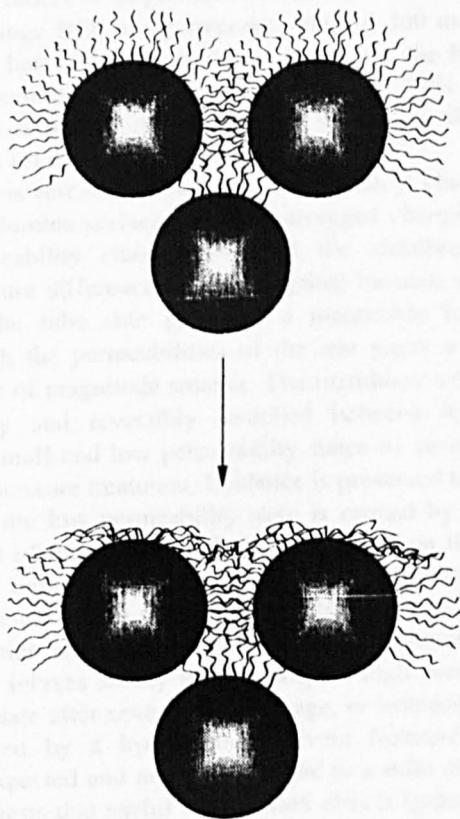
Fig. 8. Hypothesis of the morphology change, induced by the pressure treatments.

side) does not (also) create a low permeability state once more, but merely restores the high permeability (relaxed) state. This implies that there is no mechanism by which octadecyl chains may block the pores of the active layer at its interface with microporous support. This may be because at this interface there is no free external surface to provide the excess of hydrocarbon chains capable of entering the pores, but only a transition to the much wider pores of the support. Alternatively, one might imagine that efficient silanisation of the active layer is largely confined to outer surface of the tube side (face 1) and immediately adjacent pore surfaces. This latter hypothesis might be justified, firstly, if the octadecyl trichlorosilane, which is large relative to the pore dimensions, may not easily diffuse through the pores, and secondly, because each molecule which reacts with a hydroxylated site within porous active layer

will further obstruct the access of following molecules to sites deeper in the porous structure.

A further factor in this phenomenon is the observation that the creation of the low permeability state and restoration of the original high permeability state is quickly and easily achieved by 10 min application of a pressure of 1 atm against a vacuum (here 1 mmHg). An equal applied pressure difference of 2 bar against 1 bar (the experimental conditions for measuring permeation) neither creates the low permeability form as evidenced by the constancy and reproducibility of all the original permeability data of Fig. 3, nor, in reverse, restores the high permeability form, as seen in Fig. 6. Even pressure difference of 4 bar versus 1 bar have little effect, Fig. 7.

The reasons for this are not clear. Under standard permeation conditions (face 1, 2 atm, face 2, 1 atm) nitrogen permeability of the membrane in its low permeability state is constant and reproducible over many hours. It was of interest to measure the permeability of propane in this membrane since it is very soluble in hydrocarbons and so might be expected to cause a relaxation of the octadecyl chains and consequently have a high permeability. Contrary to this expectation, the permeability of propane was low (35×10^{-6} mol s^{-1} m^{-2} bar^{-1}), stable and very similar to that of nitrogen ($40\ 10^{-6}$ mol s^{-1} m^{-2} bar^{-1}). Therefore, it seems that propane is not able, by itself, to induce a fast membrane morphology modification. However, when the membrane, in its low permeability state, was dipped in toluene (solvent) for 10 min and air dried, its nitrogen permeability measured immediately thereafter was 315×10^{-6} mol s^{-1} m^{-2} bar^{-1} (Fig. 7). This indicates that solubilisation of the octadecyl chains causes a return to the fully relaxed high permeability state.

5. Conclusion

The alumina membrane can be easily modified by grafting a monolayer of and organic trichlorosilane molecules. Octadecyltrichlorosilane, used in this study, formed a chemically stable monolayer on an alumina membrane. The modification was permanent blocked the original 5 nm pores effectively and reduced the gas permeability of the membrane for the test gases (He, Ne, Ar, N_2, CO_2, CH_4, C_3H_8) by

three orders of magnitude. All have permeabilities in the range 10% of the average value of 360 mol s^{-1} m^{-2} bar^{-1}, except methane which has the highest permeability, 481 mol s^{-1} m^{-2} bar^{-1}. This membrane is not of obvious use for separation of these gases on the basis of this study.

This research shows that the octadecyl chains on the alumina surface may be rearranged changing the permeability characteristics of the membrane. A pressure difference of 1 atm against vacuum applied on the tube side produced a metastable form in which the permeabilities of the test gases were an order of magnitude smaller. The membrane could be easily and reversibly switched between its high (original) and low permeability states by reversal of the pressure treatment. Evidence is presented to show that the low permeability state is caused by movement of the surface hydrocarbon chains on the tube side moving into the pores (a self fouling phenomenon). This state is metastable and gas permeabilities are easily measured. The membrane however relaxes slowly into its original high permeability state after several days storage, or immediately if treated by a hydrocarbon solvent (toluene). This unexpected and novel effect, due to a mild pressure, suggests that useful rectification effects (gated transport) might be easily achieved, as here with pressure, but also with suitable functionalisation of chain substituents by electric or other forces.

Acknowledgements

References

[1] J. Randon, P. Blanc and R. Paterson, Modification of ceramic membrane surfaces using phosphoric acid and alkyl phosphonic acids and its effect on ultrafiltration of BSA protein, J. Membrane Sci., 98 (1995) 119–129.

[2] R.E. Johnson and D.I. Ford, Stability and reactivity of dimethylethoxysilane, in J.J. Pesek and I. Leigh (Eds.), Chemically Modified Surfaces, The Royal Society of Chemistry, 1994, pp. 164–184.

[3] J.J. Pesek, Conversion of oxide surfaces to hydride surfaces, in J.J. Pesek and I. Leigh (Eds.), Chemically Modified Surfaces, The Royal Society of Chemistry, 1994, pp. 1–23.

[4] C. Leger, H. De L. Lira and R. Paterson, Preparation and properties of surface modified ceramic membranes. Part II. Gas and liquid permeabilities of 5 nm alumina membrane modified by a monolayer of bound polydimethylsiloxane (PDMS) silicone oil, J. Membrane Sci., 120 (1996) 135–146.

[5] A.R. Bassindale and P.G. Taylor, Reaction mechanisms of nucleophilic attack at silicon, in S. Patai and Z. Rappoport (Eds.), The Chemistry of Organic Silicon Compounds, Part 1, Interscience Publications London, 1989, pp. 839–892.

[6] M.J. Wirth and H.O. Fatunmbi, Spectoscopic and chromatographic characterization of a self-assembled monolayer as a stationary phase, in J.J. Pesek and I. Leigh (Ed.), Chemically Modified Surfaces, The Royal Society of Chemistry, 1994, pp. 203–209.

[7] A. Larbot, J.P. Fabre, C. Guizard and L. Cot, New inorganic ultrafiltration membranes, J. Am. Ceram. Soc., 72 (1989) 257.